Daniel Filipe Martins
Mestrado em Engenharia Física

40 K Neon Liquid Energy Storage Unit

Dissertação para obtenção do Grau de Doutor em Engenharia Física

Orientador: Prof. Doutor Grégoire Bonfait, Associate Professor, Universidade Nova de Lisboa
Co-orientador: Prof. Doutora Isabel Catarino, Assistant Professor,Universidade Nova de Lisboa

Júri:

Presidente: Prof. Doutora Maria Adelaide de Jesus
Arguentes: Doutor Johan Bremer
Eng. Thierry Tirolien

Vogais: Prof. Doutor António Joaquim Rosa Amorim Barbosa
Prof. Doutor Manuel Leite de Almeida
Prof. Doutor Grégoire Marie Jean Bonfait
Prof. Doutora Maria Isabel Simões Catarino

FACULDADE DE
CIÊNCIAS E TECNOLOGIA
UNIVERSIDADE NOVA DE LISBOA

Dezembro 2014

Acknowledgments

I would like to thank Prof. Grégoire Bonfait and Prof. Isabel Catarino for their commitment and availability throughout the course of this work and for all the opportunities they provided me since 2007. They have largely expanded my horizons both professionally and at a personal level. It has been a pleasure to work with them.

I extend my gratitude to my colleagues of the Laboratory of Cryogenics, Josiana Afonso, Luís Ribeiro, João Franco and Patricia Borges de Sousa, for their constant availability in the development of this work. My sincere thanks goes also to João Faustino due to his assistance during the development and manufacturing phases.

I also thank Prof. Carla Machado, Prof. Alberto Martinho and Prof. Pámies Teixeira (Mechanical and Industrial Engineering Department of FCT-UNL) and Dr. Lionel Duband (INAC-CEA Grenoble) for their technical advices.

To my friends Paulo Ferreira and César Soares, I would like to thank for all the help and the friendship. They have always been helping and encouraging.

For her support, patience and help during this important phase of my life, a special thank goes to my girlfriend, Ines Afonso.

To my parents, I would like to express my gratitude for all they have done, tirelessly, to help me achieving my goals. Without them, none of this would be possible.

I also thank *Fundação para a Ciência e a Tecnologia* for the SFRH/BD/70427/2010 scholarship and the Physics Department of Faculty of Sciences and Technology and CEFITEC.

- This work was partially supported by: Fundação para a Ciência e Tecnologia: PTDC/EME-MFE/66533/2006; PTDC/EME-MFE/101448/2008; PEst-OE/FIS/UI0068/2012-2014);
- FCT-Embaixada de França — Programa Pessoa 2011/2012. Estabilizadores de Temperaturas criogénicas.

Abstract

Cryocoolers have been progressively replacing the use of the stored cryogens in cryogenic chains used for detector cooling, thanks to their higher and higher reliability. However, the mechanical vibrations, the electromagnetic interferences and the temperature fluctuations inherent to their functioning could reduce the sensor's sensitivity. In order to minimize this problem, compact thermal energy storage units (ESU) are studied, devices able to store thermal energy without significant temperature increase. These devices can be used as a temporary cold source making it possible to turn the cryocooler OFF providing a proper environment for the sensor. A heat switch is responsible for the thermal decoupling of the ESU from the cryocooler's temperature that increases when turned OFF.

In this work, several prototypes working around 40 K were designed, built and characterized. They consist in a low temperature cell that contains the liquid neon connected to an expansion volume at room temperature for gas storage during the liquid evaporation phase. To turn this system insensitive to the gravity direction, the liquid is retained in the low temperature cell by capillary effect in a porous material.

Thanks to pressure regulation of the liquid neon bath, 900 J were stored at 40K. The higher latent heat of the liquid and the inexistence of triple point transitions at 40 K turn the pressure control during the evaporation a versatile and compact alternative to an ESU working at the triple point transitions.

A quite compact second prototype ESU directly connected to the cryocooler cold finger was tested as a temperature stabilizer. This device was able to stabilize the cryocooler temperature (($\approx$ 40K ±1 K) despite sudden heat bursts corresponding to twice the cooling power of the cryocooler.

This thesis describes the construction of these devices as well as the tests performed. It is also shown that the thermal model developed to predict the thermal behaviour of these devices, implemented as a software, describes quite well the experimental results. Solutions to improve these devices are also proposed.

Resumo

Os criorrefrigeradores, maquinas térmicas cada vez mais fiáveis e compactas, têm vindo gradualmente a substituir os sólidos e líquidos criogénicos nas cadeias criogénicas utilizadas para arrefecer detectores. No entanto, factores como as vibrações mecânicas, interferências electromagnéticas e as flutuações de temperatura inerentes ao funcionamento dos criorrefrigeradores podem reduzir a sensibilidade do sensor. Para minimizar estes problemas, neste trabalho são estudadas unidades de armazenamento de energia térmica (ESU) dispositivos capazes de armazenar calor sem grande aumento de temperatura. Estes dispositivos tornam-se assim fonte fria temporária que permitem desligar o criorrefrigerador criando as condições mais adequadas para o funcionamento do sensor. Para proteger o ESU do aumento da temperatura do criorrefrigerador, quando este é desligado, é utilizado um interruptor térmico..

Este trabalho envolveu o dimensionamento, construção e caracterização de vários protótipos de unidades de armazenamento de energia baseado no calor latente do néon liquido para operar acerca de 40 K. Estes dispositivos consistem numa célula a baixa temperatura, com néon líquido, conectada a um volume de expansão para armazenar o gás durante a evaporação deste líquido. Para tornar estes sistemas insensíveis à direção da gravidade, o líquido é retido dentro da célula por um material poroso.

Através do controlo da pressão na célula de baixa temperatura, foi possível armazenar 900 J a 40K. A inexistência de pontos triplos nesta zona de temperatura e o elevado calor latente do líquido torna este tipo de dispositivo uma alternativa, mais compacta, ao uso das transições de ponto triplo.

Foi ainda desenvolvido um estabilizador de temperatura que consiste num pequeno ESU diretamente conectado ao dedo frio do criorrefrigerador. Este dispositivo mostrou ser capaz de manter uma temperatura estável (≈ 40K ±1 K) apesar de picos repentinos de potência correspondendo ao dobro da potência frigorífica do criorrefrigerador.

Esta tese descreve a realização destes dispositivos assim como os testes efectuados. Mostrou-se também que o modelo térmico desenvolvido, implementado na forma de uma aplicação informática, descreve bem os resultados experimentais. Soluções para melhorar estes dispositivos são também apresentadas.

Contents

List of Figures

List of tables

List of Symbols

$\dot{Q}$	Heat load
A	Area
c	Specific Heat
C	Heat capacity
E	Energy stored
F	Force
f_{ress}	Resonance frequency
H	Enthalpy
h	Height
k	Conductivity
K	Conductance
L	Latent heat
m	Mass
n	Moles number
P	Pressure
p	Pitch
Q	Heat
r	Radius
R	Ideal gas constant
S	Entropy
s	Section
T	Temperature
t	Time
T_{fin}	Final temperature
T_{ini}	Initial temperature
U	Internal energy
V	Volume
α	Expansion coefficient
γ	Heat capacity ratio
Δ	Gap width
θ	Contact angle
ρ	Density
σ	Surface tension
σ_{yield}	Yield strength

Acronyms

CTSU	Cryogenic thermal storage unit
DV	Dual volume
ESA	European Space Agency
ESU	Energy Storage Unit
GGHS	Gas gap heat switch
HX	Heat exchanger
LPTC	Large pulse tube cooler
PCM	Phase change material
PTR	Pulse tube refrigerator
QWIP	Quantum-well infrared photodetector
RT	Room Temperature
SQUID	Superconducting quantum interference devices
SS	Stainless steel
TSU	Thermal storage Unit

Introduction

The cooling of infrared detectors is one of the major applications for space cryogenics. Infrared vision provides useful information for earth observation and meteorology missions as well as for space tracking and surveillance programs[1]. For space observation missions, Infrared detection brings us unique information about star and planet forming regions, supernovas and the structure of the early Universe (Herschel [2]). Moreover, apart from the operational temperature range of these sensors, a low vibration and low electromagnetic interference environment is always required to avoid sensors sensitivity loss.

Different cooling techniques, among cryogenic fluids and mechanical cryocoolers, can be used to cool the infrared detectors down. Nevertheless, nowadays, mechanical coolers have become more and more attractive[3], thanks to their increasing reliability, and due to the intrinsic short lifetime of cryostats using stored cryogens.

However, even with pulse tube coolers, without moving parts at low temperature, some vibrations are induced either by the compressor and by the pressure oscillations inherent to the operation of cryocoolers, and these vibrations can limit very high precision measurements. One way to stop these vibrations during the measurement is to stop the cryocooler but this procedure leads to a fast temperature increase that results in a quite short time for measurements under a vibration-free environment.

To slow down this fast temperature rise, the sensitive sensors could be connected to a thermal Energy Storage Unit (ESU) that will act as a temporary cold source in a vibration-free environment. The idea is to couple a high enthalpy reservoir to the cold finger through a thermal switch, which is responsible for the thermal coupling or decoupling of the ESU from the cold source. During the sensor operation, the cryocooler is stopped and the heat switch isolates the temporary could source from the fast temperature drift occurring at the cold finger when the cryocooler is stopped. During this phase, the thermal energy dissipated by the sensor is then absorbed by the ESU and, thanks to its high enthalpy, does not lead to a severe temperature increase.

A solution to slow down this fast temperature rise in the 40 K temperature range is the objective of this present work. This concept, using a heat switch, can also be used to maintain the temperature of some cryogenic device constant in the case of cold source temperature fluctuations: the ESU is “charged” (i.e. cooled) whenever the cold source temperature is lower than the ESU and thermally decoupled while the opposite occurs and becomes ready for being “discharged” when needed.

Another objective of this work is the use of the 40 K enthalpy reservoir as a thermal buffer, where it is directly coupled to the cold source and to the cryogenic device in order to absorb sudden heat bursts. This principle was studied and demonstrated by Bugby[4] in the 35 K range.

One of the target applications of this 40 K ESU are the rather recent very long wavelength infrared sensors, the so-called Quantum-Well Infrared Photodetectors – QWIPs[5], used for space observation missions, earth observation and military applications. The Operational Land Imager for the Landsat Data Continuity Mission (Landsat 8) [6] is an example of the QWIP-based infrared instrument (launched in February 2013) used in an earth observation mission.

The ESU being a high enthalpy reservoir able to store heat without a large temperature drift, high specific heat materials can be good candidates to integrate this kind of system and turn the ESU system very simple. On the other hand, phase change materials (PCM), such as cryogenic fluids, can also lead to an efficient solution due rather large latent heat associated to their phase transitions. Some ESU were developed by our group to operate between 3-6 K[7] and 11 – 20 K[8] using the specific heat of lead and Gd_2O_2S, respectively. An ESU based on the liquid to vapor transition of the nitrogen was also studied to operate in the 70 K – 80 K range[9].

The triple point is also attractive for the development of an ESU because it corresponds to a phase transition occurring naturally at constant temperature, as is the case of the Thermal Storage Unit developed at *Lockheed Martin*[10]. This device operates at a constant temperature and uses the triple point transition of nitrogen at 63.2 K.

In the present work, the development of an ESU operating in the 40 K range is studied, the heat storage is obtained by the latent heat associated to the liquid-to-vapor transition of neon. It is shown that it presents a compact and light solution to store up to 1000 J in the 40 K range.

This text is divided in five chapters, where the different steps for the 40 K ESU sizing, manufacturing and testing are presented. In the first chapter, the solutions to store thermal energy below 100 K are discussed, and some examples of ESUs using those principles are presented.

In the second chapter a detailed description of the three operational working modes of an ESU using the liquid-vapor transition is given. This device can operate as a temporary cold source in a vibration-free environment by turning the cryocooler off. The direct coupling of the ESU to the cold source improves the temperature stability, which would be difficult to maintain stable in case of sudden heat bursts. Operation at constant temperature is also possible, similarly to the triple point transitions, by controlling the pressure in the enthalpy reservoir during the evaporation phase with a pressure control valve. It is shown that the liquid-vapor ESU working in this mode can be much more compact at low temperature than the triple-point based ESUs due to the higher latent heat of the liquid-vapor transition. In the same chapter, a thermal model is presented and adapted for each operational mode. With this thermal model a pre-dimensioning tool software was created, which is useful for system sizing and to predict the experimental results.

As already mentioned, the target applications of such ESUs are space applications, and, within this goal, this device must be gravity insensitive. For that reason, the confinement of liquid neon inside of the low temperature cell is needed for proper device operation. The adopted solution is liquid confinement in a porous media by capillarity effects. However, at 40 K, neon approaches its critical point and its surface tension is rather low, which means a decrease in the capillary forces. This fact adds an extra challenge in the liquid confinement inside the cell. Tests of the capability of some porous materials to confine the liquid neon at 40 K are presented and discussed in the third chapter. The experimental setup and the ESU components sizing are also described in this third chapter. The system is composed by a small cold cell containing the liquid neon and, to minimize the pressure increase during the evaporation phase, an expansion volume at room temperature is used. To operate with liquid neon within this temperature range, a cryogenic cell suitable to withstand 25 bar was required. This fact leads to the development of different cells to test each of the operational modes and test materials to confine the liquid inside the cell. An orientable stand, developed to change the cryocooler orientation in respect to gravity in order to allow the study of the ESU performance as function of the orientation, is described in the same chapter. In this description, the sizing of whole mechanical interfaces of the cold cell and the gas gap heat switch inside of the cryocooler that clamp all set in operation is also included. The gas gap heat switch used to allow the enthalpy reservoir thermal coupling and decoupling from the cold source was previously developed[11] but, to operate in the 40 K range, it is was necessary to implement and test a new cryopump. The characterization of the heat switch is presented in the third chapter.

In the fourth chapter, all of the functional tests of the ESU modes are presented: the "temperature drift mode" and the "temperature controlled mode". In both modes the heat switch allows the operation in a "quasi-adiabatic" environment, which facilitates the measurement of the stored energy within the ESU. The cyclic operation tests (Cooling process followed by the ESU) are also shown, where a detailed description of each phase is given. For the tests of the ESU booster mode, a smaller cell (12 cm^3) was directly coupled to the cryocooler cold finger to attenuate its temperature variation in case of sudden heat bursts. This configuration was sized to absorb 400 J within a temperature drift of 1 K at the 40 K range. Tests to study the influence of this configuration in the cryocooler temperature (with a cooling power of 4.5 W at 40 K) when subjected to high heat loads (14 W) and variable heat load profiles were applied and are presented. During all these tests, the experimental results are compared to instead of with those obtained by the thermal model.

The last chapter summarizes the results and the lessons learned from them. Some insight is given in order to improve future ESU working along the liquid-gas saturation curve.

1 The use of cryocoolers

The reliability of the cryocoolers is presently so high that they can integrate cryogenic infrastructures, where the stored cryogen systems were used in the past. Since the 1960s the possibility of cooling with a very long lifetime cryocooler instead of a limited lifetime provided by the liquid reservoirs has attracted their use in space cryogenic missions. But, at that time, the temperatures obtained using cryogens were more competitive. For instance, a system using solid cryogen was able to obtain temperatures as low as 6 K. This solid state was kept by the vacuum of space and was stable in zero *g* operation. To achieve lower temperatures it was necessary to use liquid cryogens (helium). But some factors like zero-*g* fluid management complicate the use of cryogenic liquids. These systems are characterized by their simplicity when compared with the cryocoolers and the non-existence of vibration. But the typical lifetime of 1-2 years was a limitation of cryogen systems.

These facts stimulated the investments to achieve lower temperatures, high power efficiency, high cooling power and low vibrations. The number of cryocoolers in space missions is growing rapidly, thanks to their high level of maturity. Pulse Tube, Stirling and turbo-Brayton cryocoolers have been reliably used in space missions involving infrared sensors. Many single-stage cryocoolers (50-100K range) are approaching 10 years of on-orbit operation, maintaining their cooling performance [3, 12]. Beyond of the non-existence of intrinsic lifetime limit, the cryocoolers have significantly lower mass than stored cryogens of comparable cooling capacity.

The Stirling cryocoolers use the Stirling engine principle. In the 1970s, at Oxford University the engineers developed and qualified a reliable long-life Oxford Stirling cooler for space[3]. The cooling process is a result of compressions and expansions of the working fluid, helium, in 2 chambers through a regenerative heat exchanger. Two pistons are responsible for these compressions and expansions. The Oxford engineering made innovations in the moving mechanisms increasing the reliability of these coolers[13]. The first closed-cycle mechanical cryocooler in orbit was the Malaker Stirling cooler that cooled an infrared radiometer, in July 1971[3]. The cooling power of each Stirling was 2 W at 100 K with 40 W input. The two coolers periodically cooled the detectors to 105 K during the radiometer operation (3 to 4 h periods). The total run time on the coolers during the mission was less than 1000h [3]. The Ramaty High-Energy Solar Spectroscopic Imager (RHESSI) used a Sunpower M77B Stirling cooler to cool a detector array to 75 K (Figure 1-1 a))[14]. This was the first low-cost commercial cooler to achieve multi-year operation in space [3, 14].

Another type of cryocooler that is often used is the pulse tube refrigerator (PTR). The PTR is a closed-cycle regenerative mechanical cooler, like the Stirling coolers, but without moving parts at low temperature. This leads to an increase of the lifetime and to a reduction of the vibration level. Cooling powers of ~1.5 W at 4.2 K and ~40 W at 45 K can be obtained with the modern Pulse Tubes refrigerators. An example of multi-year cryocooler operation in space is the TRW pulse-tube cooler used to cool two different infrared focal planes to 62 K on JPL's Tropospheric Emission Spectrometer instrument (TES)(Figure 1-1 b). The TES was launched in 2004 and worked during more than 16000 h without any problem [3]).

Turbo-Brayton cryocoolers are known by their low resonant vibration[15]. The turbomachines are used to compress and expand the working gas as part of a reverse-Brayton cycle. The moving parts of these cryocoolers are the small turbomachines that operate at several thousand rotations per second. The emitted vibrations are very small and occur at high frequencies. Manufacturing these small turbomachines is a challenge and the moving parts at the cold end can compromise the reliability of the cryocooler. Due to the damage occurred in solid –nitrogen dewar of the NICMOS in

1999, a Turbo–Brayton cryocooler (7.1 W at 70 K (Figure 1-1 c) was installed on the Hubble Space Telescope in 2002[3].

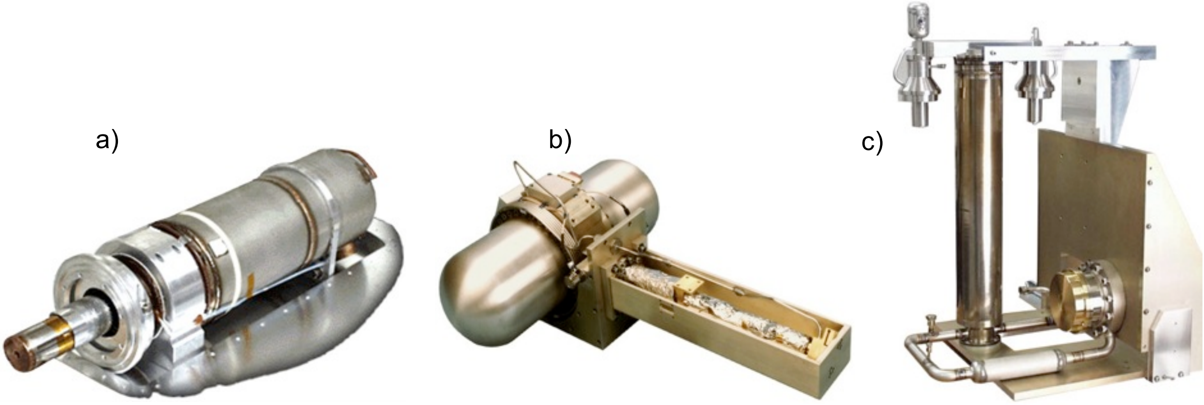

Figure 1-1 - a) Sunpower M77B Stirlling cryocooler used on the RHESSI radiator structure[3]; b) NGST TES pulse tube cryocooler[3]; c) The Turbo- Brayton cryocooler in preparation for installation on Hubble Space Telescope[3].

The main drawback in the use of cryocoolers are the vibration. Most of the cryocoolers used for earth Observation missions or surveillance tracking programs are Stirling or Pulse Tube cryocoolers and are based on compression-expansion cycles of helium. The pressure oscillations due to these cycles leads to vibrations that can affect the instrument performance. Moreover, the vibration effect on instrument noise is hard to model, hence hard to predict. A lot of developments were made in Pulse Tube and Stirling cryocoolers to reduce these vibrations [16, 17]. In addition to the mechanical vibrations, the magnetic interferences induced by the motor of the mechanical cryocoolers can influence certain measurements. That is the case, for instance, of the cryocoolers used to cool SQUID magnetometers [18].

1.1 Cooling below 50 K

The development of very long wavelength infrared devices for space or earth observation missions for civilian and military applications has increased the demand for reliable cryocoolers to work below 50 K. It is the case, for example, for the cooling of the very long wavelength infrared devices (Quantum-Well Infrared Photodetector - QWIP) where temperatures as low as 40 K are required for these devices to work properly[6].

The GaAs/AlGaAs QWIPs rely on intersubband transitions between quantized states within conduction band and their range of detection is 8 – 13 μm. These QWIPs are usually used in the array form. Some thermal imaging cameras are based in QWIPs arrays [19]. The QWIPs characteristics are very dependent of the temperature: at 45 K their performance can be the half of that at 40 K [20]. In addition to the temperature stability for a properly working, a low vibration and electromagnetic interference environments are required.

The thermal infrared sensor (TIRS) of Landsat 8 (launched on February, 2013) is a on orbit example of QWIP based instrument[21]. A mechanical two-stage cryocooler is responsible for the focal plane cooling at 43 K.

For missions of Earth Observation or Surveillance Tracking programs, CEA/INAC/SBT and Air Liquid have developed the so-called “Large Pulse Tube Cooler” (LPTC) for the temperature range of 40 – 60 K (Figure 1-2)[22]. This cooler appears as an alternative to the Stirling coolers for applications where a low vibration level is a requirement. This LPTC has a cooling power of 2.3 W at 50 K and 1 W at 40K and a minimum temperature around 31 K [22].

Figure 1-2 – Coaxial Large Pulse Tube[22].

Other pulse tube coolers were created to cool infrared detectors down to 50 K with low vibrations. It is the case of the Stirling-type pulse tube cryocooler developed by Wang[20] to cool GaAs/AlGaAs QWIPs that require the cooling power of 0.3 W at 40 K. This cryocooler provides a cooling power of 420 mW at 40 K. Also to cool this type of infrared detectors a single stage coaxial pulse tube cooler was developed by Dang[23]. This model can provide 860 mW of cooling power at 40 K.

The demand for low vibration coolers in this temperature range is patent and, for instance, ESA (European Space Agency) published the following call in 2013: "Two Stage Cooler for Detector Cooling between 30 K and 50 K". Using the actual pulse tube and Stirling technologies in a double stage configuration the cryocooler should be able to provide 800 mW at 35-40 K (cold stage) and 1500 mW at 100 – 130 K in the higher temperature stage to intercept parasitic heat load. This cooler will be used to provide temperatures around 35 K – 40 K to enable the operation of big QWIP detector matrices for earth observation missions (ESA Intended Invitation To Tender nº 11.127.02).

1.2 Storing thermal energy below 50 K

In the last section some low vibration mechanical cryocoolers, which were developed for cooling infrared sensors bellow 50 K, were summarily described. Even with pulse tube coolers, without moving parts at low temperature, some vibrations are induced by the compressor and by the pressure oscillations inherent to its operation. Sometimes these vibrations can be incompatible with very high precision measurements. In addition, the electrical motor of the compressor can origin undesirable electromagnetic noise. One-way to stop/reduce these vibrations is to stop the cryocooler, or simply decrease its frequency to avoid the mechanical stresses due to repeated starts and stops[9]. However, these stops lead to a rapid increase of the temperature that results in a very short time for measurement without vibrations. To reduce this rapid temperature drift, a thermal energy storage unit (ESU) can be used and will play the role of a temporary cold source in a vibration-free environment. The idea is to thermally link the sensitive sensors to this high enthalpy reservoir (ESU). As depicted in Figure 1-3 the ESU is coupled to the cryocooler cold finger through a thermal heat switch. This thermal heat switch is responsible for the coupling or decoupling of the ESU from the cold source.

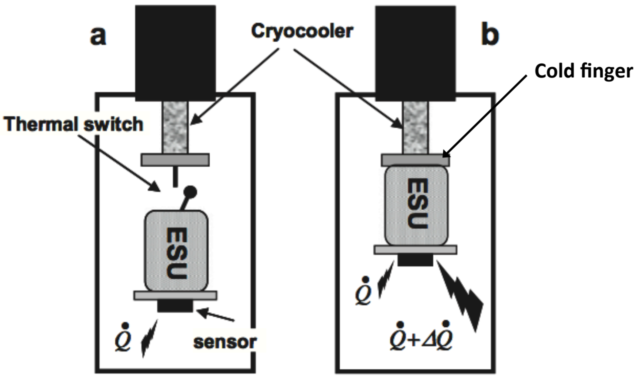

Figure 1-3 - A schematic integration of an energy storage unit (ESU) in a cryocooler for: a) “vibrationless configuration”; b) cooling power booster. In both cases the sensor is coupled to the ESU. Adapted from [9].

In the first phase of the operation with an ESU, the pre-cooling phase, the enthalpy reservoir is cooled down to the lowest temperature achievable by the cryocooler. During this first phase the thermal heat switch is maintained in its higher conducting state (ON state) to allow cooling. When the ESU is cold, the second phase, the so-called “ESU mode” can start: the heat switch is toggled to the OFF state (the poor conducting state) leading to the thermal decoupling of the ESU from the cryocooler. At this time the cryocooler is turned off and the cold finger temperature starts to increase (the rate of increasing being dependent of the cryocooler’s characteristics as well as the thermal inertia coupled). During this phase, thanks to the thermal decoupling from the cryocooler and the high enthalpy of the ESU, the temperature of the ESU also starts to increase from pre-cooling temperature but at a much slower rate. During the temperature drift the ESU actuates as thermal ballast and the rate of this drift is going to be dependent of the ESU enthalpy [7, 8].

The ESU can also be directly coupled to the cold finger of the cryocooler and used to temporarily increase the cooling power of the cryocooler – this mode will be called in the following as “cooling power booster mode” (Figure 1-3 b). In this mode, the main task of the ESU is to absorb sudden heat bursts dissipated by the sensors, which are cooled by a cryocooler with a lower cooling capacity than the sudden heat bursts. As illustrated in Figure 1-4, the heat load profile can be modelled as dissipating $\dot{Q}_{H,MAX}$ during δt and $\dot{Q}_{H,MIN}$ in $P- \delta t$, where P is the period. For an efficient use of the ESU, the cooling capacity ($\dot{Q}_C$) must be higher than the medium heat load ($\dot{Q}_{H,MIN}$). When the heat load from the sensor is less than Q_C,, some cooling energy is being stored. The laying area between the cooling and heat load curves, when the cooling capacity is higher, represents the stored energy (E_S). When the opposite scenario occurs the cooling energy (E_U) is being used. In a cyclic ESU operation the minimum cooling power ($\dot{Q}_{C,MIN}$) occurs when the E_S=E_U is ensured [13].

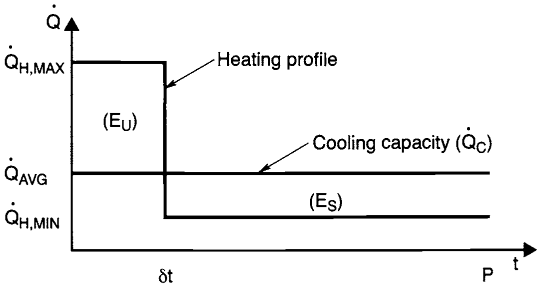

Figure 1-4 – ESU operation with a variable heating profile, adapted from[13].

For some astronomy applications the focal plane QWIPs array operates at 43 K (nominally)[6]. With the number of QWIPs sensors increasing in the arrays, to obtain higher resolution images, more cooling capacity is required. In the case of using these sensors in short times events, an ESU, working in the booster mode, would allow the use of low power consumption cooler. Such a configuration, providing a high thermal inertia also leads to a better thermal stability of the cold finger on short time, which is a very important requirement for QWIPs, a temperature stability of circa 0.01 K.

Following, in the next section, some ESU concepts are presented.

1.2.1 Sensible heat energy storage

A very simple way to store heat (*Q*) with a limited temperature drift ΔT is to dissipate it in a high heat capacity (C) block ($\Delta T = Q/C$). Materials with high specific heat are then good candidates for thermal energy storage units. Such ESU are sometimes called as sensible heat ESU by opposition to the latent heat ESU where the heat absorption is accompanied by a first order change of state like the liquid to gas transition. The sensible heat energy storage concept was used to obtain a "Solid State" cold source without mechanical, thermal and electromagnetic perturbations for sensitive applications or microgravity issues. Two ESUs of this type were developed by our group some years ago: The materials chosen to store thermal energy using sensible heat were the lead[8] between 11 K and 20 K and the Gd_2O_2S (GOS)[7] between 3K and 6 K. In Figure 1-5 the specific heat of these two materials is plotted. The high specific heat peak of GOS at 5.2 K is due to a paramagnetic-antiferromagnetic phase transition whereas the relatively large Pb heat specific is due to its low Debye temperature. Both ESU's were sized to store 36 J during the aforementioned temperature intervals.

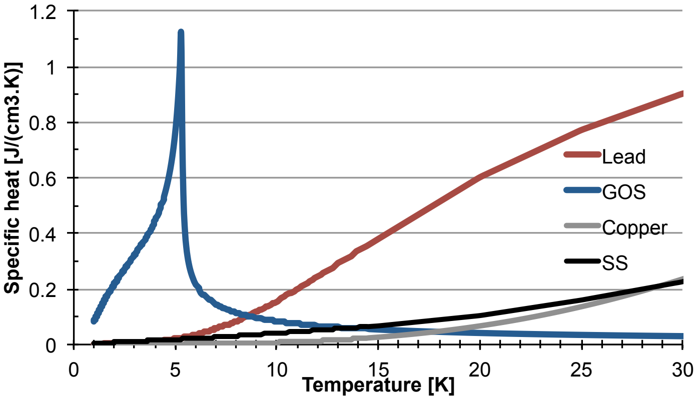

Figure 1-5 – Specific heat of the Gd_2O_2S (GOS) and lead compared to the copper and stainless steel[24].

In both GOS and Pb ESUs, the enthalpy reservoir, which contains the high specific heat material, is connected to the cold finger of a cryocooler through a gas gap heat switch. With such a setup it is possible to use the ESU as a simple cold source, free of vibrations and electromagnetic noise. When the ESU is cold (initial temperature - T_{ini}), the cryocooler may be turned OFF and the heat switch switched to the poor heat conduction state (OFF). By this time the sensors, placed on a temperature controlled "Sensor Platform", could operate in a completely vibration-free environment and be decoupled from the temperature increase of the cryocooler. In these solid state ESU's, any heat exchange only change its temperature. Therefore, the amount of heat stored by the ESU between the initial (T_{ini}) and final temperature (T_{fin}):

$$Q = \int_{T_{in}}^{T_{fin}} m.c(T)\,dT = H(T_{fin}) - H(T_{in}) \qquad (1.1)$$

where *m* is the mass and *c* the massic specific heat of the material used to store the energy and *H* the enthalpy of the ESU. In these two ESU's, the sensor are attached to a "Sensor Platform" loosely copled to the enthalpy reservoir (Figure 1-6), instead of directly coupled on it. With this configuration, the temperature of the platform can be maintained strictly constant at a temperature higher or equal to T_{fin} during the ESU mode despite the temperature drift of the ESU [7].

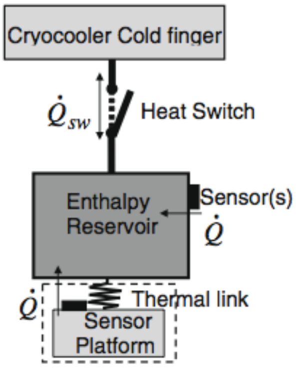

Figure 1-6 – General scheme of the ESU [8]. A "Sensor Platform" to maintain a constant temperature during the ESU-mode is used.

A complete cycle of an ESU mode (continuous operation and duty cycles) using the GOS, with the "Sensor Platform" maintained at constant temperature is demonstrated in Figure 1-7:

- At the beginning with the "Enthalpy Reservoir" at T_{ER}=3.67 K (T_{ER} - black line), and the switch in the OFF state by cooling the cryopump (T_{sorb} - green line) below ≈ 10 K, the cryocooler is stopped and its temperature increases (T_{cf} – blue line).
- The platform is controlled at a constant temperature (T_{pf} – red line) equal to 6 K during the ESU-mode. In this phase the platform temperature was stable within 5 mK.
- "A little before" the temperature of the enthalpy reservoir achieves the temperature of the platform, the ESU mode finishes (*t* ≈ 38 min). To continue to control the temperature of the platform it is necessary to recycle the enthalpy reservoir: The cryocooler is turned ON and the ESU is cooled again by toggling the heat switch into the ON state (cryopump was heated). This phase of the cycle is called "duty-cycle".
- When the ESU achieves 3.4 K the ESU is considered "recycled" (*t*≈51 min). The cryopump heating is stopped in order to toggle the switch into the OFF state.
- At *t*≈53.5 min, the switch is considered OFF and the cryocooler can be stopped again, starting the second ESU-mode.

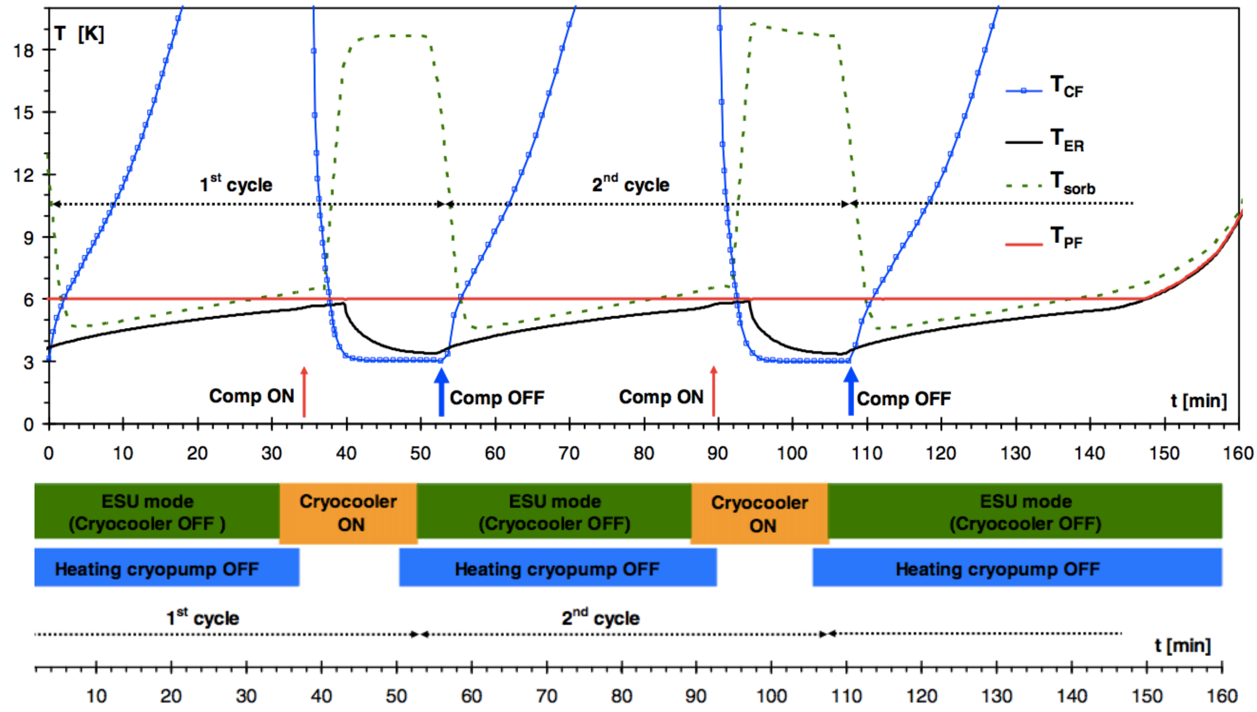

Figure 1-7 – Temperature variations during three cycles with ESU GOS. The platform temperature was maintained stable at 6 K during 2.5h (adapted from [7]).

During these 3 cycles (≈2.5 h), the platform temperature was stable within 5 mK whereas the cryocooler was maintained stopped during ≈1.8 h. Nearly 70 % of the time the sensor was in a completely vibration-free environment.

Looking back for our target, a way to store energy at 40 K, this “sensible heat ESU” concept is possible to be used in order to have a cold source free of vibrations, or simply used as booster mode to absorb the heat peaks. However, to choose a high specific heat material, two important factors needs to be taken into account: the mass and/or volume. Table 1.1 presents the comparison between specific heat of different materials. To make easier the physical comparison between these materials, the mass, the volume and the size of the ESU are calculated to store 1000 J (e.g. 1 W during ≈ 17 min.) between 38 K and 42 K.

Table 1.1 - Specific heat of some selected materials at 40 K [24]. The ESU volume and mass are calculated to store 1000 J between 38 K and 42 K. The ESU was chosen cylindrical with its height equal to the diameter.

Material	**Density** (kg/m^3)	**Specific heat** $(J/(cm^3K))$	**mass** (kg)	**Volume** (L)	**Diameter** (cm)
Copper	8960	0.53	4.27	0.48	8.46
Aluminium	2713	0.23	3.00	1.11	11.21
SS	8000	0.45	4.44	0.56	8.91
Brass	8802	0.66	3.33	0.38	7.84
Ice Water	920	0.33	0.70	0.76	9.88
Lead	11340	1.07	2.65	0.23	6.68
Er0.73Pr0.27	≈9000	1.32	1.70	0.19	6.22
Nickel	8908	0.34	6.55	0.74	9.78
Solid N_2	1022	1.34	0.19	0.19	6.19

The solid nitrogen appears as the most competitive high sensible heat material, in mass and volume point of view. However, if maintained in this small volume, at room temperature, the nitrogen will be in its gaseous phase at a very high pressure (> 2000 bars). For such pressures, the technical requirements would lead to a mass of the reservoir that exceeds the mass of the solid N_2 and the advantages of using N_2 become quite questionable. Discarding this solution, the erbium-based alloys like $Er_{0.73}Pr_{0.27}$, from the volume point of view are the most interesting whereas, for the mass optimization, the ice water provides the lightest solution. The difference of water densities between the liquid and solid state being lower than 10 %, a simple volume filled at 90% of water at room temperature could provide a solution.

The ice water has already been tested to use as an ESU (called as “heat capacitor” by the authors) in a magnetically levitated vehicles (maglev) [25]. The main idea was to operate the High Temperature Superconducting magnets detached from a cooling source and without a vacuum pumping system after their cooling. The range 20 K – 50 K was assumed as the operational temperature range of this system.

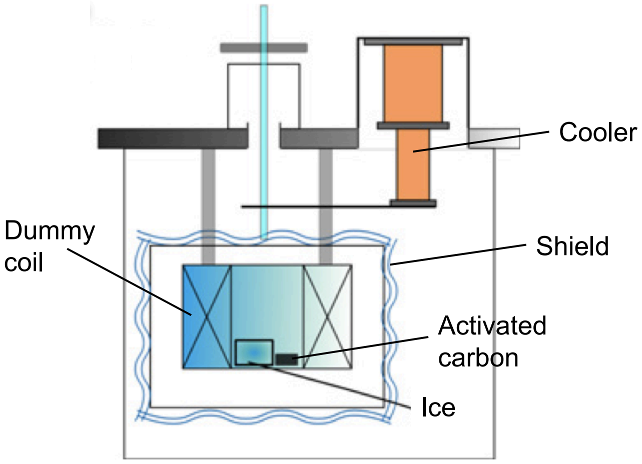

Figure 1-8 – Schematic drawing of the annex place of the ice water. Adapted from [25].

A test system was built and tested with a total amount of 1 kg of ice water being used as a heat capacitor (Figure 1-8), in the dummy coil (9.28 kg of copper to simulate the real coil) and in the radiation shield (1.86 kg of aluminium). The activated carbon attached on the dummy coil is responsible to adsorb the residual gas (during the operation no vacuum pumping system was used). After cooling the dummy coil at 20 K with a Gifford Mac Mahon cryocooler, and the shield at 50 K, the cryocooler was decoupled and turned off. The use of ice water increased in 2 hour the drift time of the dummy coil between 20 K and 50 K, for a total drift time of 8 hour. The idea is, considering scale effect, to have 1 day of cold storage in a full-scale magnet for Maglev vehicles.

The integration of such heavy or voluminous ESUs displayed in Table 1.1 can be disproportional or even incompatible in some compact cryogenic systems or small cryocoolers. Other alternative solutions, which take in account a reduction of the mass and volume at low temperature, are going to be discussed in order to be used as thermal energy storage unit.

1.2.2 Phase change materials

In the case of sensible heat based ESU, the high specific heat of the materials reduces the temperature drift as thermal energy is absorbed. But, in the case of the liquids or even solids, the absorption of thermal energy does not necessarily lead to a temperature increase. Instead of the temperature increase, a first order phase change can occur (Figure 1-9 a)). These first order phase changes are accompanied by an energy exchange, also called Latent Heat ecchange and heat absorption can occur at constant temperature. The transitions solid – vapor, solid- liquid and solid-vapor are examples of first order transitions.

The latent heat, the energy released or absorbed by a body during a phase change at constant temperature, is given by:

$$L = T\Delta S \tag{1.2}$$

The ΔS is the entropy difference between the final phase and initial phase (e.g. gas –liquid). If the process is conducted under constant pressure, the latent heat can be rewritten as function of the variation of the enthalpy (ΔH):

$$L = T\Delta S = \Delta H \tag{1.3}$$

Figure 1-9 b) gives the generalized layout of a Temperature-Enthalpy (*T*-*H*) diagram for a pure substance. This diagram provides a way to determine the amount of exchanged heat when a substance undergoes a phase change. As the latent heat is a measurement of the difference of the enthalpy between the final and initial state, the enthalpy of the different states presented in this diagram allows to realize the differences between the latent heat of the different transitions: liquid-vapor transition (green shade), the solid- vapor transition (red shade) and the solid-liquid (blue shade). The solid and liquid states present lower entropy (and enthalpy) when compared with the entropy of the vapor, which explains the higher latent heat of the S-V and L-V compared with the S-L state.

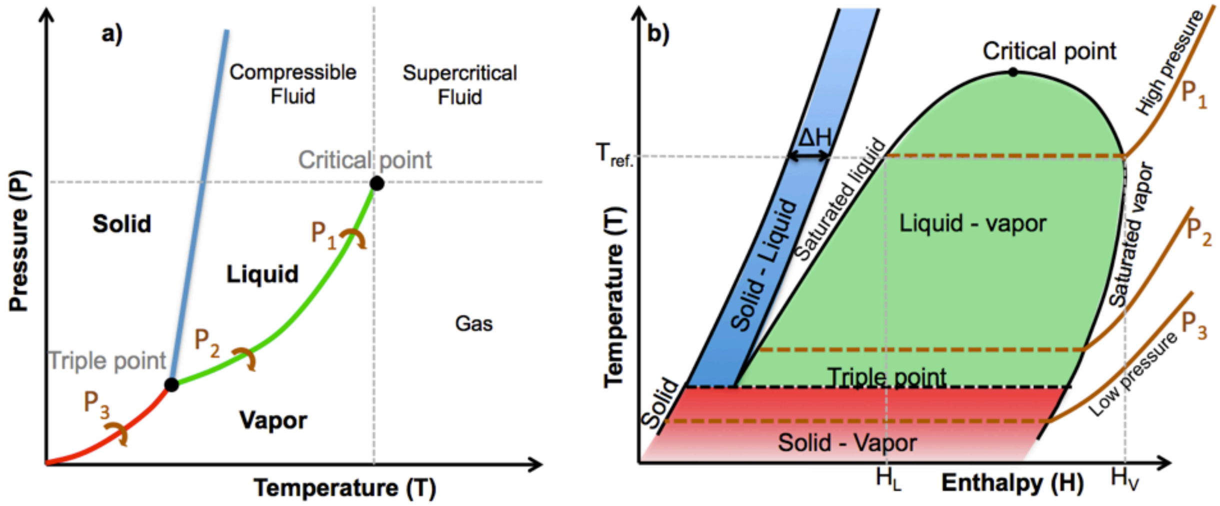

Figure 1-9 – P-T (a) and T-H (b) phase diagrams of a pure substance; Three phase changes are represented in both diagrams.

Consider the three phase changes presented in both diagrams (at constant pressure): P_1, P_2 and P_3. P_1 represents the transition between the liquid to a vapor state at T_{ref} temperature. The exchanged energy during this transition is given by the difference of the enthalpy of the final state and the enthalpy of the initial state:

$$Q_{transition} = H_V - H_L \tag{1.4}$$

the width of the green band at T_{ref} gives the energy involved in the transition. In the example at lower pressure P_2 and lower temperature (liquid- vapor transition) the length of the green zone is larger there than at the P_1 transition, i.e. the energy transferred during this transition is larger than at P_1.

Close to the critical point the liquid and vapor become indiscernible presenting similar entropy, which means that the latent heat is zero at and beyond this critical point (second order phase transition). This explains the lower latent heat involved in the transition P_1 when compared than at P_2. This reduction of the latent heat in the *S*-*V* transition close to the critical point is evidenced in annex 3 and 4.

The P_3 point is an example of solid to vapor transition (at constant pressure). In this transition (red band) the difference of enthalpies is higher than the liquid-vapor transition. This transition occurs for lower pressures and temperatures than for the triple point.

The solid to liquid transition is also available in the $T - H$ diagram and it is represented by the blue band. For example, for the temperature T_{ref}, the energy transferred during this transition is rather low when compared to the liquid-vapor transition (P_1) at the same temperature.

The energy involved in this transition is similar to a solid-liquid transition. The first energy storage units were developed based in this transition at fixed pressure and temperature[10, 26]. Typically a single closed volume filled with a pure substance composes these triple point based ESUs. In such cell, at the triple point, at fixed pressure and temperature, most of the energy absorbed by the ESU contributes to the solid melting. The other part of the energy is used to condense some of the vapor in order to maintain a constant pressure. As far as, the 3 phases coexist in the ESU this melting process occurs at constant pressure and temperature, which makes this ESU concept so attractive: it possible to store energy at constant temperature.

Two types of designs of thermal energy storage units using Phase Change Materials (PCM) are possible: single and dual volume[4] (Figure 1-10). In a single volume type all the fluid is contained in the low temperature cell that must be filled at quite high pressure to obtain a reasonable amount of liquid or solid when cooled. For instance, for nitrogen, a pressure of ≈ 3800 bars at RT would be necessary to obtain the liquid density at the triple point. Such high pressures being not safe, usually, the volume is only partially filled with liquid when cold, this means a volume for the low temperature cell significantly larger than the volume of PCM really needed. The thermal storage unit using hydrogen triple point, developed in CEA[27], storing ≈ 10 J at 14 K in a cold volume of 22.2 cm^3 is an example of a single volume ESU type.

In the dual volume configuration, the low temperature cell is connected to a room temperature storage volume (expansion volume) by a small diameter tube. Using this storage volume, the filling pressure (at room temperature) needed to obtain the cold volume 100% full is much lower than for the single volume type. Beyond safety issues, this allows the use of a thinner walled and then lighter low temperature cell.

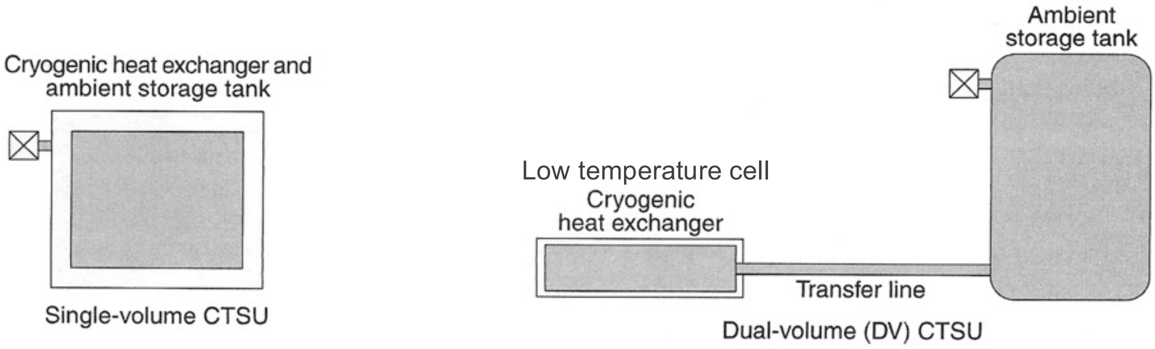

- High fill pressure
- Thick-walled heat exchanger
- Partially filled when cold
- Larger and heavier heat exchanger than for dual-volume design
- Higher parasitics than dual-volume design

- Low or high fill pressure (user selects)
- Thin- or thick-walled heat exchanger
- Fully filled when cold
- Smaller and lighter heat exchanger than for single-volume design
- Lower parasitics than single-volume design

Figure 1-10 - Single- and dual-volume CTSU (cryogenic thermal storage unit) designs; Some advantages and disadvantages of each design. Adapted from [4].

An example of the use of the dual volume concept for space applications is the ESU at 56.6 K using the Solid-Solid transition of the nitrogen trifluoride (NF_3), that uses a 16.7 liters storage tank at room temperature[28]. This system was successfully flight demonstrated in October 1998 aboard the STS-95 Shuttle mission for AFRL customer.

Different ESU using first phase transitions are described below.

Triple point energy storage unit

A nitrogen triple-point thermal storage unit was developed in the Netherlands by A.P. Rijpma et al. [18]. The idea was to use a cryocooler to cool down a SQUID (superconducting quantum interference devices), which are highly sensitive magnetic field sensors, to monitor fatal heart signals. To reduce the magnetic and mechanical interferences from the cooler, they intend to switch it off during the measurements. To maintain the system cold when the cryocooler is OFF, an energy storage unit based on the triple-point of the nitrogen (63.15 K) is used providing a good temperature stability during the measurements. A phase diagram of nitrogen is available on Annex 1.

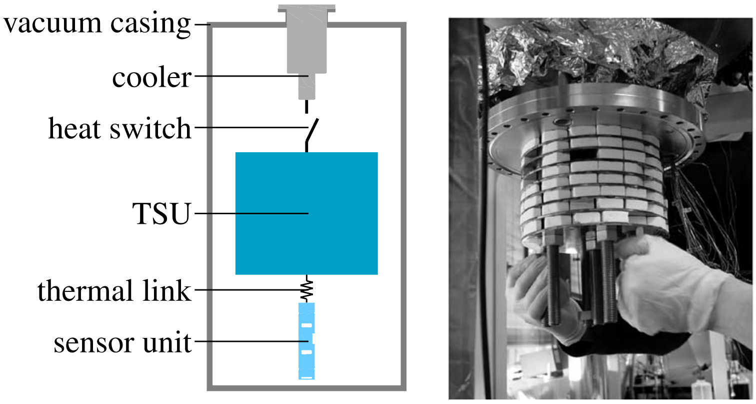

Figure 1-11 - a) Schematic view of a cryocooler system and TSU; b) picture of the TSU with the copper disks and the blocks of porous materials[18].

The triple point N_2 thermal storage unit was sized to be operational for a full working day (≈10 h) with an estimated heat load from the sensor unit of about 1.5 W (54 kJ). The TSU is connected to the second stage of a Gifford Mac Mahon cryocooler through a heat switch. The heat switch is used to allow the decoupling of the TSU from the cryocooler during the measurements. The sensor unit is connected to the TSU by a thermal link (Figure 1-11 a). To establish a good thermal contact between the casing of the TSU and the nitrogen, a structure with layers of copper and porous material (highly porous alumina) was used.

During the measurements only nine layers of porous material were used, as shown in the Figure 1-11 b) and some blocks of porous material were left out. With this configuration the capacity the TSU should be 30 kJ (8.3 Wh). To avoid elevated pressures inside the system at room temperature, the solid nitrogen compartment was connected by a tube at room temperature to drain the excess fluid. The experimental results show that the capacity of the system was around 85% of the expected 30 kJ. This reduction of the capacity was attributed to a lack of nitrogen during the filling process. To achieve the total capacity of 54 kJ with a stable temperature all of the copper layers and porous material need to be incorporated and an improvement in the filling procedure needs to be done [18].

Liquid energy storage unit

In our laboratory, in the framework of a ESA project, the latent heat of the liquid to vapor transition of the nitrogen was used to develop an energy storage unit in the temperature range 60-80 K[9]. A temporary cold source if the cryocooler is stopped or a thermal buffer to attenuate temperature fluctuations due to heat bursts are the main objectives of this liquid nitrogen ESU. This work was developed during J. Afonso's master and PhD thesis [29] in our group.

In this system, contrarily to the system described in the previous section, the nitrogen was used in a closed cycle along its saturation curve then a storage reservoir for the nitrogen vapour is needed and a pressure and temperature increase are the results of the evaporation process. Compared to the liquid volume, a very large volume would be required to attenuate the pressure/temperature increase. To avoid the use of a heavy and large volume at low temperature an expansion volume at room temperature was used leading to a configuration similar to the dual volume solution. In the low temperature side was used a small cell (ESU) connected to the expansion volume at room temperature (RT) as shown in Figure 1-12 a). The evaporated nitrogen expands to this RT volume limiting the ESU temperature increase. The low temperature cell is connected to the cryocooler through a thermal switch that allows the thermal coupling or decoupling of the cell from the cryocooler. This switch enables the ESU operation in a free vibration environment: is possible to turn off the cryocooler during the ESU operation avoiding the vibrations inherent to the cryocooler working. By thermal decoupling the cell from the cryocooler is provided a thermal insolation from the sudden cryocooler temperature increase when it is OFF.

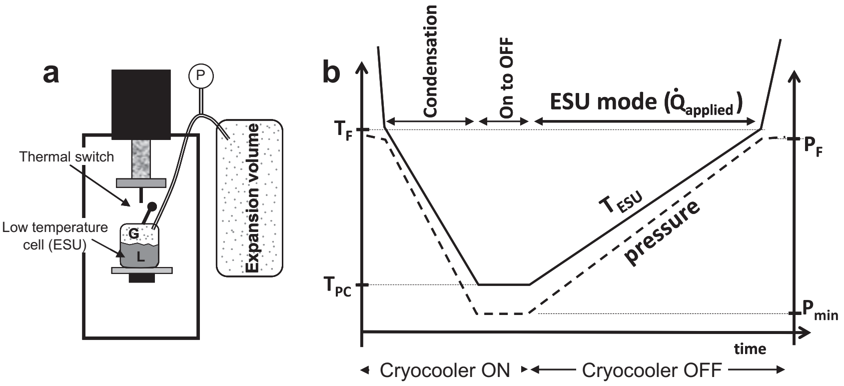

Figure 1-12 - Scheme of the nitrogen liquid ESU set-up (a) and of timing operation (b)[9].

At the beginning (pre-cooling phase), the ESU is cooled down with the thermal switch in its high conductance state (ON state). During this pre-cooling phase, below a certain temperature T_F, the nitrogen starts to condense inside of the ESU. When it is full of liquid (T_{PC}), the switch is toggled to its low conductance state (OFF state) and the ESU is ready to store energy. The last phase ("ESU Mode") starts when the sensors are turned OFF and start to dissipate power: thanks to the high enthalpy of the liquid to vapor transition, the power dissipated by the sensors is absorbed without rapid temperature increase. During this ESU mode, due to the stopping of the cryocooler, a time limited cold source without vibrations is available.

During the evaporation (ESU mode), the pressure and temperature in the ESU are interconnected due to the coexistence of the two phases in equilibrium (Figure 1-12 b)). By limiting the increase of the pressure it is possible to decrease the temperature drift: then a large expansion volume will limit the pressure increase and consequently the temperature drift during the ESU mode. An extreme case is an infinite expansion volume that leads to evaporation at constant pressure and temperature. Also we will see later that the capacity of the expansion volume is going to be determinant for determining other parameters for the ESU.

Figure 1-13 shows results of a typical temperature drift during an ESU mode. In this experiment a 6 L expansion volume filled with 1.95 bar of nitrogen was used. Assuming that the liquid and vapor are in equilibrium the liquid temperature was obtained by the cell pressure measurement. At beginning, at t≈0, the cold finger and the ESU temperature (pre-cooling temperature) were ≈ 65 K. At this time, when the ESU was almost full of liquid, the switch was toggled to the OFF state and a heating power of 1 W was applied in the ESU (blue and green lines) and cold finger temperature (red line) was swept at a rate of 0.8 K/min to simulate the natural warming of the cryocooler cold finger after stopping. After ≈ 62 min the temperature stabilization of the liquid temperature (black line) and the sudden rate increasing of the ESU temperatures indicate that all the liquid evaporated: no more heat is absorbed by the latent heat. The stable pressure obtained once the liquid finished is explained by the end of the coexistence of the 2 phases in equilibrium and the liquid temperature has no further meaning.

During this ESU mode the whole system absorbed 3720 J with ≈ 19 K of temperature drift (65 K – 84 K).

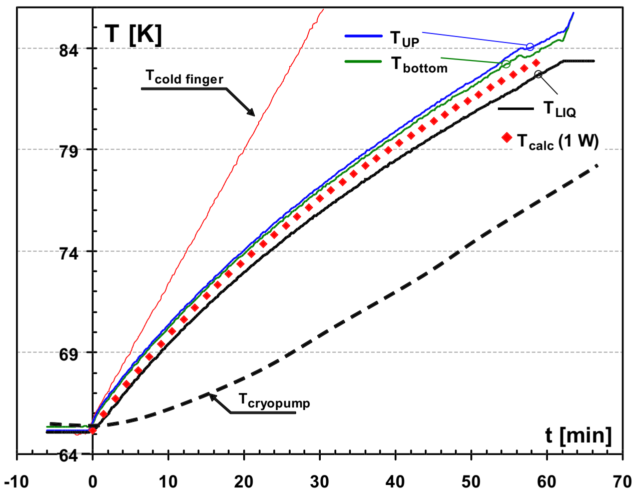

Figure 1-13 - Typical temperature drifts for an ESU mode (1W applied), using 6 L expansion volume[9].

In this work, another experiment was performed absorbing more or less the same energy (3900 J) within a reduced temperature drift of only 5 K (76 K - 81 K): To reduce this drift a bigger expansion volume was used, 24 L instead of 6 L.

A constant temperature and pressure during the evaporation of the nitrogen, like in a triple-point transition, was also successfully demonstrated in this work. As the liquid and vapour coexist in equilibrium inside of the cell, by controlling the pressure inside the cell using a pressure control valve it is possible to maintain a stable temperature/pressure inside of it, as in Figure 1-14. This working principle was also used in the present work with neon and a detailed explanation is presented later.

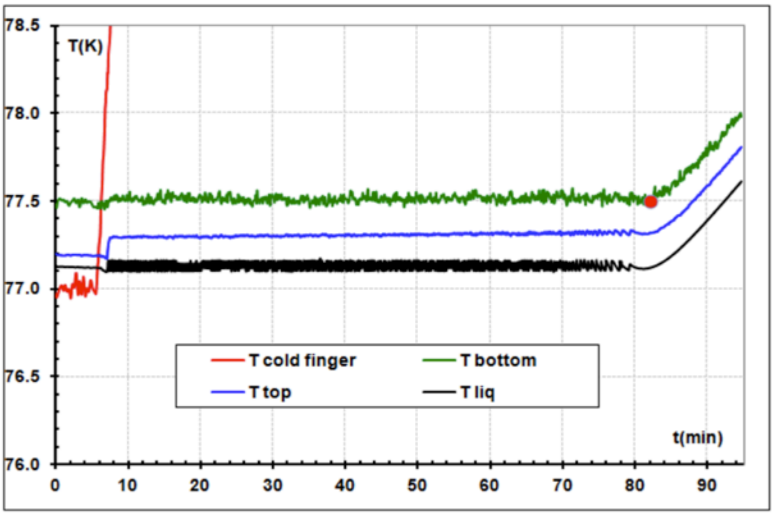

Figure 1-14 – Temperature control at 77.1 K using a 24 liter expansion volume, with filling pressure of 1.25 bar. 0.5 W of applied power in the ESU

In the example of Figure 1-14 the control temperature was 77.1 K, corresponding to a pressure controlled at ≈ 1 bar. When the evaporation process is running, the evaporated gas is stored in the expansion volume. When the pressure inside of the cell equals the pressure of the expansion volume the valve can no longer control the pressure and the ESU control mode is finished. In this example the temperature control mode finished at ≈ 80 min.

The advantage of using the triple point transitions is the constant temperature during the energy storage phase. With this ESU mode, it is possible also to store energy at constant temperature. Below 100 K only few triple-points are available. Using the liquid ESU in the temperature controlled mode a much larger range of temperatures is covered. The higher latent heat of the liquid to gas transitions when compared to the triple point transitions turn this mode into a promising solution to obtain a constant temperature ESU.

Stored solid cryogen systems

The high latent heat of the solid to vapor (sublimation) transition and the absence of problems with fluid management in microgravity, make the frozen state an attractive way to store cryogens to cool detectors in space. The operating range of this concept is below the triple point temperature/pressure along the sublimation line (red line in Figure 1-9 a). The temperature is then dependent of the vapor pressure achieved. For example in the case of nitrogen, the triple point temperature and pressure are 63 K and 125 mbar. By pumping down to 0.1 mbar the temperature of 43 K is achieved. In the case of hydrogen, the triple point at 14 K and 74 mbar, by pumping down to 0.1 mbar the temperature of 8 K can be achieved. To maintain these small pressures, a vent line to the space vacuum is used (Figure 1-15)[4].

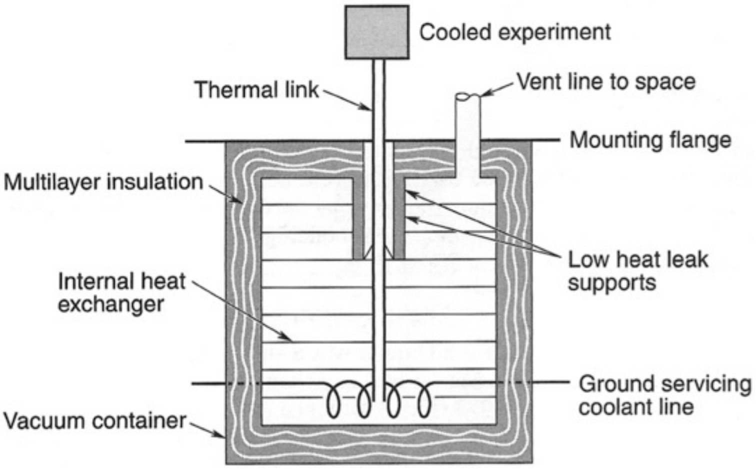

Figure 1-15 - solid cooler design concepts[4]

The solid cooler can be designed to obtain a specific temperature, which requires the exhaust vapour to be maintained at a constant pressure. The use of this concept in a closed cycle, using an expansion volume to re-use the sublimated gas instead of pumping it is not suitable due to large $\partial P/\partial T$ along the sublimation line. For example, in the case of nitrogen, the *P*-*T* diagram (Annex1) for nitrogen indicates that a small increase of the pressure on the sublimation line induces a large temperature increase that becomes incompatible with most of the stability requirements.

Solid to solid transition of nitrogen 35 K

A change in a crystalline structure of the nitrogen at 35.6 K is also attractive to be used in an energy storage unit. This phase change corresponds also to a triple point (two solid phases in equilibrium to the gas) then a possibility for temperature stability. The latent heat associated to this solid – solid transition of nitrogen is 9 J/cm^3.

A dual-volume (DV) cryogenic thermal storage unit (CTSU) was developed by Bugby[26] based on this solid-solid transition of nitrogen, to enable the duty-cycle of temperature sensitive cryogenic devices at 35 K. The idea is to reduce the cryocooler cooling power without sacrificing the temperature stability of the cryogenic devices. The CTSU – heat exchanger (CTSU-HX) is placed between the 35 K cooler and the cryogenic component (Figure 1-16 a)). To store the nitrogen and avoid very large pressures when all the system is at room temperature, a 23 litres storage tank, located at room temperature, is connected to the CTSU-HX.

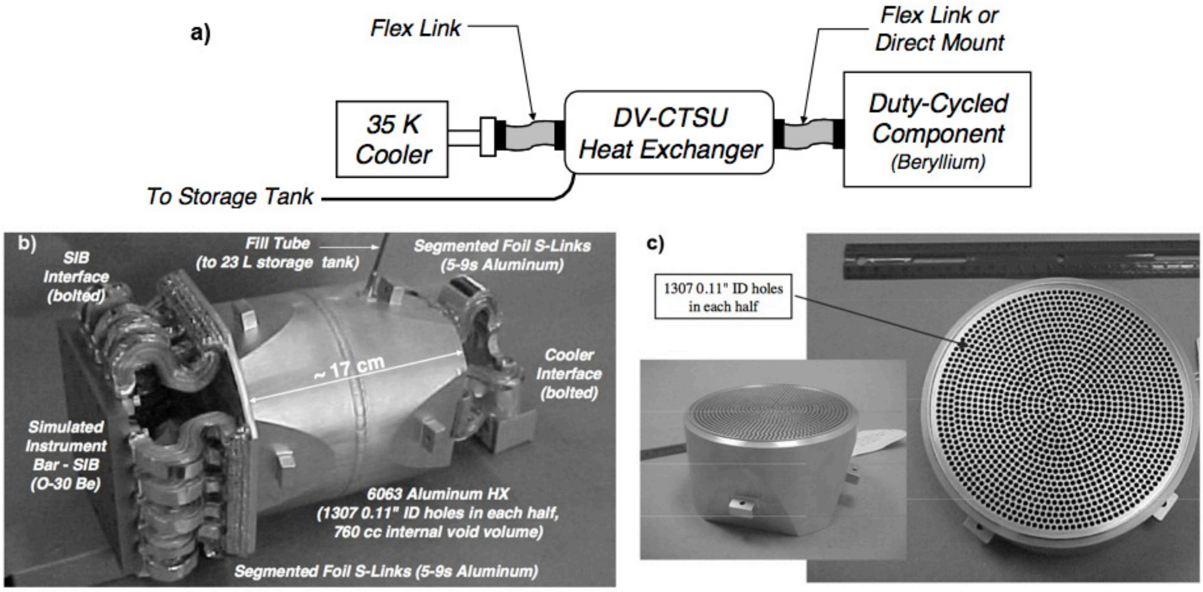

Figure 1-16 – a) Conceptual Diagram of the 35 K dual-volume cryogenic thermal storage unit; b) Design of the 35 K CTSU –HX details; c) The 2 drilled-hole aluminium halves of the heat exchanger; adapted from [26]

Figure 1-16 b) shows the design of the 35 K CTSU-HX. The heat exchanger is formed by welding together two drilled-hole aluminium halves (Figure 1-16 c)). The void volume of the CTSU-HX to fill with nitrogen is 760 cm^3, to store 5600 J. The working pressure at 35 K is ≈ 3 mbar, and using a 23 litres storage tank, the filling pressure at room temperature is ≈ 23 bar. The total mass of the CTSU-HX is 6 kg.

The CTSU is going to be responsible to intercept and store the excess heating from the components when it is ON and is cooled thanks to the excess cooling of the 35 K cooler. Due to this configuration, beyond the high heat capacity, the CTSU-HX should have also a high thermal conductance.

Using a cryocooler with 1.5 W of cooling capacity the duty-cycle component has been subjected to a heat load profile: square-wave with a peak of 3.7 W during 27 minutes and a minimum of 0.7 W for 73 minutes. The temperature stability of this component was better than the 0.01 K/min required, during the tests.

1.2.3 Storing solution at 40 K

The main objective of this present work is to store around 1000 J with a small temperature drift at around 40 K using a low mass and low volume at low temperature device. In the former sections, some possibilities to integrate high specific heat materials and phase change materials in an energy storage unit are presented.

Table 1.1 presented the comparison between some high specific heat materials in the 40 K range. The mass and volume for each material to store 1000 J with a temperature drift between 38 K and 42 K was calculated. The erbium based alloys present the larger volumetric specific heat (1.3

J/(cm^{3}K)). The low density of the ice water (compared with the alloys) turns its massic specific heat very competitive when compared to the metal alloys.

However, the latent heat of some phase transitions of cryogenic fluids presents the lightest solutions to integrate an energy storage unit. The Figure 1-17 gives the comparison between the latent heat associated to the liquid-gas transition, the triple-point and the solid-solid transition for substances below 100 K. Unfortunately, in the 40 K range, no triple points are available, then taking advantage of a constant temperature and pressure would be only possible by using the solid-solid transition of nitrogen at 35.16 K, the associated latent heat being only 9 J/cm^3.

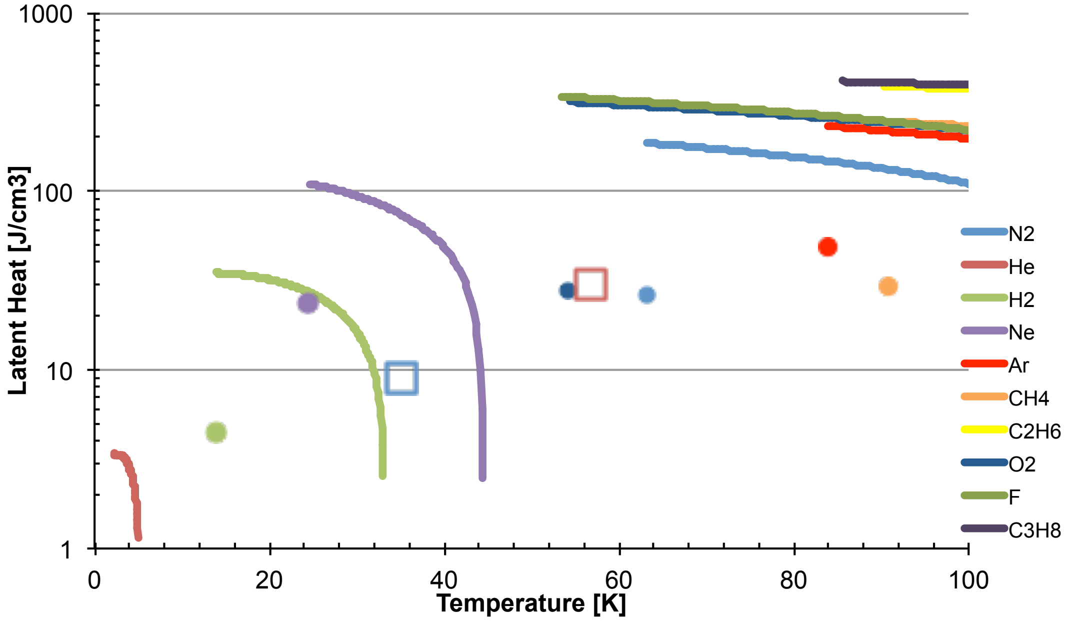

Figure 1-17 - latent heat for phase transitions below 100 K; the lines represent the liquid – gas transition; the circles are the triple-points; the solid-solid transitions are represented by the squared symbols.

Looking at the liquid-gas transitions in this range the only available substance at 40 K is the liquid neon. The associated latent heat at the 35.16 K is 73 J/cm^3, ≈8 times larger than the S-S transition of nitrogen. In other words, at this temperature 13.7 cm^3 of liquid neon are enough to store 1000 J compared with the 111 cm^3 of the solid nitrogen. The smaller volume at lower temperature is another advantage of the use of liquid neon. Moreover, the range of the operation of the neon is not limited of one temperature discrete point. On the other hand, the stable temperature during the S-S N_2 transition can be very interesting for some applications whereas the temperature drift of the liquid-gas transition would be dependent of the expansion volume size.

Back to our objective, to store around 1000 J at 40 K using a device with a cold volume as light and small as possible, an ESU based on the liquid to vapor transition of the neon appears as a promising solution. Table 1.2 gives the comparison between some viable solutions for the 40 K ESU.

A voluminous or heavy ESU, using the sensible heat of ice water or $Er_{0.73}Pr_{0.27}$ can be incompatible or disproportional with the small cryocoolers that work in this range. In those solutions the only way to reduce the temperature drift is by increasing the amount of the high specific heat substance in the ESU.

Table 1.2 –Comparison between some solutions to integrate a 40 K ESU to store 1000J.

Concept	Substance	Heat @40K	Cold vol.(cm³)	Mass (g)	T range (K)	T drift (K)
PCM S-S	nitrogen	9 J/cm³@35 K	111	≈109	35.2 K	Constant T.
PCM L-G	neon	50 J/cm³	20	19	25 K – 44 K	*
Sensible heat	Ice water	0.33 J/cm³K	760	700	< 273 K	4
Sensible heat	$Er_{0.73}Pr_{0.27}$	1.32 J/cm³K	190	1700	No limit	4

*The T drift in this case is dependent of the expansion volume size.

The constant temperature and pressure during the transition in the crystalline structure of the N_2 at 35.2 K could be attractive. In this solution it is possible to use the single volume configuration of an ESU. However, the use of a single volume configuration requires a significant larger cold volume than the volume of solid nitrogen necessary and a thick-walled volume is needed for standing the high pressures at room temperature, turning the cold volume heavy and voluminous.

Like in the work of the liquid nitrogen ESU a constant temperature during the transition L-V of neon can be obtained. By controlling the pressure inside of the cold volume it is possible to obtain a constant temperature during the evaporation of the liquid, like in the triple-point. The triple-point and the S-S transition represent only some discrete temperature points (Figure 1-17). Using a liquid to gas transition turns a wide range of temperatures available, even working in the temperature-controlled mode. Besides the temperature tuning capability, the cold size can be reduced when compared to a triple point solution, as the liquid-vapor latent heat is larger than that of the triple-point and S-S transitions.

To limit the temperature increase, the dual volume configuration in an ESU using the liquid to gas transitions of the neon is required. But at room temperature the volume constraints are much less drastic than at cold temperature. Even in the ESU using the triple point, due to the reasons previously discussed, a large volume at room temperature is common in this kind of devices.

After the comparison with other possibilities to store energy in the 40 K range, while aiming the lightest volume at low temperature, the transition liquid-vapor of the neon was chosen.

2 Liquid neon energy storage unit

This chapter describes the working principle and the different configurations tested with the energy storage unit using the latent heat of the liquid neon as storage medium. A pre-dimensioning tool was created to help dimensioning the cold volume and the expansion volume. This software is based on a thermal model and allows the user to simulate the different ESU operational modes.

As the target application of this system is the integration in a satellite, some problems are associated to the microgravity environment: the way used to solve this issue is described.

2.1 Working principle

The large latent heat of the neon liquid to vapor transition at 40 K range was chosen to provide a temporary cold source to be used after stopping the cryocooler allowing a vibration-free environment. In this case, a thermal decoupling of the energy storage unit from the turned OFF cryocooler is required to avoid that the natural warming of the cold finger sends a high heat load on the ESU. The energy dissipated by a sensor array will be absorbed by the liquid neon evaporation, limiting its temperature after stopping the cryocooler.

On another hand, a thermal energy storage unit can also be directly coupled to the cold source, allowing a temporary increase of its cooling power. In the case of using sensor arrays for short time events, this mode allows the use of a low power consumption cryocooler instead of over dimensioning it just for taking care of sporadic peaks (*Power booster mode*). This operation mode was used by Bugby at 35 K [26], and was already described in the last chapter (Section 1.2.2).

The ESU tested during this work can operate in three different configurations: the *Temperature drift mode;* the *Temperature controlled mode* and the *Power booster mode*. The first two configurations are developed to operate in a vibration-free environment.

ESU Temperature drift mode

In this mode the ESU actuates as a temporary cold source while the cryocooler is stopped, to allow the sensors to work in a vibration-free environment.

Figure 2-1 schematizes the integration of the liquid neon energy storage unit in a cryogenic system to cool a 40 K range sensor. The enthalpy reservoir is used as a thermal buffer being connected to the cold finger of a cryocooler through a gas gap heat switch to allow the thermal decoupling of the enthalpy reservoir from the cryocooler. When the cryocooler is turned OFF the switch will thermally isolate the ESU from the temperature increase of the cryocooler. A heater is connected to the enthalpy reservoir to simulate the heat load dissipated by the 40 K sensor. To limit the pressure increase inside the enthalpy reservoir during the evaporation of the liquid neon, an expansion volume at room temperature with few liters of capacity is used to expand the evaporated vapor. As already mentioned, because the liquid and the vapor coexist in thermodynamic equilibrium inside of the cell, the existence of this large volume limits the temperature increase. The two volumes are permanently connected, in other words the pressure is similar (except for pressure drops) in both volumes.

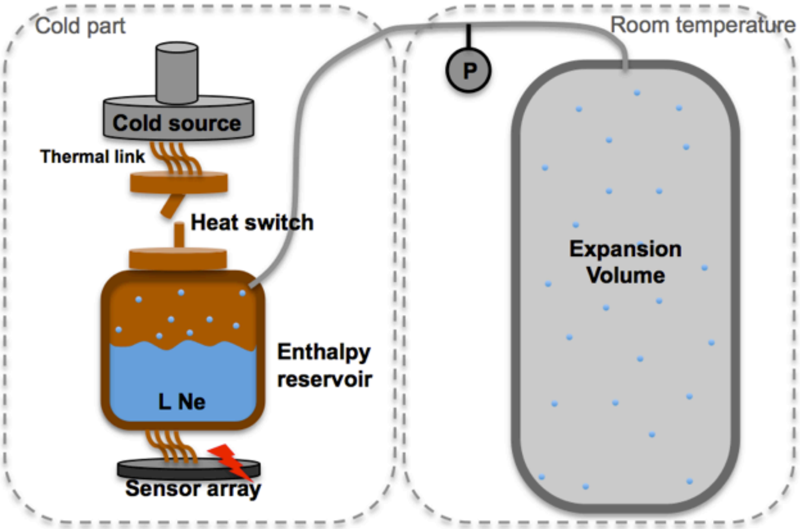

Figure 2-1 - Scheme of the liquid neon energy storage unit as *Temperature drift mode ESU*.

At the beginning, when the cryocooler and the enthalpy reservoir are at room temperature, the system (enthalpy reservoir + expansion volume) is filled with neon gas. The cryocooler is turned ON and the gas gap heat switch is toggled ON (high thermal conductance state) to allow the enthalpy reservoir cooling. During this cooling, the density of the gas increases in the cell leading to a small pressure decrease (phase 1 of Figure 2-2). When the temperature of the enthalpy reservoir is equal to the saturation temperature for the pressure of the system, the neon starts to condense (phase 2) and the liquid quantity begins to increase. The enthalpy reservoir and the expansion volumes are pre-dimensioned according with the minimum temperature requirement (precooling temperature) in order to maximize the liquid quantity at this temperature. Achieved this temperature, the heat switch is toggled OFF and the cryocooler may be turned OFF in order to provide a vibration-free environment. At this time the ESU is ready to operate and the phase 3 (Temperature drift ESU mode) starts when the heat load is applied. A direct consequence of this heat load is the neon evaporation, increasing the pressure and temperature of the ESU. During this phase, the temperature increase is attenuated thanks to the absorption of the latent heat of the liquid to vapor transition of the neon.

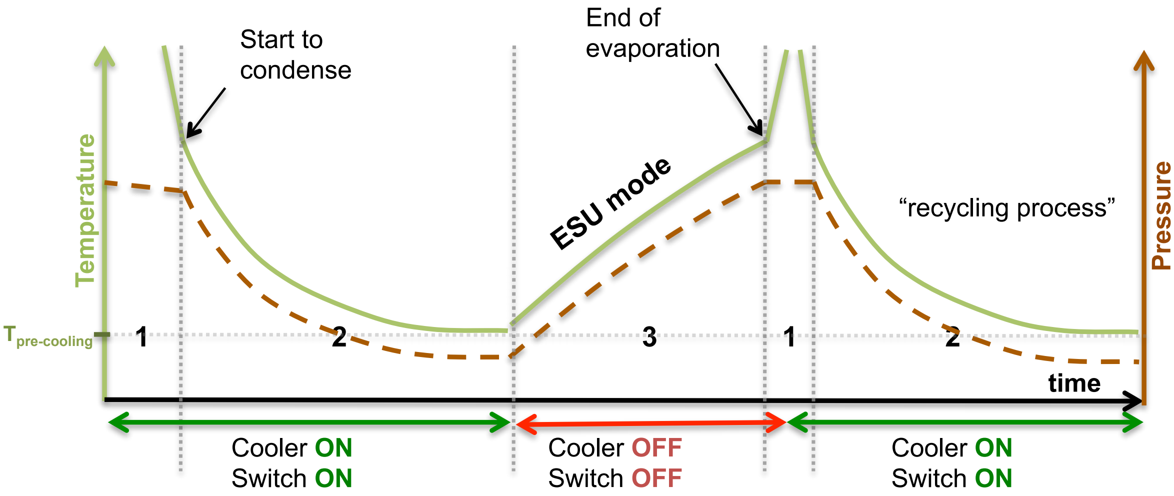

Figure 2-2 – Representation of the evolution of the pressure and temperature of the ESU during the different phases of *Temperature drift mode.*

When the low temperature cell is "empty" of liquid (phase 1), the ESU mode vanishes and the temperature of the enthalpy reservoir increases faster, as no more latent heat is available. At this time, it is necessary to turn ON the cryocooler and toggle the switch to the ON state to recycle the ESU (phase 2). The initial filling pressure determines the final temperature of the ESU mode, i.e. the temperature at which the evaporation finishes. To obtain a final temperature of 40 K, according to the annex 2 (the liquid-vapor saturation diagram of neon), the filling pressure should be 14.6 bar.

ESU Temperature controlled mode

Working at a constant temperature, like in a triple point transition, in a vibration-free environment is possible with this temperature controlled configuration. As a matter of fact, as far as the liquid and vapor coexist, to obtain a constant temperature during the evaporation of the fluid it is necessary to maintain a constant pressure inside of the enthalpy reservoir. This is possible introducing a pressure control valve at room temperature between the enthalpy reservoir and the expansion volume (Figure 2-3), and maintaining the configuration of the cold part (the same as in Figure 2-1). This operation mode was demonstrated by J. Afonso [29], using the liquid to vapor transition of the nitrogen at 80 K range.

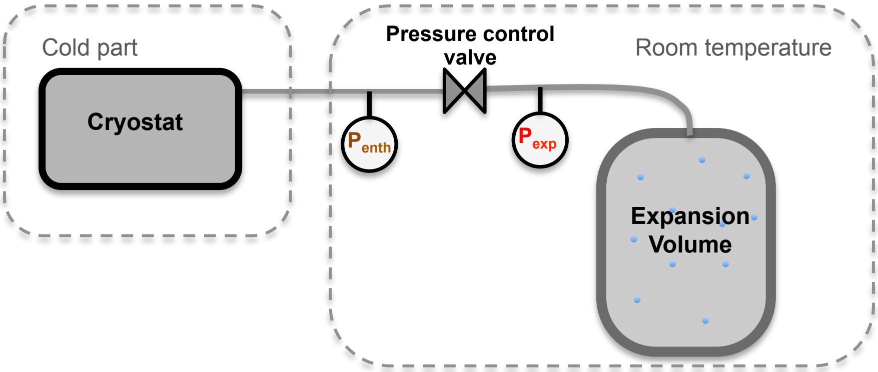

Figure 2-3 - Scheme of the liquid neon energy storage unit as *Temperature controlled mode ESU*. The same configuration at the cold part of the *Temperature drift mode ESU* is used in this controlled mode (Figure 2-1).

As in the previous mode, at the beginning it is necessary to fill the system with neon gas. In phase 1 and 2, of Figure 2-4, the cryocooler and switch are maintained in the ON state. During these two phases the pressure control valve is maintained completely opened, which results in an equal pressure in the enthalpy reservoir and in the expansion volume ($P_{\text{expansion volume}}$ = $P_{\text{enthalpy reservoir}}$).

Similarly to the previous ESU mode, the system is sized to maximize the liquid quantity at the pre-cooling temperature. Once the pre-cooling temperature achieved, the pressure control valve is closed. At this time the cryocooler and the heat switch may be turned OFF and is necessary to heat the ESU from the pre-cooling temperature up to the control temperature (phase 3 in fig 2-4). With the valve closed and a heated up ESU, all the evaporated neon remains inside of the cell, which results in a quick pressure/temperature increase as observed in figure 2-4 (phase 3). At the end of phase 3, the pressure in the expansion volume is lower than the pressure existing in the cell and the expansion volume will act as a gas buffer. Before the ESU mode (phase 4) the pressure controlled valve is set to control at a setpoint of pressure or temperature. According to the saturation diagram (annex 2) to control at 40 K, the control pressure setpoint is 14.6 bar.

The ESU mode (phase 4) starts when the heat load is applied and at this time the valve is actuated using a feedback ON-OFF control to obtain a constant pressure inside of the enthalpy reservoir, expanding the evaporated neon for the expansion volume at a lower pressure. This expansion process results in an expansion volume pressure increase. As the liquid is available in the enthalpy reservoir and its pressure is higher than the pressure in the expansion volume, a stable temperature is obtained while the heat load is applied. When the pressure in the expansion volume achieves the setpoint pressure the valve can no longer control the pressure in the enthalpy reservoir and the ESU temperature controlled mode stops. If at this time some liquid remains in the reservoir and the heat load continues to be applied, the valve continues open (because the $P_{\text{enthalpy reservoir}}$ is higher than setpoint) and the temperature continues to increase like in the *ESU temperature drift mode* (phase 5).

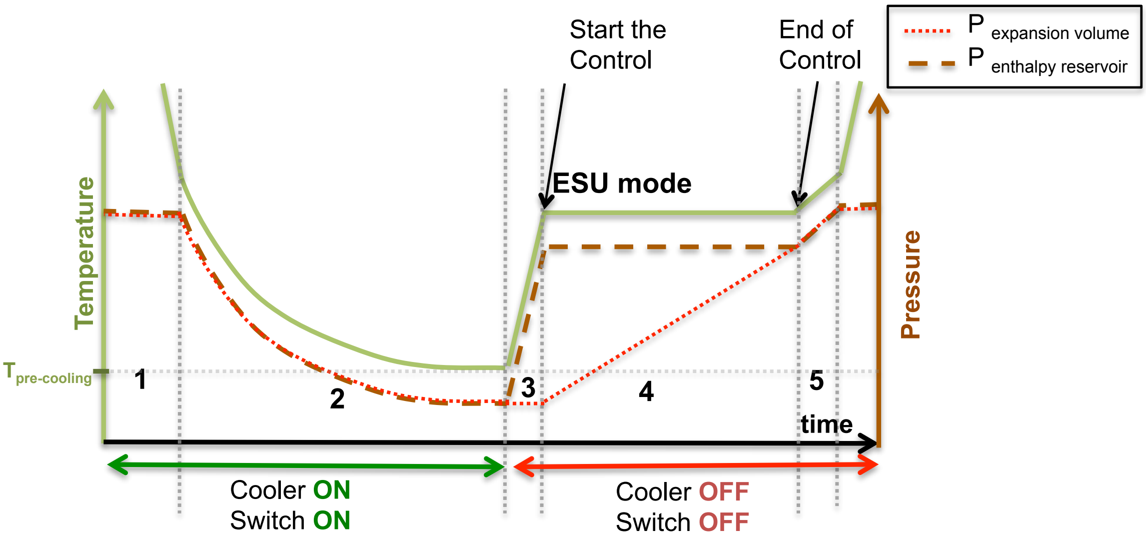

Figure 2-4 – Representation of the evolution of the pressure and temperature of the ESU during the different phases of *Temperature controlled mode.*

When the liquid runs out, the ESU temperature increases very quickly, becoming necessary to “recycle” the system.

With this controlled mode, the heat is absorbed at constant temperature like in a triple-point ESU but it takes advantage of the high latent heat of the liquid to vapor transition instead of solid to liquid one in closed triple point cell.

ESU Power booster mode

With the increase of the array size of infrared sensors for an improved resolution, more cooling power is required. In case of using such arrays only for short time events, a thermal energy storage unit directly coupled to the cold source allows to temporarily boost its cooling power, allowing the use of a low power consumption cryocooler. As described in section 1.2.2, this concept was developed by Bugby[26] to reduce the cooling capacity needed without sacrificing the temperature stability of temperature sensitive cryogenic devices during its duty-cycle.

Even in cases of low dissipated power sensors, such configuration can also be used as a temperature stabilizer.

This configuration consists of an enthalpy reservoir directly coupled to the cold finger of the cryocooler to absorb the heat bursts of a sensor array (Figure 2-5), limiting the increase of the cold finger's temperature. In this mode the cryocooler is permanently working. A good thermalization between the components (cryocooler, enthalpy reservoir and sensor array) is fundamental in this operation mode.

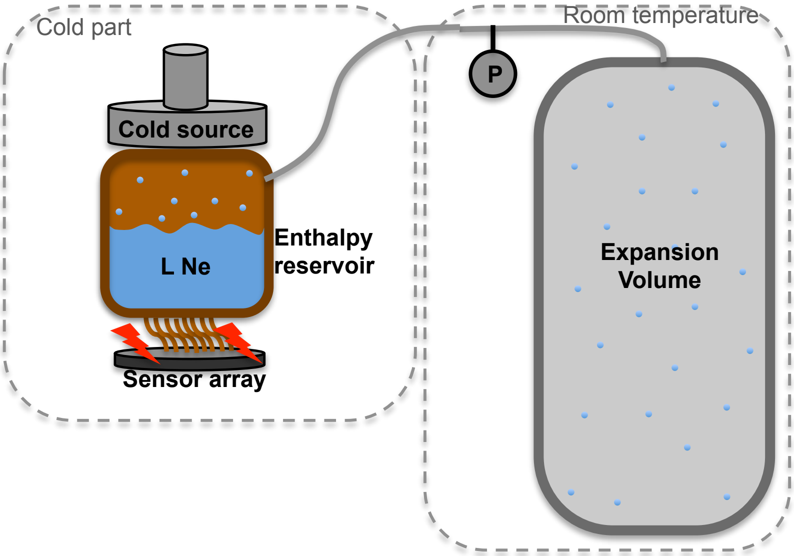

Figure 2-5 - Scheme of the liquid neon energy storage unit as *Power booster mode ESU*. In this case the enthalpy reservoir is directly connected to the cold finger of the cryocooler.

In Figure 2-6 the evolution of the ESU's temperature using a *Power booster mode* when a heat profile is applied is schematized. Like in the other ESU modes, the first phase is the pre-cooling phase. When the low temperature cell is cold, with the cryocooler in continuous operation, the sensor array can start to operate (phase 2). For a short time, some heat power higher than the cooling capacity of the cryocooler is dissipated on the ESU. In these transitory events, the high latent heat of the liquid to vapor transition of the neon compensates the higher heat load. When the heat load becomes smaller than the cooling capacity of the cryocooler the ESU (phase 3) is going to re-cool in a recycling phase. During this process, if the temperature crosses the T_{limit} (no more liquid neon available) it results in a quick temperature increase of the system.

According to the heat load profile of a particular sensor array and the cooler characteristics, the dimensioning of the available energy storage (amount of liquid neon) is possible so the device may run in a cyclic process reducing the cryocooler in power consumption without sacrificing the sensor temperature stability.

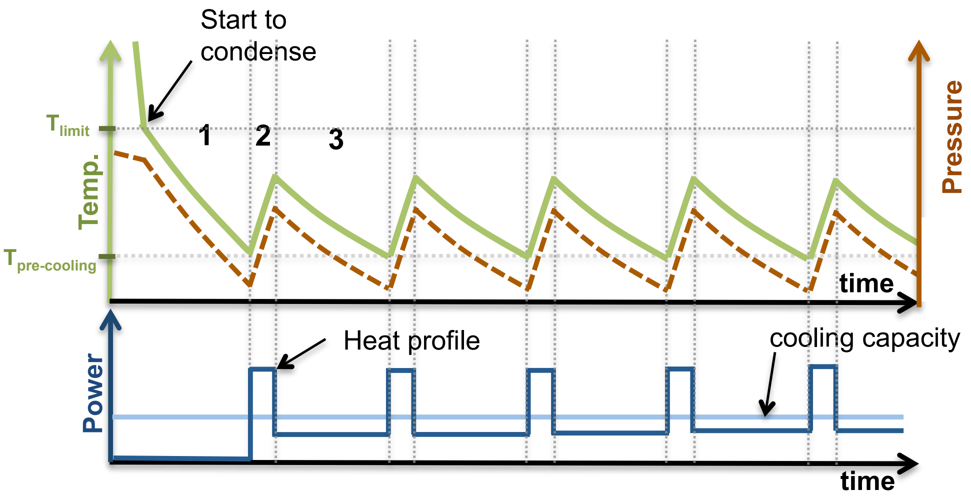

Figure 2-6 - Schematic of the evolution of the pressure and temperature when a heat profile is applied. The green line represents the temperature of the ESU, the cryocooler and the sensor array.

2.2 Thermal model

The development of a thermal model is fundamental for a predimensionning of the energy storage unit. Scaling the expansion volume and the enthalpy reservoir, to store the required energy within a temperature drift, is possible using this model.

In a liquid energy storage unit, when energy is provided to the liquid, a part will evaporate. This evaporation is going to result in a increase of the pressure, and consequently in an increase of the temperature. With this thermal model it is intended to quantify the evaporated amount for a provided energy and the resulting system temperature increase for a given expansion volume. Thermodynamics for open system will be used in the next section to solve to this problem.

2.2.1 Calculation of the energy stored entre T e T+DT in the ESU drift mode

In Figure 2-7 the enthalpy reservoir is represented schematizing our low temperature cell in which liquid and vapor coexist. When a heat power is applied in the system, some particles evaporate from the cell and go to an expansion volume at room temperature. Due to the exit or entrance of matter, our low temperature reservoir (Fig. 2.7 left) must be considered as an open system.. By using a imaginary piston moving in order to enclose the “evaporated particles”, we can define this new volume (volume limited by the red dashed line) as closed (control volume technique).

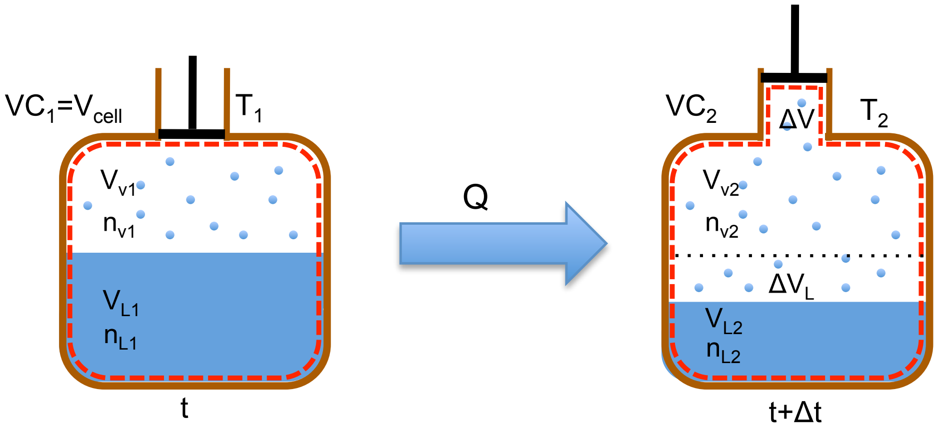

Figure 2-7 – Control Volume evolution in the enthalpy reservoir during the evaporation.

Considering our control volume, in a given instant Δt, the total number of moles of the system ($n_{VC,1}=n_{VC,2}$) is maintained. Applying the first law of thermodynamics:

$$Q=\Delta U-W \tag{2.1}$$

For an amount of heat Q received by our control volume, part of this energy is converted in work ($W=-P_2\Delta V$) done by the imaginary piston and the other part translates into an internal energy variation ΔU. We can write the $\Delta U=U_{VC,2}-U_{VC,1}$ where:

$$U_{VC,1}=U_{VC,1}\left(T_1,P_1\right)=n_{v1}u_v\left(T_1,P_1\right)+n_{l1}u_l\left(T_1,P_1\right) \tag{2.2}$$

$$U_{VC,2}=U_{VC,1}\left(T_2,P_2\right)+U_{\Delta V}\left(T_2,P_2\right)=n_{V2}u_V\left(T_2,P_2\right)+n_{V\Delta V}u_V\left(T_2,P_2\right)+n_{L2}u_L\left(T_2,P_2\right) \tag{2.3}$$

Where the n_v and n_L are the number of moles of the vapor and liquid, respectively. Considering $\Delta V=(V_{V2}-V_{V1})-(V_{L2}-V_{L1})=\Delta V_V-\Delta V_L$, and using the Eq. 2.1:

$$\begin{aligned}Q&=U_{VC,2}\left(T_2,P_2\right)-U_{VC,1}\left(T_1,P_1\right)+P_2\Delta V\\ Q&=U_{VC,1}\left(T_2,P_2\right)-U_{VC,1}\left(T_1,P_1\right)+U_{\Delta V}\left(T_2,P_2\right)+P_2\Delta V\end{aligned} \tag{2.4}$$

The enthalpy of a system is given by the $H=U+PV$ then the previous equation becomes:

$$Q=U_{VC,1}\left(T_2,P_2\right)-U_{VC,1}\left(T_1,P_1\right)+H_{\Delta V}\left(T_2,P_2\right)=\Delta U_V+H_{\Delta V} \tag{2.5}$$

Where $H_{\Delta V}$ represents the enthalpy of the gas in ΔV, i.e. exiting the cell:

$$H_{\Delta V}\left(T_2,P_2\right)=h_g\left(T_2,P_2\right)\Delta n \tag{2.6}$$

Δn represents the evacuated number of moles of the reservoir. The coexistence of the liquid and vapour inside of the reservoir set the system to a saturation situation.

During the heating, the vapor that leaves the enthalpy reservoir is expanded to the expansion volume at room temperature. In another words, in an instant Δt, the evacuated Δn is going to increase the quantity of mole of the expansion volume, n_h:

$$\Delta n = n_h(t+\Delta t) + n_h(t) \tag{2.7}$$

Due to the conservation of the total number of moles of the whole system n_t (enthalpy reservoir and the expansion volume, this system is really closed!) it is possible to write:

$$n_t = n_g + n_L + n_h \tag{2.8}$$

To establish a relationship between these three quantities, we can write the volume of the cell, V_c:

$$V_c = \frac{n_v}{\rho_v} + \frac{n_l}{\rho_l} \tag{2.9}$$

Where ρ_v and ρ_l represents the vapor and liquid densities respectively. Considering the gas in the expansion volume as ideal:

$$n_h = \frac{PV_h}{RT_h} \text{ and } n_t = \frac{P_0 V_h}{RT_h} \tag{2.10}$$

T_h representing the temperature of the expansion volume (room temperature), V_h the capacity of expansion volume, P the pressure of the system during any part of the experiment, P_0 the filling pressure of the expansion volume at room temperature at the beginning of the experiment. With the last three equations we can determine the number of moles in the liquid and gaseous states. Inside of the enthalpy reservoir:

$$\begin{aligned} n_l &= \left(\frac{RT_h V_c \rho_v - P_0 V_h + PV_h}{RT_h}\right)\left(\frac{\rho_l}{\rho_v - \rho_l}\right) \\ n_v &= \frac{P_0 V_h - PV_h}{RT_h} - \left(\frac{RT_h V_c \rho_v - P_0 V_h + PV_h}{RT_h}\right)\left(\frac{\rho_l}{\rho_v - \rho_l}\right) \end{aligned} \tag{2.11}$$

Beyond the variation of the internal energy of the cell and the enthalpy of the expanded vapour to the expansion volume ($Q=\Delta U_{cell}+h_h\Delta n$), it is necessary to take in accounts the enthalpy of the cell materials. The cell also contributes to the energy storage in the form of sensible heat ($C\Delta T$, C being the heat capacity of the cell and $\Delta T = (T_2 - T_1)$. In conclusion, the stored energy in the *temperature drift mode* between T_1 and T_2 is:

$$Q = \Delta U_{cell} + h_v \Delta n + C\Delta T \tag{2.12}$$

With this result is possible to take into account the energy needed for the ESU temperature increase of ΔT. The use of this result in a practical application is presented in the next section.

2.2.2 Practical application

In the last section, was presented the thermal model to quantify the energy storage in a temperature drift (from *T* to *T+ΔT),* the *temperature drift mode*. With this result is also possible to model the other ESU operational mode, the temperature controlled mode.

In the next section is described how to model the different ESU modes and the energy needed to "recycle the system", i.e. during the pre-cooling phase that is a common phase to all ESU modes.

Pre-cooling phase

Before each ESU mode it is necessary to fill the cell with liquid. In this phase, the vapor of the expansion volume condenses inside the cell by cooling it. The energy to extract for cooling down the vapor from the room temperature (T_{room}) to the cell temperature is given by the enthalpy:

$$H_{cooling} = H(T_{cell}) - H(T_{room}) = \left(h(T_{cell}) - h(T_{room})\right).\Delta n = h_{cooling}\Delta n \tag{2.13}$$

where *Δn* it is the moles number that enter in the cell and $h_{cooling}$ the molar enthalpy difference of the gas between the initial *T* and the final one. This result assumes a small variation of pressure between the beginning and the final of the process. In the pre-cooling process, the exchanged energy to cool down the cell from *T* to *T-ΔT* is identical to that described in the previous section. The total heat to be removed is given by:

$$Q = \Delta U_{cell} + h_g\Delta n + C\Delta T + h_{cooling}\Delta n \tag{2.14}$$

Let us note that, in the case of a liquid neon ESU at 40 K, the enthalpy of the vapor cooling from room temperature to 40 K ($H_{cooling}$) is as high as twice that needed to condense it. In order to store a given amount of energy in the ESU, it is necessary to remove more than three times this energy during the pre-cooling process: this the price to pay to store the gas at room temperature where the space restrictions are much lower.

With this equation it is possible to modelling the cooling for the different configurations of the ESU.

ESU temperature controlled mode

By controlling the pressure inside of the cell it is possible to take advantage of the latent heat of the liquid to vapor transition to store energy at constant temperature (section 2.1) like in the triple point transition. A pressure control valve can be used to control the expansion of the vapor to the expansion volume, when the pressure inside of the cell is higher than the setpoint.

To model this operation mode, two distinct phases were considered (Figure 2-8). After the pre-cooling phase, while the cell temperature is lower than the control temperature the pressure control valve is closed (phase 1), keeping the cell isolated from the expansion volume. The phase 1 consists in heating the cell in order to achieve the setpoint temperature. The evaporated fluid in this phase remains inside the cell, leading to a pressure increase. When the pressure/temperature in the cell is equal to the control pressure/temperature, the valve starts to control (phase 2) letting the evaporated fluid escape to the expansion volume to maintain constant the temperature inside of the cell.

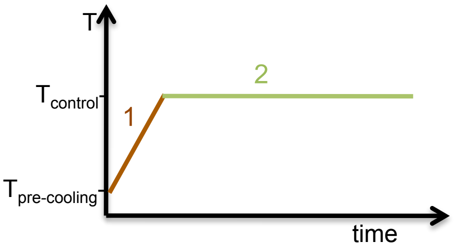

Figure 2-8 - The 2 phases of the modelling of the *ESU temperature controlled mode*.

First phase

In the first phase, the valve is closed because the pressure is lower than the setpoint pressure. The evaporated liquid, which remains inside of the cell, is going to contribute to the increase of the pressure inside of the cell. The given energy to increase the temperature of the cell from T to $T+\Delta T$ is only given by the variation of the internal energy in the cell and the enthalpy of the cell materials:

$$Q = \Delta U_{cell} + C\Delta T \tag{2.15}$$

Let us note that this energy must be supplied to the system.

Second phase

When the temperature of the cell achieves the control temperature, the pressure control valve starts to operate and maintains a constant pressure inside of the cell during the evaporation. During this process due to the constant pressure there is no variation of the molar internal energy (u_v and u_L) and the molar enthalpies (h_v and h_L). For the same reason there is no absorption of energy by the cell materials.

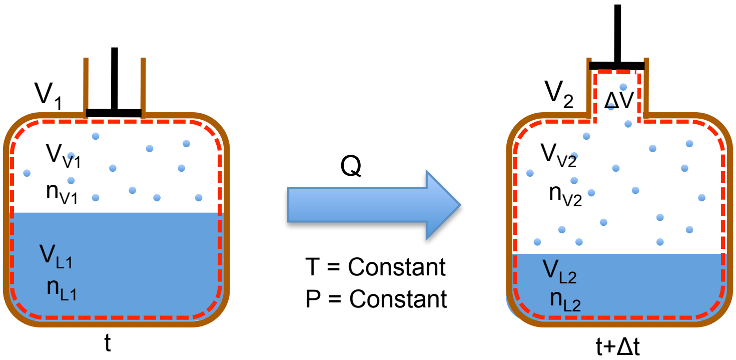

Figure 2-9 – Control volume evolution in the enthalpy reservoir during the evaporation at constant temperature/pressure.

Re-writing the Eq. 2.1 in this form:

$$Q = \Delta U + P\Delta V = U_{Vcell2} - U_{Vcell1} + P\Delta V \tag{2.16}$$

where $\Delta V=(V_{l2} - V_{v2}) - (V_{l1} - V_{v1})=V_2 - V_1$. Attending to the equation of the enthalpy $H=U+PV$, it is possible to write:

$$Q = U_{Vcell2} - U_{Vcell1} + P\left(V_{cell2} - V_{cell1}\right) = H_2 - H_1 \tag{2.17}$$

The initial and final enthalpies are given by:

$$H_1 = n_{V1}h_V + n_{L1}h_L \\ H_2 = n_{V2}h_V + n_{L2}h_L \tag{2.18}$$

The number of moles evaporated n_{eva} is given by $n_{V2}-n_{V1}=n_{eva}$ and $-(n_{L2}-n_{L1})=n_{eva}$. With this result, the stored energy as function of the latent heat and the number of moles evaporated can be written as:

$$Q = n_{eva}\left(h_v - h_l\right) \tag{2.19}$$

as expected for a system working at constant pressure.

When a given amount of liquid is evaporated, the amount of vapor expanded to the expansion volume is not the totality of the evaporation result ($h\Delta n$). A small part of this vapor is going to fill the volume of the evaporated liquid, to maintain the pressure inside of the cell. Using our experimental data for the volumes and temperatures used during this work, less than 1% of the evaporated liquid moles stay inside of the cell. Then it is a good approximation to consider $n_{eva} \approx \Delta n$.

ESU Power booster mode

In this configuration the cryocooler is continuously working and the cell, directly coupled to the cold finger of the cryocooler, is used to absorb heat bursts. In this mode, like in the *Temperature drift mode* the cell is directly connected to the expansion volume. This configuration allows the absorption of the sudden peak loads and the continuous recycling of the ESU.

When the dissipated power from the sensor array is higher than the cooling capacity of the cryocooler the cell temperature is going to increase from T to $T+\Delta T$. Like in the *ESU temperature drift mode* the amount of energy to make the temperature increases is given by the Eq. 2.12:

$$Q = \Delta U_{cell} + h_v \Delta n + C\Delta T \tag{2.12}$$

Inversely, when the cooling capacity of the cryocooler is higher than the dissipated power the cell is going to cool from T to $T-\Delta T$. During this phase, the cell is re-filled with liquid, recovering a part or the totality of the energy storage capacity. Like in the pre-cooling phase, to cooling the ESU of a ΔT it is necessary to remove the energy correspondent to the variation of the internal energy, the enthalpy of the vapor, the heat capacity of the cell and the energy to cooling the vapor from the room temperature (expansion volume) to the cell temperature. This energy is given by the Eq. 2.14:

$$Q = \Delta U_{cell} + h_g \Delta n + C\Delta T + h_{cooling}\Delta n \tag{2.14}$$

The term correspondent to the vapor cooling dictates the difference between the cooling and heating process in the *ESU power booster mode*. In other words, to maintain the ESU mode in continuous operation, more cooling energy than the energy dissipated by the sensor array is required.

2.3 Expansion volume

In the case of the energy storage units based on triple points, the use of an expansion volume is not a fundamental requirement. It is used “only” to decrease the pressure when all the system is at room temperature. During the ESU mode of such a device, the expansion volume does not play any thermodynamic role.

When the liquid to vapor transition of a fluid is selected to built an ESU, an expansion volume is indeed required: beyond the reduction of the filling pressure at room temperature, the expansion volume decreases the rate of the pressure/ temperature increase during the evaporation.

To store a given amount of energy, the volume of the cold cell is mainly given by the specific latent heat (J/cm^3) in the working temperature range whereas the temperature drift, the difference between the final and the pre-cooling temperature, will be determined by the expansion volume.

The mandatory use of an expansion volume is a disadvantage of the liquid to vapor energy storage unit. The bigger the expansion volume used, the smaller is the temperature drift during the ESU working, but for several application its big size could be a limitation. The size of the expansion volume required varies with the working fluid as well as its temperature. The possibility of using a compact expansion volume coupled to a liquid based ESU is analysed and discussed in next paragraphs.

The energy stored (d*E)* during a small temperature difference dT is function of the evaporated moles number dn and the latent heat of the evaporation L.

$$dE = Ldn \qquad (2.20)$$

From the equation of state of a classical ideal gas, $PV=nRT$, where P is the pressure, V the constant expansion volume, n the number of moles, R the gas constant and T_{exp} the constant temperature of the expansion volume, we can write:

$$dn = dP\frac{V}{RT_{\exp}} \qquad (2.21)$$

Along the saturation line of the connected liquid cell, with T the temperature of the cold cell:

$$dP = \left(\frac{\partial P}{\partial T}\right)_{Sat} dT \qquad (2.22)$$

Re-writing Eq. 2.21, from the ideal gas law:

$$dn = \left(\frac{\partial P}{\partial T}\right)_{sat} \frac{V}{RT_{\exp}} dT \qquad (2.23)$$

With this result, the variation of the energy (Eq. 2.20) is given by

$$dE = Ldn = \left(\frac{\partial P}{\partial T}\right)_{sat} \partial T \frac{V}{RT_{\exp}} \tag{2.24}$$

$$\left(\frac{\partial E}{\partial T}\right) = \left(\frac{\partial P}{\partial T}\right)\frac{VL}{RT_{\exp}} \tag{2.25}$$

The Eq. 2.27 gives the energy stored between T e $T+dT$ for an expansion volume V. This equation is only valid for a small dT. Considering a 1 litre expansion volume the last equation gives the effective energy stored between T_{min} and T_f per litre of expansion volume.

For a fixed dT of temperature drift the stored energy efficiency per litre of expansion volume grows with $\partial P / \partial T$. Looking at the P-T diagram of neon in Annexe 2, the slope increases with the temperature. The first chart of Figure 2-10 displays the slope $(\partial P / \partial T)_{sat}$ for neon, nitrogen and oxygen. For these fluids this slope increases with the temperature up to the critical point: then by working close to the critical point it is possible to take advantage of this factor to decrease the expansion volume capacity to store the same amount of energy for a dT temperature drift. This fact traduces simply that the same dP corresponds to smaller temperature drift. However the effective stored energy is also dependent on the latent heat of the evaporation.

The latent heat of the same fluids is presented in Figure 2-10: it decreases with the temperature increase, reaching 0 at the critical point where no more distinction exists between the liquid and gas phases. Close to the critical point this slope is higher. These facts are general to all fluids and is seen in annex 4.

Knowing the behaviour of both the $(\partial P / \partial T)_{sat}$ and the latent heat with the temperature, it is possible to calculate the energy stored for a temperature drift of 1 K, $(\partial E / \partial T)$, per litre of expansion volume (Figure 2-10). For the three fluids displayed it is possible to observe the increase of the stored energy per litre of expansion volume (due to the dominant effect of dP/dT) and the reverse tendency near the critical point: close to this temperature the decrease of the latent heat is more significant than the $\partial P / \partial T$ increase. For neon, to obtain the maximum of energy stored per litre of expansion volume in a determined temperature drift, the best solution is to work around 40 K range. This fact was one motivation of this work. In the case of nitrogen and oxygen it is at 115 K and 140 K range, respectively. Let us note that dE/dT at 40 K for neon is much higher than for nitrogen between 63 e 80 K where were performed the first experiments described in section 1.2.3.

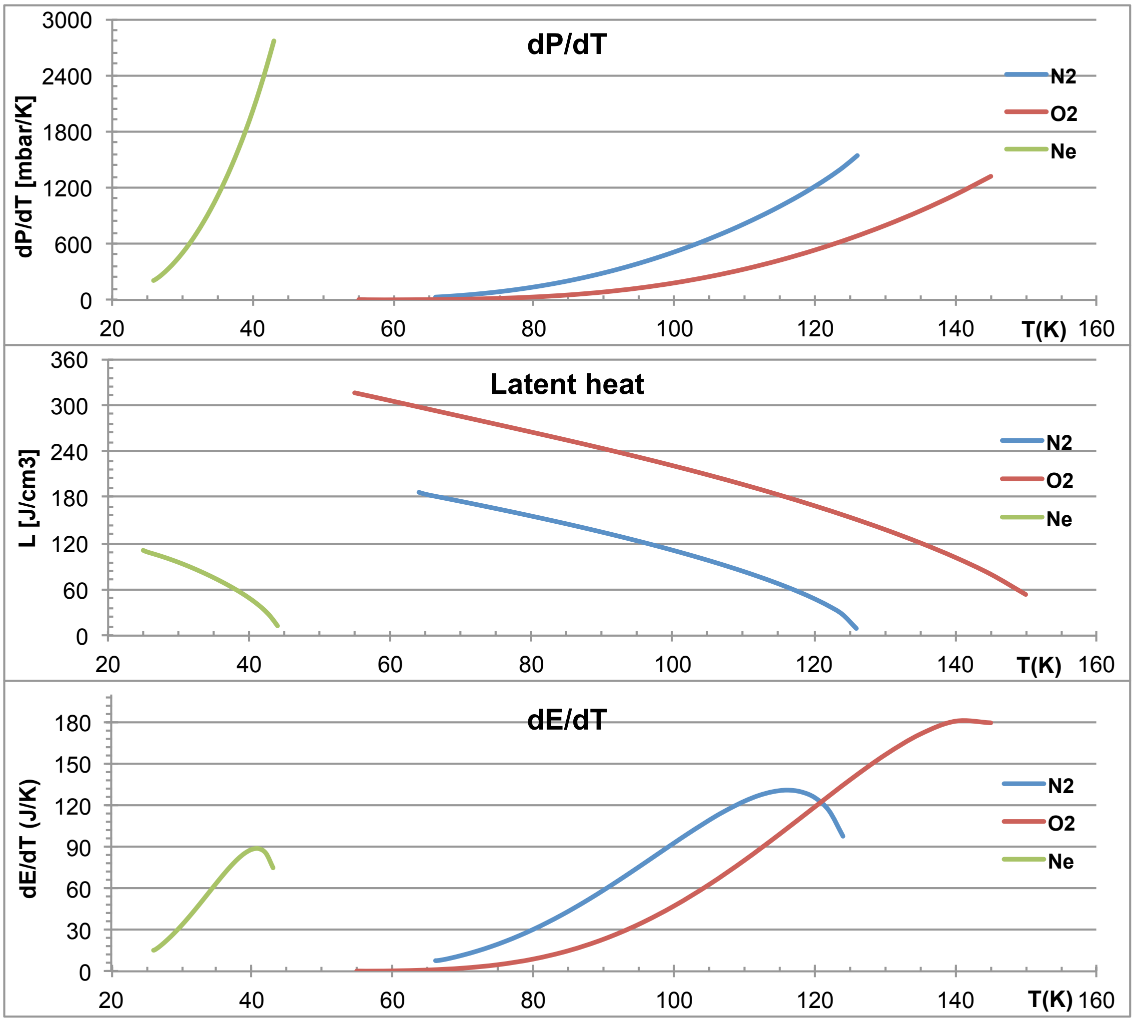

Figure 2-10 – Upper plot: $(dP/dT)_{sat}$ along the saturation line as a function of the temperature for neon, oxygen and the nitrogen. Middle plot: latent heat of these three fluids as function of the temperature. Bottom plot: energy stored per temperature drift and per litre of the expansion volume.

In can be seen also, for instance, that despite the high latent heat of the oxygen at 70 K compared to the neon at 40 K, to store the same amount of energy with the same temperature drift a smaller expansion volume is needed with neon. At 70 K, a 40 times bigger expansion volume is needed, in the case of oxygen, to store the same amount of energy with the same temperature drift than for the neon at 40 K. However, looking at the low temperature side, the larger latent heat of oxygen turns the low temperature cell smaller than the neon's cell to store the same amount of energy.

Using the equation of the energy needed to increase the temperature from T to $T+\Delta T$ (Eq. 2.12), the pre-cooling temperature for an ESU using neon and storing 1000 J around 40 K (final temperature) was calculated as a function of the expansion volume and the results are displayed in Figure 2-11. The volume of the cell is ≈21 cm^3 and the final temperature is 40 K.

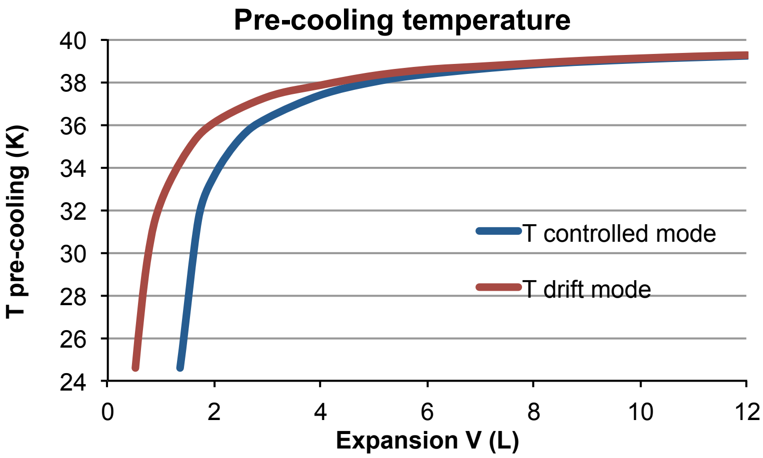

Figure 2-11 – Predicted pre-cooling temperature as function of the expansion volume capacity to store 1000 J between the pre-cooling temperature and 40 K using the neon in the T drift mode and T controlled mode.

This plot was obtained using the results of the pre-dimensioning tool described in section 2.5. As it can be seen in this figure, a 6 liters expansion volume allows storing 1000 J between 38 K and 40 K. A smaller volume requires a lower temperature of pre-cooling to completely fill the cell with liquid neon. As mentioned, with a 6 liters volume a small temperature drift of 2 K is obtained, but in the case of use a 2 liters volume the resultant temperature drift is 4 K.

To store 1000 J at 40 K it is necessary to evaporate 21 cm3 of liquid neon. But for lower pre-cooling temperatures, it is possible to take advantage of the higher latent heat in this zone (far from the critical point) decreasing the amount of liquid needed to store the same 1000 J. Consider the following example in Table 3: the liquid amount required to store 1000 J for different expansion volume sizes.

Table 2.1 – Liquid amount needed to store 1000 J for different expansion volume size. In all the examples the final temperature is 40 K.

Volume	Energy	T. drift	Liquid amount
1 L	1000	8 K	11 cm^3
3 L	1000	3 K	15 cm^3
6 L	1000	1.4 K	18 cm^3
12L	1000	0.8 K	20 cm^3

Contrarily to the temperature drift mode, in the pressure controlled mode, the evaporation occurs at constant temperature: independently of the expansion volume, the pre-cooling temperature must be enough to condense 21 cm^3 of liquid at 40 K to store 1000 J. In Figure 2-11 the pre-cooling temperature to store 1000 J at 40 K is calculated as a function of the expansion volume capacity. In generally the pre-cooling temperature in this mode for the same expansion volume is lower than the ESU drift mode to store the same energy.

With these results it is possible to pre-dimension the expansion volume in order to optimize this parameter versus the temperature drift during the ESU modes.

2.4 Liquid confinement

A potential application of the liquid neon energy storage unit is the integration in a satellite to cool sensitive sensors. Then such application requires that the ESU may operate in a microgravity environment and it becomes necessary to ensure the confinement of the liquid neon inside the cell during its operation. Before the integration in the final application the system should be gravity insensitive in a laboratory environment or, in other words, in a ground demonstration it is necessary to ensure the liquid confinement in the cell in any orientation in respect to the gravity direction without significant performance degradation. The energy stored by the ESU being strongly dependent of the liquid amount in the cell, expulsion of liquid through the capillary tube that connects the cold cell to the expansion volume during the ESU mode would be dramatic. One solution, often used to solve such an issue, is to use a porous material inside the cell to confine the liquid by capillary effect[18]. The use of cryogenic liquids embedded in porous materials for confinement is a recurring solution for space applications[30]. The use the alumina foam in a sorption cooler integrated in the Herschel satellite [31] is an example of application where this kind of porous material was successfully used to confine the liquid. The liquid nitrogen energy storage unit[9] also used this kind of alumina sponge for similar purpose.

To choose the porous material used in this work to confine the liquid neon in the cell during the ESU operation, it was necessary to predict its capability to confine the liquid neon. By assuming that the pore spaces correspond to small capillary tubes, with the diameter equal to the average pores sizes, it is possible to calculate the capillarity height, corresponding to the maximum height that a liquid can rise against gravity through the capillary tubes. In Figure 2-12 an electronic microscope image of the Procelit P160® used to confine the liquid in the nitrogen energy storage unit[9] is shown. This porous ceramic manufactured by RATH is constituted by 90% of Al_2O_3 and 10% of SiO_2, with an estimated void volume of ≈92% and the “pore size” is 50-60 μm.

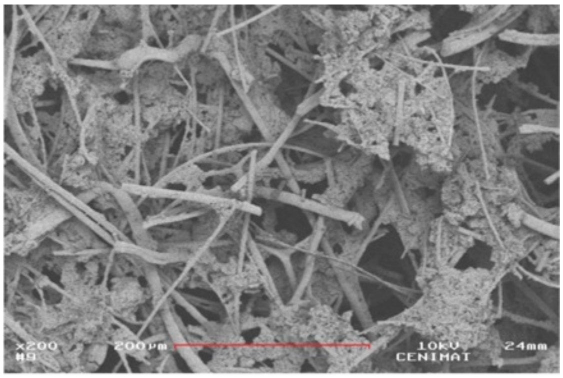

Figure 2-12 - Electronic microscope image of Procelite 160 (UNL/FCT/CENIMAT). The red scale represents 200 μm.

In a first approximation, to ensure the liquid confinement in the porous ceramic it is necessary to have a capillarity height at least equal to the cell’s height. In Figure 2-13 the capillary height of 2 different diameters tubes is schematized. Balancing the total weight of the liquid column and the tensile force acting along the contact line (capillarity force) it is possible to estimate the height *h* that a liquid can raise through a capillary tube with *r* radius[32]:

$$\left(\pi r^2 h\right)\left(\rho_L - \rho_V\right) g = \left(2\pi r\right)\sigma\cos\theta \tag{2.26}$$

where ρ_L represents the liquid density ρ_L and ρ_v the vapor density, σ the surface tension (N/m), and θ the contact angle between the liquid and the tube walls: the height that a liquid can rise in a capillary tube (Jurin's law) is[32] then:

$$h = \frac{2\sigma\cos\theta}{r\left(\rho_L - \rho_v\right)g} \tag{2.27}$$

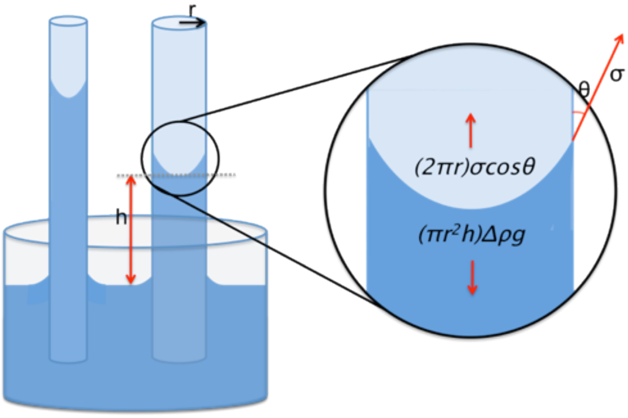

Figure 2-13 –Scheme of the capillarity effect in two capillary tubes with different diameters.

The contact angle θ quantifies the wettability of the solid surface by a liquid. When the liquid wets the wall of the capillary, the surface is concave in shape; for complete wetting, the contact angle takes small values, $\theta << 90°$. When the liquid does not wet, the capillary walls, the meniscus becomes convex and appears a depression of depth h. In this case the contact angle takes values between $90 < \theta < 180°$. In general, the cryogenic fluids present a good wettability, which means that a contact angle close to $\theta \approx 0°$[33] is a good approximation and will be taken in the following calculations.

In the liquid nitrogen ESU, the average pore size of the ceramic (Procelit P160) used was ≈ 60 µm and the cell's height was 35 mm. In these conditions, the nitrogen liquid confinement between 70 K and 80 K was successfully demonstrated. In the case of the liquid neon ESU the working temperature range is 40 K, quite close to the critical temperature (44.5 K) where the liquid and vapor states become indiscernible and where the surface tension tends to 0 (annex 5). A direct consequence is the decrease of the capillarity height close to the critical point, turning more difficult the process of liquid confinement. Let us note however that the difference of densities (ρ_l - ρ_v) also decreases near the critical point zone which attenuates the decrease of the capillarity height.

Using the Jurin's law (Eq. 2.27), the capillarity height for the nitrogen and neon using a porous size of 60 µm (Procelit P160) are compared in Figure 2-14.

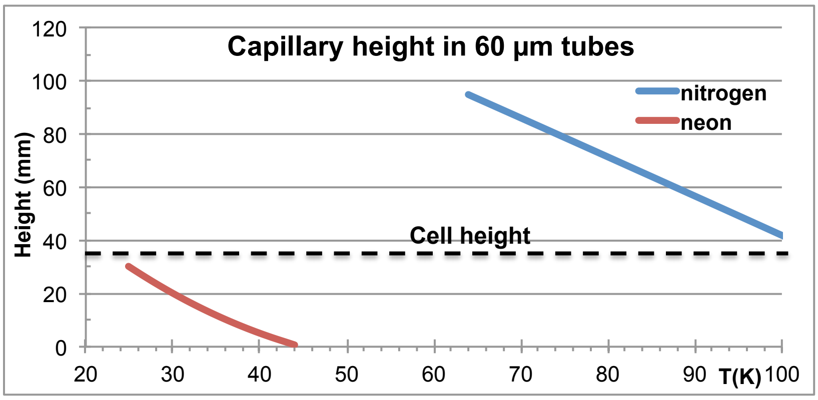

Figure 2-14 - Determination of the capillarity height in capillary tubes with 60 µm of diameter for both neon and nitrogen using the Jurin's law.

Considering 35 mm for the cell's height, in the case of neon, the liquid cannot reach the top of the cell by capillarity effect for any temperature. This figure shows that actually at 40 K, with this pore size, the liquid neon will only climb ≈ 5 mm against gravity.

In Figure 2-15, the capillarity height is determined for different tube diameters: to enable the ESU to work at least up to 42 K, a porous material with < 5 µm of pore size is required.

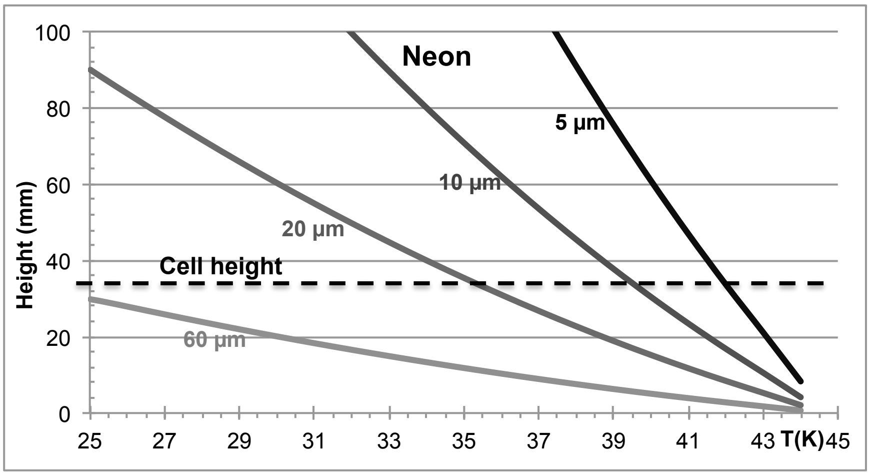

Figure 2-15 – Determination of the capillarity height in tubes with different diameters for neon.

Some porous ceramics similar to the referred P160 but with different dimensions are available from the same manufacturer RATH®. But, in preliminary tests, the minimum of ≈ 20 µm of porous size was found in this ceramic material, which is not sufficiently narrow. Other porous materials were searched in order to reach the aimed capillary height at 42 K.

In the experimental setup section some experiments to test the capability of some porous materials to confine the neon will be presented.

2.5 Pre-dimensioning tool

Another objective of this work is to associate the thermal model developed for this system to an user-friendly software, in order to easily and rapidly obtain an idea of the dimensions necessary to satisfy a “customer” requirements while using it as a pre-dimensioning tool. This software must be able to describe each individual system and various configurations as far as possible.

The MATLAB® software was used for this pre-dimensioning tool. By introducing the initial conditions and the working fluid the pre-dimensioning software gives the evolution of temperature for the three different operation ESU modes: the *temperature drift mode*, the *temperature controlled mode* the *power booster mode*. The cooling process is also possible to be simulated as far as the cryocooler’s cooling power is known.

Several inputs need to be provided to this pre-dimensioning software: the working fluid, the filling pressure, the expansion volume size, the volume of the cold cell, the mass of its materials, the initial temperature, the cryocooler cooling capacity and the heat load profile. By pressing the simulation button available for each ESU mode or the cooling process, the evolution of the temperature is plotted and the intermediate calculations (number moles evaporated, energy stored, liquid percentage in the cell, pressures…) are displayed in a table. All these intermediate and final results of the calculation can be saved in a “.txt” file. A screen shot of the software interface is presented in Figure 2-16, where an example of the cooling process with a constant cryocooler temperature at 35 K is presented. In this calculation, the gas gap heat switch conductance was taken into account as another input.

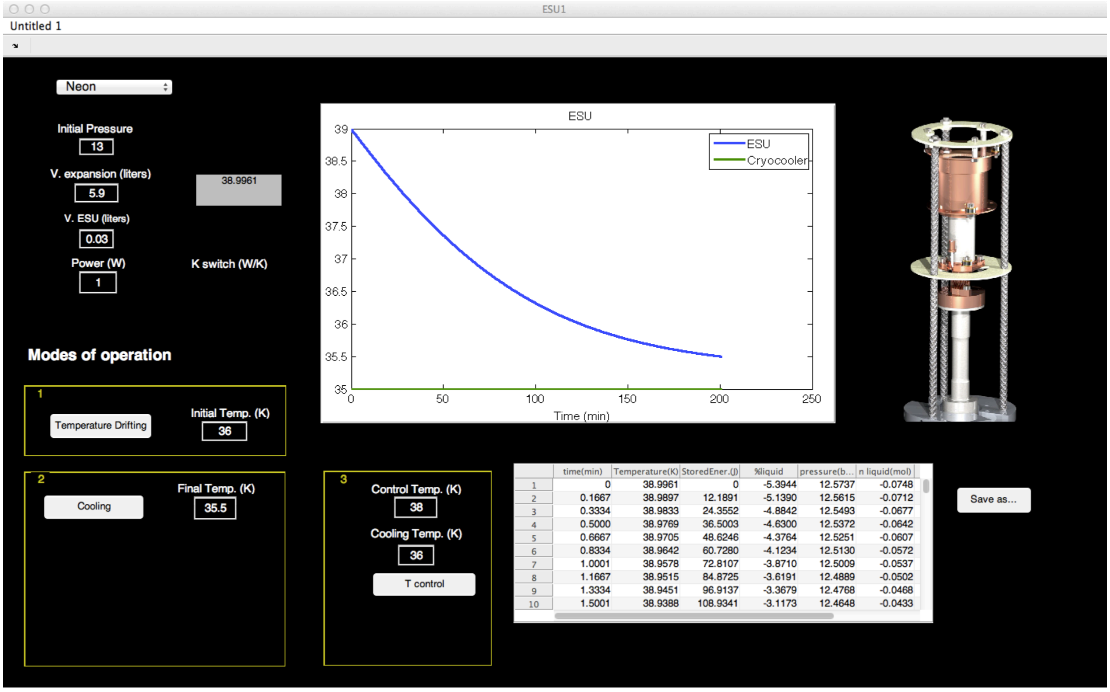

Neon

Initial Pressure 13

V. expansion (liters) 5.9

V. ESU (liters) 0.03

Power (W) 1

38.9961

K switch (W/K)

Initial Temp. (K) 36

Final Temp. (K) 35.5

Control Temp. (K) 38

Cooling Temp. (K) 36

	time(min)	Temperature(K)	StoredEner.(J)	%liquid	pressure(b...	n liquid(mol)
1	0	38.9961	0	-5.3944	12.5737	-0.0748
2	0.1667	38.9897	12.1891	-5.1390	12.5615	-0.0712
3	0.3334	38.9833	24.3552	-4.8842	12.5493	-0.0677
4	0.5000	38.9769	36.5003	-4.6300	12.5372	-0.0642
5	0.6667	38.9705	48.6246	-4.3764	12.5251	-0.0607
6	0.8334	38.9642	60.7280	-4.1234	12.5130	-0.0572
7	1.0001	38.9578	72.8107	-3.8710	12.5009	-0.0537
8	1.1667	38.9515	84.8725	-3.6191	12.4889	-0.0502
9	1.3334	38.9451	96.9137	-3.3679	12.4768	-0.0468
10	1.5001	38.9388	108.9341	-3.1173	12.4648	-0.0433

Figure 2-16 – Graphical user interface of the pre-dimensioning software developed to simulate the *ESU pre-cooling process*, the *temperature drift mode* and the *temperature controlled mode*. This is a typical simulation of the pre-cooling using a constant temperature of the cryocooler.

Two different iterative processes can be used to calculate all the operational modes: temperature increments or time increments. Due to these two different ways to calculate, the pre-dimensioning software was divided in two separators. The first one (Figure 2-16), using increments of temperature, makes possible to simulate the *cooling process*, the *temperature drift mode* and the *temperature controlled mode*. The second iterative process was developed to simulate the *power booster mode*. In this mode, the ESU is directly coupled to the cold finger of a cryocooler to attenuate heat bursts. For this reason, a heat load profile, simulating the heat power entering the system as a function of time, and the cryocooler cooling profiles need to be loaded. The temperature drift and its slope (positive or negative as corresponding to a cooling or a heating process) are dependent on the variable heat power transferred to the system. In this case, using a given heat load profile, the calculation is performed using time increments. A screen shot of this part of the software is available in Figure 2-17. The two different iterative processes and how they are applied for each working mode are described in the following section.

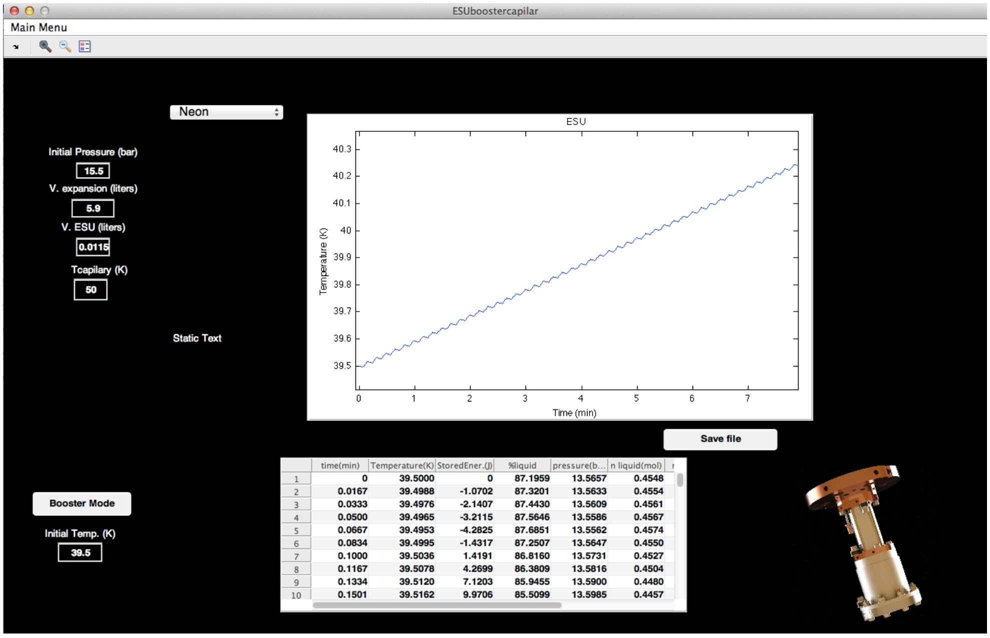

Initial Pressure (bar) 15.5
V. expansion (liters) 5.9
V. ESU (liters) 0.0115
Tcapilary (K) 50
Initial Temp. (K) 39.5

	time(min)	Temperature(K)	StoredEner.(J)	%liquid	pressure(b...	n liquid(mol)
1	0	39.5000	0	87.1959	13.5657	0.4548
2	0.0167	39.4988	-1.0702	87.3201	13.5633	0.4554
3	0.0333	39.4976	-2.1407	87.4430	13.5609	0.4561
4	0.0500	39.4965	-3.2115	87.5646	13.5586	0.4567
5	0.0667	39.4953	-4.2825	87.6851	13.5562	0.4574
6	0.0834	39.4995	-1.4317	87.2507	13.5647	0.4550
7	0.1000	39.5036	1.4191	86.8160	13.5731	0.4527
8	0.1167	39.5078	4.2699	86.3809	13.5816	0.4504
9	0.1334	39.5120	7.1203	85.9455	13.5900	0.4480
10	0.1501	39.5162	9.9706	85.5099	13.5985	0.4457

Figure 2-17 – Graphical user interface of the software developed to simulate the *ESU booster mode. The simulation using a variable heat load profile is possible, by uploading the heat load profile as a txt file format.*

Temperature iterations

The software developed to simulate the *temperature drift mode* and the *pre-cooling process* is based on temperature iterations (Figure 2-17). All the molar values (internal energies, enthalpies, densities,..) are obtained along the saturation line via REFPROP[34] and are integrated in the software. Using the inputs described in the begining of this section (filling pressure, volumes, heat load applied), the correspondent energy Q, for a given temperature drift (T_1 → T_2) or (T_2 → T_1), can be directly obtained, by using the Eq. 2.12 and Eq. 2.14 respectively:

$$Q\left(T_1 \to T_2\right) = U_{cell}\left(T_2\right) - U_{cell}\left(T_1\right) + h_v(T_2)\Delta n + C\left(T_2 - T_1\right) \tag{2.28}$$

$$Q\left(T_2 \to T_1\right) = U_{cell}\left(T_1\right) - U_{cell}\left(T_2\right) + h_v(T_1)\Delta n + C\left(T_1 - T_2\right) + \Delta n\left(h_{Troom} - h_{T_1}\right) \tag{2.29}$$

Δn represents the mole number that leaves or enters in the cell during the drift (T_1 → T_2) or (T_2 → T_1). The time of this increment is obtained knowing the applied heat power in the ESU and the energy calculated. A temperature dependent cooling capacity of the cryocooler is used in the pre-cooling instead of an applied heat power. For small temperature increments it is also possible to simulate the cryocooler's temperature during the pre-cooling process using the heat switch ON conductance (input of the software). A pre-cooling process is simulated in Figure 2-16, the blue line and the green line in the plot of the screen shot represent the temperature of the cell and the cryocooler, respectively.

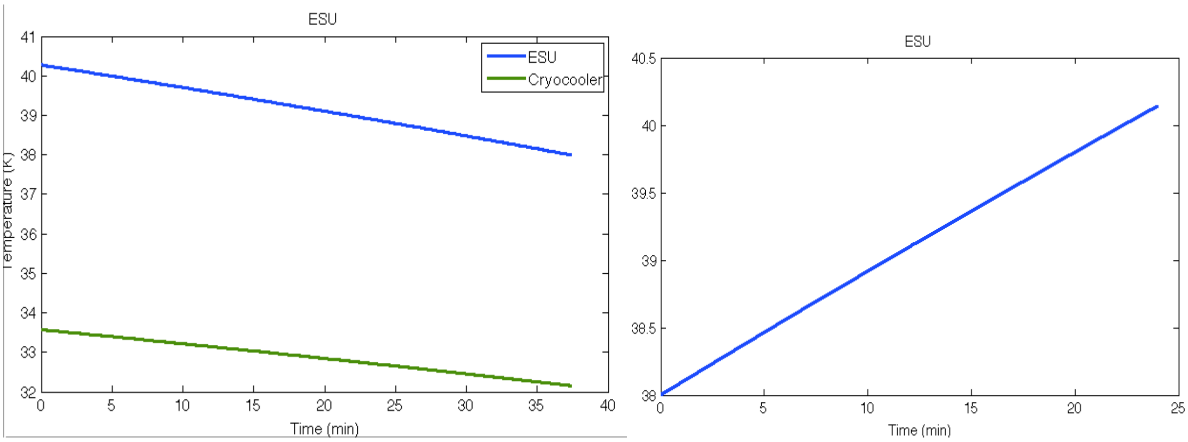

Figure 2-18 - Example of the pre-dimensioning tool result of the cooling process (left) and temperature drift mode (right). In the simulation of the cooling process, the cryocooler cooling capacity is taken into account to simulate its temperature.

The amount of vapor that leaves or enters the cell (*Δn*) results from the difference of total moles number in the cell in each temperature increment. The total moles number in the cell is given by the sum of the liquid and vapor moles number (Eq. 2.11). The determination of the liquid and vapor moles number gives the filling ratio of the cell: this value is important particularly to know the pre-cooling temperature needed to completely fill the ESU cell. Moreover, when this number vanishes, the ESU becomes "dry" and the ESU mode ends.

The temperature iterations are also used in the software to simulate the *temperature controlled mode*. At the beginning, after the pre-cooling phase, the pressure control valve is closed. With the valve closed, when a heat power is applied the temperature increases very fast. The total amount of moles inside the cell is maintained during this phase. From the pre-cooling temperature to the control temperature the correspondent energy *Q*, for a given temperature drift (T_1 → T_2) can be directly obtained, by using the Eq. 2.15:

$$Q(T_1 \rightarrow T_2) = U_{cell}(T_2) - U_{cell}(T_1) + C(T_2 - T_1) \qquad (2.30)$$

Similarly to the temperature drift mode, the time correspondent to the drift (T_1 → T_2) is the ratio of the calculated energy to the applied heat power. The number of gaseous moles inside the expansion volume is maintained constant during this phase. It is necessary to take this closed system into account while determining the liquid and gaseous moles number inside the cell during a temperature increment, using Eq. 2.11.

In the second phase (Figure 2-19) when the temperature of control is achieved the valve starts to control it and the evaporated liquid is expanded to the expansion volume, in order to maintain constant the pressure inside the cell. Using Eq. 2.19, the energy to evaporate all the liquid inside of the cell at constant temperature is given by:

$$Q = \Delta n\left(h_v\left(T_{control}\right) - h_l\left(T_{control}\right)\right) \tag{2.31}$$

This calculation does not need an iterative process. When the controlled pressure is higher than the filling pressure, the number of evaporated moles *Δn is* given by the total liquid moles number available in the cell after the valve to be closed. In this case the control stops when the liquid ends, which means that *Δn* corresponds to the total liquid moles number in the cell. When the controlled pressure is lower than the filling pressure the control stops due to the equalisation of the cell and expansion volume pressures, even before the end of the liquid. In this case, the number of liquid moles for the control temperature at the end of the control is calculated using Eq. 2.11 and it is possible to obtain *Δn* for a given control temperature. Such calculations allow obtaining the energy stored at constant *T* and, for a constant applied heat power, the time of control.

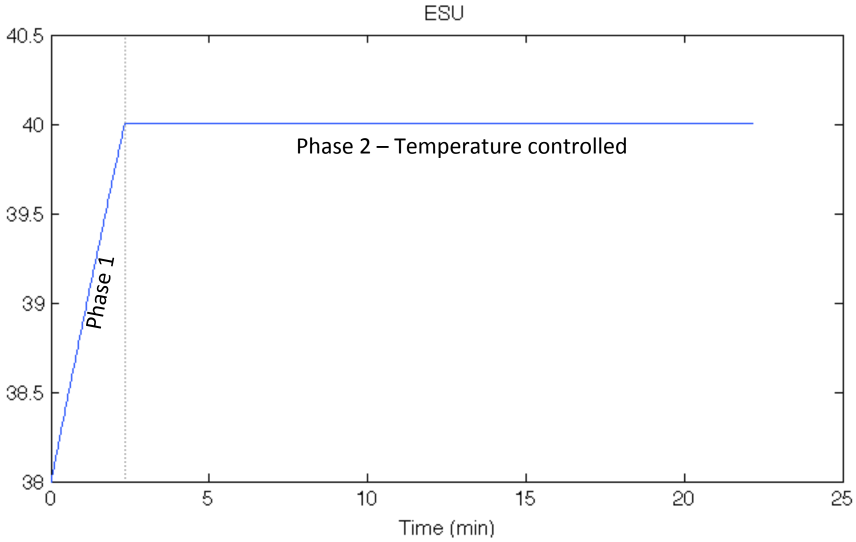

Figure 2-19 - Example of the pre-dimensioning tool result of the temperature controlled mode at 40 K.

Time iterations

The second part of the software was developed to simulate the *power booster mode*. A screen shot of this part is displayed in Figure 2-17. For this *power booster* function, a .txt file with the heat load profile (heat power applied versus time) needs to be loaded. For this part, instead of computing the stored energy for a given temperature drift ΔT a reverse process is used. For a given amount of energy ΔQ (or an heat load in a period of time Δt) the temperature change is computed resulting in a temperature drift $T_1 \rightarrow T_{solve}=T_1+\Delta T$. This turns possible to obtain the temperature change for a variable heat load profile. All the parameters are dependent of the temperature (internal energy, enthalpy of the vapor, the evaporated amount), so it is necessary to solve the following equations to find T_{solve}):

$$Q\left(T_1 \to T_{solve}\right) = U_{cell}\left(T_{solve}\right) - U_{cell}\left(T_1\right) + h_v(T_{solve})\Delta n + C\left(T_{solve} - T_1\right) \tag{2.32}$$

$$Q\left(T_1 \rightarrow T_{solve}\right) = U_{cell}\left(T_{solve}\right) - U_{cell}\left(T_1\right) + h_v(T_{solve})\Delta n + C\left(T_{solve} - T_1\right) + \Delta n\left(h_{Troom} - T_{solve}\right) \quad (2.33)$$

When the energy Q transferred to the system during a time increment is positive the first equation (eq. 2.34) is used, corresponding to an increment of temperature. When Q is negative, the energy is removed from the system and the equation correspondent to a cooling process (eq. 2.35) is used. To solve this equation and find the T_{solve}, a recursive algorithm was developed. This algorithm finds the T_{solve} with a maximum error of 1×10^{-4} K.

An example of an ESU booster mode simulation using a variable heat load profile is presented in Figure 2-20. A squared 10 s period wave with a maximum heat load of 9 W and -1 W of minimum heat load was used in this example. In the simulation it can be clearly observed the steps of temperature increase and decrease: when the heat load applied is 9 W (during 5 s) the ESU temperature increases; when the heat load is the minimum (-1 W) a part of the liquid neon evaporated is re-condensed, corresponding to a temperature decrease.

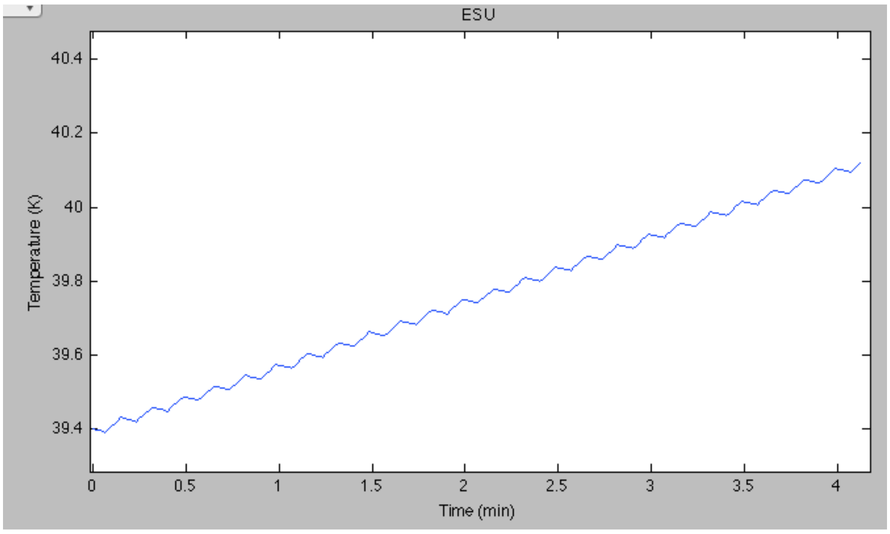

Figure 2-20 - Result of a simulation example of the booster mode using a variable heat load profile: A squared wave with 9 W max and -1 W min and a period of 10s.

In the Experimental Results section, the calculations obtained with this software will be compared with the experimental results. During the tests of the ESU, this software has been upgraded in order to simulate specific experiments. Recurrently the software is used to predict the pre-cooling temperatures and the filling ratio. All the sizing of the cell and expansion volume capacity was done using this software.

3 Experimental setup

In this section the experimental apparatus and all the sizing of the different parts of the ESU system are described. Due to the potential applications, the ESU must be able to operate in a microgravity environment: the system should be gravity insensitive in a laboratory environment. In order to demonstrate such a feature in a laboratory environment, the system developed has the capability to change the orientation. Tests with different porous materials to confine the liquid inside of the cell are presented in this chapter.

3.1 Cryocooler

To test the liquid neon energy storage unit a Gifford-McMahon (GM) cryocooler MODEL 22 of CTI-CRYOGENICS® (2W@20 K) was purchased. The required space for this ESU being larger than the vacuum shroud usually sold with this cryocooler model, we purchased only the bare cryocooler, without the vacuum shroud and instrumentation skirt, which was designed and built locally during this work.

To demonstrate the capability of the ESU to work properly in any orientation (gravity insensitive) it was necessary to develop a orientable support of the cryocooler. This argument was considered in the sizing of the instrumentation skirt and in the vacuum shroud, building them as light as possible to facilitate the rotation movement.

A drawing of the cryocooler as it was purchased is presented in Figure 3-1 (1). The ESU system (gas gap heat switch and cell) will be coupled to the cold finger (2nd stage). The instrumentation skirt (Figure 3-1 2)) is made of stainless steel 304 with 5 vacuum feedthroughs KF16 welded to the cylindrical walls. The feedthrougs are used to pass the electrical wiring for thermometers and heaters as well as the capillaries used both to connect the cell to the expansion volume and to supply the gas for the gas gap heat switch.

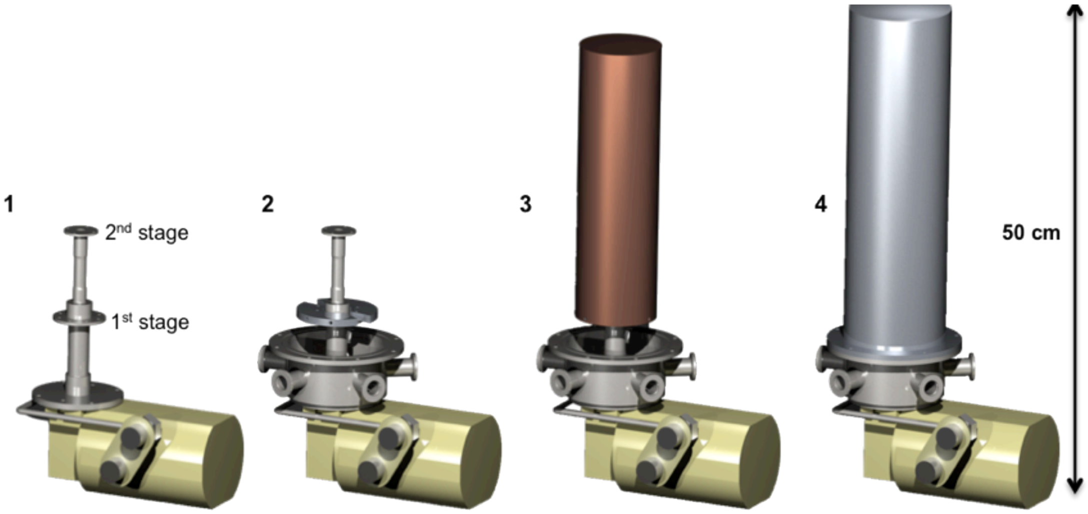

Figure 3-1 – Drawing of the different stages of the cryocooler assembly. 1 – cryocooler as purchased; 2 – cryocooler with the instrumentations skirt and two half flanges to support the 50 K thermal radiation shield; 3 – thermal radiation shield; 4 – vacuum shroud.

The minimum temperature range of the 1st stage is 40 K – 45 K, close to the working temperature of the ESU. A copper thermal radiation shield, thermally coupled to the 1st stage through two aluminium half flanges, is used to isolate the ESU from the heat radiated from the 300 K shroud. A 0.5 mm thick copper sheet was used to made this radiation shield with 90 mm of diameter (Figure 3-1 3)).

The vacuum shroud (Figure 3-1 4)) was designed starting from 3 different parts: a cylindrical 2 mm thick tube, one flange and a flat bottom. The flange and the bottom were welded to the cylindrical tube. The aluminium was chosen as the building material for the shroud, for its lightness. The length of the shroud is 350 mm with 110 mm of diameter. One of the instrumentation skirt feedthroughs is used to pump the vacuum shroud. An Edwards vacuum system (turbomolecular pump) is responsible for the system pumping.

3.2 Cell sizing

To work with liquid neon at 40 K range, the cell and the expansion volume must withstand ≈ 25 bar. On the other hand, to test different porous materials on their capability to confine the liquid neon, a low temperature cell withstanding 50 bar and with the possibility of being “easily” opened and closed was required. Its integration in an orientable system required the development of a light cell in order to avoid high torques on the thin tubes of the cryocooler. When the adequate porous material was found, another cell with more appropriated thermal properties (higher thermal conductance) to use as enthalpy reservoir was designed.

A smaller cell was sized for the booster mode. With the cryocooler in continuous operation the objective of this enthalpy reservoir is absorb the sudden heat bursts, limiting the temperature increase and providing a better thermal stability of the cryocooler. Beyond the high thermal conductance of the cell itself and high thermal conductance between the cell and the cold finger, a good thermal contact between the walls of the cell and the liquid is also required.

In this section the sizing of the three different mentioned cells, using a finite elements software COSMOS® (Solid Works®) will be described.

3.2.1 Multipurpose cell

This multipurpose cell was developed with the main objective of testing porous materials to confine the neon liquid inside of it. In order to be easily opened and closed, the lid of this cell is sealed using screws and an indium ring. The cylindrical cell with 38 cm^3 (38 mm of diameter and 35 mm of height) must withstand 50 bar. A trade-off between materials for building the cell was done and took into account both its thermal conductivity and its mass. The operational temperature range of this cell is 40 K – 300 K. The “ultimate stresses” of different materials for temperatures below 300 K are shown in Figure 3-2.

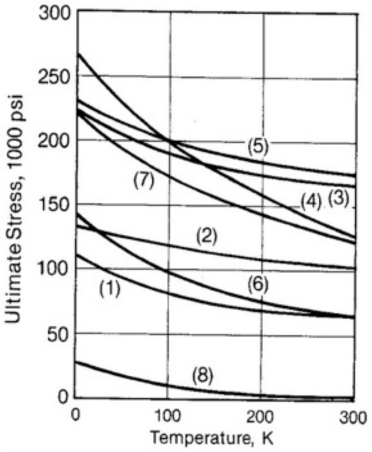

Figure 3-2 - Ultimate stress for some materials[35]. (1) Aluminium 2024 – T4; (2) copper-beryllium; (3) "K Monel"; (4) titanium; (5) stainless steel; (6) Carbon steel C1020; (7) Steel- Ni 9%; (8) Teflon.

Because the mechanical resistance (yield strain and ultimate stress) of the different types of materials decreases for higher temperatures, in the operational temperature range of this cell, the lower yield strain and the ultimate stress at 300 K were used.

For the multipurpose cell design, five different materials commonly used at low temperature were considered: copper, stainless steel 316; aluminum 6063; aluminum 6061; aluminum 2024- T4 (duralumin).

In order to compare the mass of a cell made of these different materials, the minimum thickness of the cylindrical walls of the cell to withstand the pressure of 50 bar was calculated. To determine this thickness two different stresses in the cylindrical walls are calculated (Figure 3-3): the cylinder walls are subjected to a tensile stresses due to the pressure (*q*) on the lid and the radial pressure (*q*) directly applied in the cylindrical walls. In this phase no deformations in the lids of the cell were considered (top and bottom).

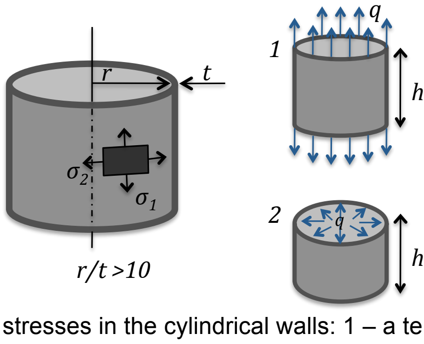

Figure 3-3 - The two different stresses in the cylindrical walls: 1 – a tensile stress; 2 – radial pressure.

In the first case, an annular section of the cylindrical walls is subjected to a tensile stress. The resultant stress (σ_1 and σ_2, according to Figure 3-3) in this case is:

$$F = qA_{lid} = \sigma_1 2\pi rt \leftrightarrow \sigma_1 = \frac{qr}{2t} \text{ and } \sigma_2 = 0 \qquad (3.1)$$

Where the q is the pressure, A_{lid} the lid area, r the radius of the cylinder (and of the lid) and t the wall thickness. In the second case the resultant tensions are given by the applied force on a longitudinal section of the cylindrical walls:

$$F = 2rhq = 2\sigma_2 2th \Leftrightarrow \sigma_2 = \frac{qr}{t} \text{ and } \sigma_1 = 0 \qquad (3.2)$$

To avoid any plastic deformation in the material, the resultant stress in the materials needs to be lower than the yield strength of the material ($(\sigma_1,\sigma_2) < \sigma_{Yield}$). Then, using equations 3.1 and 3.2, the minimum thickness to avoid any permanent deformation is given by [36]:

$$t_{\min} > \frac{qr}{\sigma_{Yield}} \qquad (3.3)$$

With this result it is possible to estimate the minimum thickness and the mass of the cell (Figure 3-4) based on the properties of the 5 materials in the Table 3.1:

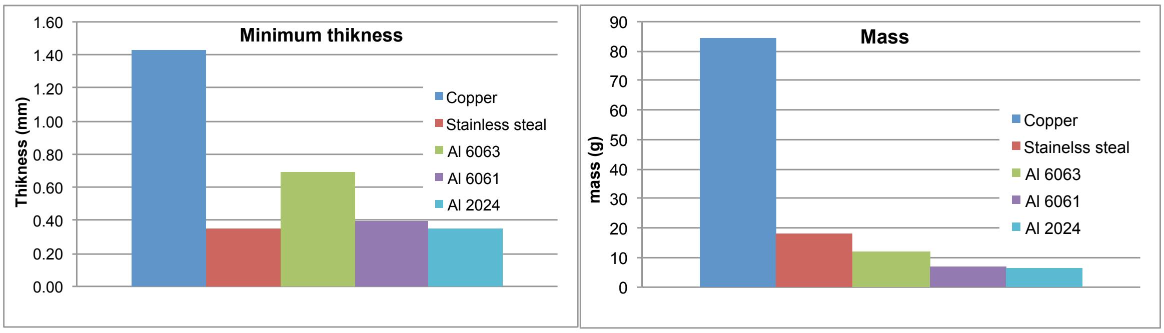

Figure 3-4 - minimum thickness of cylindrical walls to avoid any plastic deformation when subjected to 50 bar. The mass is estimated with the minimum thickness for the 5 different materials. The mass of the cell is estimated by considering the minimum thickness and two lids (bottom and top) with the same calculated thickness.

Table 3.1 – Properties of the different materials considered to the cell design. The yield strength, and young modulus are given for the temperature of 300 K.

Properties	Copper	SS 316	Al 6063	Al 6061	Al 2024-T4
Density (kg/m^3)	8930	7990	2700	2700	2780
k (W/(m.K)) @ 40K[24]	1150	5	220	55	45
σ_{Yield} (MPa)[37]	70	290	145	255	290
Young modulus (GPa)[37]	115	193	68,9	68,9	73,1
$\Delta L/L_{300\,K}$ (%) @ 40 K[24]	0,323	0,296	-	-	0,394

Considering the previous results as a trade-off about choosing the construction material of the cell, the copper does not seem to be a very good solution due to its mass, despite its high thermal conductivity. The thermal conductivity of the cell is an important factor that could avoid thermal gradient along the cell during heating phases. The stainless steel presents a poor thermal conductivity, making the aluminium the best choice to build the cell. The main drawback for using aluminium is the need for soldering a filling capillary to the cell while the soldering process on aluminium is not a trivial process. However, an appropriated soft solder and flux for the aluminium-SS junction (Castolin® 1827[38] and Alutin 51L[39] both from Castolin®, respectively) was found and preliminary tests showed good results for soldering process between 6000-aluminium series and stainless steel SS. Having chosen the aluminium for building the cell, the higher yield strength of Al 6061 turns this one the selected alloy. Giving priority to the cell mass, the issue of capillary soldering being solved and the aluminium presenting relatively good thermal conduction properties, an aluminium (Al 6061) cell was decided.

A finite elements analysis (FEA) software (COSMOS®) was used to validate the analytical determination of the minimum thickness of the cylindrical walls. For this simulation the aluminium 6061 was considered. This software was also used to determine the thickness of the cell lid.

The detailed the sizing of the fastening elements used to close the lid and maintaining it leak tight when subjected to a 50 bares of internal pressure at 40 K are presented in appendix A. For this effect, nine M3 stainless steel screws were used with the initial tightening torque between 400 – 460 N.mm. In this calculation the differential contraction of the fastening elements and the cell material (aluminium) was taken into account.

The final design of the multipurpose cell is presented in Figure 3-5. The total height of the cell is 50 mm (including the lid). The nine stainless steel screws and bolts are responsible for closing the lid as just described. At the bottom of the cylindrical walls a hole is drilled to sold the filling capillary tube. In the base of the cell, four threaded holes (M3) are available to couple it to the gas gap heat switch. The leak tightness of this cell is insured by an indium wire O-ring. Due to the malleability of the indium wire it can fill small imperfections creating an impervious boundary between two surfaces. A rectangular groove was designed in the lid to hold the indium wire. The body of the cell fits in this groove, compressing the indium wire to obtain a leak tight join. Three M3 threaded holes were added to the lid for helping its disassembly from the body of the cell. During the ESU operation, these holes are used to attach the heaters and thermometers.

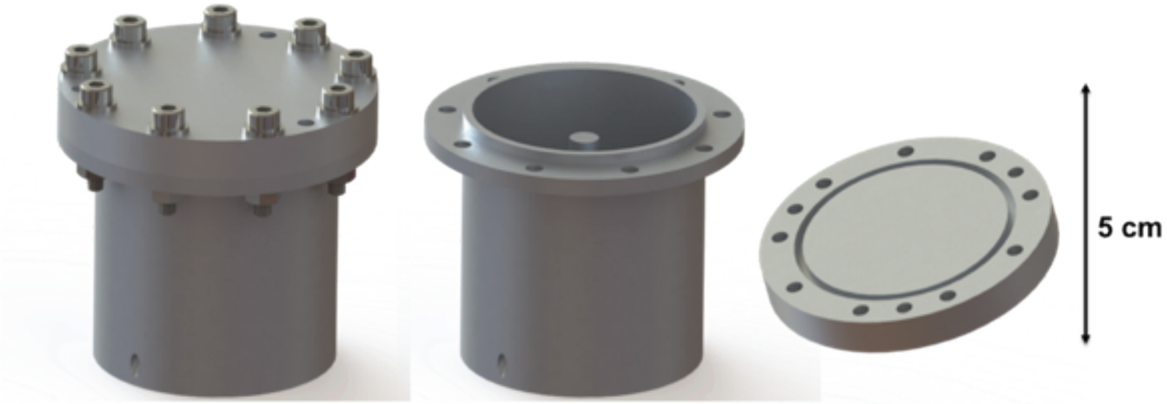

Figure 3-5 – Tri-dimensional design of the multipurpose cell. An O-ring indium wire is used to the cell sealing. The cylindrical walls and lid thickness are 1.5 mm and 7 mm, respectively. Total weight is 100 g.

A pin in the axis of the cell was designed with the objective to improve the temperature homogeneity in the cell. The cylindrical wall is 1.5 mm thick, thicker than the minimum required to withstand the 50 bar in order to improve the thermal conductance of the walls and the lid thickness is 7 mm. Those thicknesses were sized using a finite element analysis software (COSMOS®). The total weight of the cell is 100 g.

The difficulty in obtaining a leak-tight soldering for the capillary in aluminium led to a search for other solutions. By changing the material of the lid (copper or stainless steel) instead of having the venting exit on the bottom of the cell it could be put on the top of the lid. In this case the soldering process in copper or in the stainless steel would be easier and safer.

A copper lid with 4 mm thickness was considered in a preliminary FEA. In this simulation the initial tightening of the screws was considered. From the stress point of view, the maximum nominal stress values result smaller than the yield strength of copper (70 MPa) for the applied pressure load of 50 bar. But from the deformation point of view, the difference between the cell and the lid groove displacement could compromise the indium sealing. A thicker lid would then required but the density of copper compared to the aluminium results in a significantly heavier solution. Hereupon this solution was disregarded and the stainless steel (SS) was considered. Even reducing the thickness, a decrease of the lid displacement is obtained in the simulations by using the SS. But the poor thermal conductivity of the SS turns the use of the lid for coupling the heaters and the thermometers inadequate. The aluminium solution was then finally chosen offering the best compromise mass-thermal conductance.

The finite element analysis results using aluminium 7 mm thickness lid is represented in Figure 3-6. In this simulation a 450 N.mm tightening for the screws, a temperature of 300 K and 50 bar pressure load in the cell were considered. The maximum stress obtained in the lid is of the same order of the cylindrical walls (≈60 MPa). In the displacement point of view, the maximum occurs in the middle of the lid (35 μm). In the sealing groove zone the differential displacement can achieve a maximum of 10 μm. We “bet” that this displacement would be compensated by the indium malleability and by somehow self-sealing due to the design of this part.

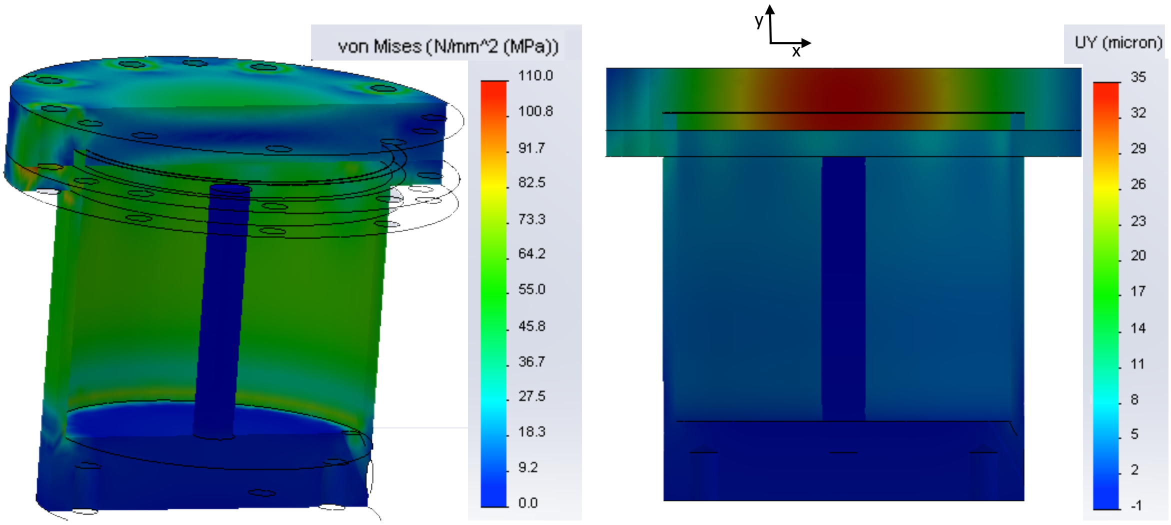

Figure 3-6 –Finite element analysis results: von Mises diagram and displacement in Y axis. The cell was pressurized with 50 bar and the initial tightening of 450 N.mm was considered in this simulation. Results obtained with COSMOS®.

The final drawings of this multipurpose cell are available in Appendix C. After the construction of the cell a stainless steel capillary tube with 2 mm of diameter was soldered to the bottom of the cylindrical walls with a soft solder and its flux adapted to SS-aluminium junction. Various attempts were necessary to obtain a leak tight soldering. Small porosities appeared in the interface zone, resulting sometimes in multiples leaks. Fortunately, despite of this difficulty, this cell was successfully used to test the liquid confinement in different porous materials and performed numerous ESU tests in the *temperature drift mode* and the *controlled temperature mode*.

During the tests, some leaks appeared in the capillary soldering and were immediately fixed. However, after some successfully soldering processes, due to unknown reasons, a leak tight soldering became impossible. Moreover, as it will be shown later, the temperature difference between the top and the bottom of the cell was significantly higher than expected high. These two reasons implied to design a new cell made in copper to solve these two problems simultaneously.

3.2.2 Copper cell

In order to avoid the problems explained in the last section, a new copper cell was designed and a light and functional solution was sought in order to avoid the rather heavy solution (thick lid + screws + indium sealing). We choose to design a 4.5 mm thick lid directly screwed on the cylindrical walls of the cell, the sealing being obtained by a soft soldering process at the junction of these two parts. A hole in the lower part of the cylindrical walls was drilled to connect the capillary, just like in the multipurpose cell. The final design of the copper cell is presented in Figure 3-7. Two platforms, one at the top and the other at the bottom, are used to attach the heaters and the thermometers. In addition, the top platform was used to mechanically decouple the cell from the structure while change the orientation of the cryocooler (described after in this section). Four holes in the base were made in order to couple the cell to the heat switch. A thin cylinder in the middle of the cell is used to enhance the dissipation of the applied power to the liquid and to obtain a better temperature homogeneity between the cell and the liquid.

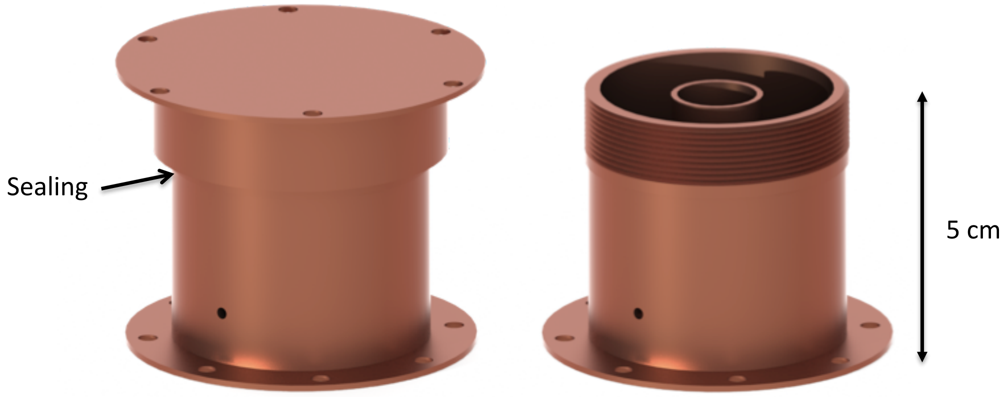

Figure 3-7 - Tri-dimensional design of the copper cell and respective screw cap. A soldering alloy is used to seal the cell along the marked zone. The cylindrical walls and the lid thickness are 2mm and 4.5 mm respectively. The capacity of the cell is 35 cm^3. The thread pitch is 1 mm over 10 mm

Based on the previous calculations, the minimum thickness to avoid any plastic deformation in the cylindrical walls is 1.4 mm. The use of 2 mm for the walls thickness was decided for safety.

The finite elements analysis was used to size the lid thickness. A simplified model was drawn for the simulations. Using a 4.5 mm lid the inlet pressure of 50 bar was simulated. The thread was not simulated and a perfect contact in this zone was defined to avoid any separation of the elements. The result of this simulation is presented in Figure 3-8. The mean stress obtained in the cylindrical walls is of the same order of the stress in the lid, ≈ 45 MPa. Only a superficial stress concentration is observed in the middle of the lid, ≈ 70 MPa (close to the yield strength of copper σ_{Yield}≈70 MPa), which is negligible because it is a superficial stress concentration. Recalling that this cell was sized to work at 50 bar whereas the working pressure of this cell will never exceed 25 bars, a safty factor of 2 was used. The maximum displacement obtained from the FEA in the aforementioned conditions is around 27 µm in Y axis. This value corresponds to a 0.01% of the diameter of the lid. By using a soft solder to maintain the cell leak tight, these deformations should not affect the sealing.

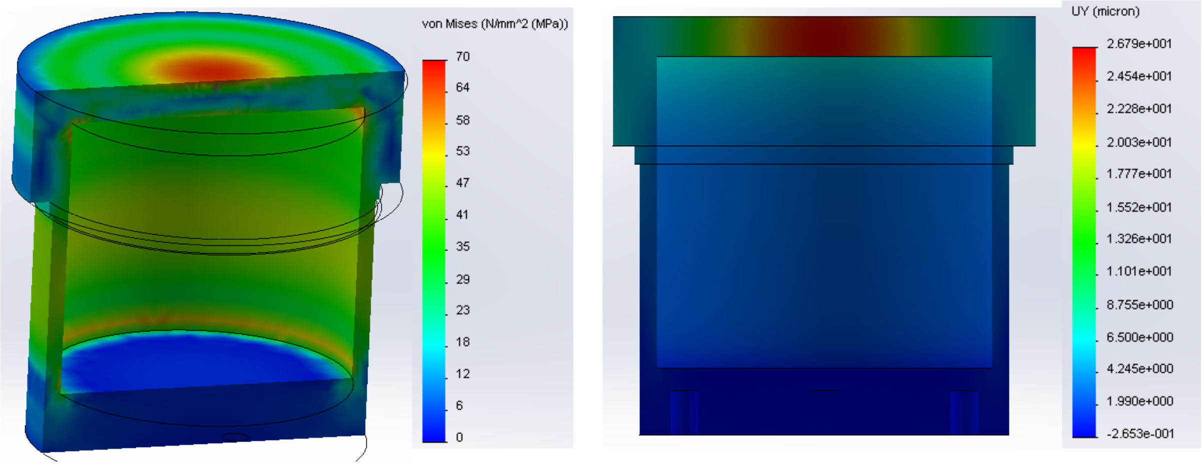

Figure 3-8 - Finite elements analysis results for the copper cell: von Mises diagram and displacement in Y axis. The cell was pressurized with 50 bar. The thread was not considered in this simulation. Results obtained with COSMOS®. The yield strength of the copper is ≈ 70 MPa.

The thread to hold the lid has a pitch p=1mm along H=10 mm length as previously described. The stress in the thread due to the pressure of 50 bar inside the cell can be estimated using Eq. 3.4 and the parameters defined in Figure 3-9:

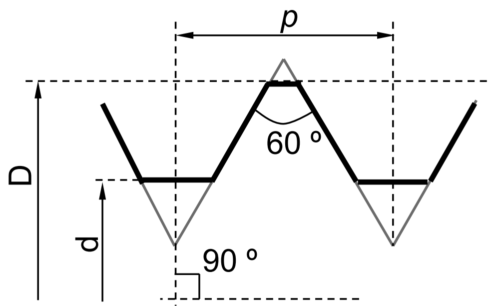

Figure 3-9 - scheme of the thread. The parameters used in the thread sizing.

The stress in the thread is given, based on the Eq. 3.4 and attending to the parameters of the Figure 3-9, by:

$$\sigma_{thread} = \frac{4Fp}{\pi H\left(D^2 - d^2\right)} \approx 17 \text{ MPa} \tag{3.4}$$

The estimated stress in the thread due to a pressure of 50 bar inside of the cell, $\sigma_{\text{thread}} \approx$ 17 MPa, is lower than the yield strength of the copper (σ_{copper} = 70 MPa). Moreover, a soft solder alloy (60% Sn-Pb 40%) was used to seal the cell at interface lid-cylindrical walls. By ensuring the migration of the solder along the thread, the solder could also help to the mechanical resistance of this part.

The total weight of this cell is 310 g, three times heavier than the aluminium previous cell while keeping the same inner volume of 35 cm^3. The drawings of this copper cell are available in Appendix D.

3.2.3 Power booster cell

For the ESU power booster mode a more compact cell was developed. In this mode the cell is directly coupled to the cold finger of the cryocooler to increase, for a short time, its cooling capacity. In this mode higher heat powers are sporadically used. The copper was chosen to maximize the thermal conductance of the cell. The successful way to insure leak-tighting described in the previous section was imported for the power booster cell: a threaded lid and a soft solder sealing process to make it leak-tight. Figure 3-10 displays a tri-dimensional design of the cell. This cell is 3 cm height and its inner volume of 12 cm^3 storing ≈400 J at 40 K when filled up with liquid neon. A small hole on the top of the lid is used to connect the capillary tube (2mm) connected to the expansion volume. Four holes in the base and in the top of the cell were drilled to couple the cell to the cold finger (in the base) and for other devices (on the top) like an intermediate flange. The 6 mm hole through the base of the cylindrical walls is for a 50 W cylindrical heater used to control the temperature of the cold finger.

The thread to hold the lid has a pitch p=1 mm along H=7 mm length instead of 10 mm used in the copper cell. Attending to Eq. 3.17 the stress in this thread continues far from the yield strength of copper.

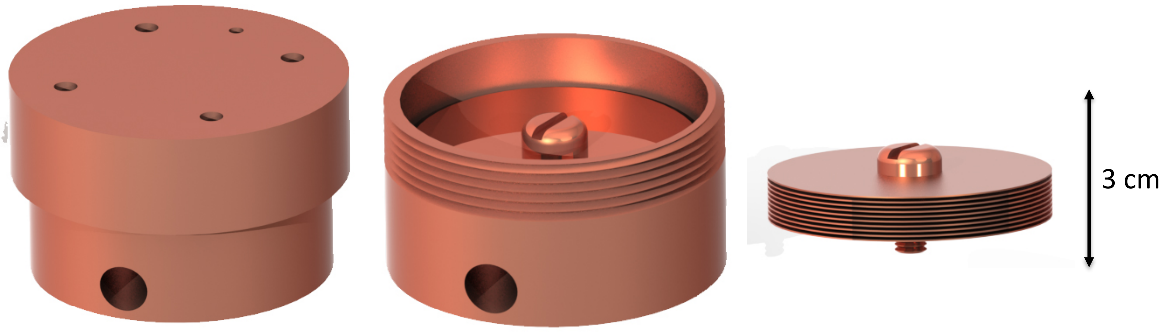

Figure 3-10 - Tri-dimensional design of the “power booster cell”. The inner volume of the cell is 12cm^3. The cylindrical walls and the lid thickness are 2mm and 4.5 mm respectively. The copper heat exchanger is composed by 10 circular plates (35 mm diameter and 300 µm of).

In this operational mode, heat powers in the range 10-15 W will be applied to characterize the ESU. In this case it is necessary to take in account the possibility to exceed the “critical heat flux”. The critical heat flux is the maximum heat flux admitted to avoid the formation of a gas film on the heated surface due to a very intense evaporation process. Such a continuous gas film result in a dramatic decrease of the efficiency of the heat transfer and then to huge overheating of the heated surface (Leidenfrost effect or boiling crisis). The critical heat flux is dependent on the pressure of the working fluid and is weakly dependent of the geometry of the heated surface[40]:

$$\frac{\dot{Q}}{A} = C h_{fg} \rho_v \left[\frac{\sigma g \left(\rho_L - \rho_v \right)}{\rho_v^2} \right]^{\frac{1}{4}} \qquad (3.5)$$

C represents a geometry constant (C=0.131 for large horizontal cylinders and spheres finite heated surfaces), h_{fg} the latent heat of vaporization, ρ_L and ρ_V the liquid and vapor densities and σ the surface tension. For neon at 40 K the critical heat flux is $\dot{Q}/A \approx 5$ x10^4 W/m^2. In the case of our cell, the maximum heat flux will be around 1.5 x10^4 W/m^2. Attending to this estimation, during our tests the maximum heat load used (15 W) is lower than the critical heat flux. However, in order to increase the thermal homogeneity between the cell and the liquid, a copper heat exchanger (HX) was built (Figure 3-10). This HX is composed by 10 circular 300 µm thickness plates and with a diameter almost equal to the inner diameter cell as shown in Figure 3-10. Small 500 µm thickness washers were used as spacers to separate the different plates. The plates and the washers are soldered to a copper screw fastened in the inner base of the cell,

A finite elements analysis was used to size the lid and wall thickness of this booster cell. In this case the lid is thicker (7 mm) than needed for pressure purposes only to allow 4 threaded holes to attach other devices. The base is also thicker in order to allow the heater cartridge introduction (6 mm diameter). The walls are 2.5 mm thick to promote a good thermal homogeneity between the top and the bottom of the cell. The thread was not simulated and a perfect contact in this zone was defined for computing. The sizing of this part was also considered by the estimation of the stress in the thread when subjected to an inner pressure of 50 bar (Eq. 3.17). The results of this analysis for the case of 50 bar pressure are presented in Figure 3-11.

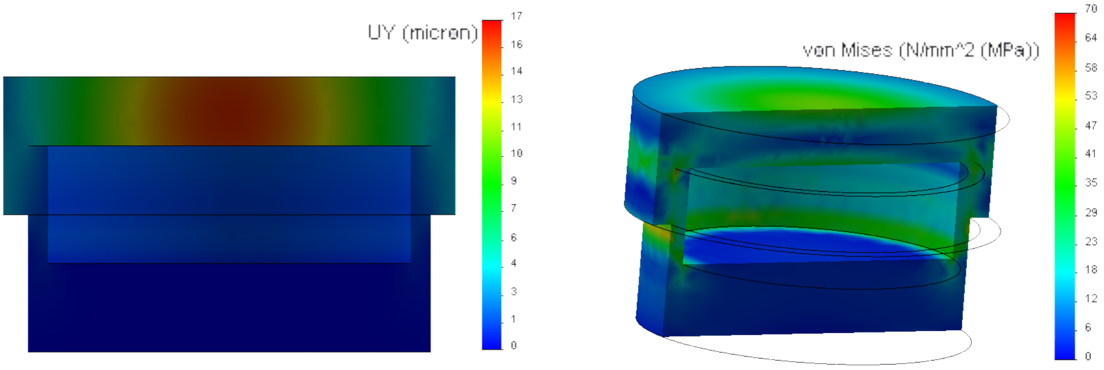

Figure 3-11 - Finite elements analysis results obtained with COSMOS® for the copper cell: displacement in Y axis and von Mises diagram for a pressurized with 50 bar cell. (The yield strength of the copper is ≈ 70 MPa).

The maximum stress in the lid and in the cylindrical walls is around 45 MPa, lower than the yield strength of copper. In this case, no stress concentration appears (like in the copper cell) on the top of the lid due to its higher thickness. The same reason explains the lower displacement in the Y axis.

The total weight of this cell is 245 g and the inner volume is 12 cm^3. The drawings of this “booster cell” are available in Appendix E.

3.3 Gas gap heat switch

A heat switch, responsible for the thermal coupling or decoupling of the enthalpy reservoir from the cold finger of the cryocooler, is a fundamental device in the ESU system for the ESU temperature drift mode and temperature controlled mode as well as for thermal characterization of the ESU performance. The heat switch used during this work is a Gas Gap Heat Switch type: in such a device, the absence of moving parts turns it ideal for use in space applications[31, 41]. Generally, this kind of heat switches is built upon two copper blocks separated by a thin gap and a thin stainless steel support shell (≈100 μm thickness) encloses the gas and sustains the two blocks separated (Figure 3-12). A small sorption pump can be used to manage the gas pressure in the gap between the two blocks to provide the different conduction states. The sorption pump is composed by activated charcoal. When the pump is cold, the charcoal adsorbs the gas leading to a very low pressure in the gap and then a poor conduction state (OFF state). This poor conduction state is defined by the conductance along the supporting shell. The good conduction state (ON state) is obtained by desorbing the gas between the two copper blocks while heating the pump. The quantitative knowledge of the adsorption properties of the gas–adsorbent system allows the conversion of ON/OFF pressures into pump temperatures[42].

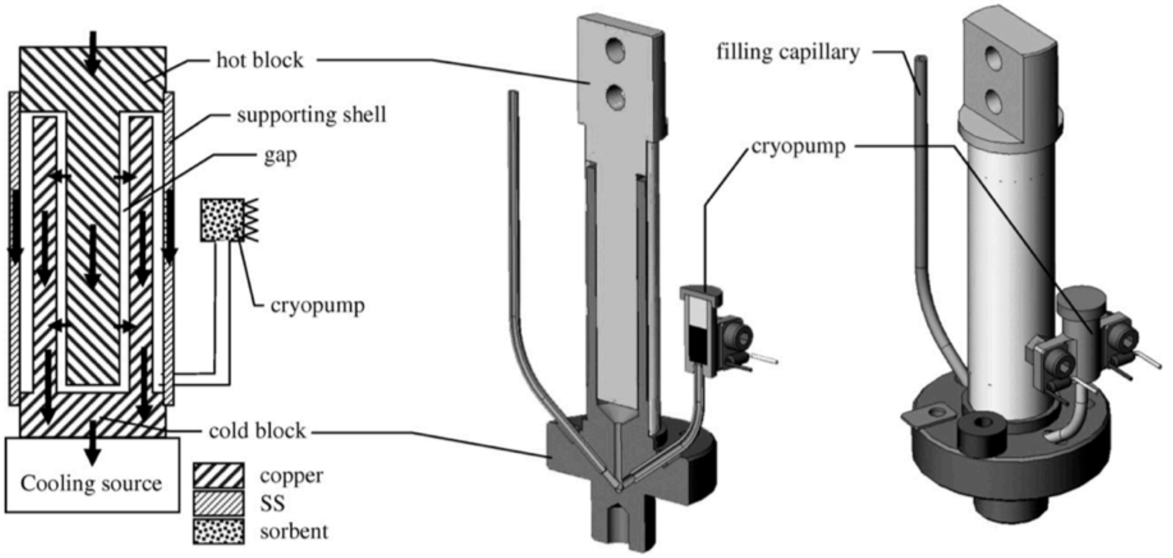

Figure 3-12 - scheme of a cylindrical gas gap heat switch[43]

A GGHS with two cylindrical blocks separated by a gap is schematized in Figure 3-12 [43]. This device was successfully used for other ESU applications[7-9].

The recycling time of the ESU is dependent of the ON conductance of the heat switch used. In order to decrease this recycling time, a different prototype, with higher ON conductance, was used [11, 44] and characterized. Two copper blocks with 5-6 parallel leaves spaced by a 100 μm gap compose this GGHS. Each copper leaf has ≈2 mm of thickness. To enclose the gas inside the device and sustain the two copper blocks a 100 μm thin stainless steel supporting shell is used. The OFF conductance is then dominated by the thermal conductance of this thin support. The stainless steel was chosen due to its appropriated mechanical properties to support the two blocks and due to its low thermal conductivity.

This model was developed, built and tested (without cryopump) during a master thesis [11] and Figure 3-13 (left) displays the two copper blocks with leaves and the thin shell before the welding process.

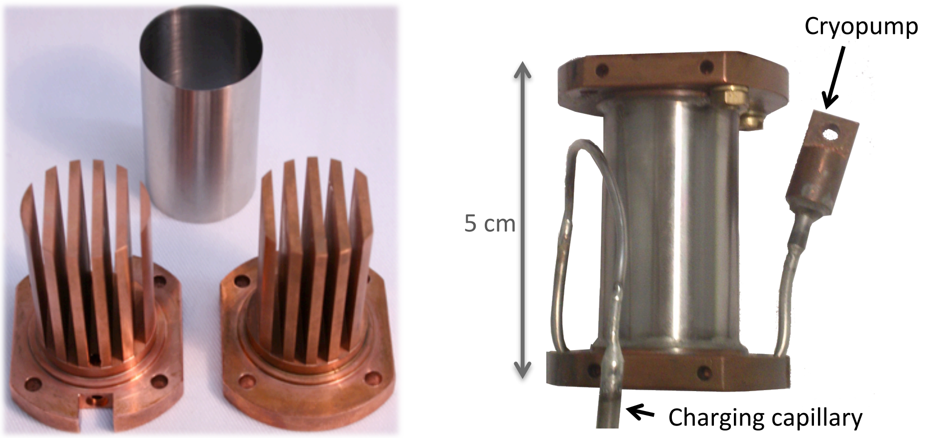

Figure 3-13 – Gas gap heat switch with leaves. The very thin stainless steel support shell encloses the gas inside the device and sustains the 2 blocks.

A small cryopump is responsible for the commutation between the ON and the OFF state. It is composed of a small amount of activated charcoal (~50 mg) placed in one miniature copper casing (Figure 3-13, right). This cryopump is connected to the switch through a thin stainless steel tube that also insures its cooling by thermal conduction. A small platinum resistor and a small heater are used to monitor and control the temperature. The gas and the activated charcoal of the cryopump were chosen according the required actuation temperatures (temperatures to have the ON and the OFF states). The choice of the gas, charcoal type and amount is reported in the next sections.

3.3.1 Conduction model

The states of the gas gap heat switches are driven by the heat transfer regime which is determined by the ratio between the mean free path (λ) of the gas molecules[43] (which is both pressure and temperature dependent) and the gap width ($\varDelta$). The maximum heat conductance (ON state) is obtained when the viscous regime is fully established ($\lambda << \varDelta$). This conduction state is pressure independent. For reaching the minimum heat conductance (OFF state) the molecular regime ($\lambda >> \varDelta$) should be obtained: in this regime, the heat transfer is linearly dependent of the pressure and, with a vanishing pressure, the device conduction decreases asymptotically down to a minimum corresponding to the stainless steel supporting shell conductance K_{ss}, which short-circuits the gas conduction.

The Eq. 3.6 and Eq. 3.7 give the effective conductance of fully developed molecular (K_m) and viscous (K_V) regimes[42] respectively (two extreme values of the effective conductance).

$$K_m = A\alpha \frac{\gamma+1}{\gamma-1}\sqrt{\frac{R}{8\pi MT}}P \qquad (3.6)$$

$$K_V = k(\bar{T})\frac{A}{\Delta} \tag{3.7}$$

Here $K = \dot{Q}/\Delta T$ ("effective conductance"), where $\dot{Q}$ represents the thermal power flowing along the GGHS and ΔT is the temperature difference between the two blocks; A is the surface area for the gas exchange, α is the accommodation factor, Δ is the gap width, $\gamma = C_p/C_v$ is the heat capacity ratio, M is the molar mass of the gas, R is the ideal gas constant, P is the pressure, and $k(\bar{T})$ is the gas conductivity at the average temperature. To determine the intermediate regime, the gas conductance is approximated as the harmonic sum of the molecular and viscous conductance in parallel with the shell, as shown on Eq. 3.8.

$$K_{eff} = \frac{1}{\left(1/K_m\right)+\left(1/K_V\right)} + K_{SS} \tag{3.8}$$

Where

$$K_{SS} = \frac{\dot{Q}_{SS}}{\Delta T} = \frac{1}{\Delta T}\frac{A_{SS}}{l_{SS}}\int_{T_{CB}}^{T_{CB}+\Delta T} k_{ss}\,dT \tag{3.9}$$

In Eq. 3.9 K_{ss}, A_{SS} and L_{SS} are the cross section area and length of the supporting shell respectively. Thanks to this model, the effective conductance K_{eff} is obtained as a function of gas pressure.

With the target temperature of 40 K for this GGHS operation, it was necessary to verify which gases could be adsorbed and desorbed in the switch's cryopump in this temperature range. Other requirement is to ensure that the gas does not condense at the operation temperature of the switch. In Figure 3-14, the shaded zone shows the operational range for each gas, which is limited by the sorption properties of the charcoals. For 40 K only neon and hydrogen can be used and the higher thermal conductivity of the hydrogen turns it to the best choice.

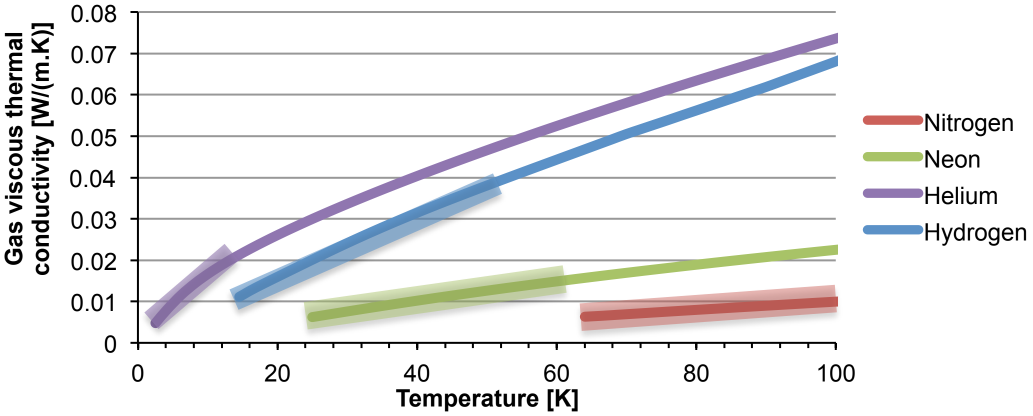

Figure 3-14 – Gas viscous thermal conductivity. The shaded zones represent the workable temperature ranges for this device with each gas.

Using predetermined sorption properties of the charcoals[42] it is possible to obtain the cryopump's temperature from the gas pressure. The next equation of state models the relation between the pressure inside the device (P), the temperature of charcoal (T) and the amount of adsorbed gas per amount of adsorbent (Q).

$$\ln P = \left[a - b\ln(Q+c)\right]\left(1-\frac{1}{T}\right) + e + \ln Q + \ln 100 \quad ^{[42]} \tag{3.10}$$

The constants *a, b, c, d, e* were obtained from our adsorption data measurements and are dependent of the type of charcoal and the gas[42]. Combining the models, Eq. 3.8 and Eq. 3.10, the mass of charcoal and the volumes of the switch, it is possible to obtain the effective conductance of heat switch as function of the cryopump temperature. This model was used to determine the best choice about the charcoal type and mass to use in the cryopump of the switch to operate in the liquid neon ESU between 35 K and 43 K.

The cryopump being connected to the switch on the ESU side, its minimum temperature is the ESU temperature, and then an OFF state maintained at least up to 45 K is required. Preliminary calculations, using the previous model, showed that obtaining the OFF state at 45 K is a limit situation. This way the charcoals with more adsorption capability at this temperature range are selected. The charcoal B and charcoal C (according to the denomination of [42]) were chosen for a short list. The predicted behaviour of these two types of charcoal is shown in Figure 3-24, using 100 mbar and 500 mbar of hydrogen and 45 mg of each charcoal. The charging pressure of 100 mbar and the Charcoal type C allow the OFF state up to ≈ 43 K and this configuration seems to be the best choice. Choosing a lower pressure would help to obtain the OFF state for higher T but would not permit a fully developed viscous regime (ON state) in this temperature range and then would limit the switch conductance in the ON state.

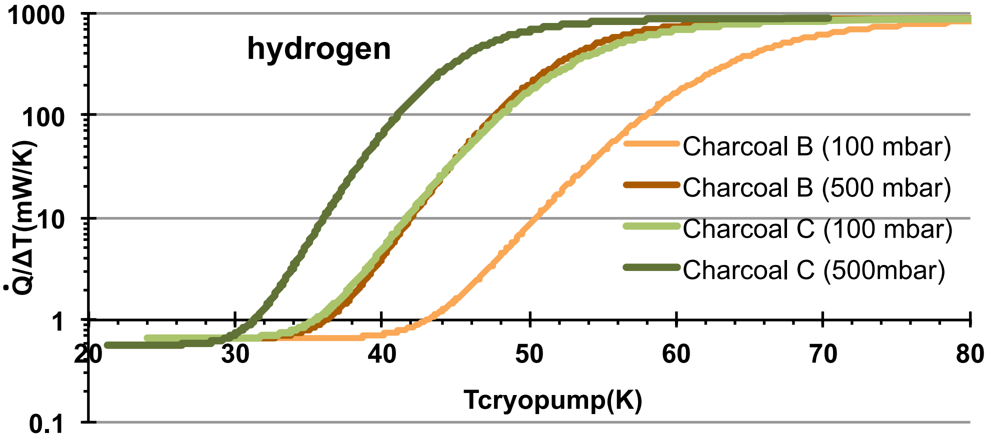

Figure 3-15 - Comparison between the calculated conductance for the two types of charcoals as function of the cryopump temperature. An equal amount of charcoal B and C was taken into account (m=45 mg). Let us note that increasing the mass helps to increase the OFF temperature but the On temperature is going to be affected too.

Based in this model, the charcoal B evidences advantages for this application and was chosen.

3.3.2 Thermal characterization of GGHS

In order to verify the model and our choice, the gas gap heat switch was thermally characterized with two different types of charcoals, type B and C. To obtain the switch thermal conductance ($\dot{Q}/\Delta T$), a copper block of the switch (cold block) was coupled to a cold finger of the cryocooler. Fixing the temperature of the cold finger at 25 K, a heat power ($\dot{Q}$) was applied in the other copper block (hot block), waiting for its temperature equilibrium. Doing this for different temperatures on the cryopump allows obtaining the conductance of the heat switch as a function of the cryopump's temperature. When the conductance is very low (OFF state) the stabilization time can be very long: the thermal stabilization can take up to 24 hours. To avoid such long stabilization times, we chose to use a dynamic method[11] for measuring the low conductance. In this method the cold block of the heat switch is fixed at constant temperature and the hot block is heated up to ≈ 60 K and let cool down spontaneously without applying any heating power, this cooling down being obtained thanks to the heat power flowing along the GGHS. Knowing the heat capacity of the hot block C (the only part that is cooling down, in this model) and the temperature change rate $\dot{T}$, we can obtain the heat power flowing along the switch $\dot{Q}$:

$$\dot{Q} = C\dot{T} \tag{3.11}$$

and then calculating the $\dot{Q}/\Delta T$ changing the temperature of the cryopump during the cooling down turns possible to measure $\dot{Q}/\Delta T$ versus $T_{cryopump}$. With this method the lower conductances are quickly obtained as a function of the cryopump temperature. For high conductance states, the stabilization times being short, the static method previously described was used.

The same amount of 45 mg of the each charcoal (B and C type) was inserted in the cryopump's body. Figure 3-17 shows the comparison between the experimental and calculated values for both charcoals. Three charging pressures (100 mbar, 500 mbar, 1000 mbar) of H_2 are shown.

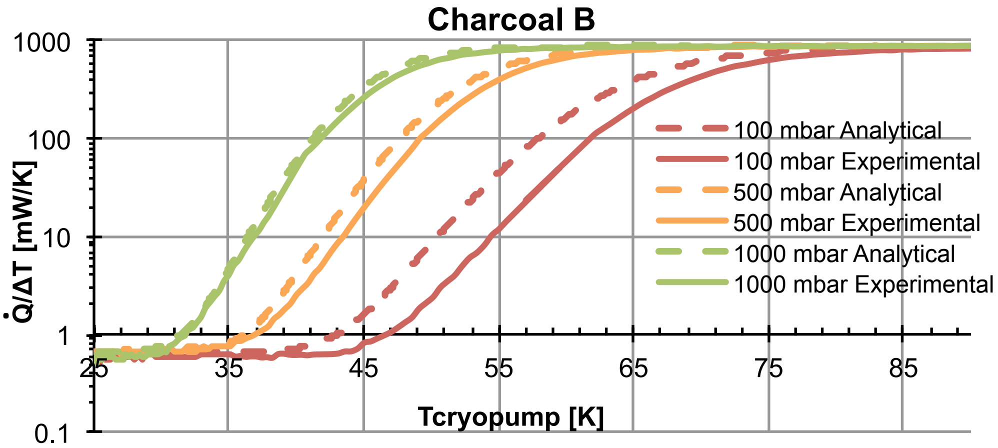

Figure 3-16 - H_2 characterization of the GGHS conductance with leaves for different filling pressures and 45 mg of the "charcoal B". The base temperature is 25 K. The dashed curves correspond to the analytical results.

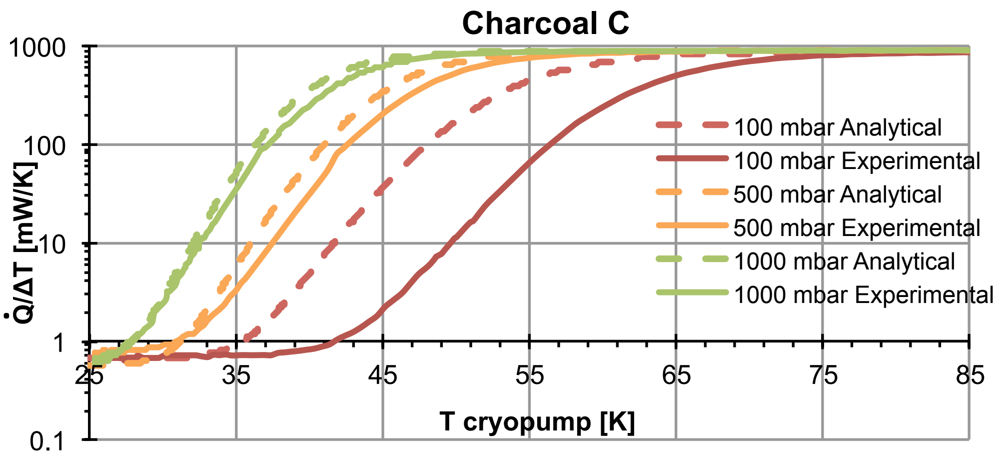

Figure 3-17 - H_2 characterization of the GGHS conductance with leaves for different filling pressures 45 mg of the “charcoal C”. The base temperature is 25 K.

The model leads to a good agreement between experimental and calculated results for high filling pressure. However, the accuracy of the calculated results decreases for lower filling pressures, but the model used to predict the effective conductance still gives useful approximation. As predicted in the preliminary calculations, the charcoal B takes advantage according to the requirements for the high turning off cryopump’s temperature. The ON and OFF conductance’s obtained were 900 mW/K and 0.8 mW/K, and, as expected, these two values are independent of the charging pressure and the charcoal, depending only of the switch geometry, on the supporting shell and H_2 conductivity. For this present work the charcoal B was chosen. With this charcoal and using a charging pressure of 100 mbar of hydrogen, the OFF state is obtained for cryopump temperatures lower than 45 K and the ON state for higher than 80 K. With this temperature range, with the cryopump thermalized in the ESU side, it is possible to maintain the OFF state during the ESU mode (38 K – 43 K).

3.4 Gravity insensitive system

The target application of this liquid neon energy storage unit being the integration in a satellite to cooling infrared sensors in the 40 K range, its capability to operate in a microgravity environment is required. On earth, a way to test this feature is to prove that the ESU works independently of the gravity direction. As described previously, a porous material will be used to ensure the confinement of the liquid neon inside of the cell during the ESU operation. Different porous materials were tested in order to check their capability to confine the liquid inside of the cell. A stand was designed to allow the changing of the cryocooler orientation relatively to the gravity while testing the system’s performance as function of this orientation.

3.4.1 Orientable stand

The system allowing to change the orientation of the cryocooler tilting is shown in Figure 3-18. The main body is made of 10 cm wide square steel tube. The stand is 90 cm tall and 80 cm wide. Two stainless steel disks, with 20 cm of diameter and 2 cm thick each, enable the rotation of the cryocooler around a stainless steel thick shaft. One of the disks is fixed on the body of the stand and the other one holds the cryocooler. Sixteen holes in the stand disk allow steps of 22.5º from 0º to 360º.

The cryocooler itself is fixed in a rectangular aluminium base. This base is fastened to the disk through a stainless steel supporting frame, as shown on the close-up of the rotating part in Figure 3-18.

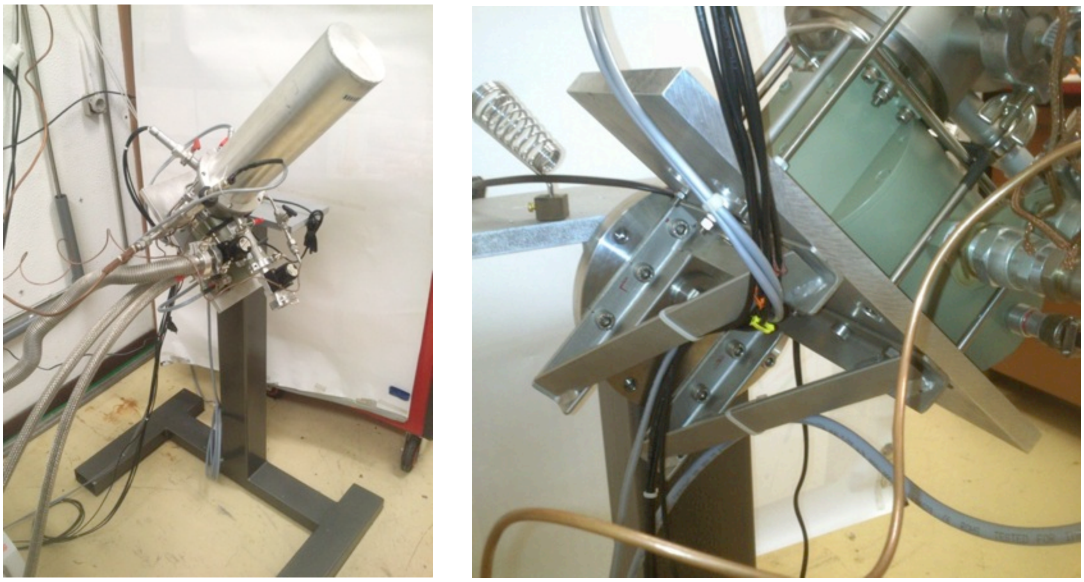

Figure 3-18 – Overall view of the rotating stand and close-up of the rotating part.

The entire stand was manufactured in the physics department workshop. A flexible vacuum bellow enabled the orientation changing without disconnecting the vacuum pump from the vacuum chamber. A copper tube (ø = 6 mm), coil shaped and flexible enough to allow deformation, makes the connection between the expansion volume and the cryocooler. A similar system was used for the 2 mm copper tube used to supply gas to the heat switch.

3.4.2 Tilting structure

Tilting the cryocooler with the gas gap heat switch and the cold cell directly coupled to the cold finger could be not safe: the torque applied to the heat switch due to the mass cell in case of working in a 90º position (Figure 3-19) could damage it by excessive efforts on the thin 100 μm stainless steel supporting shell. Adding to this torque, the heat switch is subjected to vibrations because the cryocooler is working. This two reasons lead to the necessity of a structure avoiding these efforts.

Moreover, the torque applied on the own cryocooler tubes when all the system is working horizontally by the heat switch and cell (total mass ≈ 500 g)) could be non-safe, inducing irreversible tube bending (Note: lacking of manufacture's information lead to the decision of not taking the risk).

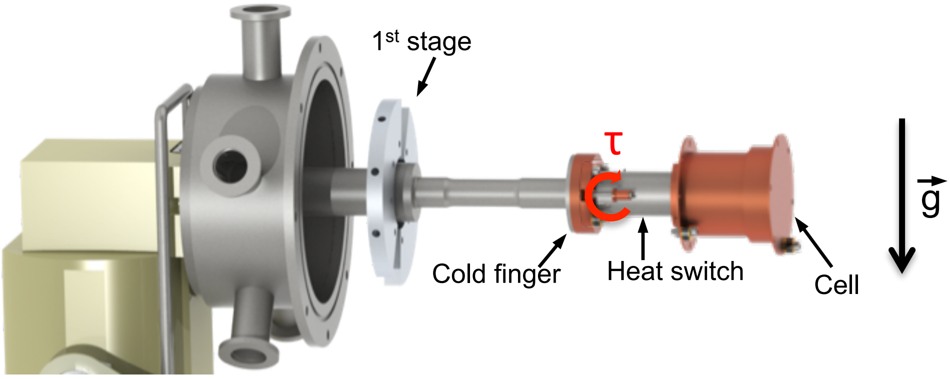

Figure 3-19 - Scheme of the assembly of the gas gap heat switch and the cell in the cold finger of the cryocooler at the horizontal position.

To reduce the stress in the heat switch it was decided to mechanically decouple it from the cold finger. For this decoupling an auxiliary structure schematized in Figure 3-20 was mounted. Three carbon fibre tubes (inner/outer diameter: 5 mm/6 mm) and two G10 fiberglass rings compose this structure. These two materials were chosen due to their good mechanical properties and low thermal conductivity. To thermally connect the heat switch to the cold finger a flexible copper thermal strap is used. Even with some displacement in whole structure (heat switch, cell and the two G10 rings) in relation to the cold finger, the behaviour of this set (heat switch, cell and the two G10 rings) is like a rigid body. Some displacement of this set is allowed without a significant stress on the heat switch.

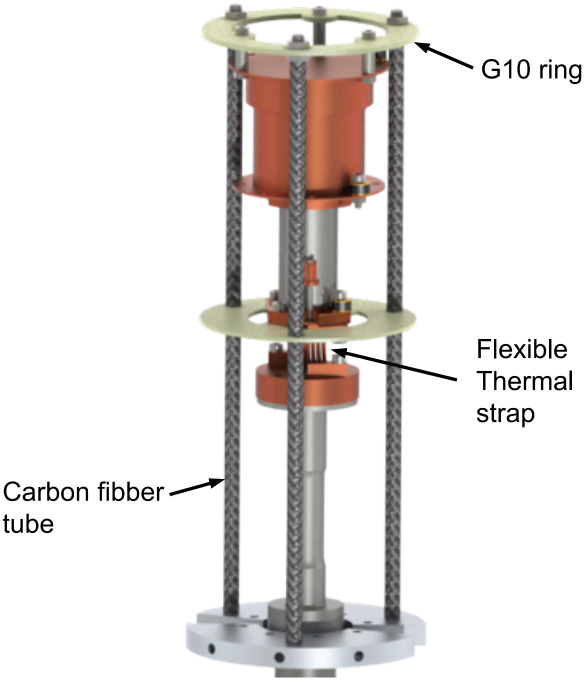

Figure 3-20 – Tridimensional drawing of structure to allow the mechanical decoupling of the heat switch from the cold finger of the cryocooler.

In this solution all the weight of the heat switch, cell and structure is supported by the 1st stage of the cryocooler. According to the manufacturer, a ≈ 60 N perpendicular force is allowed on this stage if no load is applied on the cold finger (Figure 3-21). The total weight of our set (5 N) is applied far from the cryocooler base.

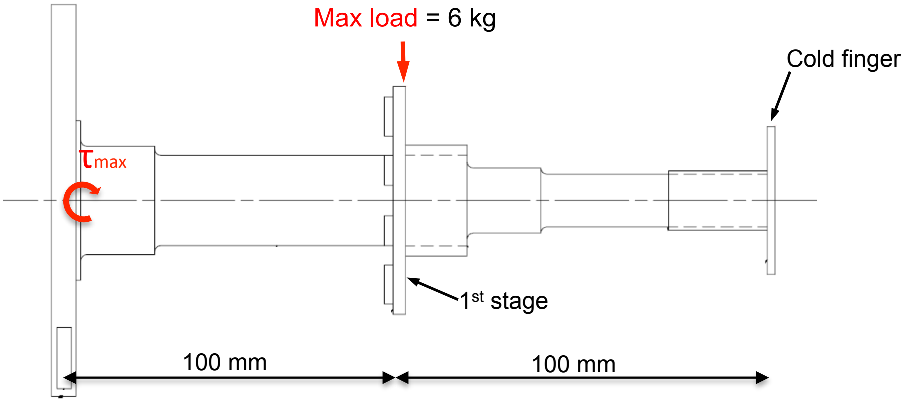

Figure 3-21 - Cryocooler manufacture requirements about the load in each stage.

Using the manufacturer's requirements it is possible to calculate the maximum torque that the cryocooler base can be subjected τ_{max} :

$$\tau_{\max} = d \times F = 100 \times 60 = 6000 \text{ N.mm} \tag{3.12}$$

The structure is connected to the 1st stage of the cryocooler. The length of the structure is 120 mm. The torque in the 1st stage due to the structure $\tau_{structure}$ is then:

$$\tau_{\max} = d \times F = (100 + 120) \times 5 = 1100 \text{ N.mm} \tag{3.13}$$

The torque in the cryocooler base due to the structure is then much lower than the maximum on indicated by the cryocooler manufacturer. In this point of view the structure can be supported by the 1st stage of the cryocooler.

The natural frequency of the auxiliary structure with the heat switch and the cell needs to be taken into account. If this resonance frequency is very close to the working frequency of the cryocooler, the structure can start to oscillate with huge amplitude (resonance). The resonance frequency calculation is shown in Appendix B, where the value found was 44 Hz, much higher than the ≈ 3 Hz of the working cryocooler.

A finite elements analysis result of our system when the structure is subjected to the gravitational force is depicted in Figure 3-22. The cylinder simulates the heat switch and the cell with the total mass of 0.5 kg. The results of the figure are amplified in order to easily have an idea of how the structure deforms.

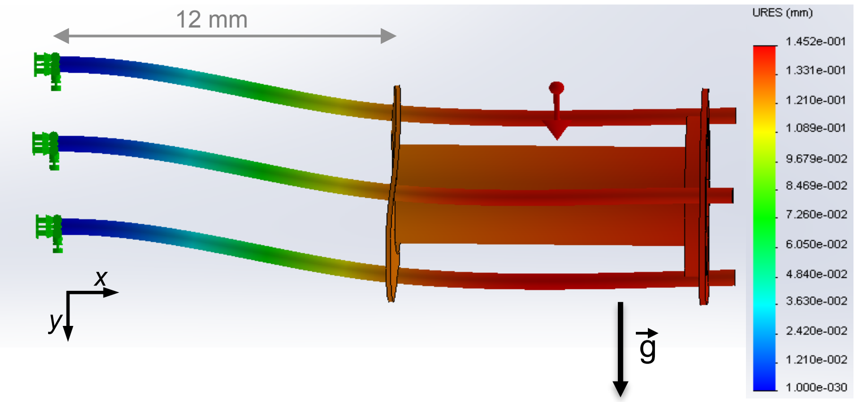

Figure 3-22 - Amplified deformation result of the displacement in y axis due to the gravity. The maximum displacement is 0.14 mm. The result was obtained in COSMOS®.

The maximum displacement given by this analysis is $y_{fCOSMOS}$= 0.14 mm. This value is very close to the calculated displacement y=0.13 mm (Appendix B).

Beyond the confirmation of how the structure is going to deform, this finite elements analysis validate our considerations in the displacement estimation. This movement correspond to the natural frequency of our structure f_{reso}= 44 Hz (calculated value).

Using an accelerometer, the natural frequency of the structure was obtained experimentally. For this propose a tri-axial accelerometer from PLUX (wireless biosignals SA)® was used. This accelerometer was installed in the top of the structure. In order to determine its natural frequency, a small shock was applied to the structure and, through the oscillations pattern (Figure 3-23), the resonance frequency is obtained using a Fast Fourier Transform algorithm. The result is shown in Figure 3-24.

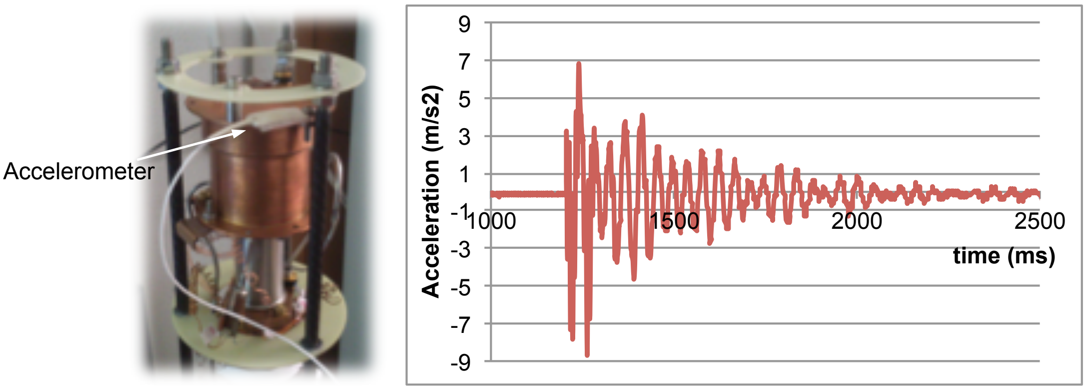

Figure 3-23 - Picture of the accelerometer placed on the top of the structure. Plot of the acceleration dumping after the small blow on the top of the structure.

With the Fast Fourier Transform of this time dependent signal (Figure 3-23), the frequency components of the signal were obtained. This result is shown in Figure 3-24.

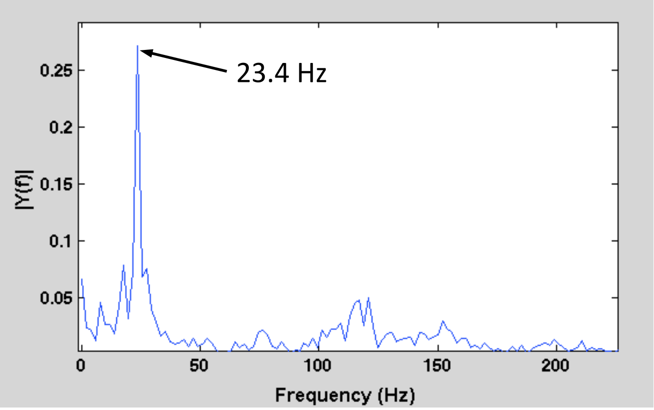

Figure 3-24 - Fast Fourier Transform of the oscillation damping. The main frequency is 23.4 Hz.

The resonance frequency obtained in this test was f_{reso}= 23.4 Hz. This result is the half of the calculated resonance frequency 44 Hz, but there are many factors that may explain this difference. These vibration tests were performed with the structure coupled on the 1st stage of the cryocooler and the measured resonance frequency corresponds to the resonant frequency of the total system (1st stage of the cryocooler + carbon fibre structure + copper braids) while the calculated 44 Hz considered a clamping carbon fibre structure as shown in the Figure 3-22. Moreover, factors like the mechanical properties of the carbon fibre are strongly dependent of the arrangement of the fibres. In these calculations, the G10 rings were considered as a perfectly rigid body. But in fact the Young modulus of this material is very low, decreasing in this geometry the resonance frequency of the structure.

Despite of this result, the working frequency of the cryocooler ≈ 3 Hz is much lower than the f_{reso}= 23.4 Hz obtained for the set of 1st stage of the cooler and structure and we can reasonably consider that the working cryocooler will not induce a high vibration level on the low temperature cell able to distort our experimental results.

Structure thermal performance

To use this structure, some thermal requirements must be met. The main one is to avoid a thermal short circuit of the gas gap heat switch when it is in the OFF state. Carbon fibre tubes and G10 fibreglass, low thermal conductivity materials, compose this structure in order to decrease the heat losses through it.

This structure thermally connects the 1st stage to the cold block of the heat switch (Figure 3-25) (cold finger) through 3 tubes of carbon fibre. The prolongation of these same 3 tubes links the cold block to the low temperature cell (figure 3-26) creating a new heat path in parallel with the supporting shell. In Figure 3-25, a scheme of the temperatures distribution along this the structure during the ESU operation is presented, with the heat switch on the OFF state. Despite the G10 very low thermal conductivity, the thermal conductance of the G10 ring is very high when compared with the carbon fibre due to its geometry (short length, relatively high cross section). For this reason, the G10 can be considered as a short circuit and an isothermal part in figure 3-28. For the thermal analysis, the carbon fibre tubes were divided in two different zones (A and B). $K_{CF\text{-}A}$ represents the conductance of three parallel carbon tubes between the 1st stage and the first G10 ring (corresponding to the hot block of the switch). The $K_{CF\text{-}B}$ represents the conductance of the three parallel carbon tubes between the first and the second G10 rings.

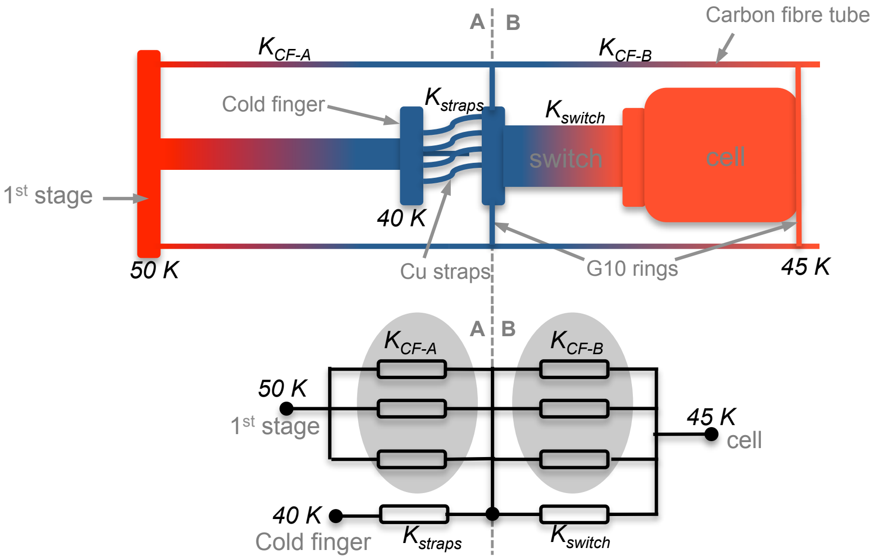

Figure 3-25 –Representation of the structure thermal design using thermal resistances.

As described in the beginning of the chapter the most important thermal requirement is to avoid the short circuit of the heat switch when it is in the OFF state, the state of very low thermal conductance. To satisfy this requirement it is necessary that the conductance of the three carbon fibre tubes in the zone B be much lower than the conductance of the gas gap heat switch ($K_{CF\_B} << K_{switch}$). The OFF switch conductance in the 40 K range is $K_{switch} \approx 1$ mW/K. Considering the cross section of each tube ($s \approx 8.6$ mm^2), L=100 mm the length of the tube and the conductivity of carbon fibre in the 40 K range ($k(40\ K) \approx 0.25$ W/(mK) [45]), the conductance of the three carbon tubes in zone B, $K_{CF\text{-}B}$ is:

$$K_{CF-B} = 3\frac{k(40K)s}{L} = 0.07 \text{ mW/K} \tag{3.14}$$

The conductance of the tubes is $K_{CF\text{-}B}$ = 0.07 mW/K, ≈10% of the heat switch conductance, and then can be considered as acceptable and this way this thermal requirement was satisfied.

In zone A, the three carbon tubes, also with $L \approx 100$ mm, connect the 1st stage ($T \approx 50$ K) with the cold block (($T \approx 50$ K). Even with the increase of the conductivity of the carbon fibre at 50 K (k(50 K)=0.35 W/mK [45]) the maximum conductance of the tubes is $K_{CF\text{-}A}$ = 0.1 mW/K. With the 1st stage at 50 K and the cold finger at 40 K this means that 1 mW goes to the cold finger from the 1st stage, which is completely negligible in regard to the cooling power of the cryocooler (4.5 W at 40 K).

During the recycling phase of the ESU, when all the available cooling power is necessary to condense the neon in the cell, the recycling time will dependent on the available cooling power. In this state, the conductance of the GGHS is $K_{\text{Switch-ON}}$ = 1 W/K. For the mechanical decoupling of the heat switch and the cell from the cryocooler, it was necessary to use flexible copper thermal straps to this thermal coupling, which acts as a thermal resistance in series with the switch. Considering the reduced available space between the heat switch and the cold finger, two thermal straps made of copper multi-wired cables were used. Each cable has around 400 thin wires with 70 µm. Each thermal strap is composed by six of these multi-wired cables, as it is shown in Figure 3-26. The cables are fixed, with a soft soldering alloy, in small holes of the copper pieces.

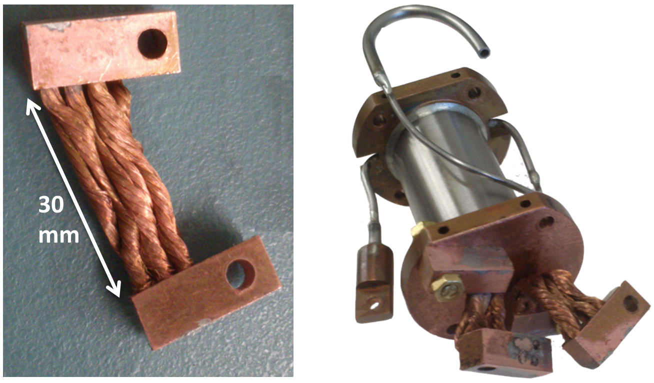

Figure 3-26 - Copper thermal strap. The two thermal straps coupled in the gas gap heat switch.

The length of these straps is ≈ 30 mm. With this geometry the total thermal conductance of the two thermal straps is 0.66 W/K. This way the total conductance K_{total} is given by:

$$\frac{1}{K_{total}} = \frac{1}{K_{straps}} + \frac{1}{K_{switch-ON}} \leftrightarrow K_{total} = 0.4 \text{ W/K} \tag{3.15}$$

instead of the previous value $K_{switch\text{-}ON}$ = 1 W/K for the directly coupled switch.

After the implementation in the structure, the conductance of the straps was measured to be 0.5 W/K, about 24% less than the calculated value of 0.66 W/K. The interface copper – soft soldering alloy in the ends of the thermal strap can decrease the overall conductance and may be in the origin of this slight discrepancy.

3.4.3 Porous materials

As described previously in section 2.4, an objective of this work is to turn the energy storage unit gravity insensitive in order to enable its operation in a microgravity environment. One possible solution is to use a porous material inside the cell to confine the liquid through the capillary forces. On a ground demonstration it is necessary to ensure the liquid confinement in the cell in any system orientation without performance degradation.

The tests in the porous materials are described in this section and also presented the results of its capability to confine the liquid. Despite of the target fluid being neon at 40 K, tests at other temperature ranges and also using helium for the different porous materials were performed in order to a better quantification and understanding of the capillarity effect in the porous materials tested.

In section 2.4 some predictions of the porous size for the ESU temperature range (38 K - 43 K) were performed. In the case of a completely filled cell, to confine all the amount of liquid neon (35 cm^3) we predict a porous material with a quite small pore size (< 5 μm). Such small size is due to the vanishing surface tension of the neon when close to the critical point (44.5 K).

The alumina ceramic foams available have a minimum of 20 μm (estimated value) of porous size. Despite of the predictions some experiments to test the capability of the ceramic foams to confine the liquid neon inside the cell were performed in order to confirm the model used to calculate it. For the tests, the ceramics P160 and P502 (RATH®) [46] with the mean porous size of ≈60 μm and ≈ 20 μm, respectively, were chosen. These ceramics present a high level of porosity, ≈ 90% of void volume. Their densities are 340 kg/m^3 and 500 kg/m^3, respectively.

The tests on the porous materials started at the beginning of this work, before designing the liquid neon ESU system. Due to this reason, the first tests of the porous materials to confine the liquid neon were performed in the existing liquid nitrogen ESU system[29]. With a similar working principle as the present neon ESU, this system was developed to take advantage of the latent heat of the liquid nitrogen to store 3600 J in the 60 K – 80 K range (described in section 1.2.2). In a quick description, the system is composed by a 35 cm^3, 34 mm height, cold cell and a 24 L expansion volume (Figure 3-27). To confine the liquid nitrogen inside the cell, the ceramic P160 with ≈ 60 μm (estimated value, see section 2.4) of mean porous size was used. For liquid nitrogen this pore size was enough to ensure that during the ESU operation all the amount of liquid remains inside the cell. Due to technical reasons the maximum pressure in this ESU system is 2 bar, limiting the working temperature with neon to a maximum temperature of 30 K.

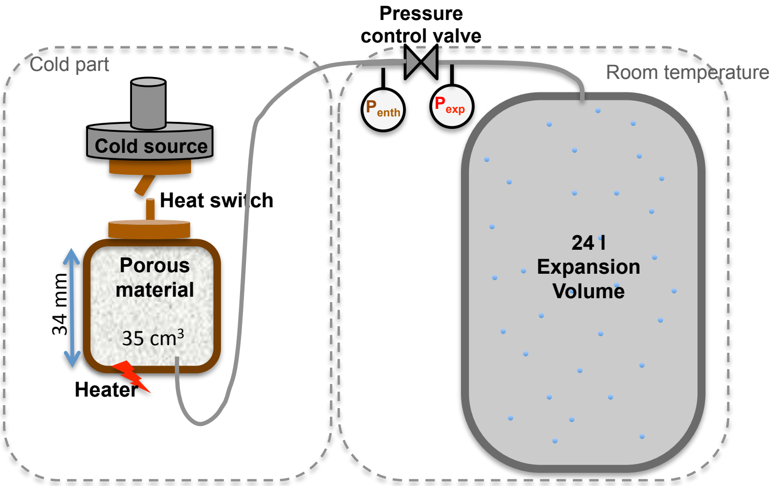

Figure 3-27 - Scheme of the experimental apparatus to test the porous materials.

As schematized in Figure 3-27 the capillary tube is used to connect the cell with the expansion volume. This tube is placed in the bottom of the cell to detect if the liquid is expelled through the capillary tube when heat is applied on the cell (ESU mode). This configuration is the worst case scenario, because the capillary forces need to win the gravity in order to avoid losing any liquid through the capillary tube. Figure 3-28 displays a picture of the cell used to characterize the porous materials with the ceramic P160 inside. The capillary tube is connected in the middle of the lid that is placed at the bottom of the cell. The pressure control valve used for the *ESU temperature controlled mode* is a solenoid valve.

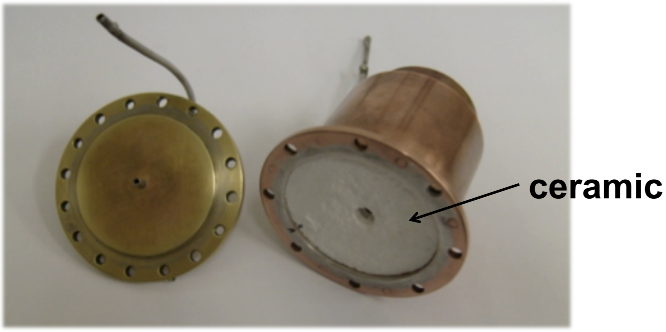

Figure 3-28 – Picture of the copper cell used to test the capability of the porous materials to confine the liquid inside of the cell. In this configuration the lid is placed on the bottom of the cell and the tube is connected in the centre of the lid.

The experiments performed to test the liquid confinement are done through a normal ESU experiment. The neon vapor flow measured at room temperature during the evaporation in the ESU mode gives information of any liquid exiting through the tube. The *temperature controlled mode* was chosen to test the capability of the porous materials. The advantage of using this mode is the possibility to choose precisely at what temperature the experiment is done. After a complete pre-cooling, the control valve is closed and with the cell completely (or almost completely) full of liquid at the controlled temperature.

As an example, an ESU temperature controlled mode experiment with neon at 30 K is shown in Figure 3-29. The red line represents the cell temperature and the black one the temperature of the liquid/vapour. This liquid/vapor temperature is calculated through the saturation pressure measurement at room temperature upstream of the valve. The liquid % represents the volumic filling ratio of liquid inside of the cell (100 % = cell full of liquid).

The heat power applied during the experiment shown in Figure 3-29 was 0.5 W. After the precooling, at 25 K, the valve was set to control at 2 bar (30 K). At the beginning, with the valve closed, a small amount of evaporation corresponds to a rapid pressure increase in the cell and consequently a fast temperature increase. When the pressure in the cell achieves the setpoint pressure, the valve starts to ON/OFF control and, if all works correctly, the temperature remains constant. However, in the displayed results, at the beginning of the ESU mode (shaded area, $t \approx 12$ min), the valve cannot control the temperature at 30 K like in the middle of the experiment. The lower graph of Figure 3-29 explains more clearly what happened during this phase. In this figure the flow across the valve (green line) is plotted, the flow being obtained from the measurement of the pressure versus the time in the expansion volume. The red line represents the maximum allowed flow through the valve, limited by the size of the orifice and the pressure differential in the valve (data obtained from the manufacturer, see next section). When this limit is reached, the valve cannot control the pressure and then the pressure and the temperature increases in the cell (12 min < t < 20 min). The instabilities occurring during those first minutes mean that some liquid has left the cell and evaporates in the capillary, resulting in a very large increase of the flow. For t > 20 min a constant temperature has been achieved and a flow of ≈ 450 cm^3/s is obtained, this value corresponding quite well with the latent heat of neon at 30 K (90 J/cm^3). Achieving the expected flow means that only evaporated neon exits from the cell. In the liquid % data is also observed an increase of the decreasing rate in the first minutes (12 min < t < 20 min). After that, when only the evaporated neon exits the cell, the rate of liquid evaporation decreases turning constant during the remaining temperature controlled mode. We consider that from this point on, the porous material can confine all the liquid avoiding any liquid losses.

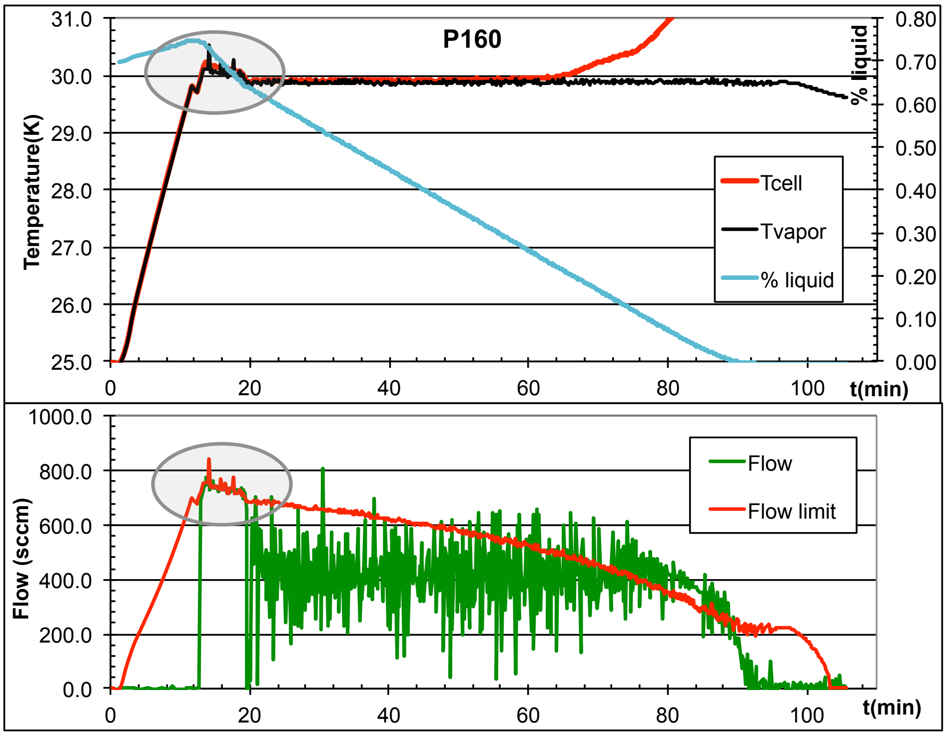

Figure 3-29 - Typical experiment to detect if any liquid exits through the capillary tube using the ceramic P160. Was used a 24 l expansion volume. The initial pressure is 2 bar of neon and the control temperature is 30 K. The heat power applied was 0.5 W.

The liquid volume ratio when the flow stabilizes indicates the maximum amount of liquid that the porous material (P160, in this case) can confine inside the cell at this temperature, called liquid threshold. In this example, 64% of liquid is the amount that the ceramic can confine without letting escape any liquid of the cell. Doing such tests for different temperatures, the liquid threshold as function of the temperature was obtained.

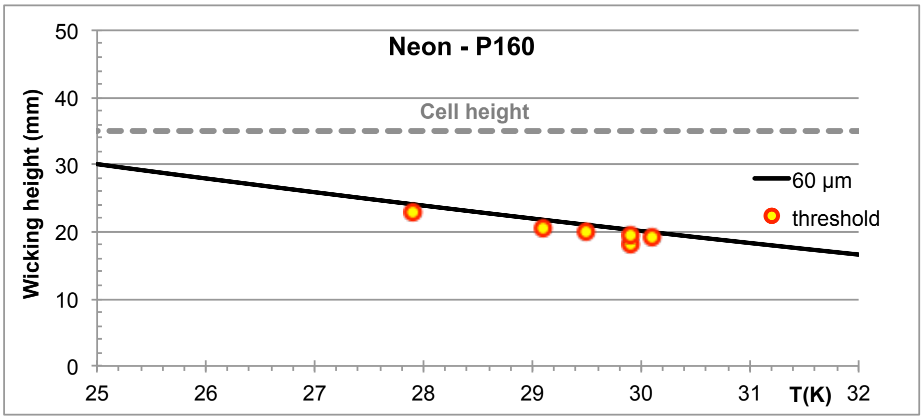

Figure 3-30 – Wicking height as function of the temperature for neon using the ceramic P160.

This liquid threshold, obtained for different temperatures, converted in wicking height (100% corresponding to 35 mm), is plotted in Figure 3-30. Considering the example, if the porous material can confine 50 % of the liquid, it is assumed that the liquid can rise up to half the height of the cell (17.5 mm). In order to compare our results with theory, we fitted the equation 2.29 using the pore size as adjustable parameter. The continuous line of the figure corresponds to this equation with a pore diameter of 60 µm.

The ESU system developed to work with nitrogen[9] is cooled down by a Gifford-Mac Mahon 1 W at 4 K cryocooler. Then, using this experimental apparatus and the same cell, it was possible to do the same type of tests to find the liquid threshold for the liquid helium at the 4 K range. The objective was to confirm that the same ≈ 60 μm of mean pore size matches the results of the liquid threshold with a different fluid.

The procedure to test the capability of the porous material to confine the liquid helium was exactly the same, but performed at lower temperature (4 K range). In Figure 3-31, the threshold height between 3 K and 5 K is presented. Due to the lower surface tension of the helium, compared with the neon, the wicking height is much smaller than the cell's height. By starting at the threshold amount (predicted using the 60 μm pore size) the expulsion of liquid of the cell was not observed in some experiments. The green points represent these experiments.

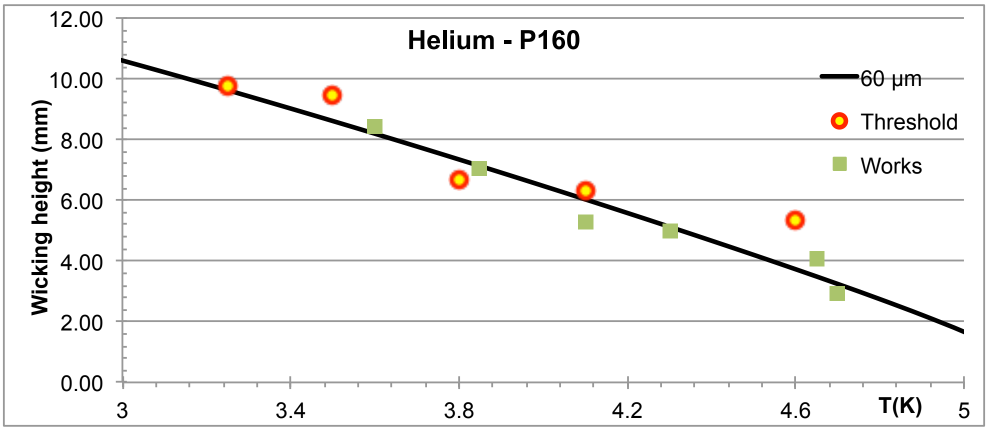

Figure 3-31 - Wicking height as a function of the temperature for helium using the ceramic P160. The same 60 μm found for the experiments with neon still match with the experimental results using helium.

The mean pore size of ≈ 60 μm still matches the results of the liquid helium threshold. A good coherence about the mean pore size was then obtained for the two fluids (neon and helium) at different temperatures. With this method, it is possible to test different porous materials with smaller porous size to use with neon near 40 K.

The ceramic P502, was also tested using the same method. For these tests, the same copper cell (Figure 3-28) was used, replacing the ceramic P160 by the P502. The first fluid tested was the helium at three different temperatures. The wicking height for three different temperatures is represented in Figure 3-32. By adjusting the mean pore size to fit the results, a diameter of ≈ 20 μm was obtained.

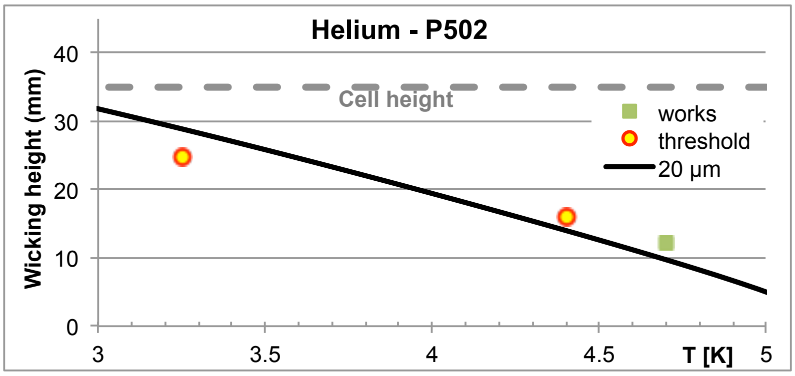

Figure 3-32 - Wicking height as function of the temperature for helium using the ceramic P502. The mean pore size of 20 μm match with the experimental results.

This result confirms that this porous ceramic material cannot also be used to confine the liquid in a 35 mm height cell for neon at 40 K range once the wicking height for neon in a 20 µm porous material is lower than 20 mm in the 40 K range (Figure 2-15), which is much below the 35 mm of the cell height.

By changing the fluid for neon, in the same cell with the same P502 material, the capability of this porous material to retain the liquid neon at 30 K was also tested. In three different tests starting with the cell completely full of liquid, no liquid expulsion through the capillary tube was observed indicating that the wicking height at 30 K is still higher than 35 mm.

With the 25 bar aluminium cell operating at 40 K range, it became possible to test the ceramic P502 with the estimated porous size of 20 µm at our target temperature. Figure 3-33 is a picture of the cold part of the experimental apparatus developed to test the porous materials and the ESU modes. The configuration is similar to the liquid nitrogen ESU system: the cold cell, designed to withstand 50 bar, is connected to the cold finger of the cryocooler through a gas gap heat switch. The capillary tube is connected to the bottom of the cell to connect with a 6 litres expansion volume at room temperature. A pressure control valve is also used to enable the ESU operation at constant temperature. The cell was filled with the ceramic P502 in order to perform the tests with neon at 40 K on this porous material.

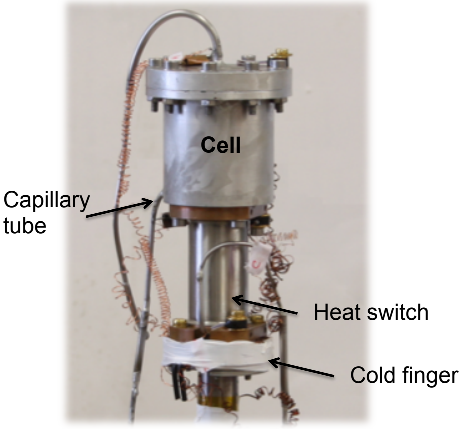

Figure 3-33 - Experimental apparatus to test the capability of the filter paper to confine the liquid neon inside of the cell at 40 K.

The experimental procedure to test the porous material at 40 K, was exactly the same than that previously described. The system was filled with 15-20 bars and after the precooling phase, with the cell full of liquid, the temperature of control was chosen. Figure 3-34 displays the experimental results for the wicking height for temperatures between 27 K and 42 K.

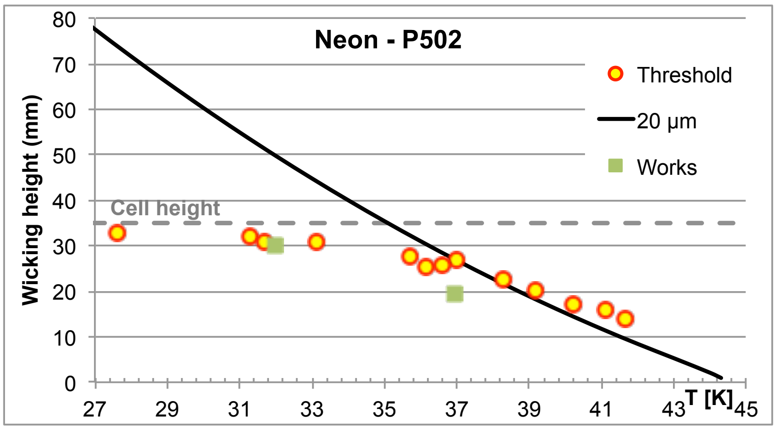

Figure 3-34 - Wicking height as function of the temperature for neon using the ceramic P502 in 27 - 42 K range.

As expected in the 40 K range, using this porous material we can only confine half of the liquid by capillarity inside the cell. The estimated ≈ 20 µm of mean porous size can predict reasonably well the experimental liquid threshold quantity.

To efficiently retain the liquid over 35 mm at ≈ 40K, different kinds of porous materials were considered. Beyond the pore size, factors like the void volume and the thermal conductivity were considered. Some metallic foams (Cu, Al) present a good thermal conductivity and a high void volume, but metallic foams with pore size below 10 µm are not available. For the ceramic foams, as previously mentioned, the minimum pore size found in this kind of material was the ≈ 20 µm pores of the ceramic P502. The aerogels are another porous materials with a very small pore size, used in thermal insulation applications[47]. But in this case, very strong confinement effects may be associated to these nano pores (5-50 nm) and, during the heating, part of liquid could remain trapped in the porous material, disturbing the evaporation process. Such effects (temperature split) will be discussed in the next sections.

The filter papers (pure cellulose) commonly used for filtration presents pore sizes between 0.5 µm to 60 µm. This pore size along with the paper lightness is very attractive for our application, but the intrinsic void volume (porosity) is lower than the alumina ceramics. These filter papers are available in plain disks and the effective void volume is then dependent of how the disks will be compressed in the cell. For having the adequate size of the pores this kind of material was tested to retain the liquid neon at 40 K. The filter paper F1250 from Filterlab® [48](Figure 3-35) was chosen for testing. The thickness of each disk of F1250 is 0.18 mm and the average pore size is 10 µm. The measured void volume was ≈ 63%, not so far from the 90% of the ceramic materials. Figure 3-35 displays the wicking height results in the filter paper in the temperature range adequate for our ESU.

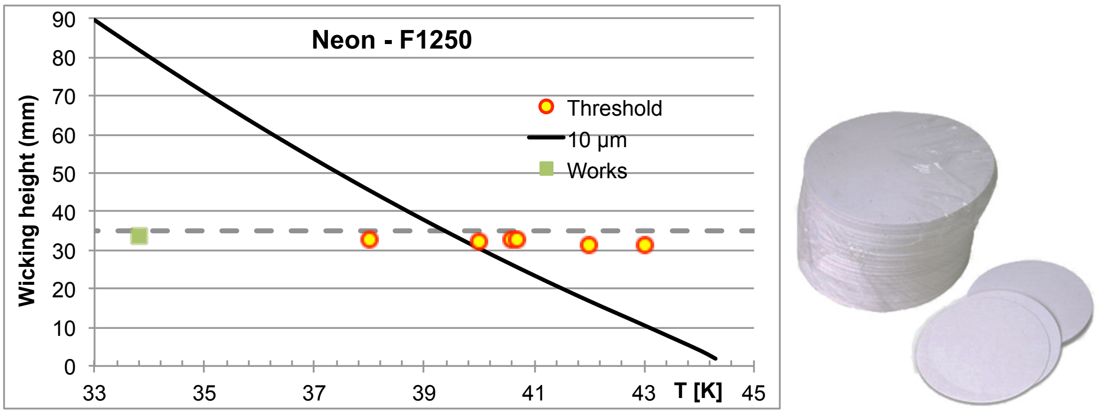

Figure 3-35 - Wicking height for neon using the filter paper F1250 with an average porous size of 10 µm at 40 K range. Picture of the filter paper used to confine the neon inside of the cell.

The wicking height results for the tests in the filter paper F1250 (Figure 3-35) show that, apparently, the amount of liquid that leaves the cell is almost independent of the temperature when it is full of liquid: Between 38 K and 43 K, the liquid threshold is about 90-95%. The estimation for the wicking height for this pore size (continuous line of Figure 3-35) indicates that this material could not confine all the amount of liquid at 43 K. Actually, at 43 K, our experiments show that a wicking height of more than 30 mm is measured allowing the normal working of the ESU system.

The smaller void volume (≈ 63%) when compared to the monoblock ceramic (≈ 90%) is a disadvantage of this material. Compared to the volume of the cell, this means less ≈25 % of liquid (compared to the volume of the cell) or, in other words, less 25 % of the stored energy.

With this filter paper it was shown that it is possible to confine the liquid neon inside the cell, even at 43 K and, despite the smaller void volume, it was decided to adopt this material. Actually, we did not find another material that is both easy to manipulate and commercially available having similar pore size and porosity.

3.5 Pressure drop

During the operation of the ESU, the liquid and the vapor are assumed to coexist in thermodynamic equilibrium inside the cell. By measuring the pressure in the cell it is possible to obtain the correspondent temperature (T_{vap}) on the saturation curve. This pressure is measured at room temperature in the tube that connects the cell to the expansion volume (Figure 3-36). Due to the vapor flow in this tube during the neon evaporation, a pressure drop can exist along it. This tube should be sized in order to decrease this pressure drop to obtain a more accurate measurement of the pressure inside the cell.

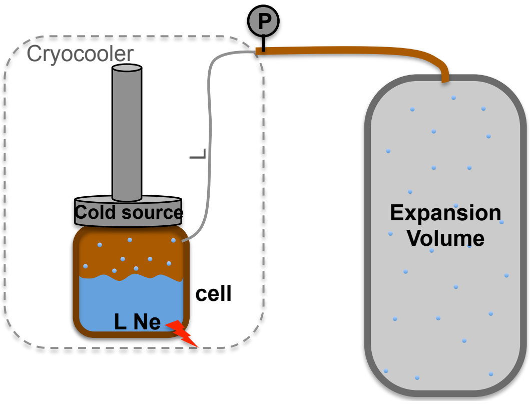

Figure 3-36 - Scheme of the connection between the cell and the expansion volume. Inside of the cryocooler a thin capillary tube with length L. The pressure is measured in the tube outside of the cryocooler (room temperature).

The pressure drop (*ΔP*) in a tube with a length *L* and a diameter *Φ* is given by [49]:

$$\Delta P = \frac{\rho v^2}{2}\frac{L}{\phi}f \qquad (3.16)$$

where *ρ* is the density of the fluid and *v* its velocity. The friction coefficient, *f,* is given by the *f*=64/*Re* in a laminar flow case. The Reynolds number (*Re*) is:

$$\mathrm{Re} = \frac{\rho v \phi}{\eta} \qquad (3.17)$$

where *η* is the viscosity of the fluid. For Reynolds numbers below $2\mathrm{x}10^3$ the flow is considered laminar. At the opposite, for larger *Re* numbers the flow is considered turbulent (> ≈ $4\mathrm{x}10^3$). In the turbulent flow the friction factor is also dependent of the roughness of the tube and it is necessary to use a Moody diagram to estimate it.

For laminar flow, rewriting the pressure drop equation as a function of the mass flow, instead of the velocity, turns easy to observe that the $\Delta P \propto L/\phi^4$. Increasing the tube diameter and reducing its length allow a reduction of the pressure drop along the tube, but increase the heat flow that comes from the hot side through the tube to the cell. A trade-off between these two effects must be found.

For meeting the thermal requirements the capillary tube is 1 m length and the inner and outer diameters are 1.5 mm and 2 mm, respectively. Beyond of the tube geometry, the pressure drop is also dependent of the thermophysical properties of the fluid. The tube being subjected to a temperature gradient between 40 K and 300 K, during the evaporation process, the vapour going to the expansion volume will progressively cool down the capillary tube. This brings an uncertainty about the temperature of the gas in the tube and consequently to the pressure drop. Figure 3-37 presents the pressure drop if all the gas is at 300 K (worst case) and if its temperature is 40 K. Instead of presenting the pressure drop as function of mass flow, it is plotted directly as function of the heat load applied ($\dot{Q} = \dot{m}L$), a more relevant variable of our system, with the ESU at 40 K (at 40 K, L=46 J/cm^3 and 2 W corresponds to 0.17 m^3/h)

This pressure drop results in a pressure, measured at room temperature, smaller than existing in the cell and then to a temperature lower than the real one temperature as deduced from the *T(P)* relation on the saturation curve. In the second plot of the Figure 3-37, the difference of temperatures due to this pressure drop as function of the heat load applied is estimated.

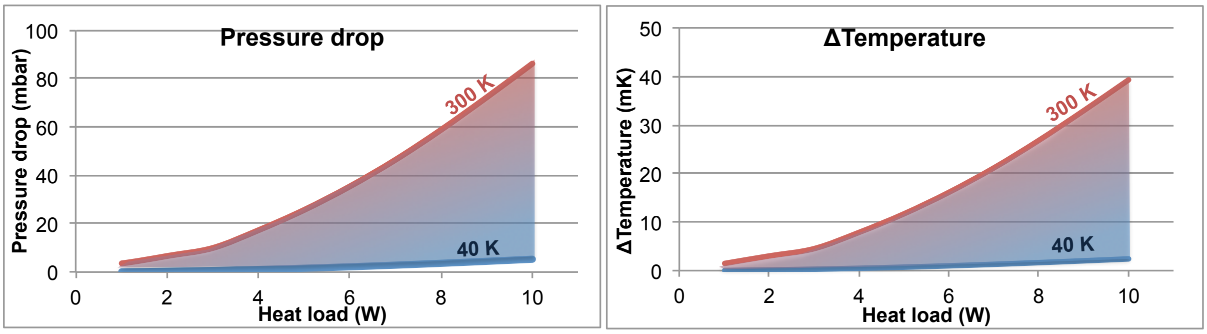

Figure 3-37 - Pressure drop as function of the applied heat loads. Difference of temperature between the measured and real temperature inside of the cell due to the pressure drop for different heat loads applied.

The pressure drop is clearly dependent of the fluid temperature in the capillary tube. However, even for the worst case scenario, supposing the capillary at 300 K, the maximum pressure drop is 80 mbar. Due to the large *dP/dT* of the saturation curve in this operational temperature range (40 K) the maximum error of the measured temperature for the real temperature is 40 mK. Even considering the worst-case scenario, this pressure drop is completely acceptable for this application in this temperature range.

3.6 Pressure control valve

As already explained, it is also possible to absorb energy at constant temperature, mimicking a triple point ESU, by controlling the pressure inside the cell during the evaporation. This control can be done inserting an electronically driven valve at room temperature between the expansion volume and the cryocooler. In our case, an ON/OFF control for the valve was used.

The better the pressure control, the better the temperature stability during the control. However, beyond the electronic control, an adequate valve to the flow characteristics during the ESU operation, i.e. one that does not limit the flow during the ESU mode, is necessary.

The flow coefficient of a valve K_v (*Cv* in the anglosaxon terminology) relates the pressure drop (ΔP) across the valve with the flow rate (Q) and is a relative measure of the efficiency of a valve in allowing the fluid flow. It is a characteristic coefficient of each valve and is dependent on the orifice size. For a gas, the flow coefficient is given by[50]:

$$K_V = \frac{Q}{18.9}\sqrt{\frac{(S.G.)}{\Delta P(2P_1 - \Delta P)}\frac{T}{293}} \qquad (3.18)$$

Were Q is the flow rate in m^3/h, *S.G.* is the specific gravity (gas density/air density), equal to 0.679 for neon, P_1 the upstream pressure and ΔP the pressure drop in the valve. In the case of this ESU system for the control at 40 K (14.6 bar), two extreme conditions of ΔP were considered *for the* K_V calculation. At the beginning of the control, 14.6 bar is the maximum ΔP *(supposing a quite low precooling temperature, the pressure of the expansion volume is also quite low).* At the end of the control, when almost all the liquid amount was expanded, the difference of pressure between the expansion volume and the cell is very small, the control vanishing when these two pressures are equal. The maximum evaporated flow, Q=0.17 m^3/h corresponding to a maximum heat load of 2 W applied to the cell was considered for the calculations. In Figure 3-38 the variation of flow coefficient during the control at 40 K in this condition is shown.

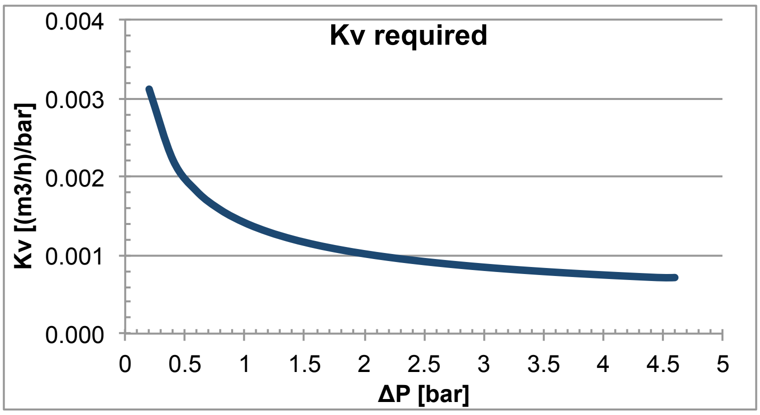

Figure 3-38 – Flow coefficient as function of the difference of pressure in the two sides of the valve during the control at 40 K.

At the beginning of the control, when the ΔP between the cell and the expansion volume is large, a minimum coefficient flow of K_v = 0.001 is enough to ensure the required pressure difference between the cell and the expansion volume for this flow (Figure 3-38). At the end of the experiment, with the decrease of the *ΔP*, K_v increases drastically. For our experimental set-up, we decided to keep a control down to a minimum of *ΔP*=0.2 bar a the flow of 0.17 m^3/h leading to a minimum K_v about 0.003 (Figure 3-38). At the beginning of the ON/OFF control, the valve will be set to open or to close in almost each cycle of a microcontroller, in order to maintain the pressure inside of the cell. But at the final of the experiment, when the *ΔP* is very small, the valve will remain a longer time in the ON state to maintain the difference of pressure for the given flow. In operation, the maximum *ΔP* of pressure that the valve will be subject is 5 bar. But for a safety reason the valve should withstand *ΔP* = 25 bar, the maximum working pressure of the system.

Attending to the requirements and the commercial available solutions, a valve of the “Series 9” of Parker® (Figure 3-39) was chosen. The maximum operating pressure is 80 bar and its flow coefficient is K_v=0.005, the current for open state is around 500 mA under 24 V.

Figure 3-39 - Pressure control valve “Series 9 valve” of Parker®. Maximum operating pressure is 80 bar. The flow coefficient is K_v=0.005.

The electronic control of this valve was based on a programmable Arduino® microcontroller. The board is connected to the pressure sensor output (10V). If the upstream pressure (cold cell pressure) is higher than the setpoint pressure the board sets the valve to be opened, otherwise the board sets the valve to be closed. A solid state relay was used to actuate the valve. A simple USB communication protocol was created to choose the pressure setpoint before the control, decreasing the response time of the controller. The advantage of this system is that, during the control, this board works independently of the computer.

3.7 Experimental apparatus

In the previous sections, all the different components of the Energy Storage Unit system were sized. Despite their similarities, each ESU mode requires different experimental configurations. In the case of the "*ESU power booster mode*", a smaller cell is directly coupled to the cold finger of the cryocooler to absorb sudden heat bursts of a sensor array. In the other two ESU modes, "*Temperature drift* and *Temperature controlled*", a gas gap heat switch is used to thermally decouple the ESU from the cryocooler to operate as an independent cold source. Both the cryocooler and room temperature apparatus were built in such a way that each ESU mode could be operated with minimum disassembling. This section gives a global description of the experimental apparatus developed, where the cold parts configurations and the room temperature apparatus are detailed.

ESU drift and controlled temperature modes

In the modes in which the heat switch is used, a structure to allow the rotation of the cryocooler without significant stresses on the switch and on the cryocooler tube was built. The sizing of this structure, composed essentially by carbon fibre tubes, is described in the section 3.4.2. Figure 3-40 shows the final structure assembly. The heat switch and the cell are mechanically decoupled from the cold finger in order to avoid stresses in the switch. These two components are connected to the carbon fibre tubes through a G10 fiberglass rings. Two flexible copper straps establish the thermal contact between the cold finger of the cryocooler and the switch. In the mentioned picture the multipurpose aluminium cell used to test the porous materials is showed. A similar cell in copper was also used in order to decrease the thermal gradient and to obtain a reliable soldering process. The dimensions of the two cells are similar and both fit in this structure. In both cells, the capillary tube connected to the expansion volume was soldered at the bottom of the cell. This structure is attached to the 1st stage of the cryocooler. This stage (≈ 50 K) is also used to support and thermalize a copper radiation shield.

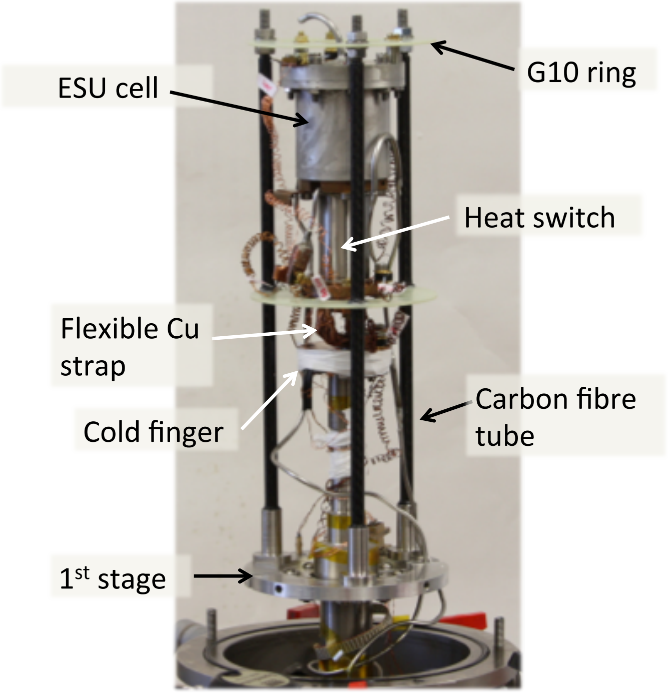

Figure 3-40 - Structural support to enable the tilting of the "cold part" components.

ESU Power booster mode

For the "*ESU Power booster mode*", the cell is directly coupled to the cold finger of the cryocooler, In Figure 3-41 the experimental configuration for this mode is shown. The smaller capacity cell (≈ 12 cm^3), developed for this proposes, is directly coupled to the cold finger. For this mode no porous material to confine the liquid inside of the cell was used. A heat exchanger inside of the cell is responsible to increase the thermal homogeneity between the liquid and the copper. The capillary tube that connects to the expansion volume is in the top of the cell, i.e., in the lid. To control the temperature of the cryocooler and to provide the heat load in the cell a 50 W heater cartridge is used, fitted on the bottom of the cell.

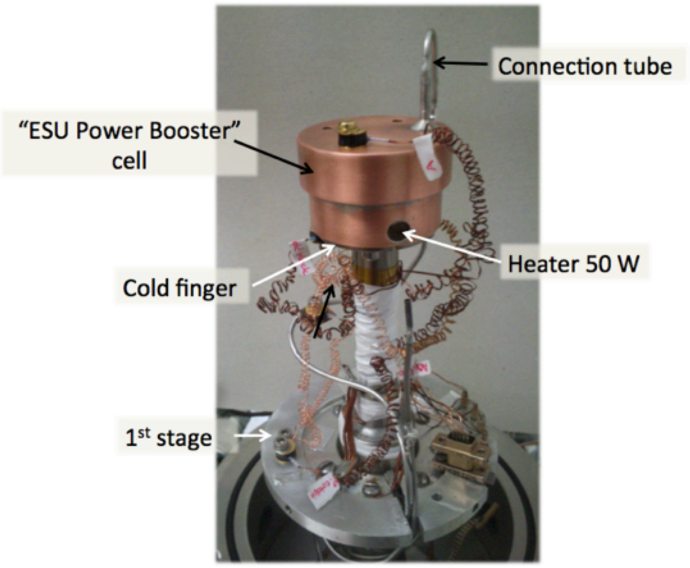

Figure 3-41 – Configuration of the ESU power booster mode. The cell is directly connected to the cold finger of the cryocooler.

Room temperature assembly

A 6 liters expansion volume at room temperature was chosen to limit the temperature increase and store the evaporated neon. This volume is an aluminium scuba diving cylinder (withstands 200 bar). Some experiments were performed with a 3 liters expansion volume and the same type of cylinder was used. In Figure 3-42 a picture of the experimental apparatus at room temperature is shown. The expansion volume and the cold cell are connected to a manifold to manage the neon gas. It allows the pumping and refilling of the ESU system with neon gas. The pressure control valve is placed between the cell and the expansion volume. This valve is just used in the controlled temperature mode and, to avoid removing this valve in the other ESU modes, a bypass circuit was installed.

The heat switch was tested with different charcoals and filling pressures. For testing the heat switch it was connected by a capillary to another manifold in order to quickly change the charging pressure inside of the switch. In the future, once found the ideal charging pressure to operate in this range, the heat switch can be charged and sealed very close the copper blocks and turn this GGHS more compact.

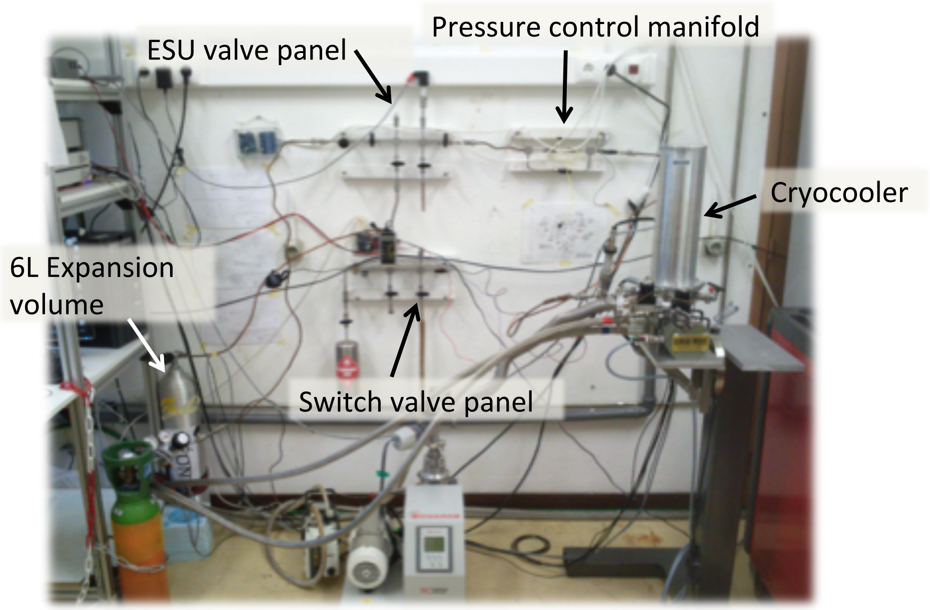

Figure 3-42 - Experimental assembly at room temperature used to test the different ESU modes.

A temperature control from Cryocon 24C® was used to control the temperature of the cryocooler and monitor the ESU temperatures. An Agilent power supply is used to provide the heat load in the ESU. For the pressure measurement are used two Keller sensors (0-100 bar range). All the temperatures, pressures and heaters are monitored and controlled using a computer software developed in Labview®. The main window of this software is displayed in Figure 3-43. All the temperatures, pressures and some preliminary calculations, as the example of the liquid ratio, are shown in the graphical interface and saved into a log file. Hardware items such as the compressor, the cryocooler, the vacuum system and the pressure control valve are also controlled using this software. During the ESU experiments this software also returns the estimate of the liquid amount inside the cell.

A Booster 292.6588
B 1st stage 292.4841
C Cold finger 292.8816
D Perm. 292.6742
T pt capilar 295.8300
T gas 26.9996
P ESU 0.978303
Tempo 101.76
% liquidacélula 2.75684
Cryopump setpoint (K) 90
Delay 10
NP 8
Inserir comentario no ficheiro
comentario no ficheiro Tudo isto parece
P ESU (bar) 0.978303
Tensão aquecimento V 0.00088
resistencia 55
Potencia celula (W) 1.408E-8
Estado Ler
P panela (mbar) 1E-5

Figure 3-43 - Labview® interface to monitor the pressures and temperatures and control the heaters.

3.7.1 System overall dimensions

In this section are presented the overall dimensions of the ESU developed.

The overall dimensions, envelope size, and mass of the cold part experimental set-up used for the ESU temperature drift and temperature controlled modes are presented in the Table 3.2.

Table 3.2 - Envelope size and masses of the cold part components used for the ESU temperature drift and temperature controlled modes.

ESU component	Envelope size (mm)	Mass (g)
Gas gap heat switch	40 x 40 x 50	210
Cold cell	50 x 50 x 50	310
Thermal straps	20 x 40 x 40	26
SS Capillary tube	-	10
CFRP/G10 structure	90 x 90 x 200	20
Total	**90 x 90 x 200**	**550 g**

For the booster mode configuration, the overall dimensions and mass of the cold par set-up are presented in the Table 3.3.

Table 3.3 - Envelope size and masses of the cold part components of the ESU booster mode.

ESU component	Envelope size (mm)	Mass (g)
Power booster cell	28 x 46 x 46*	245
SS capillary tube	-	10
Total	**28 x 46 x 46**	**255 g**

*This envelope size does not include the curvature of the ss capillary tube.

To store de the gas at room temperature a 3 and 6 liters expansion volumes was used. Both volumes are aluminium scuba diving cylinders, sized to withstand 200 bar. The masses of these 3 and 6 liters cylinders are 3.5 kg and 7.3 kg, respectively. The development of lighter volumes to use as expansion volume is not aim of this work, however, in the Table 3.4 is presented the mass estimation of two aluminium spherical volumes to withstand 25 bar.

Table 3.4 - Estimated mass of an aluminium spherical pressure volume to withstand 25 bar (using a safety factor of 2)[36].

Spherical volume (Aluminium 6061)	Wall thickness	Mass (g)
3 L	1 mm	280
6 L	1.3 mm	580

For this estimation was considered the aluminium 6061 (276 MPa of yield strength [37]) and a safety factor of 2. Based on these calculations is possible to use an expansion volume with a lower mass than 1 kg, by using a spherical shape.

4 ESU Experimental Results

The Energy Storage Unit system was developed to enable its operation in different modes as defined in section 2.1: *Temperature drift mode*, *Temperature controlled mode* and the *Power booster mode.* After being sized and assembled all the different components, these operational modes were tested. The system aims to be gravity insensitive: the performance of the ESU as a function of the cryocooler orientation was also tested. The results of these tests are shown and discussed in this chapter.

4.1 Temperature drift mode

In the temperature drift mode the cell is cooled down to a precooling temperature (T_i) to condense the neon in the cell. When the cell is filled with neon liquid and/or when the precooling temperature is reached, the ESU is ready to operate. Applying a heat load, the liquid neon evaporates and the gas expands to the expansion volume. During this evaporation the large latent heat of the liquid neon is used as temporary could source. The difference between the T_i temperature and the final temperature (T_f) during the drift is determined by the size of the expansion volume as explained and discussed in section 2.3.

In this drift mode, the gas gap heat switch is used to provide the thermal decoupling of the cell from the cold finger to allow turning off the cryocooler without fast temperature increase. Actually, in these tests, the presence of the heat switch also creates a "quasi-adiabatic" system, allowing to precisely taking in account of the exchanged energy with the ESU.

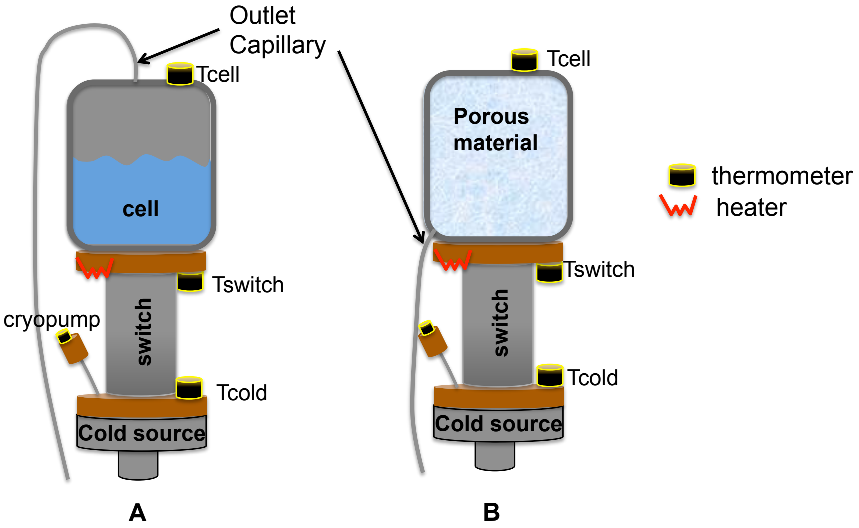

Figure 4-1 - Configurations used to test the temperature drift mode. A - without the use of porous material, the capillary tube is connected on the top of the cell. B- using porous material, the capillary tube is connected at the bottom of the cell.

In Figure 4-1 the configurations used to test the temperature drift mode are presented. In the first case (A), no porous material was used. The capillary tube is connected on the top of the cell to prevent loss of liquid due to the gravity force. This capillary connects to the 6 L expansion volume at room temperature.

At the beginning, the system (expansion volume and the cell) is filled with gaseous neon at a determined filling pressure ($P_{filling}$) that determines the final temperature of the ESU (T_f) (Cf section

2.1). This process was made with all the system at room temperature in order to easily account the total number of moles in the system. During the cooling process, the density of the gas inside of the cold cell increases leading to a small decrease of the pressure in all the system. When the temperature of the cell achieves the saturation temperature the pressure in the system is only slightly lower than the filling pressure and drops quickly from this point on.

In Figure 4-2 a typical experimental result for an temperature drift mode is displayed. In this test the configuration A ("Capillary on TOP") of the Figure 4-1 was used with the aluminium cell. After the cooling process, the cell was thermally decoupled from the cryocooler by toggling the switch to the OFF state. The ESU mode started at *t*=0, by applying 1 W of heat power. The temperature *Tvapor* represents the temperature at the liquid-vapor interface (orange line, *Tvap*) as deduced from the saturation pressure. When the heat power is applied, the bottom of the cell (light blue, *Tswitch*) becomes hotter (≈0.4 K) than its top (*Tcell*) due to the proximity of the heater resistance.

The dark blue line in the plot of fig 4.2 gives the liquid filling ratio (in volume) inside of the cell. This result was calculated through the initial parameters and the measured pressure (more information about this calculation is presented in section 2.2.1). Despite of the use of a constant heat power, the liquid decreasing amount during the evaporation is not constant. This is justified mainly by the latent heat variation along the saturation curve; as temperature increases, the latent heat decreases, and, for the same energy absorbed ($\dot{Q}\,\Delta t$), the evaporated liquid amount of neon is larger. This effect is well seen in this example with its rather extended temperature drift due to the proximity of the critical point where the latent heat decreases deeply (Cf Annex 4).

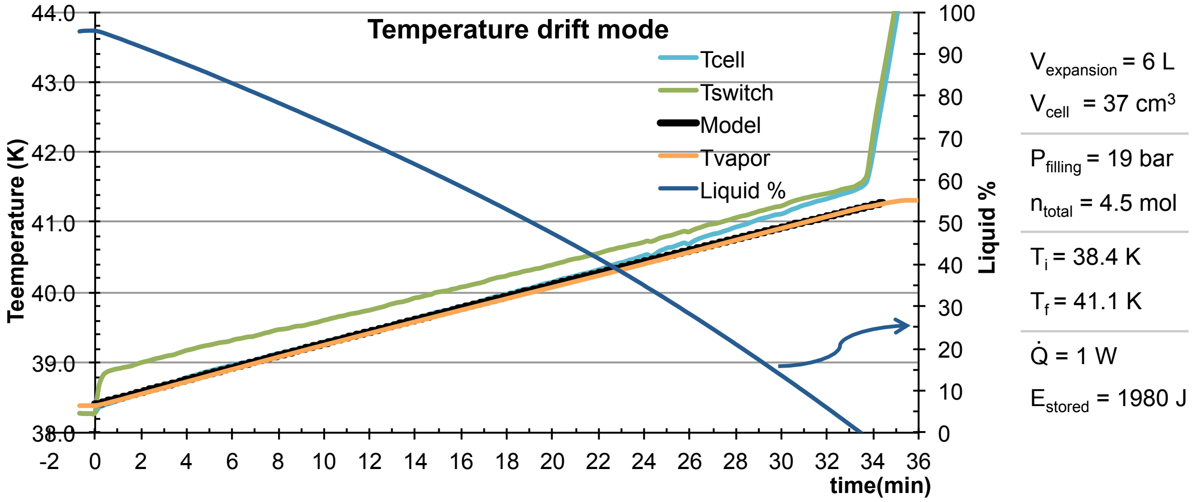

Figure 4-2 - Experimental result of the ESU drift mode (Configuration A). The temperatures are presented in the left scale. The right scale indicates the liquid percentage inside of the cell. The placement of the thermometers is indicated in Figure 4-1. The Tswitch represents the temperature of the cell in the switch side, as shown in Figure 4-1.

When the temperature T_f = 41.4 K is reached (*t* ≈ 33 min.) no more liquid is available, resulting in a faster cell's temperature increase and the pressure no longer leads to a temperature correspondence. This corresponds to the final of the ESU mode. At this time the regeneration phase must be run by re-liquefying the liquid inside the cell to allow a new ESU mode. The energy stored during this drift of 2.7 K was E_{stored} = 1980 J (1 W during 33 min). The dashed line gives the predicted result, obtained using the pre-dimensioning tool (section 2.5), in a very good agreement with the liquid/vapor temperature. This good agreement is a good contribution for the pre-dimensioning tool validation.

The influence of porous material

The liquid confinement tests with filter paper F1250 of Filterlab® showed the capability of this porous material to confine the liquid neon inside the cell at 40 K range (section 3.4.3). The measured void volume of this porous material is ≈ 63 % leading to a reduction from 38 cm^3 to 24 cm^3 for the total liquid capacity of the cell. A direct consequence of the cell's volume decrease is the reduction of the stored energy.

To test the ESU mode with the porous material the configuration B of Figure 4-1 was used. In Figure 4-3 the experimental results of the ESU mode using the porous material are shown. After cooling down to the precooling T_i = 40.3 K, the cell was filled with liquid neon and the ESU was ready to operate. The lower cell's volume turned unnecessary the cooling at a lower temperature to fill the cell, when compared with the last experiment, with the ceramic foam and more liquid capacity of the cell. With the heat switch in the OFF state the cryocooler was turned off and a heat power of 1 W was applied. A small but sudden increase of the three temperatures was observed right at the beginning of the ESU mode ($0 < t < 0.4$ min). At the same time, a quick decrease of the liquid amount (dark blue line) was observed too. An expulsion of a small amount of liquid by the capillary tube could explain this sudden temperature increase. This liquid lost evaporates very quickly in the capillary and then leads to a fast increase of the system pressure ($\Delta P \approx 0.8$ bar) and consequently of the temperature ($\Delta T \approx 0.2$ K). As it can be seen in Figure 4-3, this liquid lost corresponds to less than 10 % of the void volume.

An explanation for this initial loss could be the inadequacy of the porous material to confine all the liquid in the porous material. But this phenomenon was observed in a temperature range 38 K – 41 K where the calculated wicking height varies up to 15 mm whereas, as later experiments demonstrated, the initial amount lost seems to be independent of the temperatures. This independence from the temperature seems to exclude a possible limitation of the capillarity forces. This problem will be analysed further during the development of this work (section 4.7).

The results obtained with the pre-dimensioning tool (black line, *Model*) are adjusted to the part of the test where "nothing strange" occurs ($t > 0.4$ min) in respect to the normal behaviour of this kind of test. In this case, this adjustment corresponds simply to a time shift of the calculated $T(t)$ curve in order to join the experimental curve just after the rapid expulsion. With this shift, corresponding to $\Delta t \approx$ 80 s, it is easy to take account of the lost energy due to the liquid lost at the beginning. In this specific case, 6 % of the total liquid amount escaped through the capillary tube at the beginning of the experiment and corresponds to 80 J lost.

During the temperature drift, the two temperatures in the opposite sides of the aluminium cell is up to 1 K ((T_{cell}-T_{switch})≤ 1 K).

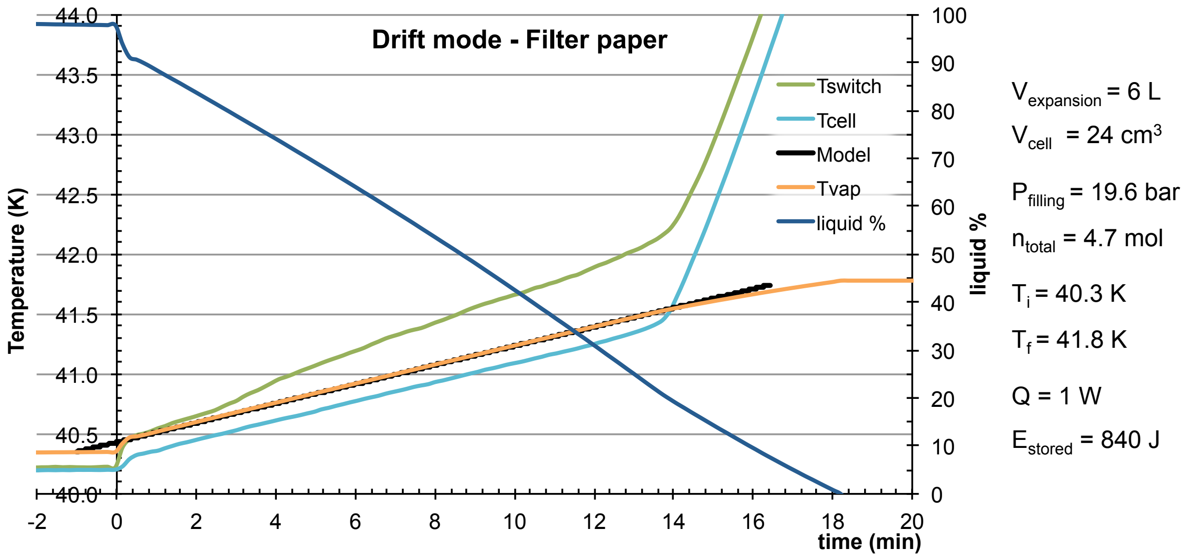

Figure 4-3 - ESU drift mode using the porous material. The temperatures are presented in the left axis. In the right axis is the liquid per cent (dark blue line). The thermal decoupling between the cell and the liquid/vapor temperature (*Tvap*) occurs when the liquid% is ≈ 20 %.

With the time shift adjustment, the calculated results (black line, obtained from the pre-dimensioning tool) present a very good agreement with the experimental results. But, when the liquid amount is ≈ 20 % (t ≈ 14 min), a rather fast thermal decoupling between the cell's temperature and the liquid-vapor interface temperature (orange line, *Tvap*) was observed. This effect, referred in the following by "temperature split", was early observed by *J. Afonso* [9, 29] in her work about the liquid nitrogen ESU. During the tests about the capability of the different porous materials reported in the section 3.4.3 this phenomenon was also observed, for both tested fluids (helium and neon) and all the different porous materials used. The amount of remaining liquid in the cell for which this thermal split is observed varies with the porous material, the fluid and the temperature. The porous geometry of the material used to retain the liquid can explain this thermal decoupling between the cell walls and the liquid temperature. As a matter of fact, below a certain filling, an amount of liquid can remain trapped in small pores by capillary effect without a continuous path to the cell walls. The bad thermal conductance of this kind of porous materials as well as the low thermal conductivity of the gaseous phase and of the porous material and the impossibility of convection in this porous geometry turns the remained liquid thermally isolated from the cell in a very efficient way. Under these conditions, the temperature of the cell walls – where the thermal power is applied — can increase significantly more than the liquid temperature/vapor interface[29]. The influence of the temperature and the heat power applied in this thermal split is going to be discussed later.

Two different phenomena have appeared with the use of the porous material: The liquid lost in the beginning of the experiment and the thermal split in the final of the ESU mode. With these two phenomena up to 26 % of the total liquid amount turned inaccessible. Despite this loss it was still possible to store a total energy of 840 J (1 W during 14 min) with the temperature drift of 2.3 K.

Copper cell

To obtain a better thermal homogeneity between the two sides of the cell (top and bottom), a copper cell was built. The difficulty in obtaining a reliable soldering of the capillary tubes in the aluminium cell also motivated the development of this copper cell. This cell (Figure 3-7) was described in section 3.2.2. The volume of this cell is the same of the aluminium cell, which means a void volume of 24 cm^3 after filling with the porous material (filter paper).

Figure 4-4 displays a typical result of a drift mode test using this copper cell. The configuration B of Figure 4-1 was maintained in this cell. After the cooling process, the switch was toggled OFF. In this test the initial temperature was *Ti* = 37.8 K, with a total of 97 % of the void volume of the cell filled with liquid, and the heat load used was 1 W. During the temperature drift, the two temperatures in the opposite sides of the cell were similar (*Tcell-Tswitch* ≤ 0.1 K) due to the better conductance of this copper cell in regard of the aluminium one. If compared with the drift mode using the aluminium cell (Figure 4-3) ((*Tcell-Tswitch* ≤ 1 K)), a significant progress for the thermal homogeneity in the cell was achieved. During these 2.3 K of temperature drift a total of 1120 J were stored (1 W during 19 min).

Like in the experiments with the aluminium cell, at the beginning, when the heat power is just applied, the temperature increases faster than the expected, This increase was not so sudden, compared with the case of the cell in aluminium, but almost the same amount of 6 % of liquid was lost in this phase.

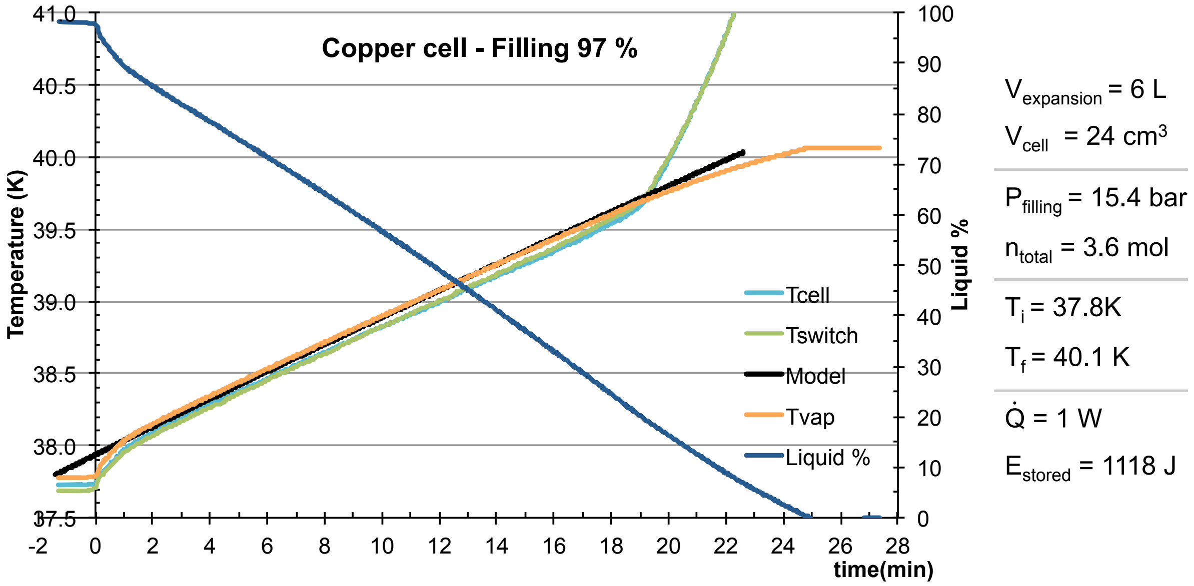

Figure 4-4 - Copper cell tested in the ESU drift mode. The filling percentage is 97 %. The temperature split (thermal decouple between the cell and the liquid) occurs when the liquid % is ≈ 20 bar.

The black line represents the temperature, calculated with the pre-dimensioning tool. After the small initial liquid expulsion, this calculation allows a good description of the temperature evolution.

The thermal split between the cell and the liquid/vapor temperature was also observed in this test with the copper cell. Same phenomenon was verified when the liquid amount is about 20 % as in the case of aluminium cell. This result indicates that this thermal split is related to the porous material and not (or just weakly) dependent of the material used for the cell. This subject is going to be discussed later in the “Summary” section (section 4.7).

In order to understand if the initial lost amount was associated to an overfilling of the cell, the same test was performed using a lower initial amount of liquid. In the experiment of Figure 4-5, the initial conditions from the last test were maintained, but, in order to obtain a lower initial filling (90 %) the initial temperature was slightly higher (*T_i*= 38.05 K).

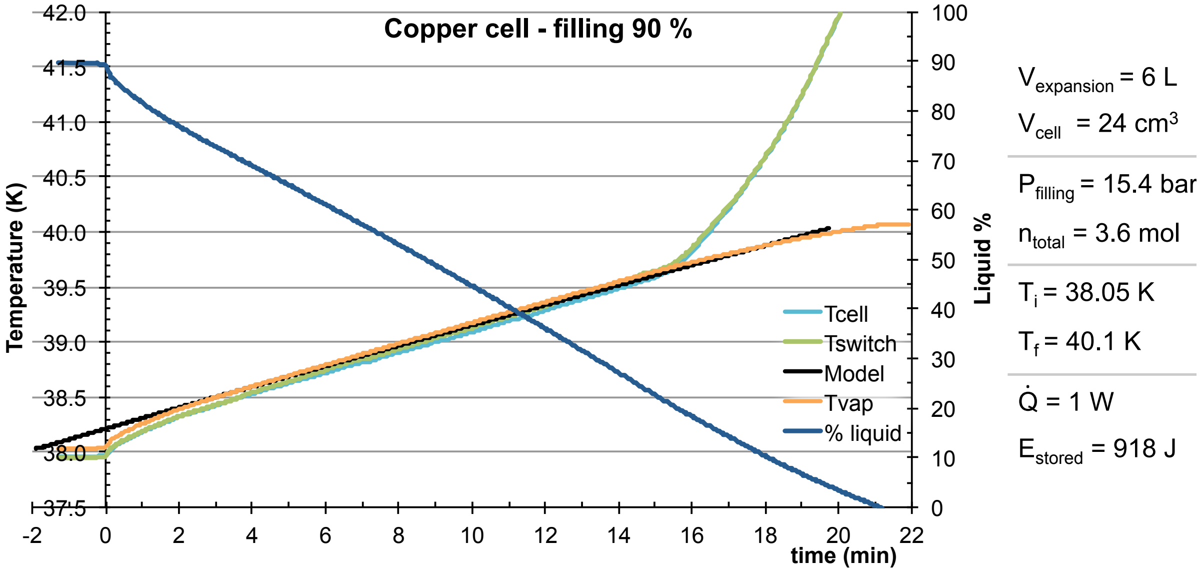

$V_{expansion} = 6$ L

$V_{cell} = 24$ cm^3

$P_{filling} = 15.4$ bar

$n_{total} = 3.6$ mol

$T_i = 38.05$ K

$T_f = 40.1$ K

$\dot{Q} = 1$ W

$E_{stored} = 918$ J

Figure 4-5 - ESU drift mode with a filled percentage of 90 %. Even with lower filled amount, the firsts 6 % of liquid were lost. The temperature split between the Rcell and the Tvap occur when the liquid amount is around 20 %.

When the heat power of 1 W was applied, almost the same liquid amount as the last example (≈ 6 % of the total void volume of the cell) was lost. Despite of the lower initial filling, almost the same amount was lost in the beginning of the ESU mode, and probably this phenomenon was not only associated to a cell overfilling. This issue will be discussed later in the development of this work (section 4.7).

In the tests of this ESU temperature drift mode, it was shown that the ESU may act as an independent cold source with the capability to store up to 1118 J with a temperature drift of less than 2 K at 40K.

Using the liquid nitrogen ESU[9] as reference, with the same expansion volume (6 liters), a significant reduction in the temperature drift was obtained with neon, for the same amount of evaporated liquid, as presented in Table 4.1. As previously discussed, the significantly higher $\partial P / \partial T$ of neon in the 40 K range (Cf. Figure 2-10) optimizes the energy stored per litre of expansion volume in a temperature drift. Despite of the same amount of evaporated liquid, the lower latent heat of neon results in a lower energy stored.

Table 4.1 - Comparison of the influence of the expansion volume in the temperature drift between the work with liquid nitrogen[9] and neon.

Fluid	***V* expansion (l)**	***V* cold (cm^3)**	***Tdrift* (K)**	**Energy (J)**
Nitrogen	6	23	65 K – 83 K	3000
Nitrogen	24	23	76 K – 81 K	3000
Neon	6	24	38 K – 40 K	1200

The results of the simulation using the pre-dimensioning tool can predict very well the experimental results and helps in the accounting of the energy lost due to two phenomena found: the initial liquid lost and the thermal split in the final of the ESU mode. These two phenomena will be analysed with more detail further on this chapter.

4.2 Temperature controlled mode

The *temperature controlled mode* (section 2.1) allows the energy to be stored in a liquid bath at constant temperature. The constant temperature is obtained by controlling the pressure inside the cell during the evaporation. A pressure control valve (section 3.6) is used to maintain the constant pressure in the low temperature cell. To test this ESU mode, the configuration B of Figure 4-1 was used. Similarly to the *temperature drift mode*, to fill the cell with liquid it is necessary to cool down the cell at a temperature lower than the control temperature (pre-cooling temperature).

An experimental result of a temperature controlled mode at 40 K is presented in Figure 4-6. In addition to the evolution of temperatures, the pressures in the cell and in the expansion volume are also presented in this figure. In this test, the system was filled with 15.4 bar of neon, a 6 L expansion volume was used and the precooling temperature was $T_{precooling}$ = 38 K. The setpoint of the valve was 14.6 bar (40 K).

During the first three minutes of the record shown in Figure 4-6, 1 W heat load was applied to the cell, until the temperature chosen for control is reached. In this phase, with the pressure control valve closed, a small evaporation in the cell corresponds to a significant pressure increase and consequently a fast rate of temperature increase was observed. During this temperature increase, a small increase of the liquid % inside of the cell was observed too due to the decrease of the liquid density for higher temperatures (the % in volume increases whereas the number of moles in the liquid phase decreases).

When the pressure of the cell achieves the setpoint, the valve starts to open and close in order to control at 14.6 bar (40 K) and a stable temperature during the evaporation is hence obtained. The cell remained 14 minutes at a constant temperature, storing a total of 840 J, with a maximum of 0.1 K of temperature noise.

When the liquid amount in the cell reached ≈ 20 %, a temperature split between the cell and liquid temperatures occurred. This phenomenon was also observed in the temperature drift mode at a similar liquid amount.

Despite of this temperature split, because the liquid continues to evaporate, the pressure in the cell, and then Tvap, is maintained constant. The liquid neon keeps evaporating until the cell is dry ($t \approx 21$ min). When both sides of the valve equalize the pressure, the valve cannot longer control. At this time ($t \approx 18$ min.) the valve remains open, and the last few amount of liquid is spent in a drift mode.

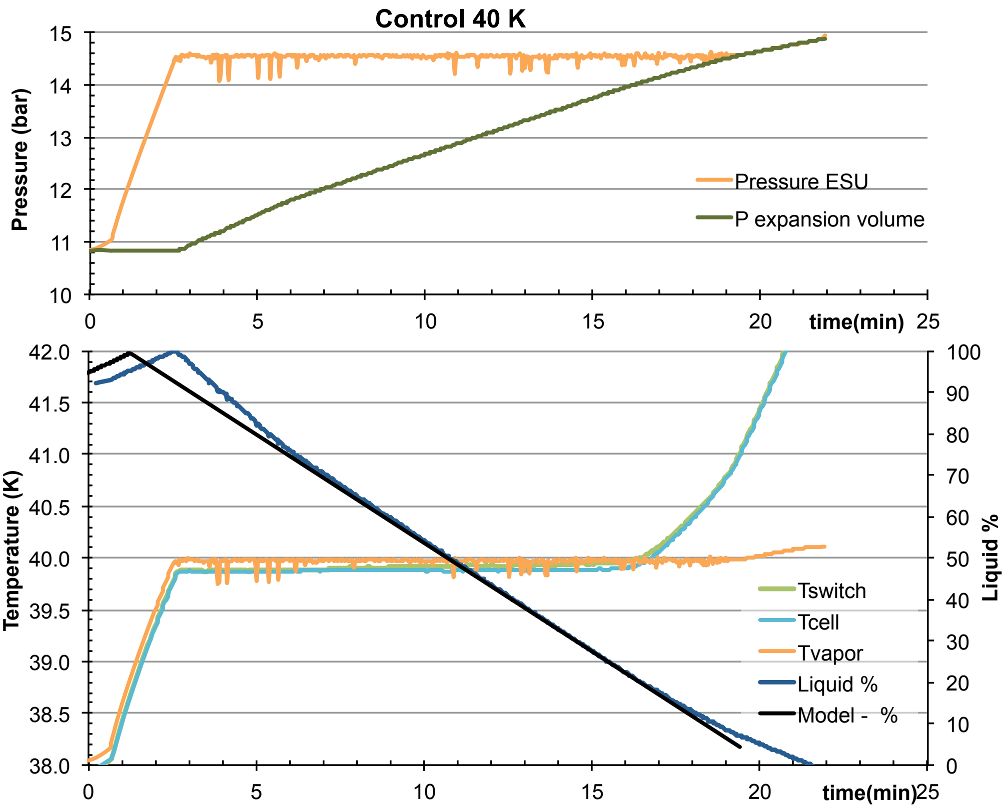

$V_{expansion}$ = 6 L
V_{cell} = 24 cm^3

$P_{filling}$ = 15.5 bar
n_{total} = 3.65 mol

$T_{precooling}$ = 38 K
$T_{control}$ = 40 K

$\dot{Q}$ = 1 W
E_{stored} = 840 J

Figure 4-6 - Temperature controlled mode at 40 K. Upper - Pressures in the cell and in the expansion volume. Lower - Temperatures of the cold part of the system. The temperature drift occurred when the liquid amount was ≈ 20 % of the total void volume of the cell.

The experimental results of Figure 4-6 was also compared with the analytical results obtained with the pre-dimensioning tool (black line). Instead of the temperatures, because it is a process at constant temperature, the liquid % was chosen to compare the experimental and the simulation results. Similarly to the process used for temperature drift mode analysis, it is necessary to shift the simulation results to obtain a good agreement between the two types of results. Like in the temperature drift mode, at the beginning, the decrease of the liquid amount was faster than expected. A small amount of liquid is lost at the beginning of the ESU mode. The amount lost is around 7 % - 8 % of the total liquid volume in the cell, estimated through comparison with the results obtained with the pre-dimensioning tool. After this initial loss, the rate of evaporated liquid shows a good agreement with the predicted results. The liquid % decreases at constant slope rate, contrarily to that obtained in the drift mode, because the latent heat of the liquid is constant during this process occurring at constant temperature.

When the cell and liquid temperatures split, another change in the rate of the liquid % was observed: Part of the provided heater power now heats up the cell, instead of just being absorbed by the liquid. This causes a decreasing in the evaporation rate.

Using the same initial conditions (filling pressure and precooling temperature) as in this experiment, it is possible to choose a lower control temperature. But, in this case, during the ESU temperature controlled mode the pressure in the expansion volume will sooner reach the saturation pressure and the controlled mode finish (or can finish) when an amount of liquid is still available. The control at higher temperatures than 40 K, with these conditions, is also possible.

The differences between the liquid and vapor phases become very small near the critical point, and the latent heat vanishes (Figure 2-10). To show this effect, three experiments at different temperatures were performed and are shown in Figure 4-7. Despite of differences between the initial conditions, the amount of evaporated liquid was similar all those three experiments.

As it can be observed in comparing the experimental data of figure 4-7, the stored energy is lower for higher control temperatures. The stored energy at 38 K is twice larger than at 43 K (*L*(38 K)= 60 J/cm^3 ; *L*(43 K= 25 J/cm^3), for the same amount of liquid neon.

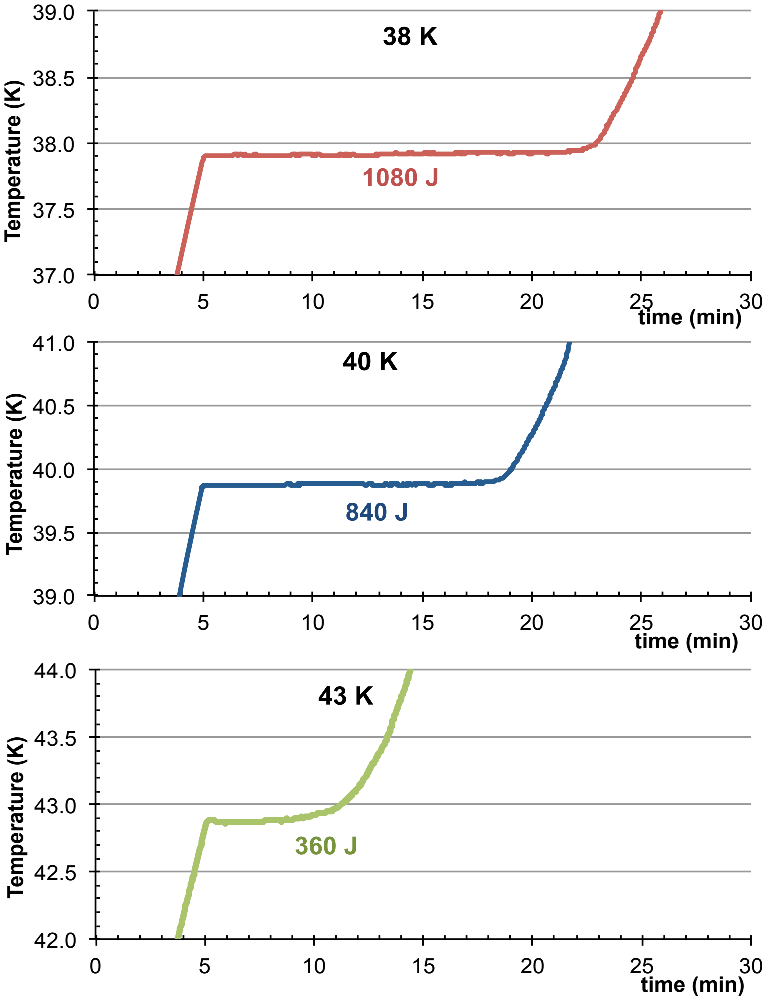

Figure 4-7 – ESU mode at controlled temperature at 38 K, 40 K and 43 K. The three experiments started with the cell full of liquid.

The temperature split between the cell and the liquid temperature occurred when the liquid amounts were 19 % at 38 K, 20 % at 40 K and 30 % at 43 K. The higher liquid amount in the temperature split at 43 K also contributes for the reduction of the stored energy when compared with the other two temperatures, but if the temperature split in this case would occur at 20 % of the liquid amount this will represent an addition of more 50 J for the total 360 J stored energy.

The initial amounts of observed liquid lost at the beginning in all these tests using the configuration B of the Figure 4-1 was similar to those previously observed. This subject is discussed after in the section 4.7.1.

All the ESU tests shown up to now were obtained using a constant heater power. To evaluate the response of the ESU system in the case of a variable heating power, a control mode at 40 K using a "random" heat load. In Figure 4-8 a controlled temperature ESU mode at 40 K using such a random heat load between 0 – 2 W is shown. Despite of the variable heat load, the system can control the pressure reasonably well and the maximum temperature variation obtained was ≈ 0.15 K.

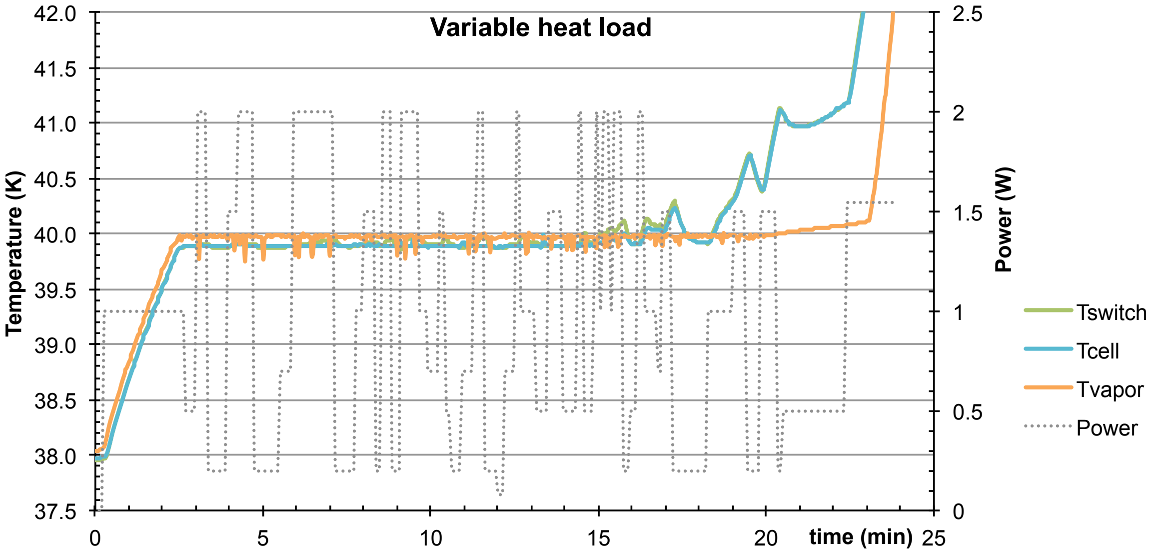

Figure 4-8 - Variable heat load profile in a controlled temperature mode at 40 K.

The temperature split between the cell and liquid temperatures is also observed in this test at ≈ 15 min., with the increase of the cell's wall temperatures in relation to the temperature of the liquid/vapor.

The tests in the *controlled temperature mode* showed the capability of this mode to obtain an auxiliary cold source with a constant temperature. By using a pressure control valve between the cell and the expansion volume it was possible to obtain a temporary cold source at constant temperature, like in the ESU's using the triple-point transitions. As already explained, the advantage of this this solution is that needs a lower mass/volume at low temperature due to the higher latent heat of the liquid to vapor transitions. The larger temperature range of operation is another advantage of this method. In the case of the triple-point transitions, only few discrete temperatures below 100 K are available. Despite of the constant temperature, the presence of the heat switch allowed to provide a vibration free environment, while the ESU acted as an independent could source.

4.3 Gravity insensitive system

Targeting this Liquid Neon ESU for space application, it was developed to be gravity insensitive. To turn the system gravity insensitive was one of the requirements to a future approval of this working principle to be used in a micrograviy environment. An orientable stand for the cryocooler and a structural support to enable the rotation of the cold components of the ESU were developed and were described in sections 3.4.1 and 3.4.2.

In Figure 4-9, the configuration of the ESU setup used to test the system performance as a function of the cryocooler orientation is schematized. The two ESU modes, *temperature drift* and *temperature controlled*, were tested at different orientations (0º, 45º, 90º, 135º and 180º). The orientation of the cryocooler was set before the beginning of the ESU cooling phase for all the performed tests.

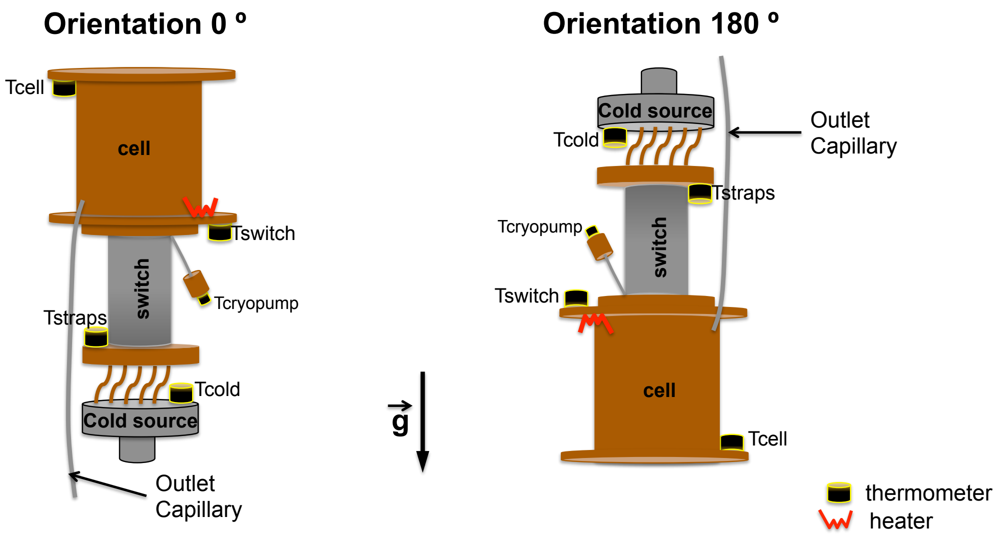

Figure 4-9 – Definition of 0° and 180° orientation and the location of the thermometers and heaters.

The case of 0º is considered the worst-case scenario. The capillary forces must overcome the gravity force, in order to avoid the expulsion of the liquid by the capillary tube during the evaporation. The lasts ESU experiments, reported in sections 4.1 and 4.2, were obtained using this 0º orientation.

<u>ESU temperature drift mode</u>

,An experiment of the ESU temperature drift mode in the 180º orientation is shown in Figure 4-10. With a filling pressure of 15.5 bars to obtain a final temperature of 40 K, the same experimental procedure as in the previous experiments was used (cf. Figure 4-4). The rate of temperature increase is faster than the expected when the heat power was applied, as observed also in the previous tests in the 0º orientation. A possible explanation relies on a small amount of liquid that initially is expelled to the capillary tube. Even in the 180º configuration, it seems that this amount was pushed out to the cell. About 4 % was the total amount of this initial liquid lost in the 180º orientation, a lower value than the one found in the case of the 0º configuration (8 %).

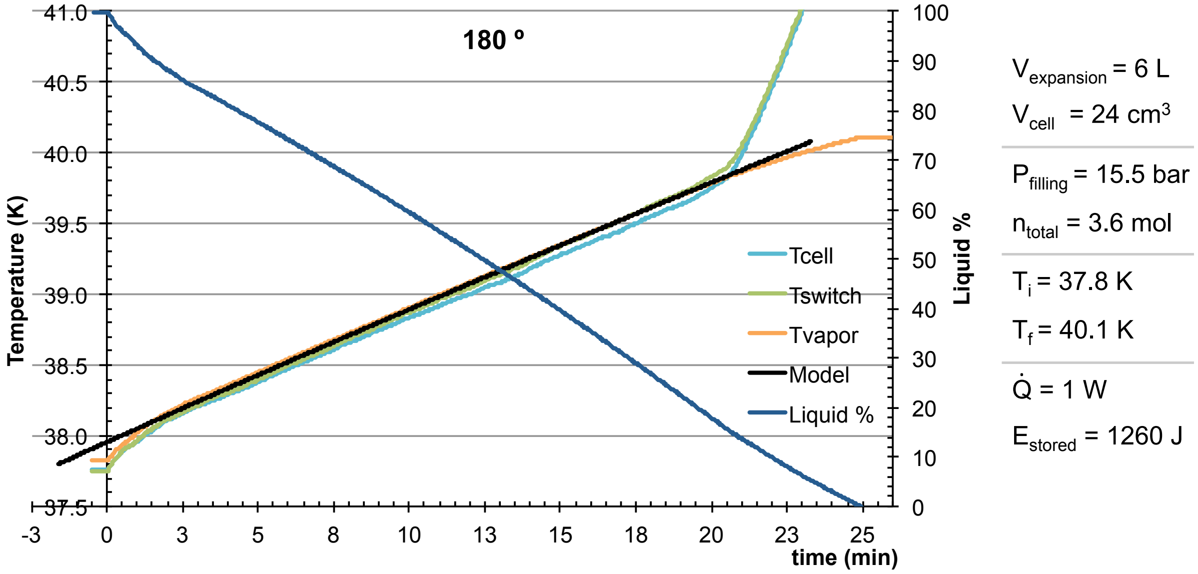

$V_{expansion} = 6$ L
$V_{cell} = 24$ cm^3
$P_{filling} = 15.5$ bar
$n_{total} = 3.6$ mol
$T_i = 37.8$ K
$T_f = 40.1$ K
$\dot{Q} = 1$ W
$E_{stored} = 1260$ J

Figure 4-10 - ESU temperature drift mode in the 180º orientation. The temperature split occurs when the liquid amount is ≈ 18 %.

With the system in the opposite orientation (180º), a temperature split between the cell and liquid temperature was observed when the liquid amount was around 18%. As previously observed, this temperature split phenomena is independent of the orientation and, as discussed in the Liquid Nitrogen ESU[9], the existence of small pores of the porous materials could provide an explanation for it: part of the liquid remains trapped in these pores without a continuous path to the cell walls that leads to a thermal gradient between this remaining liquid and the cell walls. As in the other tests, between the initial liquid loss and the temperature split, the ESU drift mode with the system in the 180º position runs like as predicted by the model implemented in the pre-dimensioning tool (solid black line).

Two opposite orientations (0º and 180º) tests are presented in Figure 4-11 for comparison. The initial conditions were equal in both experiments.

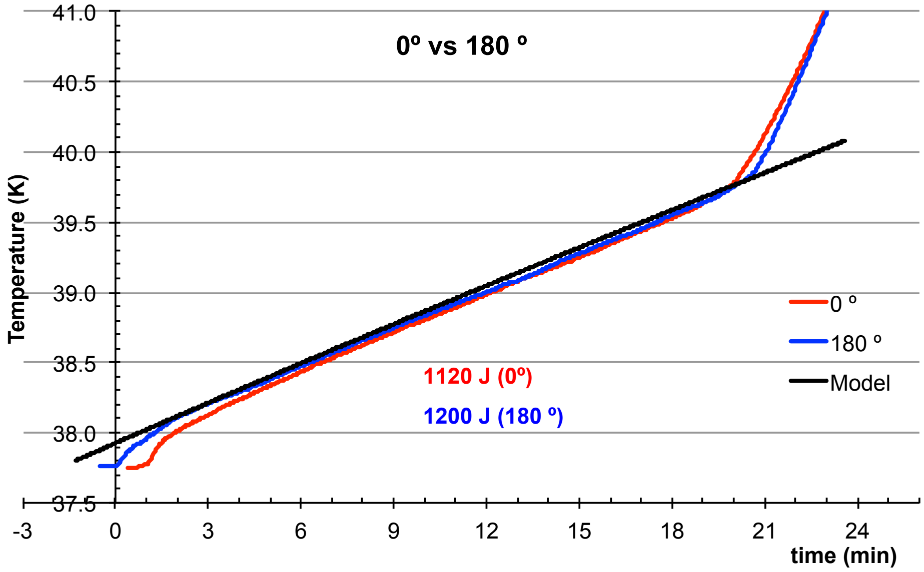

Figure 4-11 - Comparison between the temperature drift mode in the opposite orientations, 0º and 180º.

A sudden temperature increase was obtained in the beginning of the experiment at 0º configuration, which means that "as usal" a small initial liquid amount was lost. After this initial lost, a similar temperature drift was obtained for both experiments until the beginning of the thermal split. The temperature split occurs when the liquid amount is 19 % and 17 % for the 0º and 180º configurations, respectively.

A difference of 80 J in the total 1200 J stored energy (difference found based in the duration of the tests) was obtained in these similar experiments (using the same initial conditions but at different orientations). The lower energy stored was obtained in the 180º configuration due to the higher liquid lost in the beginning of the test. Nevertheless, the similar temperature drift profile obtained in the two cases evidences the capability of this ESU to operate in any direction.

ESU controlled temperature mode

An experimental test of the ESU controlled temperature mode at 40 K in the 180º configuration is presented in Figure 4-12. In this configuration, during ≈ 18 minutes, a stable temperature with 1 W of heat load power was also obtained. This duration corresponds to more 4 minutes than similar in the 0º configuration (240 J, Figure 4-6). The temperature split between the cells and liquid temperature was also observed for the same liquid remaining amount starting at ≈ 20 % of the total void volume of the cell.

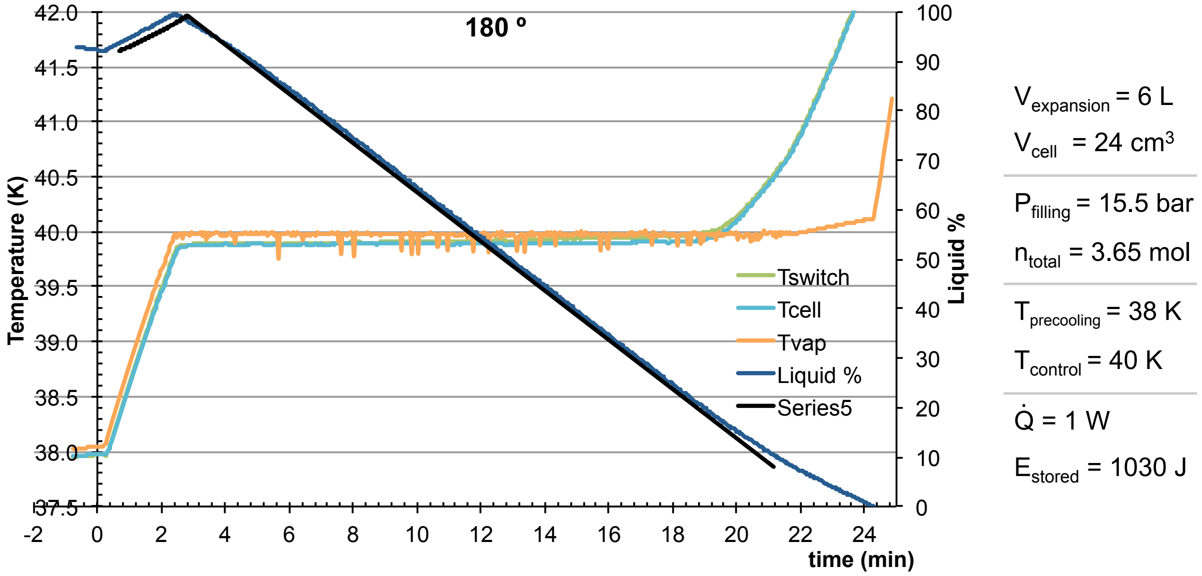

$V_{expansion}$ = 6 L
V_{cell} = 24 cm^3

$P_{filling}$ = 15.5 bar
n_{total} = 3.65 mol

$T_{precooling}$ = 38 K
$T_{control}$ = 40 K

$\dot{Q}$ = 1 W
E_{stored} = 1030 J

Figure 4-12 - ESU controlled temperature ESU mode at 40 K in the 180º configuration.

The black line is the predicted evolution of the amount of liquid inside of the cell during the control. Unlike the other tested configuration (0º), at the beginning, the rate of liquid amount was similar to the expected results: in this test, it seems that no liquid was pushed out to the cell. The difference in the energy stored in both configurations was only due to the initial liquid lost.

In order to try to clarify what happened at the beginning of the ESU mode, the controlled temperature mode at 40 K was tested for five orientations with 1 W of heat load using the same initial conditions (initial filling ratio (≈ 96%; initial temperature ≈ 38 K). The comparison between them is presented in Figure 4-13.The control time varies between 14 minutes in the case of the 0º orientation and 17 minutes in the case of 180º.

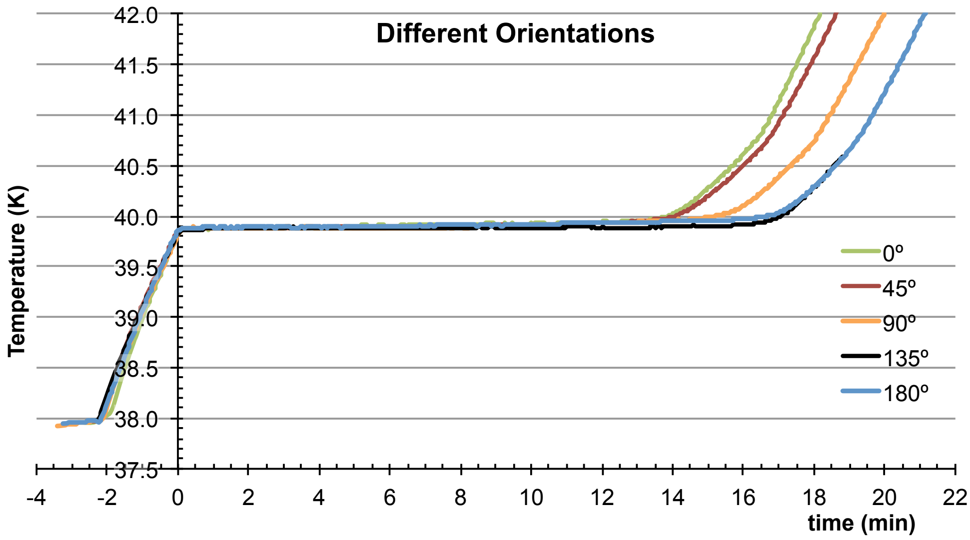

Figure 4-13 - Different orientations ESU temperature controlled mode at 40 K. The initial liquid amount is 100 % of the void volume of the cell.

The differences in the energy stored in these tests occurred in the beginning of the control. This mode operating at a constant temperature, this initial liquid lost amount is only observed through the liquid % behaviour, as the example of Figure 4-6. The amount of liquid pushed out of the cell in the beginning determines the difference between the ESU times in these five tests. From the curve of the liquid filling ratio versus time (not shown), it could be conclude that the temperature split occurs for the same liquid amount (≈ 20%) in the five tests.

The stored energy for previous tests as function of the cryocooler orientation is presented in Figure 4-14. The initial liquid amount in the beginning of all these tests was about of 100 % (squares) or 90% (circles) of the void volume of the cell.

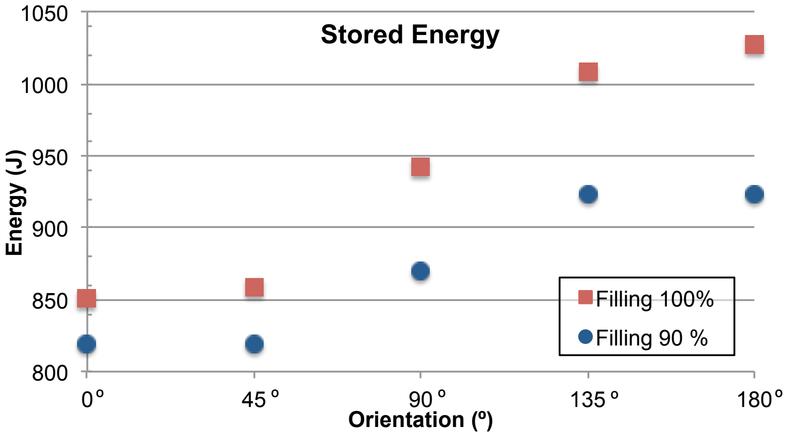

Figure 4-14 - Energy stored (at constant temperature) as function of the cryocooler orientation. The results are presented for two cases of initial filling: 100 % and 90 %.

The difference between the stored energy in the 0º and 180º orientations is about 17 % for an initial filling of 100 %. For the 90% initial filling, the difference of the performance between the opposite orientations decreases to 10%. This lower difference is due to a lower initial liquid lost in the beginning of the control. This result seems to indicate that it is possible to reduce the initial liquid lost amount by reducing the initial liquid amount in the cell. In fact, this was tested and can be observed in Figure 4-15 when the initial filling is about 75 % and this phenomenon is almost negligible. The liquid lost is lower than 1% of the total liquid amount.

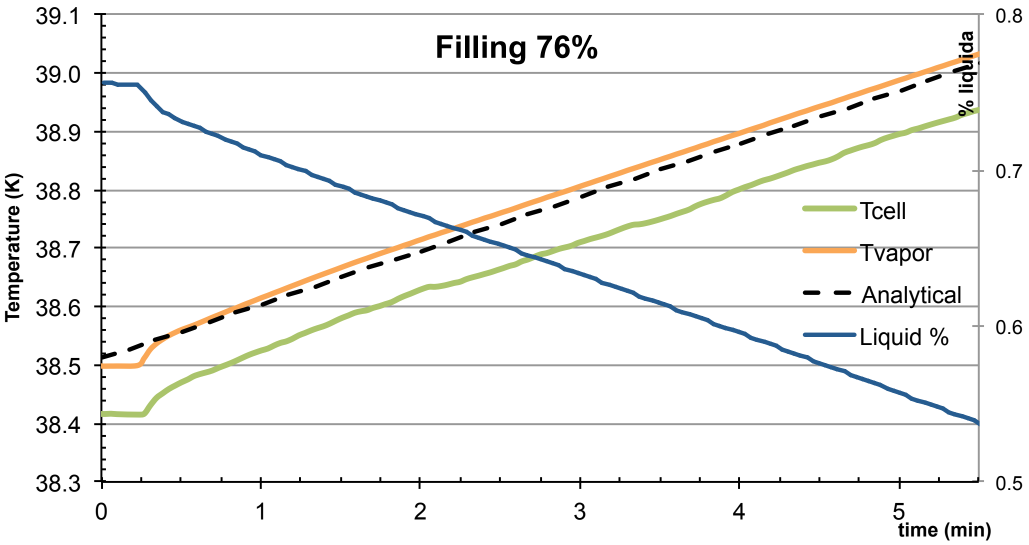

Figure 4-15 – Initial liquid lost amount in the case of the initial liquid cell filling of 76 %, applying 1 W of heat power.

4.4 Cooling process

Before any ESU mode operation, it is necessary to liquefy the neon in the cell and the duration of this process, the cooling time, is a function of the available cooling power. In this cooling process, in addition to the energy to liquefy the neon, it is also necessary to cool down the cell and the entire vapor that comes from the expansion volume at room temperature. This cooling time can be calculated theoretically using thermodynamics and these calculations were included in the pre-dimensioning tool. However, in order to obtain an accurate prediction, the knowledge of the thermal conductance of the elements that links the cell to the cryocooler is necessary. This thermal connection is made by the gas gap heat switch and the copper thermal straps (Figure 3-26). Both the elements were experimentally characterized: the total thermal conductance of the gas gap heat switch (in the ON state) and the thermal straps obtained at 40 K was $K_{total\_\exp}$= 0.4 W/K.

The temperatures during a cooling process are shown in Figure 4-16. The filling pressure was 15.5 bar using the 6 L expansion volume. The moment when the temperature of the cell achieved the saturation temperature (40.1 K; $t \approx 4$ min.) and the neon started to condense can be observed in this plot. This cooling process was performed maintaining the temperature of the cryocooler cold finger constant at 37 K and about 110 minutes was necessary to fill the cell with liquid. According to the conductance of the elements that connects the ESU to the cryocooler (switch and thermal straps), the maximum cooling power used to cooling the ESU occurred in the beginning of the cooling phase and was ≈ 1 W. Without controlling the cryocooler temperature, the cold finger would be much colder and more cooling power would be available, and a faster cooling process being obtained.

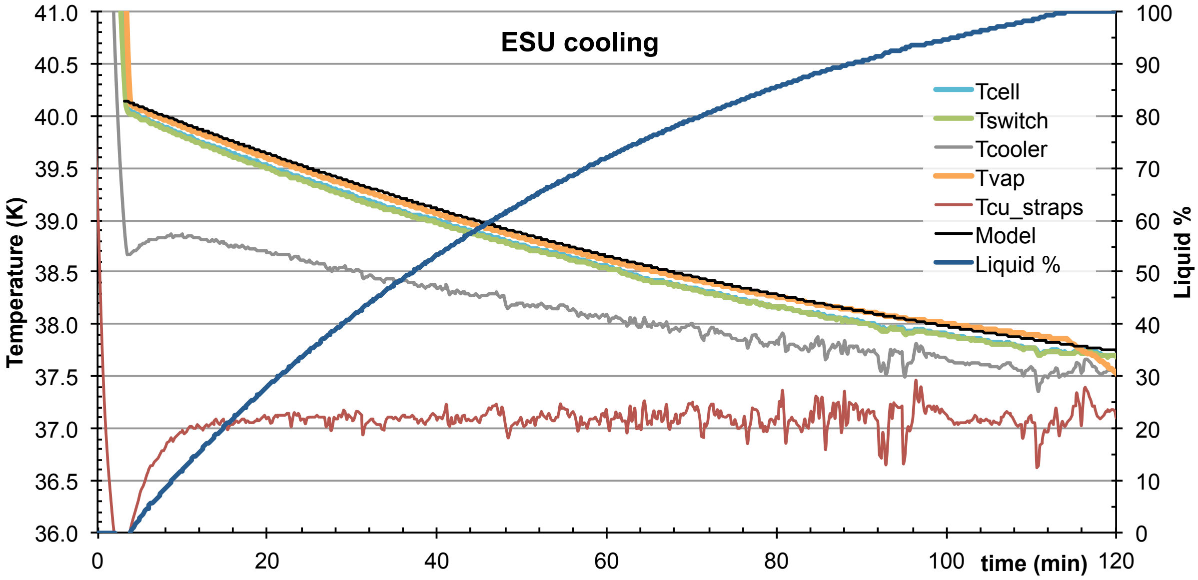

Figure 4-16 - Cooling phase of the ESU with the temperature of the cryocooler controlled at 37 K. The placement of the thermometers is available in the scheme of Figure 4-9.

For the simulation of this cooling phase, the temperature of the cryocooler and the thermal conductance of the set (switch and thermal straps) that connects the cell to the cryocooler were introduced in the pre-dimensioning tool. With these parameters the software returns the temperature of the cell as function of time. The predicted results are presented in Figure 4-15 by the black solid line. The very good agreement between these results and the experimental curve validates the pre-dimensioning tool and its use for prediction of the cooling dynamics of the ESU.

About 6500 J were removed from the system while cooling the ESU from 40.1 K to 37.8 K. About 20 % of this energy was used to transform the vapor into liquid (latent heat). This means that ≈ 80 % of this energy was exclusively used to cool the vapor from the expansion volume to the temperature of the cell. The storage of the gas at high temperature turns this process relatively inefficient, but the volume and mass budget that would be necessary to store the same fluid at a lower temperature turns the use of such a storage solution impracticable. In the example of the ESU's that operates at the triple point in a single volume configuration (section 1.2.2) as the PCM is always at low temperature the energy expended in the cooling phase is similar to the stored energy.

After this cooling, the ESU was ready to operate in the temperature drift mode between 37.8 K and 40 K. In these conditions it will be possible to store around 1300 J (20 % of the energy used to cooling the ESU), half of the energy required to cool the vapor stored in the expansion volume.

4.5 ESU cycle

Figure 4-17 shows the test performed on the ESU in a "continuous" operation. In this test the ESU was used to provide a temporary could source at constant temperature in a 180º orientation.

At the beginning ($t \approx$ -120 min) of the data plotted in Fig 4-16, the cryocooler was switched on to cool down its cold finger from the room temperature down to 37.3 K. At $t \approx$ 4 min the cell achieved the saturation temperature (≈ 40 K) and the neon started to condense inside the cell. During this **cooling phase**, analysed in the previous section, a good conductance between the cell and the cold finger is required: the cryopump was warmed up at 90 K (see cryopump characteristics, Figure 3-17) to maintain the switch in the ON state (section 3.3). Due to the condensation process, the neon stored in the expansion volume is pumped to the cell resulting in an overall system pressure decreasing. The pressure control valve was maintained open during this phase to allow the passage of the gas to the cell (see the bottom plot in Figure 4-17).

When the cell achieved the pre-cooling temperature ($T \approx$ 38 K, $t \approx$ 115 min), the ESU is charged (filled with liquid). Once achieved this pre-cooling temperature, the switch was toggled to the OFF state, by stopping the cryopump heating and allowing it to cool down. The switch commutation time (ON → OFF state) is ≈ 10 min. After cooling the cryopump, the cell was thermally decoupled from the cryocooler (switch OFF) that was turned OFF to provide a vibration-free environment.

The pressure control valve was closed and the setpoint to control at 14.6 bar was defined (to control at 40 K). The **temperature controlled mode** started by applying a heating power of 1 W ($t \approx$ 115 min). When the cell temperature achieved the setpoint (40 K), the ESU mode is starting, the valve beginning its pressure control. At this time the expansion of the evaporated neon to the expansion volume was controlled in order to maintain a constant pressure (and temperature) in the cell. During 17 minutes 1000 J were stored at constant temperature in a free vibration environment. During the expansion the pressure in the expansion volume was gradually increasing. The temperature split phenomenon between the cell and liquid temperatures appeared when the trapped liquid amount was ≈ 20 %.

When the pressure in the expansion volume become equal to the cell pressure, the valve stops to control and stays open. Until the end of the liquid, the **end of the ESU mode**, the evaporation continued like in the temperature drift mode (this phase appears clearly on the last plot). After the 1st cycle the ESU was empty and was necessary to recycle it ($t \approx$ 150 min). To start the cooling phase of the second cycle the cryocooler was turned ON again and, the cryopump was heated up again so the switch was toggled to the ON state. This process allowed the ESU to re-cooling and being re-used after (repeating the 1st cycle).

The total duration of the two cycles was ≈ 290 minutes, and during these cycles it was possible to use the ESU as an independent cold source at constant temperature with 1 W of cooling capacity during a total period of ≈ 35 minutes. In the energy point of view, in each ESU mode a total of 1030 J were stored. In this test, when in operation, the cryocooler was maintained at constant temperature T = 37.3 K.

In the presented case, a sensor that works at stable temperature dissipating 1 W was simulated. This sensor operates whenever possible, and it is only interrupted by the impossibility to maintain a stable temperature without the duty cycle.

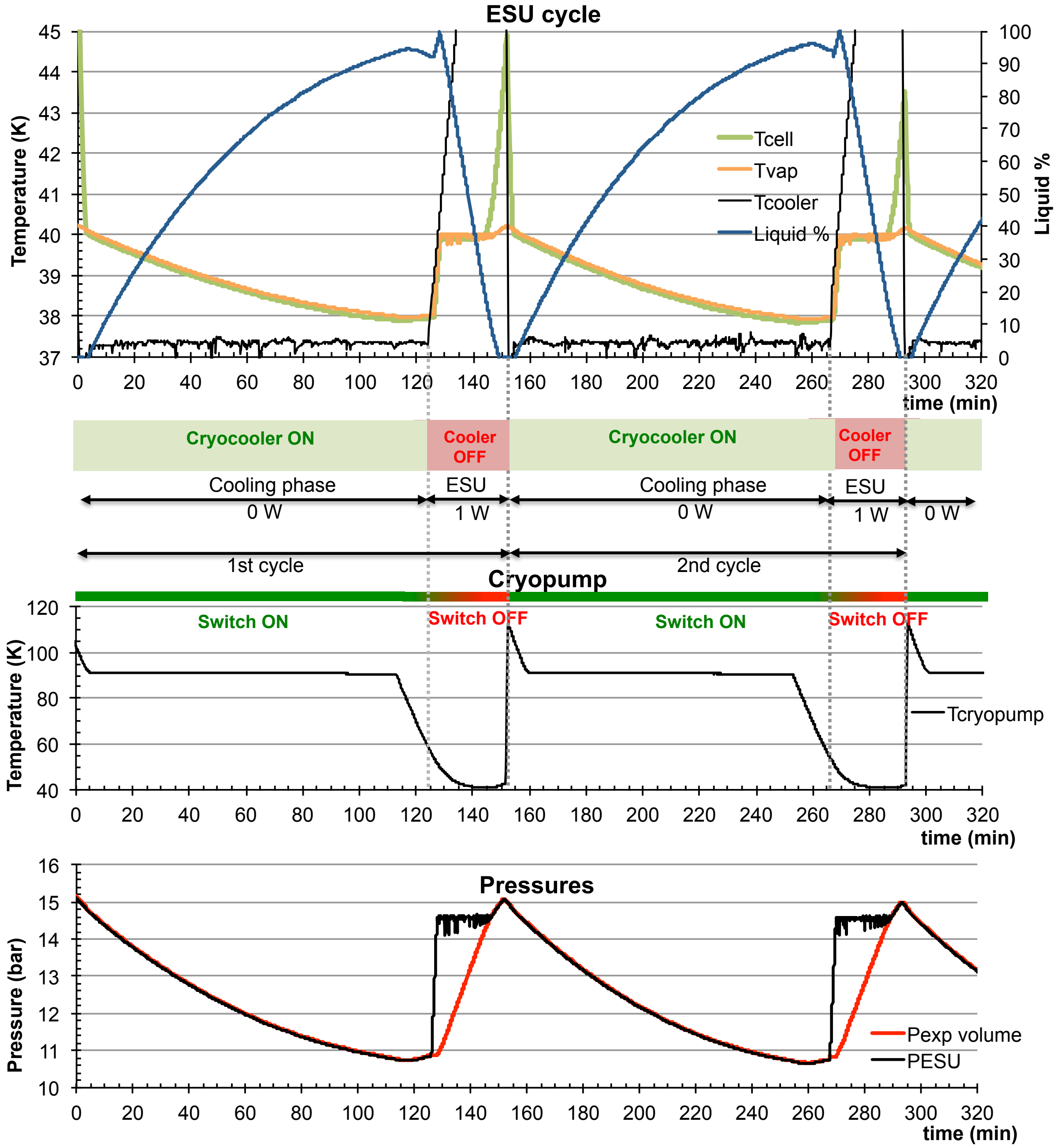

Figure 4-17 - Temperatures and pressures variations during two complete cycles: In the first plot the ESU temperatures are presented; In the second is the temperature of the cryopump; The third plot represents the pressures of the cell and of the expansion volume.

4.6 Power booster mode

The ESU power booster mode is used to temporarily increase the cooling power of a cryocooler in permanent working or to obtain a stable cryocooler temperature. In this operational mode the cell was directly coupled to the cold finger of the cryocooler as shown in Figure 4-18. Inside the cell a heat exchanger (described in the section 0) was used to increase the temperature homogeneity between the cell and the liquid (and to avoid any possibility of critical boiling). In these tests, no porous material was used and the power booster mode was only tested in the orientation described in Figure 4-18 where the liquid cannot be (in principle) be expulsed. The volume of this smaller cell is V_{cell} =12 cm^3.

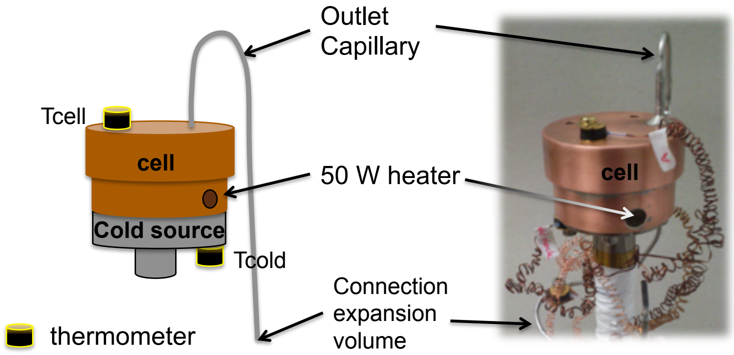

Figure 4-18 – ESU power booster mode configuration. A 50Ω/50 W heater was embedded in the cell bottom. In this mode a heat exchanger was used inside of the cell. No porous material was used. A 6 litres expansion volume was used.

The cryocooler used was the same that used to test the other ESU modes, with a cooling power at 40 K around 4 W.

The verification of the temporary increase of the cryocooler cooling capacity was the objective of the first tests performed using the ESU in this operational working mode and Figure 4-19 presents an example of such a test in which a 6 litres expansion volume was used and the filling pressure was 15.5 bar.

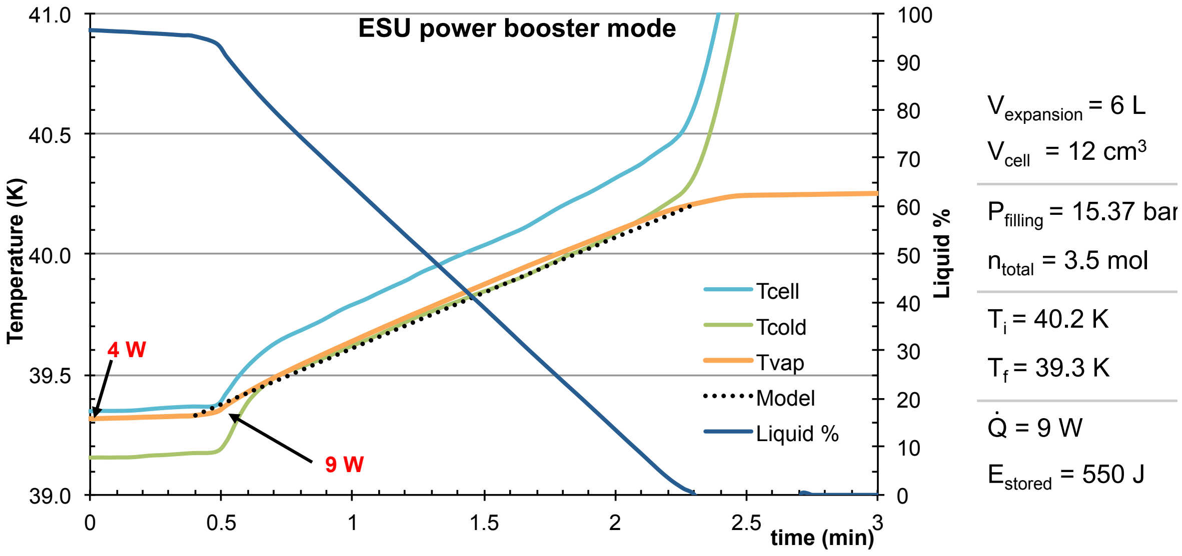

Figure 4-19 – Experimental result of the ESU Power booster mode. The heat load applied was 9 W and the cryocooler capacity is ≈ 4 W.

At the beginning of this test, a heat load of 4 W (the cooling power of the cryocooler) was applied to obtain a stable temperature (≈ 39.3 K). With the cryocooler in continuous operation at $t \approx 0.5$ min a heat load of 9 W (4 W for the cold finger control at 40 K + 5 W extra power applied) was applied in the cell. Like in the ESU temperature drift mode, the liquid neon evaporates and the gas expands to the expansion volume increasing the overall pressure and consequently the cell temperature. When all the liquid is evaporated, the ESU booster mode finishes and a large increase of the cell's temperature is observed. In this test, during 1.8 minutes, the heating power jumped from 4 W to 9 W whereas the temperature drifts only about 1 K. The cooling capacity of the cryocooler was doubled during 1.8 minutes. The correspondent stored energy was 550 J. Let us note that:

- T_{cell}-T_{cold} is more or less constant: the cell stays isotherm or no extra temperature gradient appeared during the extra heating;
- Even using a high heat load the difference of the temperature between the cell and liquid (T_{vap}) did not exceed 0.25 K evidencing the importance of the heat exchanger.

In Figure 4-19, the dashed black line represents the predicted results obtained with the pre-dimensioning tool. Using the total heat load of 5 W applied of in the ESU a reasonably good agreement with the experimental results was obtained.

In order to show the benefit of an ESU in the power booster mode, a similar test without using the ESU was also performed. Actually, the 300 g copper cell was maintained direct coupled in the cold finger but without neon inside. The total energy to increase the temperature of the copper cell in 1 K is ≈ 30 J. The direct comparison between the tests using the ESU in the cryocooler and "without the ESU" is presented in Figure 4-20. In both tests the heat load applied was 9 W. In the test without the ESU a large increase of the temperature was observed when the heat load was applied, after 2 min, its temperature would reach ≈ 51 K. The case where the ESU was used, presented in Figure 4-19, during almost 2 minutes the ESU could dissipate the heat load applied with a temperature drift lower than 1 K.

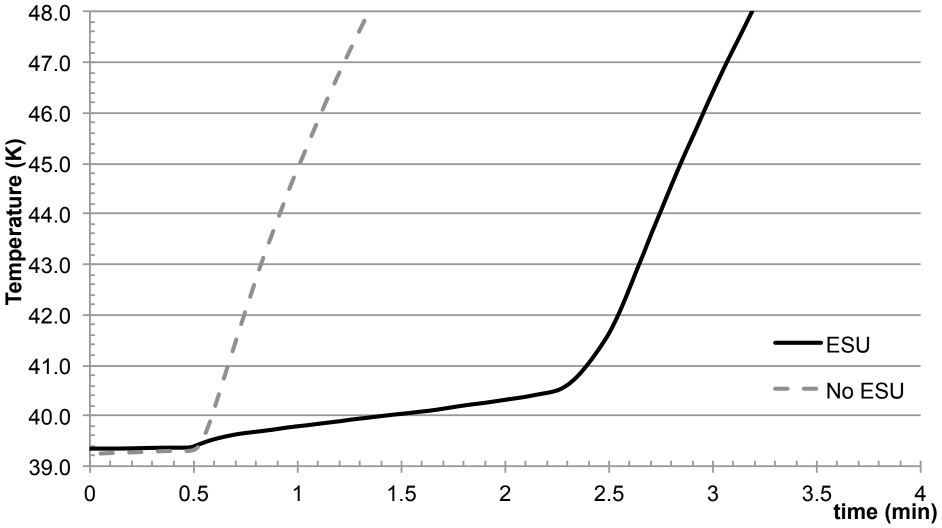

Figure 4-20 - Experimental results of the influence of use the ESU as power booster in the cryocooler. The heat load used was 9 W. The test using the ESU is the same presented in Figure 4-19.

These tests showed that using a rather small cell (V=12 cm^3) directly coupled to the cold finger of the cryocooler turns possible to double the cooling capacity of the cryocooler up to 2 minutes without a large temperature drift. This test reinforces the advantages to use an ESU in applications where short events with a large cooling power is needed, turning unnecessary the use of oversized cryocoolers.

As previously demonstrated, the pre-dimensioning tool also can predict the cooling process, but in this case the uncertainty associated to the cooling capacity of the cryocooler turn more difficult the simulation process. In this process the energy needed to cool down the gas from the expansion volume (at room temperature) is ≈ 4/5 of the total energy expended in this process. But, if the gas is cooled before entering the cell it is possible to reduce this energy parcel.

In a cyclic operation, the evaporation of the cold vapor to the expansion volume results in a cooling of the capillary tube that connects to the cell. In the following cooling process, the vapor that passes through the tube is pre-cooled before entering the cell. The capillary tube acts as a regenerator and, despite of the low mass of the capillary tube, the high specific heat of the stainless steel tube turns this pre-cooling of the vapor into a rather efficient process. An estimative of the values of each contribution is presented in Table 4.2. Considering the temperature difference between 300 K and 40 K the enthalpy of the stainless steel capillary tube (1 meter) is 1/3 of the enthalpy of the vapor (0.5 mol).

Table 4.2 - Comparison between the enthalpy of the vapor that flows through the tube while entering the cold cell and the tube itself. The obtained enthalpies are estimated between 40 K and 300 K. The length of capillary tube considered is 1 meter.

Substance	**Quantity**	**Enthalpy (T_{300} – T_{40})**
Neon gas	0.5 mol	2800 J
SS capillary	10 g	1000 J

In a real case the capillary tube is not whole at 40 K in the beginning of the cooling phase, but this effect (the enthalpy of the SS capillary) reduces significantly the total energy to be extracted by the cryocooler. In the simulation process, it is not easy to quantify the exchanged energy between the capillary tube and the vapor and this simulation process would be simplified if the temperature of the vapor that enters the cell was known.

In order to obtain a better knowledge of the vapor temperature and then to be able to test the "pre-dimensioning tool" software with more accuracy, a small heat exchanger (HX) was built and located along the circuit (Figure 4-21). A copper capillary tube (ϕ = 2 mm) with 30 cm length coiled in a copper tube with 20 mm diameter was used for this heat exchanger. The length of this capillary tube was sized to ensure the thermalization between the coil and the vapor (with temperature difference below 1 K) after its passage.

This heat exchanger intersects the outlet capillary tube, without any thermal link to the cold source. This means that its temperature is dependent on the mass flow and the temperature of the vapor passing through it. The measurement of the heat exchanger temperature, during the cooling phase, gives with a good approximation the vapor temperature when it enters the cell.

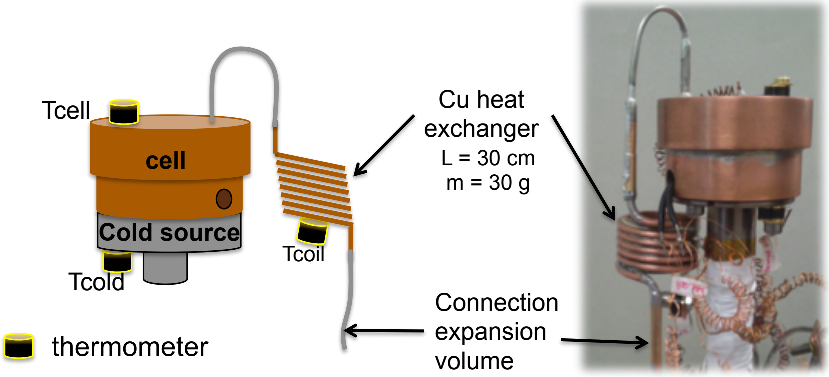

Figure 4-21 - Scheme and picture of the heat exchanger used to measure the temperature of the vapor. The length of the capillary tube coiled is 30 cm to ensure the thermalization (difference < 1 K) between the coil and the vapor in the case of the maximum gas flow.

The temperatures of the ESU and the HX coil during the cooling process experiment are presented in Figure 4-22(upper and lower part, respectively). In the beginning of the cooling process the temperature of the coil was ≈ 220 K. This temperature was significantly lower than 300 K because this test was preceded by other experiments. Even in the case of the first cooling process, the initial temperature of the coil is lower than 300 K (≈ 260 K) due to its short connection to the cell (≈ 5.5 cm of 1.5/2 mm capillary tube).

In this test (Figure 4-22), during the cooling phase, the neon gas coming from the expansion volume at 300 K leads to a temperature increase of ≈ 30 K on the HX (red line). Knowing the temperature of the gas that enters the cell, it was possible to predict the evolution of the cell's temperature during the cooling phase (black dashed line). For the simulation, the cooling power of 4.2 W was assumed and despite of the uncertainty about this value, a good agreement with the liquid temperature was obtained.

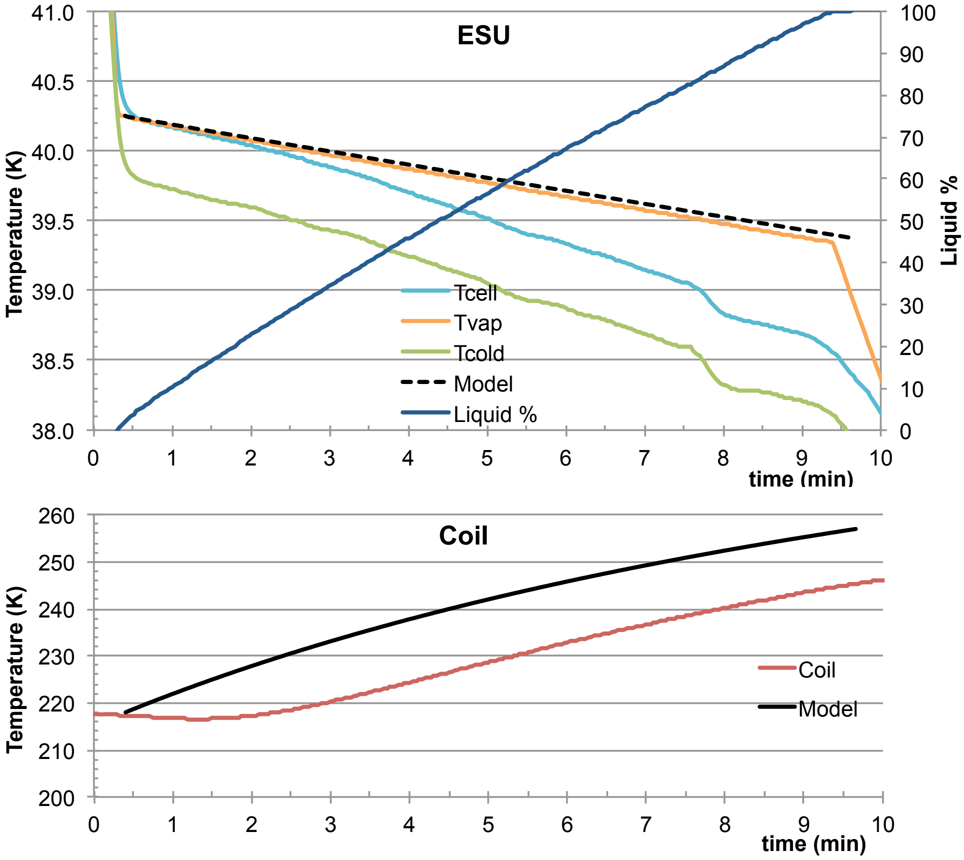

$V_{expansion} = 6$ L

$V_{cell} = 12$ cm^3

$P_{filling} = 15.5$ bar

$n_{total} = 3.6$ mol

$T_i = 40.3$ K

$T_{final} = 39.4$ K

$\dot{Q} \approx -4.2$ W

Figure 4-22 – Temperatures of the ESU and of the coil during the cooling phase.

Considering the heat capacity of the HX (≈ 30 g of copper), it was also possible to predict its temperature evolution during the ESU cooling process. The solid black line in the lower plot of Figure 4-22 represents this prediction calculated by the pre-dimensioning tool. In this simulation, a perfect thermalization between the neon gas coming from the expansion volume at 300 K and the HX was considered. The predicted result is higher than the experimental one. However this difference can be qualitatively explained taking into account that, actually, the capillary tube connecting the HX to the expansion volume is at an intermediate temperature lower than 300 K at the beginning of this test, being partially cooled down by conduction and/or by the regenerative effect of the tube that was cooled down by preceding experiments. This means that at the beginning of the test the neon reaches to the HX at a temperature lower than 300 K, the value that was assumed in the calculation. This argument can explain the higher temperature of the HX coil obtained with the model. When the temperature of the coil starts to increase, despite of the temperature difference, the temperature increasing dynamics is similar to the predicted model.

Let us note, that, in addition to allow the temperature measurement of the gas entering the cell, such an "extra heat capacity device" acting as regenerator, as it is the case of this HX, can lead to an efficient gas precooling and then to a shorter cooling time.

The existence of the HX along the capillary does not affect the evaporation process, but knowing the gas temperature while flowing through it can be useful for further simulations. In Figure 4-23 the temperatures of the cell (upper graph) and of the HX (lower graph) and their predictions during an evaporation experiment are presented. This test was performed applying a heat load of 4 W for *t* < 0.1 min and 11.5 W *t* < 0.1 min. As in Figure 4-19, the simulation of the cell temperature using the pre-dimensioning tool (dashed black line of Figure 4-23) is in quite good agreement with the experimental results.

The temperature of the coil was reduced from 215 K to 100 K due to the evaporation of all the liquid neon inside of the cell. The predicted results for the coil temperature are represented in Figure 4-23 by the solid black line and its final temperature is close to the measured temperature (≈ 95 K). The time constant of the coil wasn't taken into account in the simulation and consequently the obtained temperature profile is shifted in time.

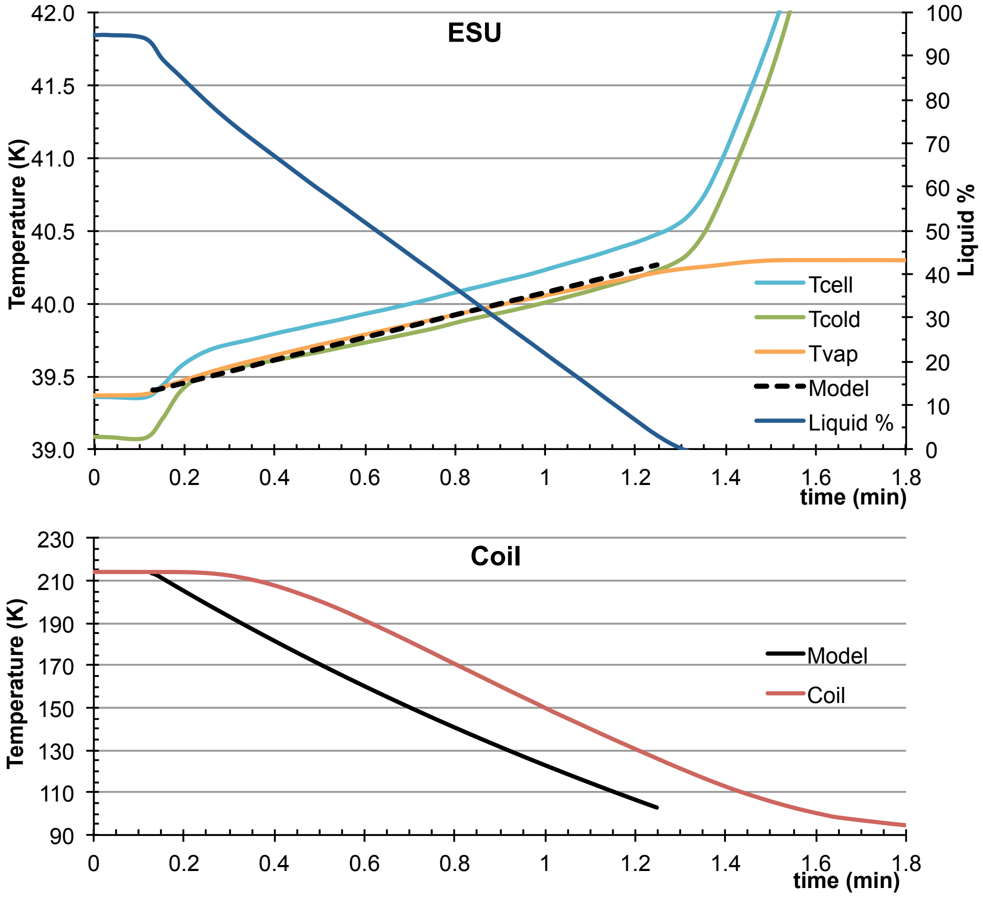

Figure 4-23 – Test of the ESU with the cryocooler in permanent working using a heat power of 11.5 W. Prediction of the coil's temperature (Model) in this case of the neon evaporation its measured temperature (Coil).

However, the calculation of the exchanged energy in the coil is more accurate for the evaporation than for the condensation process. Due to the short connection between the coil and the cell, the temperature of the evaporated neon is assumed constant until arriving at the coil. In opposition, in the condensation phase the neon gas has to travel along a rather long capillary tube (≈ 1 meter) at a temperature lower than 300 K that pre-cools the neon coming from the expansion volume. This results in a lower gas temperature at the inlet of the coil than the one assumed in the pre-dimensioning tool.

With these last results the use of the pre-dimensioning tool was validated for calculating the booster mode and as shown it can be used to predict the ESU temperatures in a cyclic operation.

Variable heat load profile

The energy storage unit can also be used to absorb sudden heat bursts, providing a better thermal stability of the cryocooler temperature. In the case of a sudden heat burst a mix of the two processes previously described, the condensation and the evaporation processes, occur. With the cryocooler in permanent operation during the ESU mode, if the heat load applied becomes lower than the cryocooler cooling power, a recycling process starts.

To test such effect, the response of the ESU when subjected to a variable heat load was studied using the heat profile depicted in Figure 4-24. The heat load profile used for testing was a squared wave with 3.5 W and 7.5 W as minimum and maximum heat loads respectively, and with a period of 10 s. As the minimum heat power in this profile was lower than the available cooling capacity (4.5 W), a partial recycling process of the ESU should occur during half of the period.

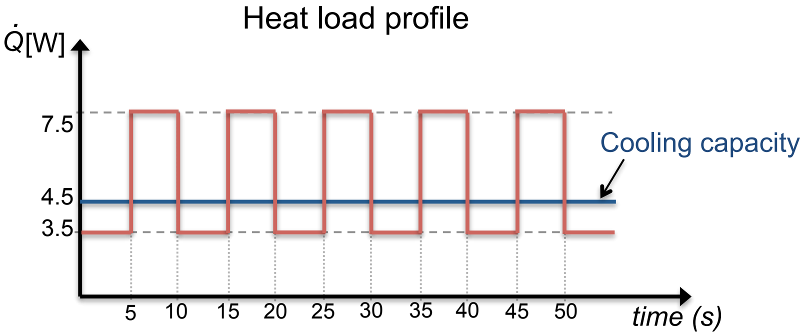

Figure 4-24 - Heat load profile applied in the ESU. The cooling power of the cryocooler assumed in the pre-dimensioning tool was 4.5 W.

Figure 4-25 depicts the behaviour of the ESU when subjected to this heat load profile. In this test, the ESU was previously pre-cooled at 39.4 K and in the beginning the coil's temperature was 180 K. During $t \approx 9$ minutes the cell's temperature increase was lower than 1 K even with the heat bursts of 7.5 W. The applied heat load profile is clearly identified by the increase and decrease of the ESU temperatures and in the liquid amount inside the cell, where part of the liquid amount was recovered (about 3 %) when the 3.5 W heat load was applied. Despite of the cell HX used, the temperature oscillations measured on the copper cell are higher than the ones obtained in the temperature of the liquid/vapor (T_{vap}). These oscillations of the liquid temperature are lower than 200 mK, similar to the predicted results of the model developed represented by the solid black line. The model also predicted the temperature of the coil and a difference of 20 K (in a total of 100K) in the final temperature was obtained.

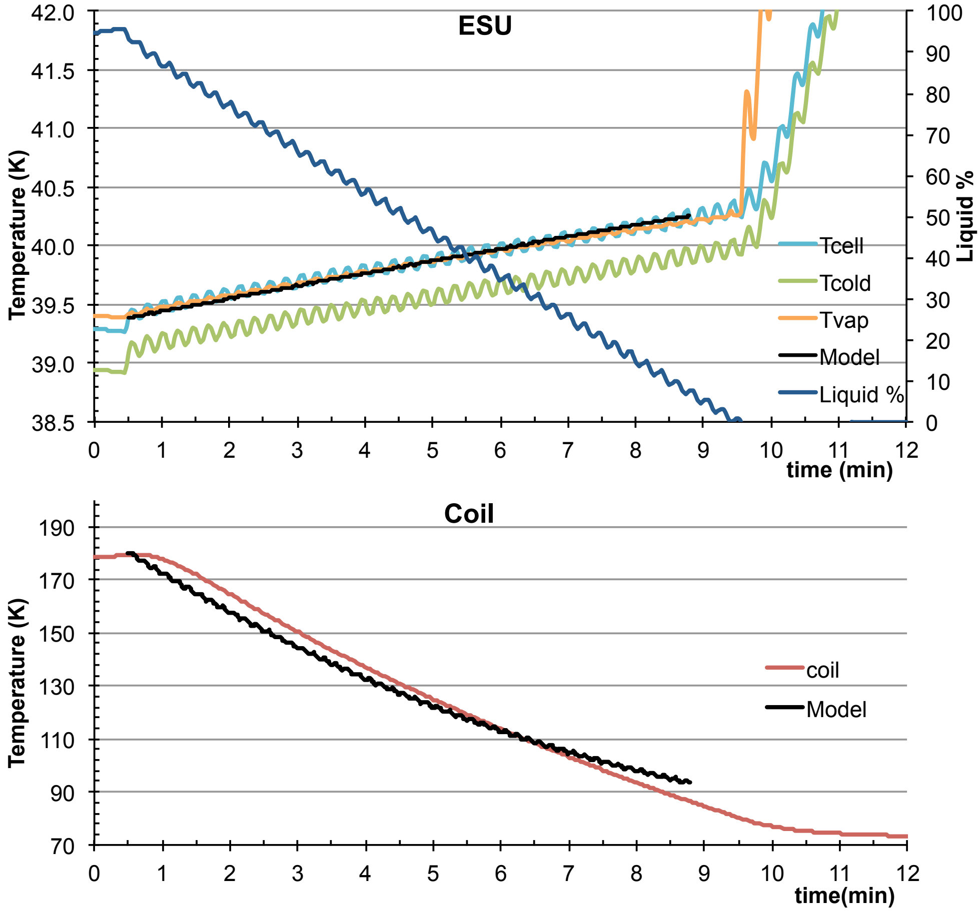

$V_{expansion}$ = 6 L

V_{cell} = 12 cm^3

$P_{filling}$ = 15.5 bar

n_{total} = 3.6 mol

T_i = 39.4K

T_f = 40.2 K

Figure 4-25 – Experimental test applying the variable heat load profile of Figure 4-24 in the ESU. The simulations of the temperatures of the ESU and the coil were performed in the pre-dimensioning tool.

The initial conditions as well as the initial temperature of the coil are the inputs of the simulation. With these input parameters, the pre-dimensioning tool calculated the coil and cell temperatures. The final coil temperature (i.e. when no more liquid exists in the cell) found was 95 K compared with the measured 74 K. But similarly as explained in the simulation of the cooling process (Figure 4-23) when the neon comes from the expansion volume towards the cell and flows through the coil, its temperature in the simulation is assumed to be 300 K while the temperature at which the neon enters in the coil is lower than the room temperature due to the cooling of the connections between the coil and the expansion volume in the evaporation processes during the precedent cycles.

A quite reduced temperature drift of the ESU was observed when it was subjected to the heat load profile of Figure 4-24 and showed its potential application for transitory events as is the case of sudden heat bursts, turning unnecessary the use of oversized cryocoolers. To point out the capacity of the ESU to absorb the sudden heat bursts, the same test without using the ESU was performed and its results are shown in Figure 4-26.

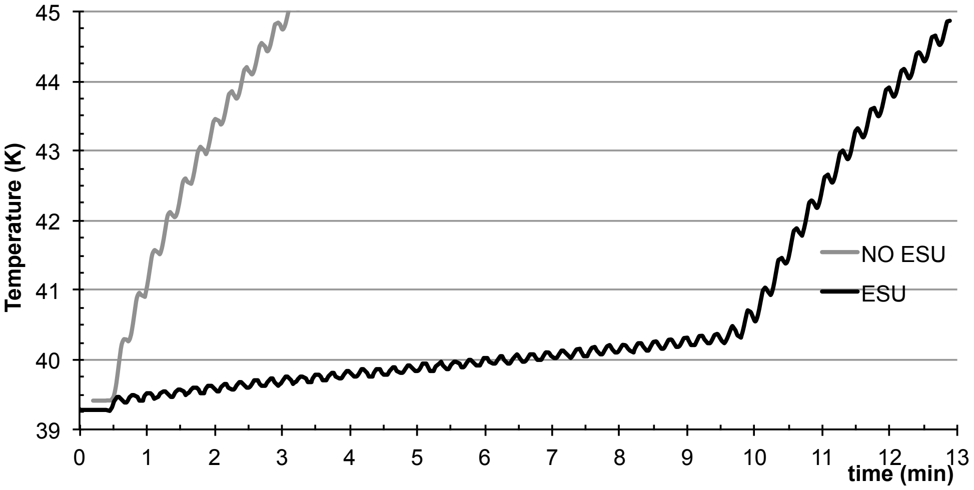

Figure 4-26 - Influence of the ESU to absorb the heat load profile of Figure 4-24

From Figure 4-26 one can read that, when the ESU was not used, in less than 20 temperature of the cryocooler increases by 1 K, whereas, the same temperature increase is obtained after 9 minutes if the ESU is used.

Smaller expansion volume

The influence of the size of the expansion volume in the temperature drift at this work was described in section 0. As the larger is the expansion volume, the lower would be the temperature drift or the difference between the pre-cooling and the control temperature in the case of the *ESU temperature controlled mode*.

In the temperature controlled mode, for a given control temperature and the same liquid amount condensed in the cell, the size of the expansion volume does not affect the stored energy, it only affects the pre-cooling temperature, temperature at which it is necessary to cool down the cell in order to fill it with liquid: the smaller the expansion volume the lower is this pre-cooling temperature.

In opposite to the temperature controlled mode, the size of the expansion volume in the *ESU booster mode* and in *temperature drift mode* affects the stored energy for the same liquid amount initially condensed in the cell. To show these effects, the same experiment in equivalent conditions was performed using 3 L and 6 L expansion volumes. In these tests, the cell was filled with the same liquid amount and the filling pressures were chosen in order to obtain the same final temperature. The two tests using a heating power of 9 W are presented in Figure 4-27.

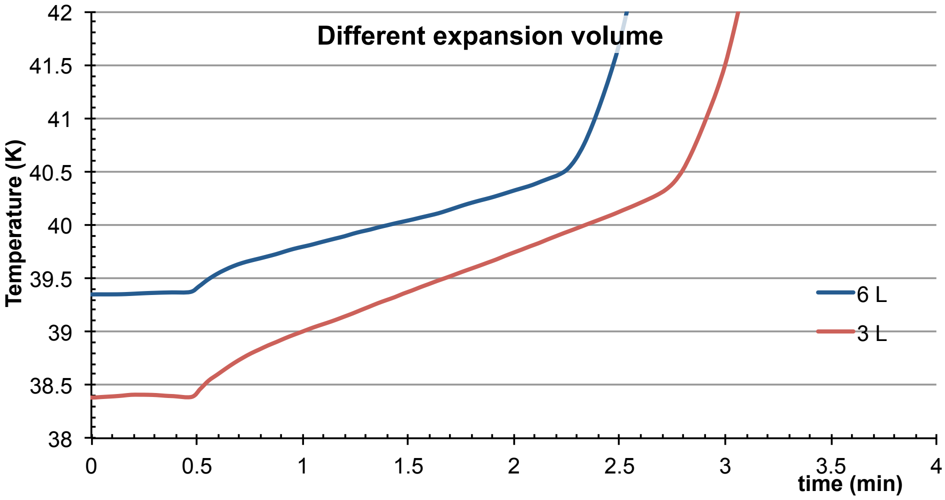

Figure 4-27 - Experiments of the ESU booster mode using 2 different sizes of expansion volume: 3 L and 6 L. The heat load power applied was 9 W.

To obtain the same initial liquid amount (100 %) in both tests, it was necessary to cool the cell down to 38.4 K and 39.4 K, for the 3 and 6 litres expansion volume, respectively. This means that the smaller volume (3 litres) leads to a temperature drift (38.4 K – 40.4 K) twice than the obtained with the larger volume as predicted in the expansion volume section (section 0).

A clear difference was observed between the duration of each ESU mode: Using 3 litres volume, the ESU duration was ≈ 2.3 min, storing ≈ 690 J whereas, for the 6 litres, in ≈ 1.8 min, some ≈ 540 J were stored. The time difference being about 30 s, represents an energy difference of 150 J in the total stored energy. This difference is due to 3 factors:

- Sensible heat of the liquid: Part of the energy is used to heat the liquid during the temperature drift. This contribution was doubled with the doubling of the temperature drift (3 L case).
- Heat capacity of the cell: The heat capacity of the cell materials (copper) was doubled with the temperature drift increase.
- Latent heat: the test with the 3 litres volume requesting a lower precooling temperature, takes advantage of the small increase of the latent heat at lower temperatures L(38.4K)= 57.8 J/cm^3 ; L(39.4K)= 52.2 J/cm^3.

The 3 factors are ordered by their influence in the increase of the stored energy when a smaller expansion volume is used.

The ESU booster mode was also tested with the 3-litres expansion volume using a variable heat load profile. This heat load profile consists in a squared wave with 13.8 W and 0 W of maximum and minimum heat loads and a period of 20 s. Figure 4-28 displays the temperature of the ESU when subjected to this heat load profile. In this figure the same test using the 6-litre expansion volume and a test “without ESU” are also presented.

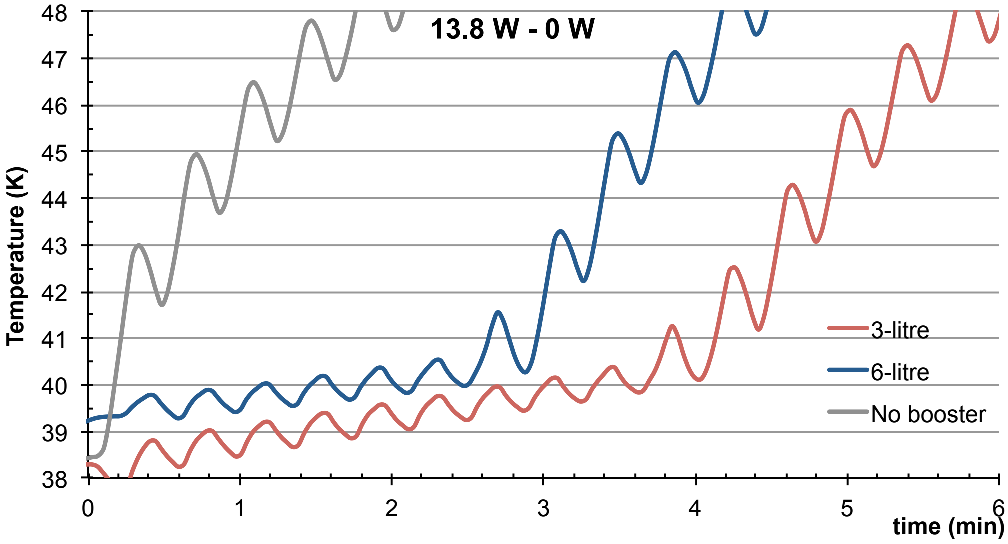

Figure 4-28 – ESU booster mode tested with a squared wave (0 W - 13.8 W - 0 W) with a period of 20 s. The ESU was tested with the 3 and 6 litre expansion volumes. A test with the same heat load profile without ESU is also shown.

As in the previous test, the temperature drift with the 3 litre expansion volume (≈ 2 K) was the double of the obtained with the 6 litre volume (≈ 1 K). Due to the 3 factors previously presented, for the same initial liquid amount, a higher stored energy with the 3-litre expansion volume was obtained and then the ESU mode is maintained during a longer time.

The heat bursts applied were three times higher than the cooling power of the cryocooler and the temperature increase in each heat burst was lower than 0.3 K. The gain obtained by an ESU to smooth this bursts is clearly evidenced when the same test was performed without ESU (grey line in Figure 4-28): A single heat burst of 13.8 W during 10 s was enough to increase the temperature of the cryocooler in 4.5 K.

We showed in this section that for Neon ESU operating at 40 K a small volume of 3 litres could be used. The use of smaller expansion volumes is also possible, but increase the temperature drift between the initial and final temperature and lead to an increase of the charging pressure, which require a thick cold cell.

4.7 Summary

In this work, energy storage units that using latent heat of the liquid neon was designed, built and tested in three distinct modes:

- *ESU temperature drift mode*: this ESU mode operates between an initial and a final temperature, defined by the expansion volume size and the system filling pressure. This operation mode was tested in a vibration free environment, turning OFF the cryocooler (in cycling operation) and using a heat switch in order to thermally isolate the ESU from the quickly cryocooler temperature increase. Up to 1200 J or 1 W during 20 min was stored between 38 K and 40 K.

- *ESU temperature controlled mode*: controlling the pressure inside the cell it was possible to obtain a constant temperature during the neon evaporation. Up to 1000 J (1 W during 17 min) was stored at 40 K. This mode could have the same functionality of an ESU working on a triple point (section 1.2.2) but takes advantage of the higher latent heat of the neon and its larger temperature range of application compared to the triple point transition. This mode was also tested in a vibration free environment, acting as an independent could source.

- *ESU booster mode*: The ESU was used to temporarily increase the cooling capacity of the cryocooler or to obtain a better cryocooler temperature stability. In this mode the ESU was directly coupled to the cryocooler, which was maintained in permanent operation. The performed tests shown the capability of the 12 cm^3 ESU to duplicate the cooling capacity of the cryocooler ($P_{\text{cryocooler}} \approx 4.5$ W) up to 2 minutes (500 J) with a temperature drift of only 1 K. The tests also showed its potential application to smooth the cryocooler temperature when it was subjected to a periodic heat bursts up to 14 W. A smaller expansion volume with half a volume (3 L) was tested and, for the same initial conditions as in the case of 6 L, the temperature drift between the initial and final temperature was doubled.

The development of the pre-dimensioning tool was a good step in the prediction of the ESU experimental results. Using this software, almost of all the experimental results presented here were successfully simulated, even in the case of the use of a variable heat load profiles. The validation of such tool allows us to confidently design another similar ESU for some real application, under a specific requirement.

The ESU temperature drift mode and the controlled mode were developed to be gravity insensitive. Tests in different cryocooler orientations showed the capability of the porous material (filter paper) to confine the liquid inside the cell. However, a difference up to 17 % was found in the ESU performance between the 0° and 180° cryocooler orientation in the temperature controlled mode and 5 % in the temperature drift mode. This phenomenon is associated to an initial liquid loss found in all the ESU tests. This phenomenon is discussed later in this section.

Another phenomenon was detected that seems related to the use of the porous material: When the remaining liquid amount is about of 20 % a thermal split between the cell and the liquid occur, turning inaccessible the use of this last liquid amount. Some tests are shown later in this section aiming to better understand this phenomenon.

4.7.1 Initial liquid lost

The initial liquid loss was observed in all the tests performed in the *ESU temperature drift mode* with the filter paper. At the beginning, we associated this phenomenon to the incapacity of the porous material to confine the liquid inside the cell. But the emergence of this phenomenon for all the cryocooler orientations as well as for liquid ratio relatively small seems to exclude this hypothesis.

To understand the causes of this phenomenon, some tests were performed to quantify this initial liquid lost: Namely, its dependence of the initial filing amount, the heat load applied on the ESU, the orientation of the cryocooler and the position of the heater on the cell.

The dependence of the initial liquid loss with the initial filing amount was tested using the same initial conditions of the experiment of Figure 4-4. The filling pressure of 15.4 bars was maintained in these tests. But, to successively obtain a lower initial liquid amount, a higher initial temperature was chosen. The cryocooler orientation was the 0º ("antigravity" orientation with respect to the capillary outlet) and the outlet capillary tube was in the bottom of the cell (configuration B of Figure 4-1). This is considered the worst-case scenario because the capillarity forces have to overcome the gravity force in order to avoid dropping any liquid by capillary tube. The results of initial liquid loss dependence versus the initial liquid filling amount tests are presented in Figure 4-29.

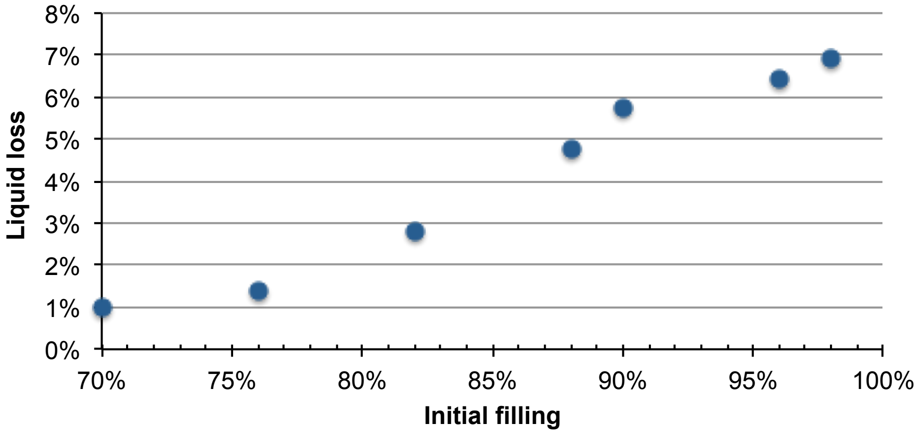

Figure 4-29 - Liquid lost amount in the beginning of the ESU drift mode as function of the initial filling. The liquid percentage loss is in relation to the initial filling. The same heat power of 1 W was used in all the tests. The initial temperature varies between 37.7 K (100 % of initial filling) and 38.7 (70 %).

In these tests, a decrease of the initial liquid loss with the decrease of the amount of the liquid at the beginning of the test and is observed. Starting with an initial liquid amount lower than 70 % of the total void volume of the cell is necessary to consider this loss negligible.

The same type of experiment with higher initial temperature (the same results of the Figure 4-29 between 38 K and 42 K) was also performed, but no measurable differences were observed for the initial liquid lost amount. The initial liquid loss seems to be only dependent of the initial filling and independent of the initial temperature. This particular result seems to exclude the incapacity of the porous material to confine the liquid inside of the cell. As a matter of fact, if it was the explanation for this lost liquid, due to the surface tension decrease for the neon with this temperature increase, the temperature dependence of the capillarity forces should cause a measurable difference in the amount of liquid lost

As was mentioned in this section, for all the cryocooler orientation this liquid loss phenomenon was observed at the beginning of the ESU tests. This was presented in Figure 4-11, in which the difference between the same test but in the opposite cryocooler orientations (0° and 180°) is shown. The initial liquid loss in these tests, with the cryocooler at 90°, is presented in Figure 4-30. In all the tests the initial liquid amount was ≈ 98 %.

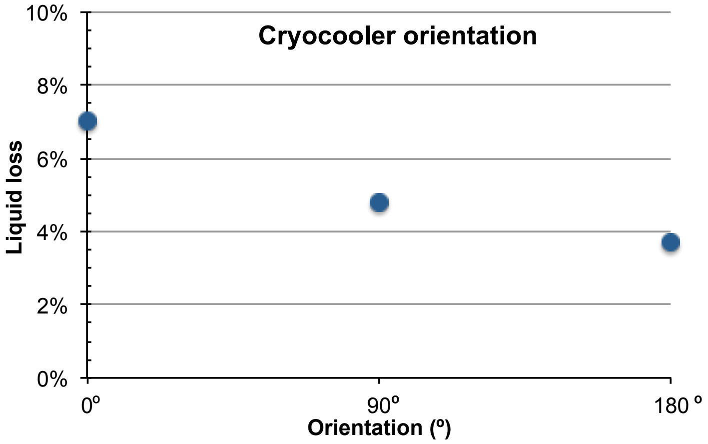

Figure 4-30 - Influence of the cryocooler orientation in the initial liquid lost amount. The three tests were performed between 37.8 K and 40.1 K with a filling pressure of 15.4 bar. The 1 W of heat power was used in all 3 tests.

Despite of the lower liquid loss amount, in the 180° cryocooler orientation, 4 % of the liquid was pushed out of the cell in the beginning of the experiment. Let us recall that in the 180° orientation, the capillary tube becomes located at the top of the cell (as is schematized in Figure 4-31) avoiding any liquid lost even if the capillary forces could not confine the liquid.

These last results seem to strongly exclude the incapacity of the porous material to confine the liquid and indeed some other effects seem to push the liquid out of the cell at the beginning of the ESU mode.

In all the ESU experiments analysed in this document, the heater was located close to the exhaust capillary tube (“capillary side” in the scheme of Figure 4-31). But when the heat load power was applied on the “opposite side” a higher initial liquid lost amount was verified. An example emphasizing the difference between heating in the two different locations at the beginning of the ESU drift mode is presented in Figure 4-31 with the cell in the 180° orientation configuration. In these figures, the black dashed line represents the result of the simulation using the pre-dimensioning tool. As previously seen, this simulated result is left shifted from the beginning of the experimental results in order to obtain a match with the time axis of the experiments where the ESU mode is running as expected. The difference between the onsets of these results allows the calculation of the liquid amount lost due to this phenomenon.

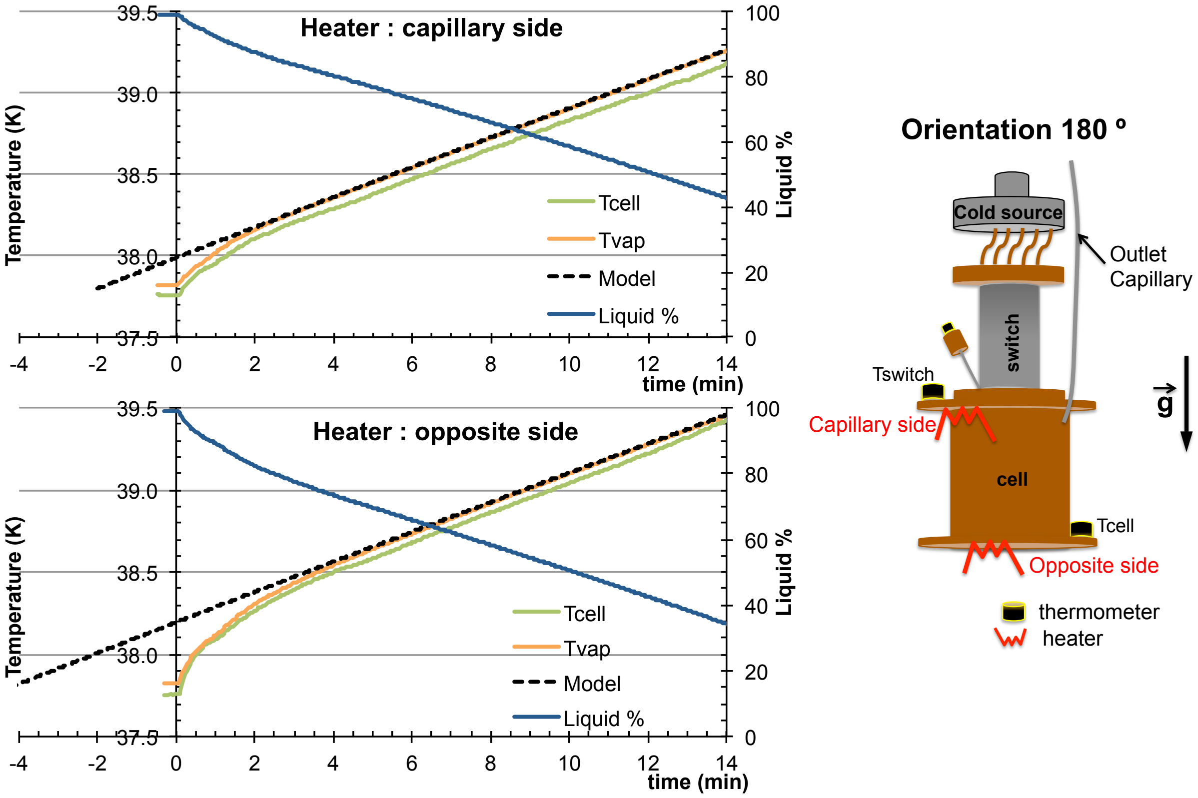

Figure 4-31 - ESU drift mode with the heater placed in two differnt locations: "capillary side" and "opposite side".

The offset of 4 min between the calculations and the experiments corresponds to about 14 % of the total liquid amount lost at the beginning of the ESU mode when the heater is located on the opposite side, compared with the lost of 7 % (2 min) in the case of the heater in the capillary side. In the 0º orientation, doing the same tests with the heaters in two opposite locations, the difference obtained between them was equivalent (≈ 2.5 min), which means no difference between the location of the heater in the 0º orientation. These results indicate a deterioration of the initial liquid lost phenomenon when the heater location is far from the outlet capillary tube for all the cryocooler orientations. This result is discussed in next paragraphs.

Moreover, the influence of the heat load applied on the ESU on the initial liquid lost was also tested to understand the causes of the initial liquid lost. In Figure 4-32, two ESU drift mode tests with two different applied heat loads, 100 mW and 4 W, are presented. These tests were performed with the same initial conditions, between 37.9 K and 40.1 K, with the cryocooler in the 0º orientation and the heater located in the capillary side. The black dashed lines represent the result of the pre-dimensioning tool, and, similarly to the previous results, the simulations are left shifted from the onset of the experimental results for an easy liquid lost calculation.

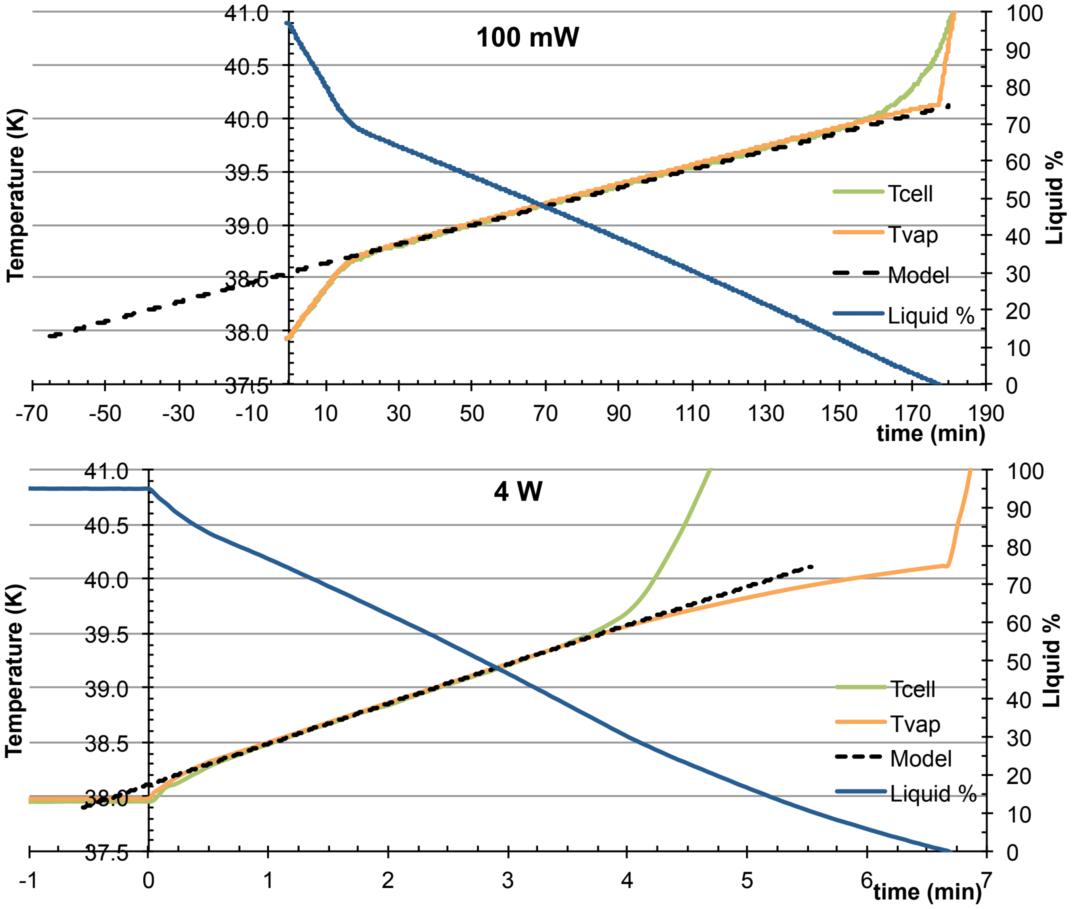

Figure 4-32 - ESU drift mode, in the cases of 100 mW and 4 W of applied heat load.

Beyond the large difference in the duration of these two tests, due to the quite different heat power, the difference between the beginning of the simulated and experimental results is also evident in the case of the lower heat load applied. In this test, the initial liquid loss is evidenced by the higher decreasing rate of the liquid amount inside of the cell. Actually, the experiment only starts to run as expected when the liquid amount was about 70 %. During these initial 15 min about of 18 % of liquid were pushed out of the cell. This result is surprising compared with the experiment using 4 W of heat load: as a matter of fact, for this higher heat load only about ≈ 6 % of the total liquid amount is lost at the beginning of the experiment.

The study on the heat load dependence for the initial liquid lost was extended to some more applied heat powers. Figure 4-33 depicts a synthesis of the liquid lost amount for the tests using different heat loads.

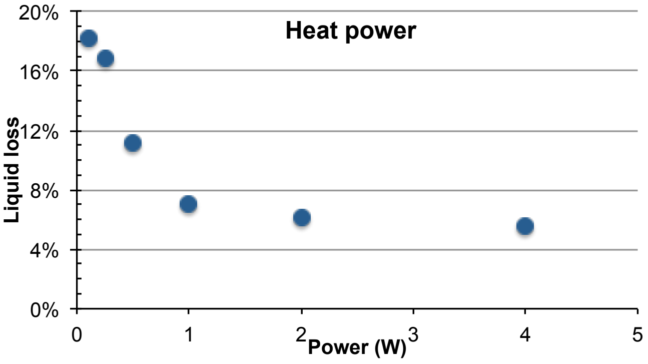

Figure 4-33 – Influence of the heat power applied in the liquid lost amount. Liquid lost amount as function of the heat power applied.

For heat loads up to 1 W, the liquid loss decreases significantly with the increase of the heat load. For higher heat loads, the liquid loss seems to stabilize at about 6 % of the total liquid amount

Combining the observed behaviour from both the influence of the heat load and the dependence on the heater location in the initial liquid loss, let us build up a hypothesis to explain this phenomenon. This hypothesis takes into account the geometry of the cell and, particularly, the flow constraints created by the 12 mm diameter copper tube located at the center of it (section 3.2.2). Consider the two opposite configurations on the left of Figure 4-34: the heater in both sides of the cell, corresponding to both experiments of Figure 4-31. Despite of the high thermal conductance of the copper cell, a small thermal gradient in the cell for higher heat powers can appear and then, the evaporation will be favoured close to the hotter spot, i.e. near the heater. When the heater is localized at the “opposite side”, the neon is evaporated also far from the capillary and has to pass through the liquid confined in the porous material to reach the cell exit. If the liquid is blocking this exit, this gas could push it directly through the exhaust. In the tests performed in this second configuration (Figure 4-34) a volume of 14 % of liquid from a full cell was initially pushed out of the cell.

In the case of the heater in the “capillary side”, the gas is formed near the exit of the cell: this turns the exhaustion of the vapor an easier process, reducing the liquid lost. But the neon that evaporates inside of the copper tube in the middle of the cell has to flow along all this tube to exits. The grey arrows in the left schema of Figure 4-34 represent the vapor path. This causes again a pushing effect, similar to the case of the hotspot in the “opposite side”. This may explain the lost of about of 7 % of the total initial liquid amount in the ESU mode begging – half the lost found with “opposite side heating”. The removal of this central heat exchanger tube or to open holes to create a more direct path for the vapor exit should reduce the initial liquid lost amount.

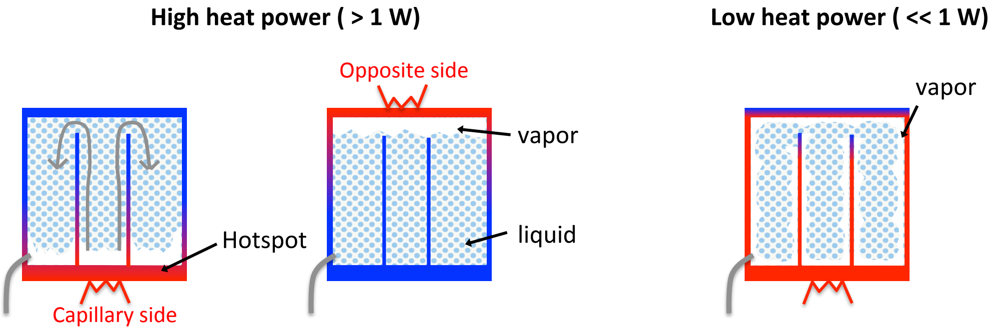

Figure 4-34 – Hypothesis to explains the variations of initial liquid lost in the various configurations tested: heater in the capillary side and in the opposite side. The high thermal homogeneity of the cell for low heat powers allows the evaporation along the area of the cell walls. (See more explanation in the text).

The hypothesis of the hotspot existence may also explain the high initial liquid lost amount for lowers heat loads applied (<1 W). Due to the decrease of the heat load applied, the thermal homogeneity of the cell is better and then increases the hotspot area as schematized in figure 4.34. In an extreme situation the evaporation can occur in whole cell walls, which turns difficult the creation of different paths to exhaust all the evaporated neon pushing the liquid out of the cell.

This hypothesis of the exhausting path from the hot spot seems reasonable to explain the initial liquid lost phenomenon, since it describes its dependence both with the applied heat load and the placement of the heater.

As demonstrated in these previous tests, the initial liquid lost effect can be minimized using the heater in the capillary tube side, reducing the liquid push effect. If our hypothesis is right, it indicates that the existence of “almost closed” volumes can lead to liquid pushing effects. The solution to avoid the high initial liquid loss when using low heat loads may be to start the ESU mode with a lower initial liquid amount, about 70 % of the total cell void volume.

4.7.2 Temperature split

For all the tests previously presented tests, a recurrent phenomenon was appearing when the liquid amount was about 20 % of the cell void volume — the temperature split, as it was called. A sudden thermal decoupling between the cell and the liquid temperature was observed when approaching this liquid ratio. This phenomena was also observed by *J. Afonso* [9] using a liquid nitrogen ESU in the 60 – 80 K range. The existence of small pores on the porous materials can explain this temperature split between the cell and liquid temperatures. Part of the liquid may remains trapped in these pores without a continuous path to the cell walls for thermalizing. The lack of this continuous path between the liquid and the cell, the pour thermal conductance of the porous material and of the gas as well as the very limited convection phenomena result in a quite good thermal isolation of this remaining liquid from the cell walls. With a heat load applied, these conditions can lead to quite high thermal gradients between cell walls and the liquid temperature[29].

Some differences in this “trapped liquid” amount when the temperature split occurred were observed for different ESU operation temperatures. The liquid ratio remaining in the cell when the temperature split occurred as function of the ESU temperature operation is presented in Figure 4-35 as a function of the ESU temperature operation. The liquid ratio is calculated according to the thermal model presented in the section 2.2.

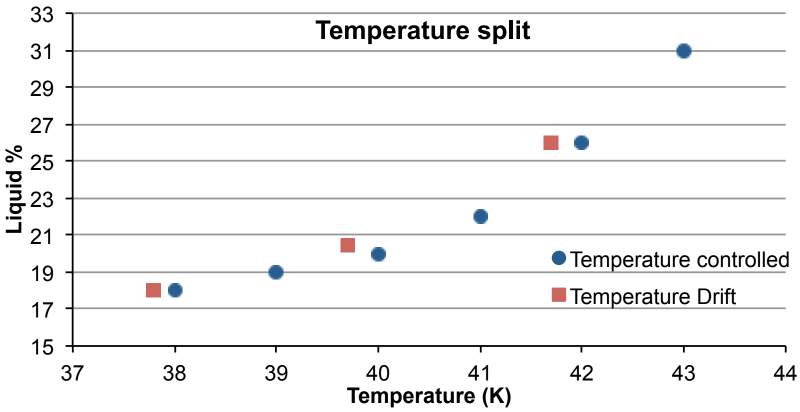

Figure 4-35 - Trapped liquid amount dependence versus the ESU temperature operation.

This Figure 4-35 shows that the trapped liquid amount increases with temperature and could reach up to 31 % at 43 K. For lower tested ESU temperatures, the trapped liquid amount is around 17 %. These results were observed in the two tested ESU modes, the temperature controlled and the temperature drift.

The temperature split also depends on the applied heat load. This dependence of the trapped liquid amount with the heat load applied is shown in Figure 4-36.

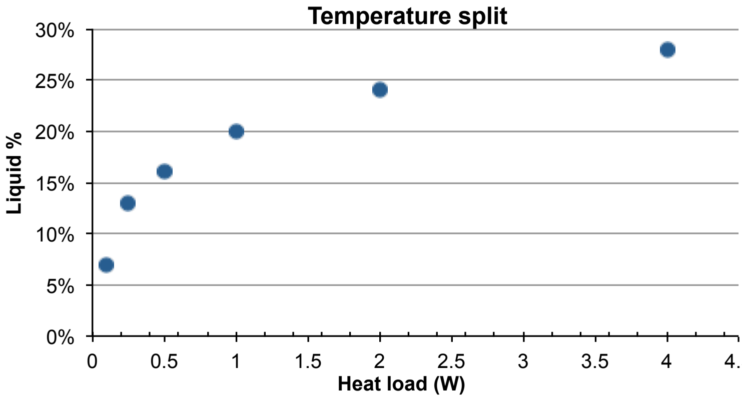

Figure 4-36 - Influence of the heat power load in the trapped liquid amount in the temperature split.

The results of Figure 4-36 were obtained using the ESU temperature drift mode between 38 K and 40 K under the same initial conditions. The liquid that remains trapped in the porous material when the temperature split occurs increases with the increase of the applied power. The temperature split phenomena could be minimized using small heat loads, enabling the use of more liquid to store energy.

During the cell sizing, the temperature split phenomenon was already known from previous works and we tried to take it into account. In the aluminium cell a cylindrical pin in the middle of the cell was used to obtain a better thermal homogeneity between cell and liquid, as shown in Figure 4-37. The estimated trapped liquid amount using the aluminium cell was about 20 % (using 1 W of heat power) of the void volume of the cell at 40 K.

In the copper cell, a copper tube with 15 mm diameter was designed. The objective was to reduce the distance between the cell walls and the most distant point of the ceramic while trying to decrease the intensity of the temperature split phenomenon. A shorter thermal path from the trapped liquid to the cell walls should lead to a smaller amount of inaccessible trapped liquid and consequently reduce the temperature split.

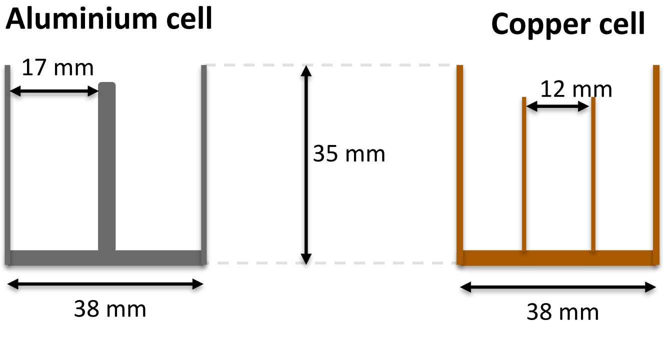

Figure 4-37 – Cell walls spacing scheme. The total internal surface area of the copper cell is 30 % bigger than the aluminium cell and the shortest distance between wall and the farthest point of the wall is, respectively, 8.5 mm and 6 mm.

Our results showed a non-measurable difference between the trapped liquid amount in the aluminium cell and the copper cell as the temperature splits were found to be quite similar. Even with the reduction of the distance between the cell walls and an increase of more than 30 % of internal surface area, the temperature split phenomenon was unchanged. This means that the remaining liquid is not localized in the middle of the porous material and reinforced the idea that this trapped less uniformly distribute in the whole volume of the porous material. This copper tube, initially designed to help the heat transfer, brings some complication for the vapour exit and is a good example of a false good idea!

5 Conclusion

For space applications, the energy storage units, providing a temporary cold source without mechanical vibrations and electromagnetic interference, could be very useful devices for cryogenics chains integrating mechanical coolers.

With the objective of a temporary cold source to absorb up to 1000 J in the 40 K range, an energy storage unit based in the latent heat of the liquid to vapor transition of neon was developed. This system is composed by a cold cell (35 cm^3) thermal coupled to the cryocooler through a gas gap heat switch allowing the ESU thermal coupling/decoupling from the cold source. The cold cell is connected to a 6 litre expansion volume used to limit the pressure increase during the liquid neon evaporation. Using this configuration, two operational working modes were tested: the temperature drift mode and the temperature controlled mode. In the temperature drift mode, with the ESU thermal decoupled from the could source, the ESU absorbed 1 W of applied heat power during a total of 18 minutes (1080 J) with a temperature drift as small as 2 K between 38 K and 40 K.

By controlling the pressure inside the cold cell during the evaporation, is also possible to absorb the heat load applied at constant temperature, like in a triple point transition. This temperature controlled mode was successfully tested: with the use of a pressure control valve between the cold cell and the expansion volume, it was possible to control the pressure inside the cold cell and to absorb the heat load applied (1 W) at constant temperature during 15 minutes. In this mode the ESU stored a total of 900 J at a constant temperature of 40 K. Let us mention that such a mode is a solution for the inexistence of triple point transitions at 40 K.

These last two modes allow the operation of sensitive sensors in a vibration free environment by turning off the cryocooler.

A cooling process to condense the neon inside of the cold cell precedes both operational modes. The duration of this cooling process is dependent of the available cryocooler cooling power, and we showed that 80 % of the energy required for this process is used to cool down the neon gas from the 300 K expansion volume. The other part of the energy (20 %) is used to liquefy the neon within the cell. This mean that the energy required to “charge” the ESU is ≈ 5 times the storage capacity of it. This lack of efficiency is the price to pay for storing the gas at 300 K.

Turning this system gravity insensitive to allow its operation in a microgravity environment was intended. It is possible thanks to the use of a porous material that, through capillarity effect, confines the liquid within the cell. However, at 40 K, the neon is near its critical point turning its surface tension quite low: a porous material with a very small porous size (<10 μm) to confine properly whole liquid inside of the cell was required. Some tests in porous materials with porous size between 10 μm and 50 μm (experimental estimated values) were performed in order to test their (un)capability to confine the liquid. A filter paper with the mean porous size of ≈ 10 μm proved to be able to confine the liquid.

In order to test the influence of the gravity in the performance of the ESU, various experiments of the ESU temperature controlled mode at 40 K were performed for various cryocooler orientations (between 0° and 180°). A difference of 17 % in the stored energy was obtained between the opposite configurations, 0° and 180°. It was verified that this difference is associated to an initial liquid loss. For filling ratio lower than 90 % of the cell void volume, the difference between the initial liquid losses in two opposite orientations (180°-0°) was shown to be lower than 10 %.

Some experiments to understand this initial liquid loss were performed and this phenomenon was observed in all the cryocooler orientations. Despite of the highest loss occurring in the 180° configuration, the results obtained exclude the incapacity of the porous material to confine the liquid and indeed some other effects seem to push the liquid out of the cell at the beginning of the ESU mode. The non-existence of a direct path inside of the cell allowing a exhaust for the evaporated neon could be an explanation for this initial liquid loss when the filling ratio is high. The operation with low (less than ≈ 70%) initial liquid filling allow the reduction of the initial liquid amount turning the performance of the ESU equivalent for different cryocooler orientation and consequently to obtain a gravity insensitive system.

Another phenomenon occurs due to the use of the porous material: a split between the cell wall temperature and the liquid one. This phenomenon, independent from the cryocooler orientation, occurs when the remaining liquid amount in the cell is about 20 % Value closed of that observed and studied in the liquid nitrogen ESU work[29]. The tests performed in this work converge for the same explanation found in the ESU nitrogen: part of the liquid may remain trapped in the smaller pores without a continuous path to the cell walls, leading to a high thermal gradient between cell walls and the liquid trapped.

The ESU booster mode was tested with the goal to maintain stable the cryocooler temperature in case of sudden heat bursts. A small cell (≈12 cm^3) directly coupled to the cryocooler cold finger (with an cooling power of 4.5 W at 40K) and connected to an 6 liters expansion volume at room temperature was built having the capability to store up to 400 J within a small temperature drift of 1 K at 40 K range. A test using 9 W of heat load (twice the cryocooler cooling power) showed that during 2 minutes the ESU succeeded to absorb this extra energy within a temperature drift of 1 K. The same test without the ESU caused a temperature increase higher than 10 K. These results make this concept ideal for applications where high cooling power is required for a short time, avoiding the use of oversized cryocoolers. Experiments using periodic heat bursts up to 14 W were performed, and the temperature increase in each heat burst was lower than 0.3 K, evidencing the influence of the ESU to smooth the temperature oscillations.

It was also shown that ESU could work with expansion volume as small as 3 liters. The direct consequence was the doubling of the temperature drift for the equivalent test using a 6 liters volume. We showed that the relevant parameter for expansion volume optimization is the $L.dP/dT$. The energy stored per liter of expansion volume for a temperature drift of 1 K is possible to obtain using this parameter. The high $(dP/dT)_{sat}$ of neon at 40 K range is the reason why such a small expansion volume as 3 liters could be used within a rather small temperature drift.

A pre-dimensioning software was developed and became a useful tool for the system sizing and to predict the experimental results. Beyond the accurate simulations of the ESU temperature controlled and temperature drift modes, the temperature of the ESU during the cooling process also was simulated by this software. The simulation of the booster mode operation in the case of a variable heat load profile, a mix of multiple temperature drift modes and cooling processes, is also possible, although it is not as precise. This pre-dimensioning tool can be directly used for other working fluids in different temperature ranges and adapted to simulate other ESU where it use can be useful.

With the analysis of the results obtained during this this work, some suggestion for future developments can be proposed. Two phenomena were detected related to the use of the porous material: the temperature split and an initial liquid lost.

The temperature split phenomena is justified due to the inexistence of a continuous path between the liquid trapped in the smaller pores and the cell walls, which causes a large thermal gradient between the trapped droplets and the cell walls. The use of a porous material with higher thermal conductivity could enhance the temperature homogeneity between the cell and this trapped liquid. The combination of a porous material with metallic foam should be considered due to the difficult in to obtain a high conductivity material with the required porous size (< 10 μm).

For the initial liquid loss, the hypotheses of the inexistence of direct exhausting path from the hot spot seems reasonable to explain this phenomenon. The thin cylinder in the middle of the cell created to test a possible enhance of the thermal homogeneity between the cell and the liquid has worsened the initial liquid loss phenomena, hindering the gas exhaustion. The thin cylinder removal and the creation of internal paths in the middle of the porous material could be an efficient solution to reduce this phenomenon, instead of starting the ESU mode with a lower initial filling rate (~70% of the cell void volume).

During the system sizing (section 2.2.2) and in the results discussion (section 4.6) was mentioned that around 80 % of the energy used during the cooling process is used to cool down the neon gas (stored at room temperature) to 40 K, where only the remain part of the energy (20 %) are required to liquefy this pre-cooled neon gas. This part corresponds to the ESU stored energy that could be used during the ESU modes. Instead of sending the cold evaporated gas for the room temperature expansion volume, part of the energy of this cold gas could be re-used to pre-cooling the neon in the next cooling cycle (principle of the regenerators in the cryocoolers!). This is possible using a heat exchanger between the cold cell and the expansion volume. In fact, the heat exchanger used in the booster mode named as “coil”, allowed to re-use part of the energy of the cold evaporated neon. This heat exchanger was created to monitor the temperature of the vapor, when it enters in the cell (during the cooling phase), for the pre-dimensioning tool validation process and was not optimized to store energy of the evaporated neon. The pre-dimensioning tool is thus a good starting point for this concept optimization, where materials like the stainless steel and copper could be a solution due it reasonable high specific heat in the 40 K – 300 K temperature range and due its ease of integration.

References

1. Collaudin B. and N. Rando, *Cryogenics in space: a review of the missions and of the technologies.* Cryogenics, 2000. **40**(12): p. 797-819.

2. Harwit M., *The Herschel mission.* Advances in Space Research, 2004. **34**(3): p. 568-572.

3. ROSS R.G., *Aerospace Coolers: A 50-Year Quest for Long-Life Cryogenic Cooling in Space.* Cryogenic Engineering, 2007: p. pp 225-284.

4. Bugby D., M.B., *Cryogenic thermal storage units.* Cryogenics, ed. S.t.c. hanbook. Vol. II. 2003.

5. Jhabvala M., *Applications of GaAs quantum well infrared photoconductors at the NASA/Goddard Space Flight Center.* Infrared Physics & Technology, 2001. **42**: p. 363-376.

6. Jhabvala M., et al., *QWIP-based thermal infrared sensor for the Landsat Data Continuity Mission.* Infrared Physics & Technology, 2009. **52**(6): p. 424-429.

7. Catarino I., et al., *6K solid state Energy Storage Unit.* Cryogenics, 2010. **50**(2): p. 102-110.

8. Bonfait G., et al., *20 K Energy storage unit.* Cryogenics, 2009. **49**(7): p. 326-333.

9. Afonso, J., et al., *Liquid nitrogen energy storage unit.* Cryogenics, 2011. **51**(11-12): p. 621-629.

10. Williams B.G., Spradley E.E., *Test Results of a Nitrogen Triple-Point Thermal Storage Unit.* Cryocoolers 10, 2002: p. pp 697-706.

11. Martins D., *Desenvolvimento, construção e teste de um interruptor térmico para baixas temperaturas*, 2010, Universidade Nova de Lisboa: Master degree thesis.

12. Shirron P., *Space Cryogenics*, in *Cold Facts*2013, Cryogenic Society of America.

13. David G. Gilmore, *Spacecraft Themal Control Handbook*, ed. T.A. Corporation. Vol. Volume I: Fundamental Technologies. 2002.

14. Boyle R., *On-orbit performance of the RHESSI cryocooler.* Cryogenics, 2004. **44**: p. 389-393.

15. Zagarola M.V. and J.A. McCormick, *High-capacity turbo-Brayton cryocoolers for space applications.* Cryogenics, 2006. **46**: p. 169-175.

16. Veprik A., Nachman I. and Pundak N., *Dynamic counterbalancing the single-piston linear compressor of a Stirling cryogenic cooler.* Cryogenics, 2009. **49**(5): p. 165-170.

17. Riabzev S.V., et al., *Vibration-free stirling cryocooler for high definition microscopy.* Cryogenics, 2009. **49**(12): p. 707-713.

18. Rijpma A.P., et al., *A nitrogen triple-point thermal storage unit for cooling a SQUID magnetometer.* Cryogenics, 2005. **45**(3): p. 231-239.

19. Costard E. and P. Bois, *THALES long wave QWIP thermal imagers.* Infrared Physics & Technology, 2007. **50**(23): p. 260-269.

20. G.P. Wang, et al., *Development of a 0.5 W/40 K Pulse Tube Cryocooler for an Infrared Detector.* The Proceedings of the 14th International Cryocooler Conference, 2006.

21. Irons J.R., Dwyer J.L. and J.A. Barsi, *The next Landsat satellite: The Landsat Data Continuity Mission.* Remote Sensing of Environment, 2012. **122**(0): p. 11-21.

22. Trollier T., et al., *Air Liquide space cryocooler systems.* Cryogenics, 2008. **48**: p. 267-273.

23. Dang H., *40K single-stage coaxial pulse tube cryocoolers.* Cryogenics, 2012. **52**: p. 216-220.

24. NIST. *Cryogenic materials properties* [cited 2013 9-2013]; Available from: http://cryogenics.nist.gov/MPropsMAY/material properties.htm.

25. Mizuno, K., et al., *Cold storage characteristics of mobile HTS magnet.* Cryogenics, 2011. 51(6): p. 321-325.

26. D. Bughy, B. Marland, and C. Stouffer, *Development and Testing of a 35 K cryogenic Thermal Storage Unit.* 41 st Aerospace Science Meeting and Exihibit, 2003: p. pp. 1-9.

27. Charles I., et al., *Thermal Storage Unit Using the Triple Point of Hydrogen.* Cryocoolers, 2011. vol. 16: p. pp. 575 - 582.

28. D. Bughy, et al., *Development of a 60 K Thermal Storage Unit.* Cryocoolers, 1997. **9**: p. 747-764.

29. Afonso, J., *Towards Cryogenic Liquid –Vapor Energy Storage Units for space applications*, 2013, Universidade Nova de Lisboa: PhD thesis.

30. Castles S. H. and Schein M. E., *Development of a Space Qualified Surface Tension Confined Liquid Cryogen Cooler.* Adv. in Cryogenic Engineering, 1988. **Vol. 33**: p. pp. 819-826.

31. Duband L., et al., *Herschel flight models sorption coolers.* Cryogenics, 2008. **48**: p. 95-105.

32. Arthur W. Adamson and A.P. Gast, *Physical Chemistry of Surfaces*. 6 ed1997: John Wiley & Sons, Inc.

33. Siegert, C.E., D.A. Petrash, and E.W. Otto, *Behavior of Liquid-Vapor Interface of Cryogenic Liquids During Weightlessness.* Technical Note D-26581965, Lewis Research Center -NASA, 1965.

34. Lemmon E.W., Huber M.L., and McLinden M.O., *NIST Standard Reference Database 23: Reference Fluid Thermodynamic and Transport Properties-REFPROP, Version 8.0, National Institute of Standards and Technology, Standard Reference Data Program, Gaithersburg.* 2008.

35. Timmerhaus K.D. and F. T.M., *Cryogenic Process Engineering*1989, New York: Plenum Press.

36. Young W.C. and Roark's., *Formulas for Stress & Strain*, ed. t. edition1989, Singapore: Mc Graw Hill.

37. *Metals handbook, Vol2 - Properties and Selection: Nonferrous Alloys and Special-Purpose Materials.*, A.I.t.E. 1990, Editor.

38. Castolin®. *Castolin 1827*. 2008 9 - 2013]; Available from: http://commerce.sage.com/bag/upload//site/default/FT/Fran%C3%A7ais/Castolin/1827.pdf.

39. Castoln®. *Alutin 51L -Decapant pour le brasage tendre*. 2009 [cited 9-2013; Available from: http://commerce.sage.com/bag/upload//site/default/FT/Fran%C3%A7ais/Castolin/AluTin51L.pdf.

40. Frank P. Incropera, *Fundamentals of Heat and Mass Transfer*2006: John Wiley \& Sons.

41. Bowman R. C. Jr, et al., *Performance of hydride activated gas gap heat switches in the Planck sorption cryocooler*, 2005, Pasadena, CA : Jet Propulsion Laboratory, National Aeronautics and Space Administration: El Segundo.

42. Martins D., et al., *Sorption characterization and actuation of a gas-gap heat switch.* Sensors and Actuators A: Physical, 2011. **171**(2): p. 324-331.

43. Catarino I., Bonfait G., and L. Duband, *Neon gas-gap heat switch.* Cryogenics, 2008. **48**: p. 17-25.

44. Martins D., et al. *Controlled actuation of a Gas-Gap heat Switch*. in *24th International Cryogenic Engineering Conference (ICEC 24)*. 2012. Fukuoka, Japan.

45. Shaughnessy B.M., et al., *Thermal conductivity measurement below 40 K of the CFRP tubes for the Mid-Infrared Instrument mounting struts.* Cryogenics, 2007. **47**: p. 348-352.

46. RATH. *ALTRA KVR High Alumina Vaccum Formed Boards*. 2012; Available from: http://www.rath-usa.com/pds-altra-krv-high-alumina.html.

47. AST. *Active Space Technologies - Aerogel*. 2012 [cited 2013 9-2013]; Available from: http://www.activespacetech.com/aerogel/aerogel_leaflet-1.pdf.

48. Filter-Lab. *Quantitative filter paper*. 2009; Available from: http://www.fanoia.com/filter-paper/quantitative-filter-paper-409.

49. António Gameiro Lopes and L.A. Oliveira, *Mecânica dos Fluidos*, ed. ETEP2010. 614.

50. JOUCOMATIC. *Enginnering Inforamtion: flow factor*. Available from: http://detector-gas-systems.web.cern.ch/detector-gas-systems/downloads/kv_calc_doc.pdf.

51. Branco C. M. and F. J.M., *Projecto de Órgãos de Máquinas*2008, Lisboa: Fundação Calouste Gulbenkian.

52. Joseph E. Shingley and C. R.Mischke, *Mechanical Engineering Design*. sixth edition ed. Mechanical Engeniering Series: MacGraaw-Hill International Edition.

53. Warren C. Young and R.G. Budynas, *Roarks's Formulas for Stress and Strain*. Seventh Edition ed2002: McGraw-Hill.

Appendices

Appendix A: Fastening elements – Aluminium cell

In this appendix the sizing of the fastening elements for the multipurpose reservoir (aluminium cell) presented in the section 3.2.1 is shown.

M3 stainless steel screws were chosen to be used for fastening the lid to the body of the cell. The minimum number of screws for fastening the 50 bar pressurized cell is calculated considering the screws subject to a tensile stress, without initial tightening, the stress in the screw is given by[51]:

$$\sigma = \frac{F}{A_t} \leq 0.7\sigma_{Yield} \tag{A.1}$$

where A_t is the effective section of the screw subject to the tensile stress (A_t = 5.03 mm^2 for one M3 screw). The total force applied on the lid is F_{total} ≈ 5700 N, result of the 50 bars on the 38 mm diameter lid. Using the yield strength of SS316 (section FF):

$$N_{M3} \geq \frac{5700}{5.03 \times 0.7 \times 290} = 5.6$$

In conclusion, six screws are necessary to withstand this force. Nevertheless it was decided use 9 screws for safety reasons. Each of the nine screws will be subject to a 630 N force due to the 50 bars inside the cell.

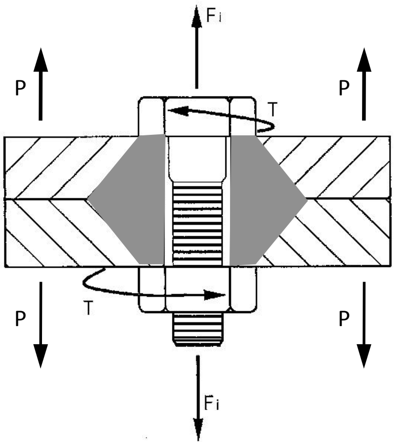

Figure 5-1 – Screw subject to a tensile stress due to the initial tightening and the pressure *P*[51]. The shadded zone represents the compressed zone of the joined elements (lid and cell).

It is intended to reach a leaktight cell, so the two surfaces (tightened by screws) shouldn't separate by applying a pressure *P*. The elasticity of the tight parts and the screw need to be considered. An initial tightening (F_i) is needed to maintain the material of the cell body and the lid subject to a compression force (F_c) to avoid the separation of the two surfaces. The force acting on the joined elements will be:

$$F_c = F_e\left(\frac{k_c}{k_c + k_s}\right) - F_i \text{ , } F_c < 0 \tag{A.2}$$

k_c and k_s are the elastic constants of the joined elements and the screw, respectively. The relation between the applied force and the resultant deformation gives these elastic constants:

$$k = \frac{F}{\delta} = \frac{AE}{L} \tag{A.3}$$

where *A* is the section, *E* the Young modulus and *L* the length. Considering a screw with 10 mm of length, *d* = 3 mm and *E*=193 GPa (1.93x10^5 N/mm^2) the constant of elasticity is:

$$k_s = \frac{\pi d^2 E}{L} = \frac{3.14 \times 3^2 \times 1.93 \times 10^5}{10} = 1.3 \times 10^5 \text{ N/mm} \tag{A.4}$$

Consider the grey area of Figure 5-1, the zone of the joined elements subject to a compression force. By the integration of the section area along the length *L* the elasticity constant of the compressed zone of the joined elements is given by[52]:

$$k_c = \frac{0.577Ed}{2\ln\left(5 \times \dfrac{0.577L + 0.5d}{0.577L + 2.5d}\right)} \approx 0.59 \times 10^5 \text{ N/mm} \tag{A.5}$$

Where *d* is the nominal diameter of the screw that joins the 2 elements. The joint length is *L*=10 mm.

With these results, it is possible to determine the minimum initial tightening force $F_{i,min}$ to ensure the absence of separation of the joined elements, due the pressure load inside of the cell. The separation occurs when F_c=0 (F_e=630 N). The $F_{i,min}$ is given by:

$$F_{i,\min} = F_e\left(\frac{k_c}{k_c + k_s}\right) = 191 \text{ N} \tag{A.6}$$

$$T_{\min} = CdF_i = 115 \text{ N.mm} \tag{A.7}$$

where T_{min} is the minimum tightening torque and *C* a coefficient related to the tightening of the screws with the value range of 0.16 and 0.2[51].

The maximum force of initial tightening can be determined by the maximum tensile stress that the screw can be subjected to.

$$F_{s,\max} = F_{i,\max} + F_e\left(\frac{k_s}{k_c + k_s}\right),\ F_{s,\max} > 0 \tag{A.8}$$

Assuming σ_{max}< 0.7 σ_{Yield} the maximum stress in the screw is σ_{max}< 240 MPa. The maximum force in the screw is $F_{p,max}$< A_t σ_{max}< 1197 N. The force and torque of tightening is:

$$\begin{aligned} F_{i,\max} &= -F_e\left(\frac{k_s}{k_c + k_s}\right) + F_{s,\max} = 757 \text{ N} \\ \mathrm{T}_{\max} &= CdF_{i,\max} = 455 \text{ N.mm} \end{aligned} \tag{A.9}$$

To avoid the separation of the two joined elements, using 9 M3 (stainless steel) screws, it is necessary to ensure the initial tightening torque between 115-455 N.mm.

The initial tightening is given at room temperature (*T*=300 K) but, the working temperature can achieve *T*= 30 K. An important consideration is the thermal contraction of the screw and the joined elements and verifying the change of the contact force F_c in the join. The contraction of the lengths of the screw (L_{ss}) and the join (L_{al}) is:

$$\Delta\delta_{screw} = \alpha_{ss} L_s \Delta T = -29.9\ \mu\text{m} \tag{A.10}$$

$$\Delta\delta_{join} = \alpha_{al} L_{join} \Delta T = -41.4\ \mu\text{m} \tag{A.11}$$

where α_{ss} and α_{al} are the dilatation coefficients of the stainless steel and aluminium, respectively. And the $\Delta\delta_{screw}$ needs to be equal to the $\Delta\delta_{join}$, this results in a variation of the force in the screw (Figure 5-2).

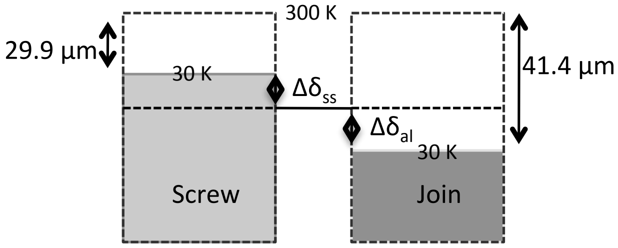

Figure 5-2 - Differential thermal dilatation between the joined elements and the screw.

The contraction of the joined elements is going to be higher than the screw's contraction. To compensate this differential contraction it is necessary to increase the initial tightening force. The force needed to add due to the differential contractions in the materials is:

$$\begin{aligned} & 41.4x10^{-3} - \Delta\delta_c = 29.9\times10^{-3} + \Delta\delta_p \leftrightarrow \\ & 41.4\times10^{-3} - \frac{\Delta F}{k_c} = 29.9\times10^{-3} + \frac{\Delta F}{k_s} \leftrightarrow \Delta F = 473\ \text{N} \end{aligned} \tag{A.12}$$

To ensure the contact of the joined materials it is necessary to compensate this force (*ΔF*=515 N) in the screw's initial tightening. The minimum initial tightening and torque is:

$$\begin{aligned} & F_{i,\min} = F_e \left(\frac{k_c}{k_c + k_s} \right) + \Delta F = 664\ \text{N} \\ & \text{T}_{\min} = 398\ \text{N.mm} \end{aligned} \tag{A.13}$$

This new initial tightening, considering the differential contraction, of $F_{i,\min}$ does not exceed the maximum allowed tightening calculated by the Eq. A.12 ($F_{p,\max}$=757 N) to avoid any deformation in the screw. Concluding, to close the lid and maintaining it leaktight the use of 9 M3 Stainless steel screws with the initial tightening torque between 398-460 N.mm were determined.

Appendix B: Resonant frequency calculation of the cryocooler structure

The analytical determination of the resonant frequency of the cryocooler internal structure to mechanical decoupling the gas gap heat switch and the cell from the cryocooler (Section 3.4.2) is shown in this appendix.

For the resonance frequency calculation, three types of movements were considered (Figure 5-3): In the 1st case, the base is fixed and the end is free. In the 2nd case, the base and the end are fixed. In the 3rd case, a small twist of the structure is considered.

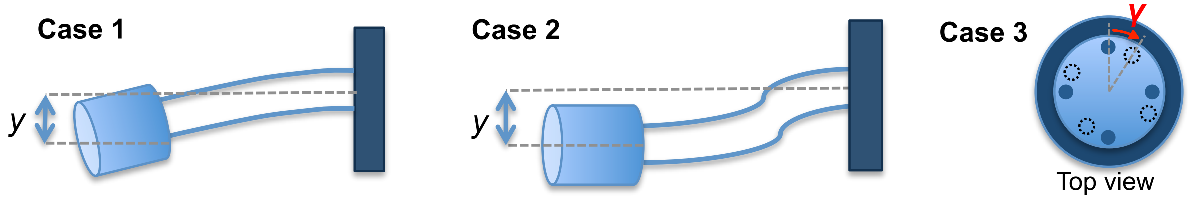

Figure 5-3 - The cylinder represents the heat switch and the cell fixed to the cold finger via a flexible thermal strap. Three types of movements are considered. Case 1: the base is fixed and the top is free. Case 2: the base and the top are fixed. Case 3: small twist of the structure.

A maximum of displacement y, an elasticity constant k and a resonance frequency f_{reso} are associated to each case. The calculation of these 3 parameters associated to each case came:

Case 1

Considering k the elasticity constant of the 3 supporting rods and y the deflection, the resultant force F (due to the gravity) in the mass m=0.5 kg (cell and heat switch) when the structure is deformed by y is:

$$F = -ky \tag{B.1}$$

In this case, of the fixed base and the free top the displacement y is [53]:

$$y = \frac{FL^3}{3nEI} \tag{B.2}$$

where L is the length of the rods, n the number of carbon tubes and E=70 GPa the Young modulus. The force is $F=m.g$ with the m=0.5 kg the mass of the cell and heat switch. I is the inertia moment of a tube around its own axis, given by $I = \pi(D^4 - d^4)/64$ [53] where D=6 mm is the outer diameter and d=5 mm is the inner diameter. The three tubes are 35 mm apart from the centre (Figure 5-4). In the case of this displacement the deviation of the tubes from the centre is going to increase the stability of the structure, or in other words, is going to increase the resonance frequency. This arrangement, namely the distance to the centre, is going to modify the way to calculate the inertia moments of each tube.

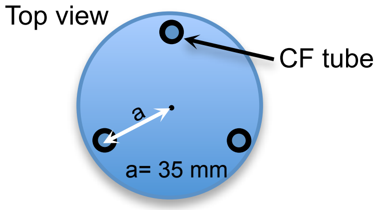

Figure 5-4 - Consideration about the inertia moment calculated using the parallel axis theorem.

Using the parallel axis theorem it is possible to obtain the inertia moment of the tube about an axis parallel to its own. Using the inertia moment (I) previously mentioned, the inertia moment for each tube 35 mm distant from the center is given by:

$$I_T = I + Aa^2 \tag{B.3}$$

where A is the cross section of the tube, and a the distance from the tube axis to the centre.

$$k = \frac{3nEI_T}{L^3} \tag{B.4}$$

With these equations considering the 3 carbon rods with lengths L=12 mm, the deflection is y=1.6 µm and the k=30 x10^5 N/m. For this case the resonance frequency f_{reso} is:

$$f_{reso} = \frac{1}{2\pi}\sqrt{\frac{k}{m}} = 390\text{ Hz} \tag{B.5}$$

For this 1st case, the resonance frequency is 390 Hz. This frequency due to this type of displacement is very far from the working frequency of the cryocooler (3 Hz).

Case 2

In this case 2, the base and the top are fixed. This time the deflection y due to the force $F=m.g$ is given by[53]:

$$y = \frac{FL^3}{12nEI} \tag{B.6}$$

In this type of displacement the arrangement of the carbon fibre tubes is independent from the stability of the structure. The distance from the centre doesn't change the elasticity constant of the structure, whereby the inertia moment is given by:

$$I = \pi(D^4 - d^4)/64 \tag{B.7}$$

The D is the outer diameter and d the inner diameter of the carbon fibre tube. The constant of elasticity for this case is given by[53]:

$$k = \frac{12nEI}{L^3} \tag{B.8}$$

In this case, the deflection in the horizontal position is y =0.13 mm, the constant of elasticity is k = 3.8 x 10^4 N/m (considering E=70 GPa). For this case the resonance frequency is:

$$f_{reso} = \frac{1}{2\pi}\sqrt{\frac{k}{m}} = 44 \text{ Hz} \tag{B.9}$$

The resonance frequency is 44 Hz, corresponding to the lower calculated resonance frequency. Despite of this lower calculated frequency, it continues to be an acceptable value when compared with the 3 Hz correspondents of the cryocooler working. This case corresponds to the type of displacement when our structure is subjected to gravitational force. We calculated the y=0.13 when the mass of the heat switch and the cell m=0.5 kg are subjected to the gravitational force.

Case 3

In this case the objective is to obtain the resonance frequency associated to a small twist of the structure. The torque associated to the twist of the structure τ is given by:

$$\tau = k_\theta \gamma_\theta \tag{B.10}$$

Where γ_θ is the angular displacement given by $\gamma_\theta=\gamma/r$ the ratio between the displacement (case 3 of Figure 5-3) and the radius of the structure. The torque can also be described by $\tau=r\times F$. With these equations we can write:

$$k_\theta = \frac{F}{\gamma} r^2 \tag{B.11}$$

In this case the linear displacement is given the same way as in case 2 (Eq. B.8). Rewriting the angular elasticity constant:

$$k_\theta = \frac{12nEIr^2}{L^3} \tag{B.12}$$

The constant is k_θ=77 N.m. To estimate the resonance frequency it is necessary to obtain the moment of inertia I_θ of the switch and the cell. The moment of inertia and the resonant frequency are:

$$I_\theta = \frac{1}{2} m r^2 \tag{B.13}$$

$$f_{reso} = \frac{1}{2\pi}\sqrt{\frac{k_\theta}{I_\theta}} \tag{B.14}$$

The resonance frequency associated to a small twist movement of the structure is f_{reso}=93 Hz. It continues to be higher than the operational frequency of the cooler.

Appendix C: Multipurpose cell

Multipurpose cell body

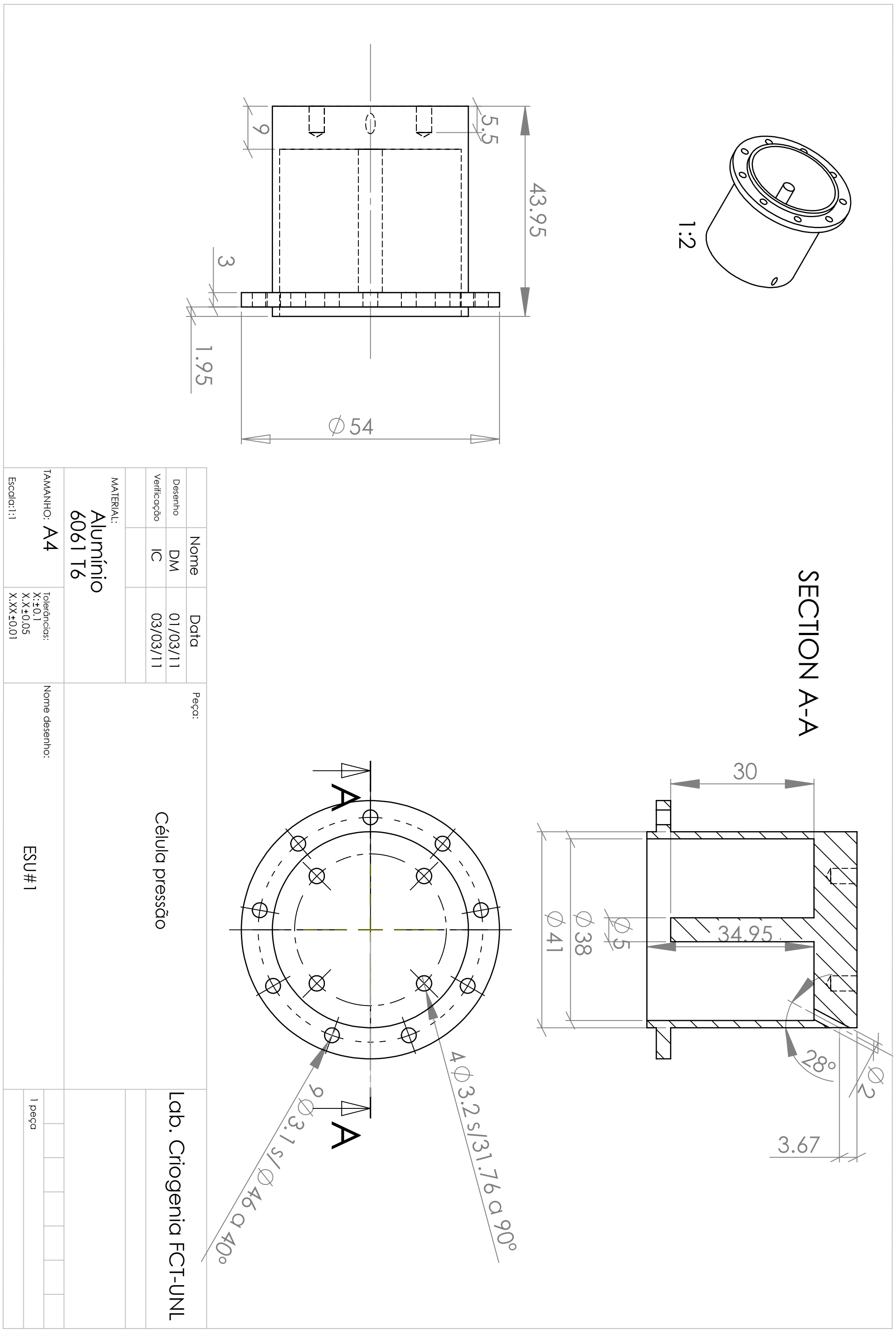

This drawing is not printed in scale.

Multipurpose cell lid

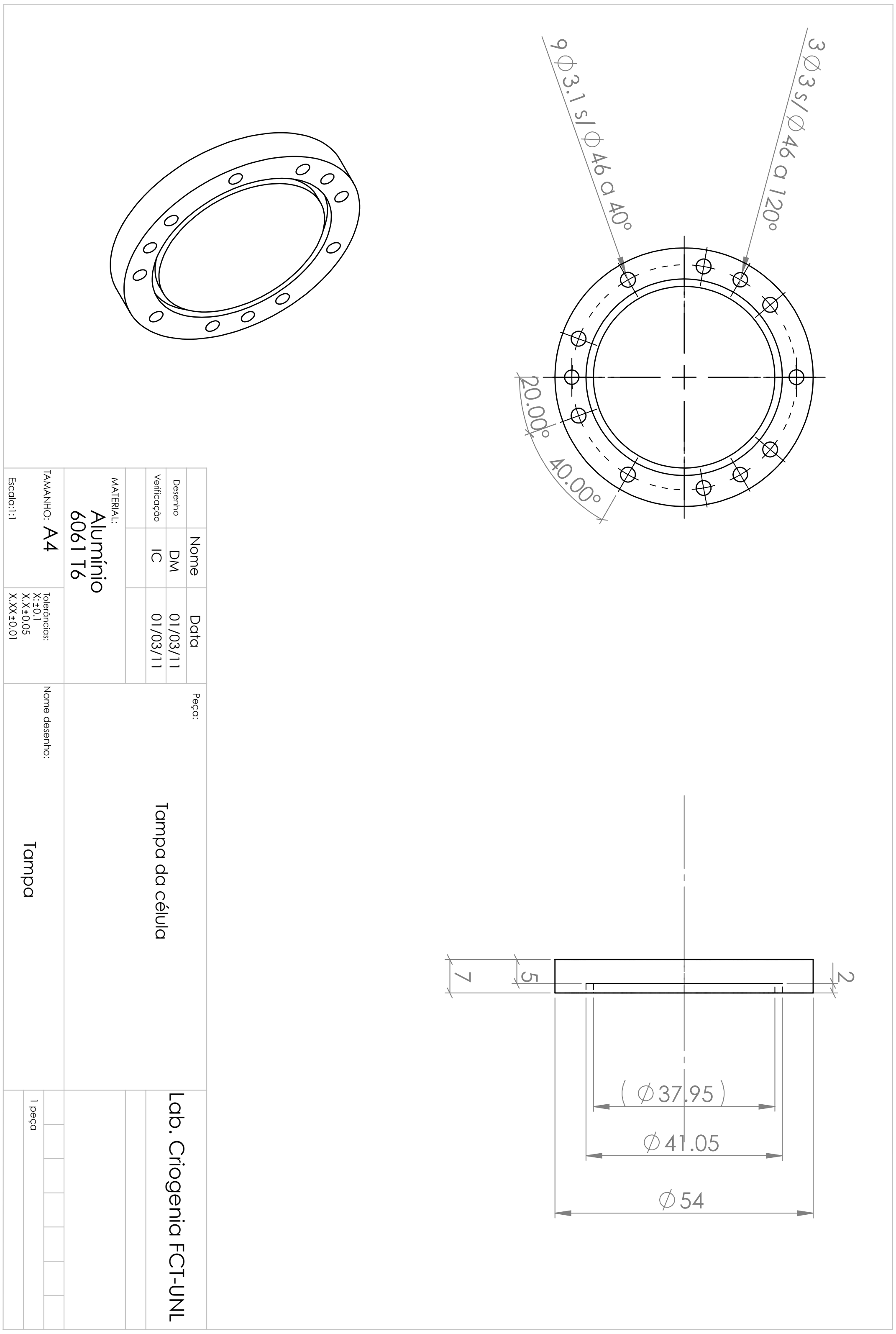

This drawing is not printed in scale.

Appendix D: Copper cell

Copper cell body

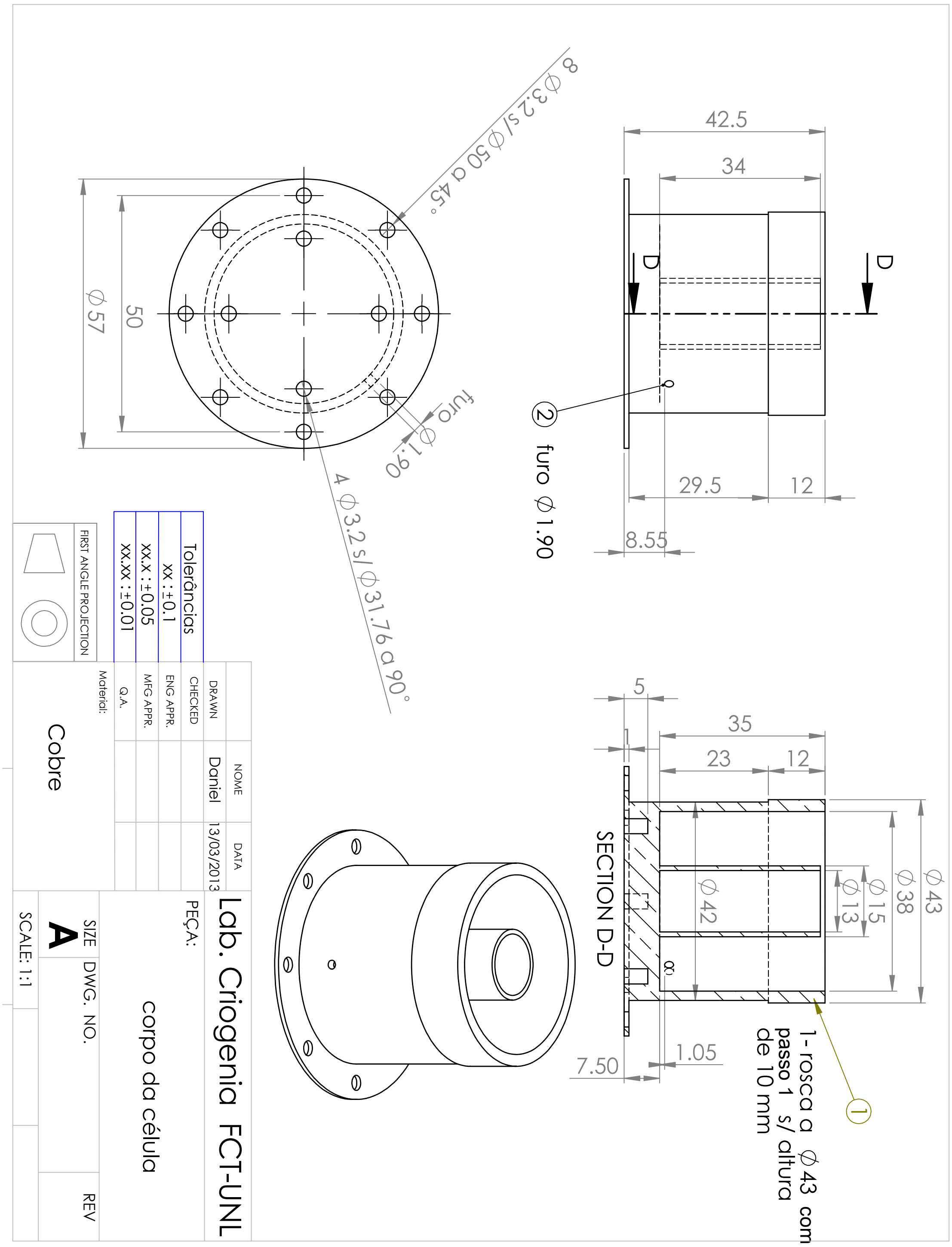

This drawing is not printed in scale.

Copper cell lid

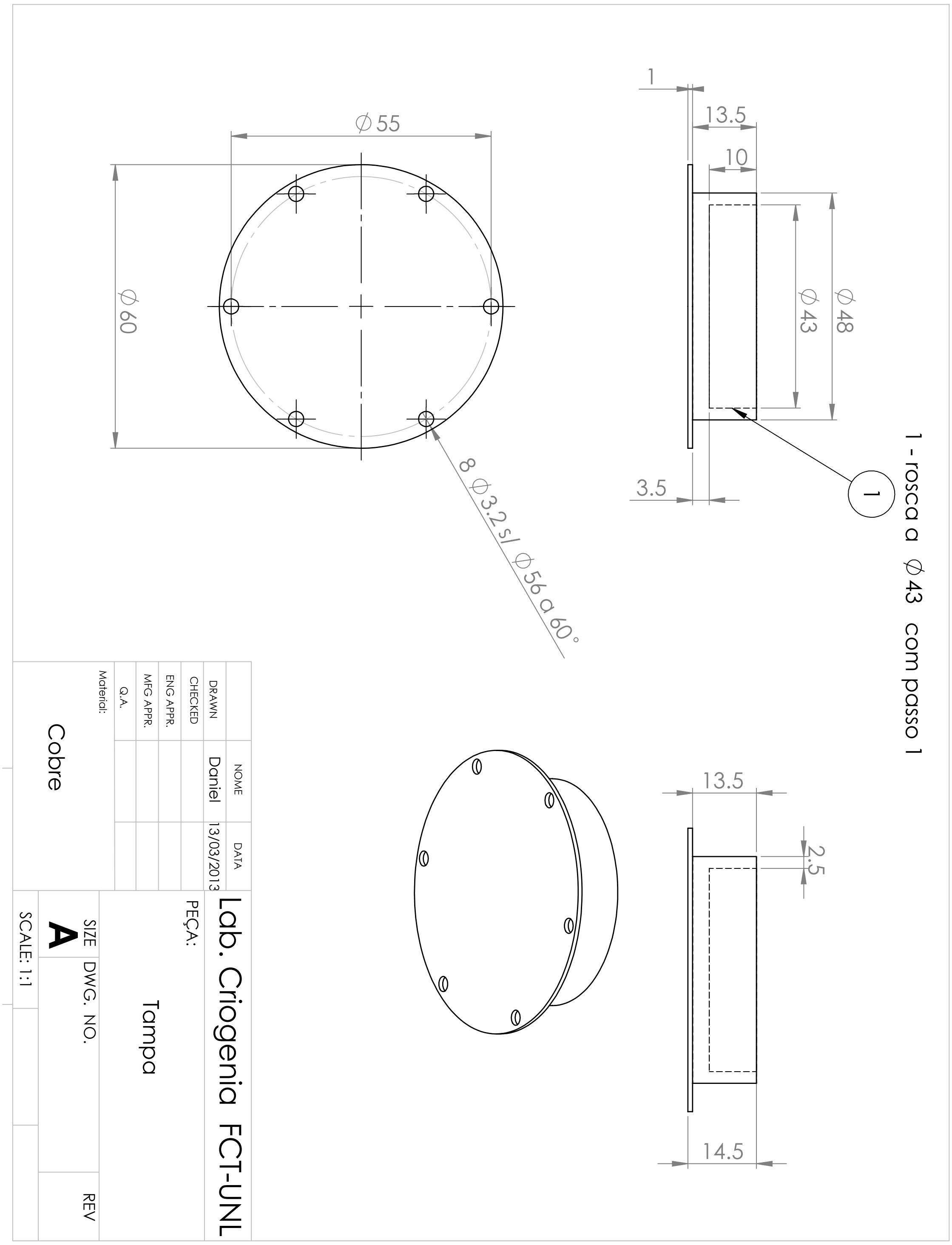

This drawing is not printed in scale.

Appendix E: Booster cell

Booster cell body

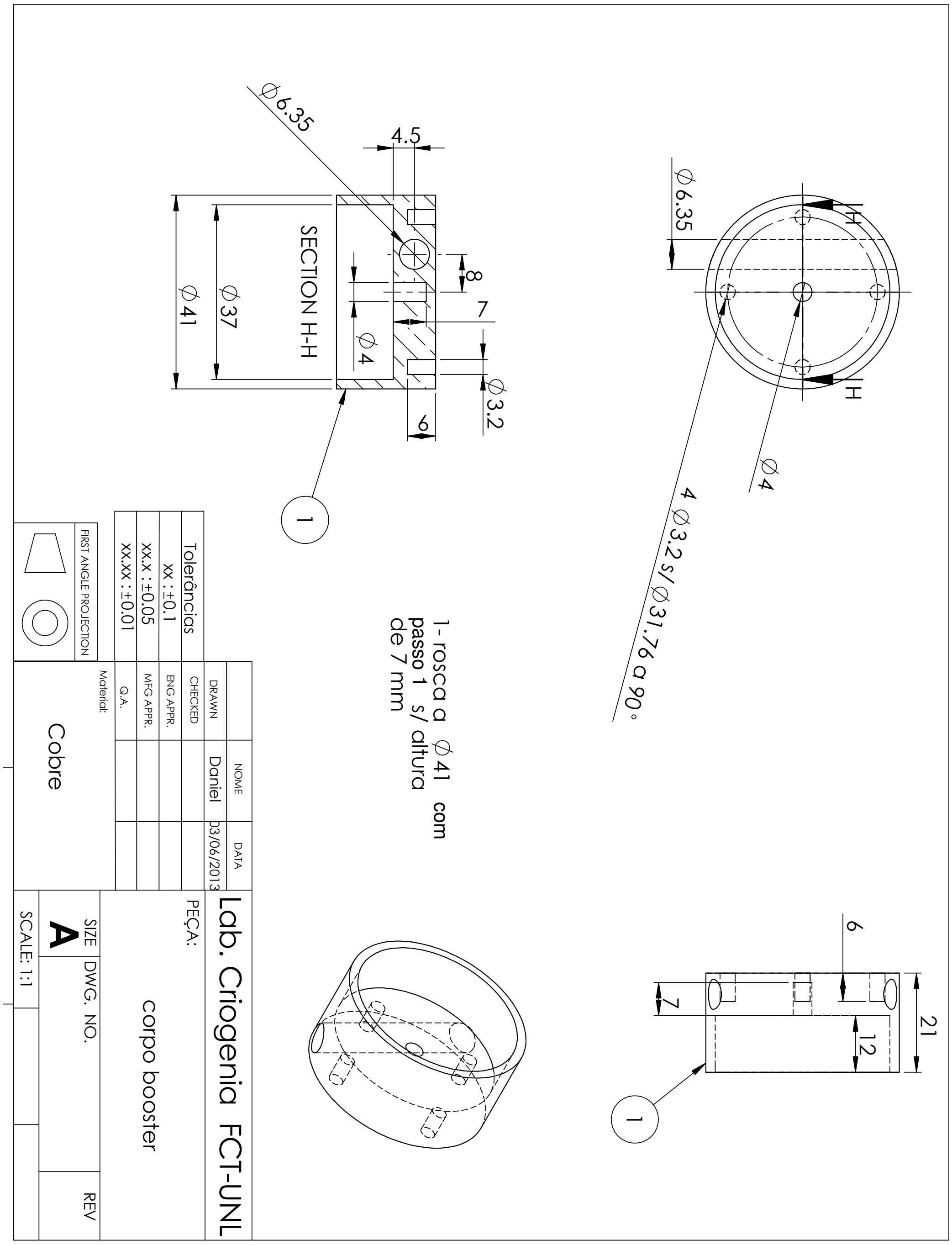

This drawing is not printed in scale.

Booster cell lid

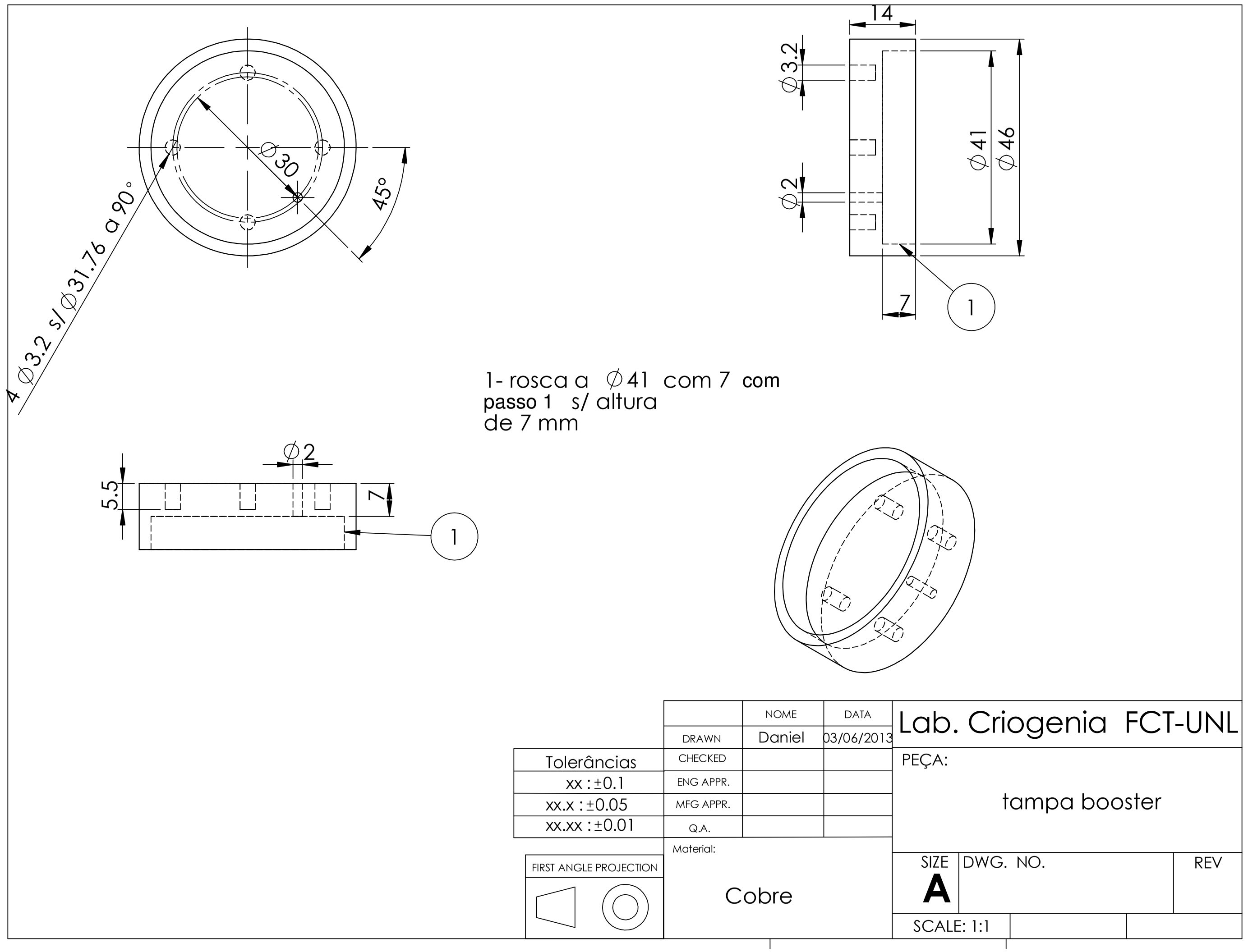

Annexes

Annex 1: P-T diagram of nitrogen.

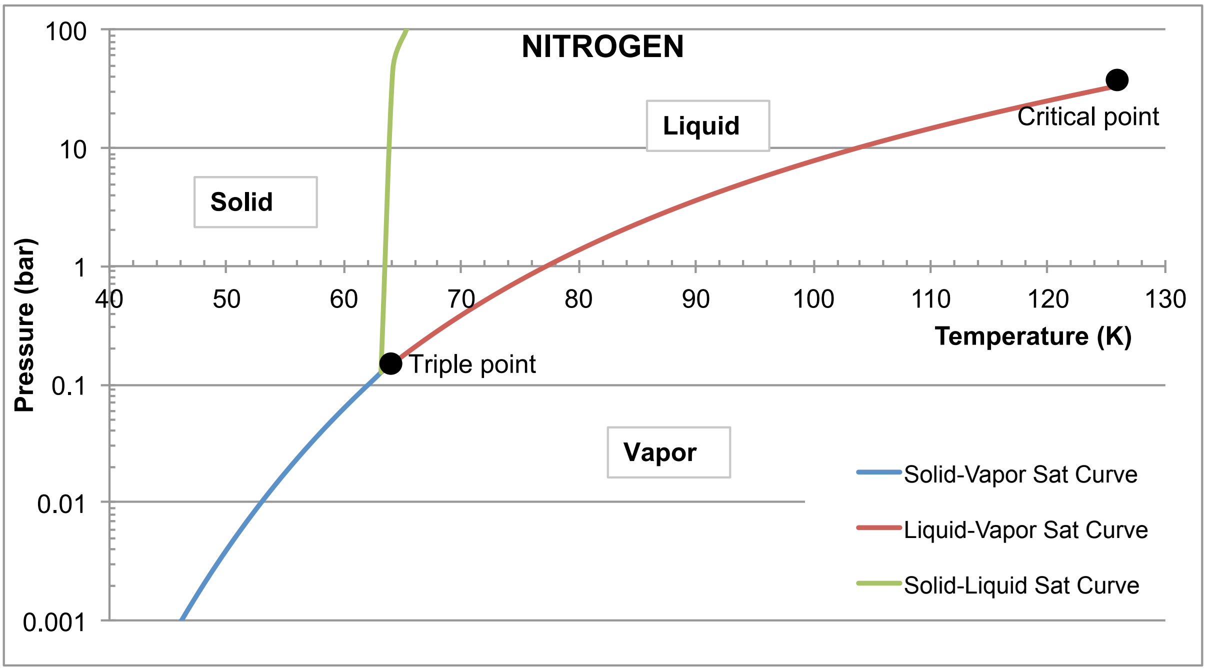

Source: REFPROP[34].

Annex 2: PT diagram of neon

The saturation diagram of liquid neon.

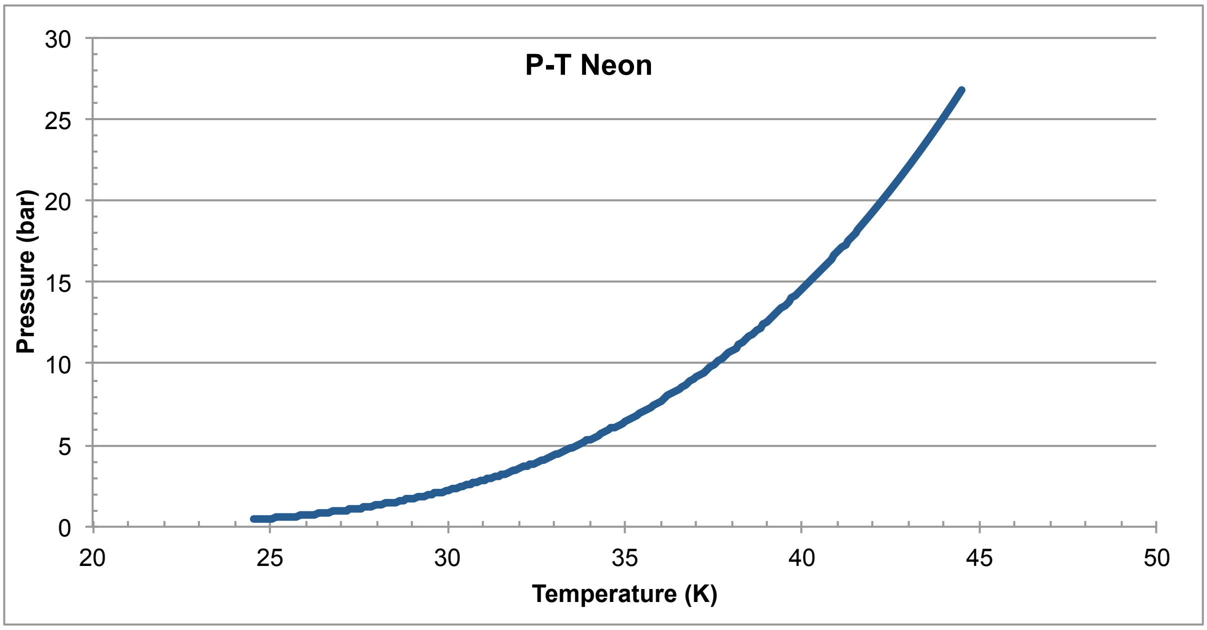

Source: REFPROP[34].

Annex 3: T-H diagram of neon.

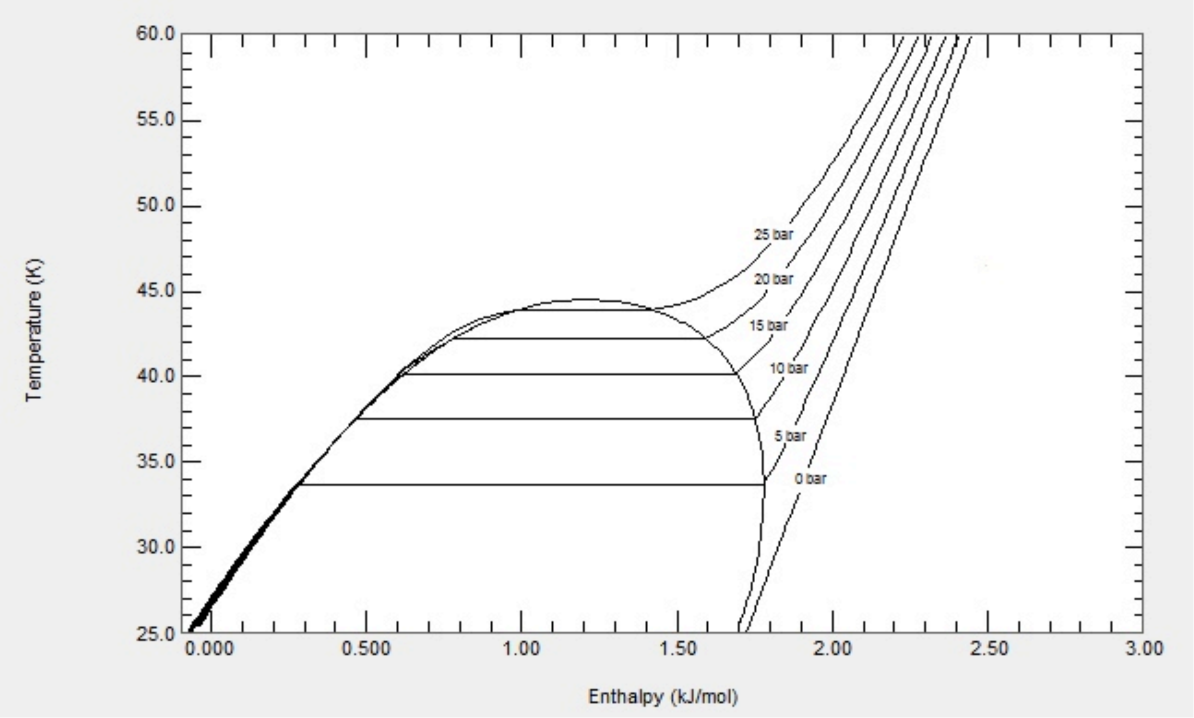

Source: REFPROP[34].

Annex 4: Latent heat of neon

The line represents the latent heat of the liquid to vapor transition of neon. The red dot is the latent heat of the triple point transition of neon.

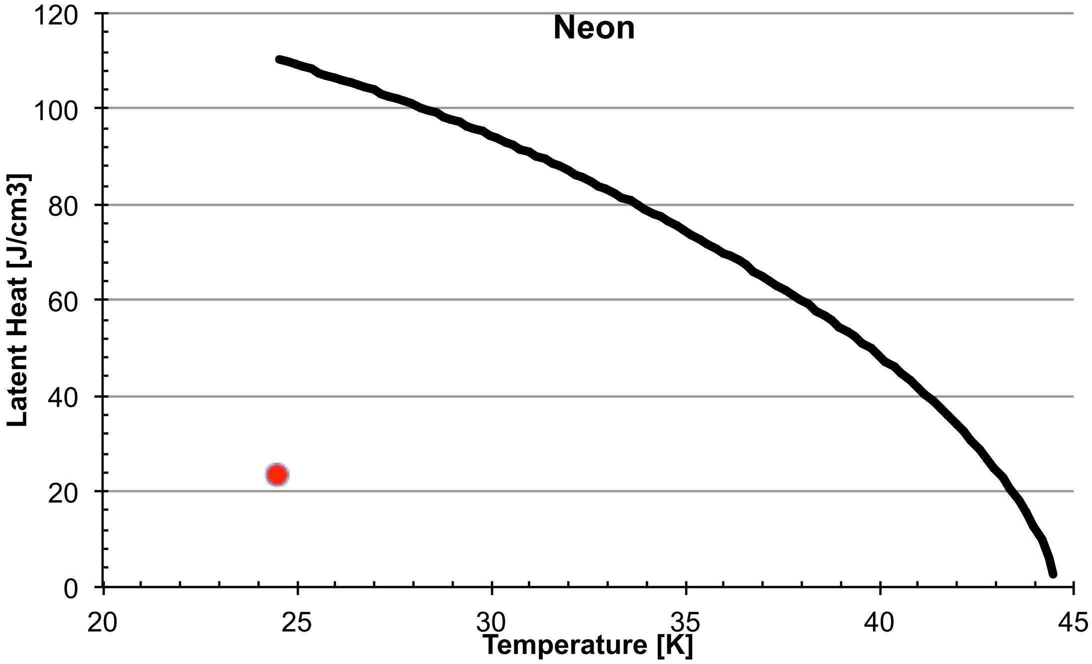

Source: REFPROP[34].

Annex 5: – Surface tension of neon and nitrogen

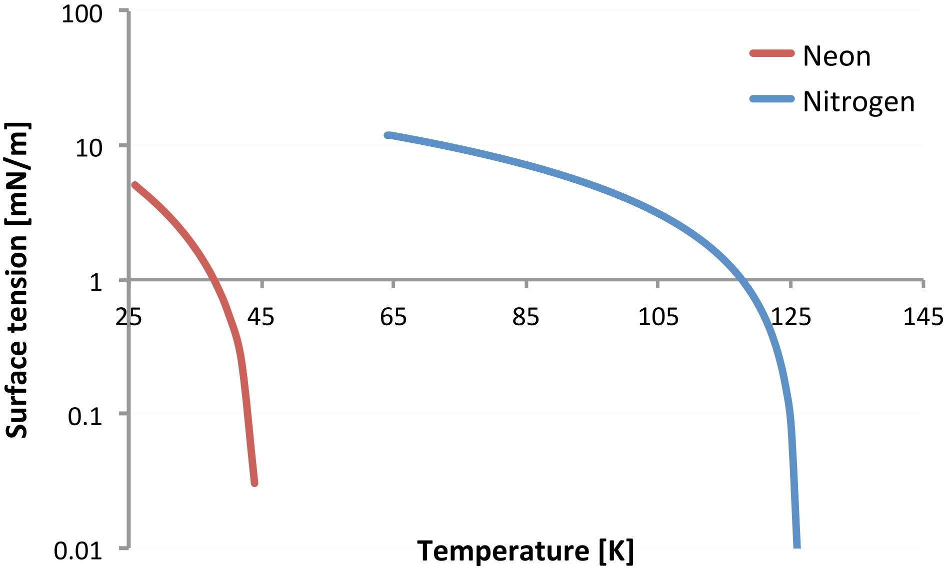

Source: REFPROP[34].